CONF-941279 --

Proceedings of the Workshop on Adaptive Grid Methods for Fusion Plasmas

A.E. Koniges
G.G. Craddock
D.D. Schnack
H.R. Strauss

Workshop on Adaptive Grid Methods for Fusion Plasmas
Pleasanton, CA
December 8-9, 1994

July 1995

Lawrence Livermore National Laboratory

Work performed under the auspices of the U.S. Department of Energy by Lawrence Livermore National Laboratory under Contract W-7405-ENG-48.

AGENDA OF TALKS

WORKSHOP ON ADAPTIVE GRID METHODS FOR FUSION PLASMAS
JOINTLY SPONSORED BY SIAC, NERSC AND NYU

DECEMBER 8-9, 1994

PLEASANTON HILTON
PLEASANTON, CALIFORNIA

Thursday Morning

8:00-8:40 AM	Registration
8:40-8:50 AM	Opening Dalton Schnack - SIAC
8:50-9:00 AM	Local Welcome Alice Koniges - NERSC

SESSION #1 at 9:00 AM; Alice Koniges Presiding

9:00-10:15 AM	Invited Talk David Bacon - SIAC "OMEGA: The Operational Multiscale Environment Model with Grid Adaptivity"
10:15-10:45 AM	Coffee Break
10:45-11:15 AM	Hank Strauss - NYU "FEMHD: An Adaptive Finite Element Method for Fluid and MHD Computations"
11:15-11:45 AM	Daniel Swift - University of Alaska "Use of Generalized Curvilinear Coordinate System in Hybrid and Electromagnetic Codes"
11:45 AM-12:15 PM	Jim Wiley - University of Texas, Austin "HP Finite Element Methods and Adaptive Grids"
12:15-1:45 PM	Lunch

Thursday Afternoon

SESSION #2 at 1:45 PM; Dalton Schnack Presiding

1:45-3:00 PM	Invited Talk Phil Colella - University of California, Berkeley "Block Structured Adaptive Grid Methods for Computational Fluid Dynamics"
3:00-3:30 PM	Andrew Kuprat/Alan Glasser - LANL "Adaptive Grid Finite Element Model of the Scrape-off Layer"
3:30-4:00 PM	Coffee Break
4:00-4:30 PM	Dennis Hewett - LLNL "A General Boundary Capability Embedded in an Orthogonal Mesh"
4:30-5:00 PM	Donald E. Burton - LLNL "FLAG: A Multi-dimensional Adaptive Free Lagrange Method for Fully Unstructured Grids".

Friday Morning

8:30-9:00 AM	Coffee Pick up lunch tickets before 9:00 AM

SESSION #3 at 9:00 AM; Hank Strauss Presiding

9:00-10:15 AM	Invited Talk Manoj Prasad - LLNL "3D Unstructured Mesh Discontinuous Finite Element Hydro"
10:15-10:45 AM	Dalton Schnack - SIAC "TRIM: A Finite-Volume MHD Algorithm for an Unstructured, Adaptive Mesh"
10:45-11:00 AM	Alice Koniges - NERSC/LLNL "Massively Parallel Systems: New Capabilities and Access for MFE and LLNL Users"
11:00-11:15 AM	Paulette Liewer - Jet Propulsion Laboratory Informal discussion on her recent Space Physics work
11:30 AM-1:00 PM	Discussion Leaders: Hirshman, Koniges, Strauss Development of Working Plan for Implementing Adaptive Techniques into MFE/ITER: needs, deliverables and relationship to edge/MHD initiatives
1:00 PM	Adjourn

Summary of Workshop on Adaptive Grid Methods for Fusion Plasmas

The Workshop on Adaptive Grid Methods for Fusion Plasmas, held on 8-9 December 1995, was sponsored jointly by NERSC, SAIC and NYU. The purpose of the workshop was to assemble workers, both within and outside of the fusion-related computations areas, for discussion regarding the issues of dynamically adaptive gridding. There were three invited talks related to adaptive gridding application experiences in various related fields of computational fluid dynamics (CFD), and nine short talks reporting on the progress of adaptive techniques in the specific areas of scrape-off-layer (SOL) modeling and magnetohydrodynamic (MHD) stability.

Adaptive mesh methods have been successful in a number of diverse fields of CFD for over a decade. The method involves dynamic refinement of computed field profiles in a way that disperses uniformly the numerical errors associated with discrete approximations. Because the process optimizes computational effort, adaptive mesh methods can be used to study otherwise the intractable physical problems that involve complex boundary shapes or multiple spatial/temporal scales. Recent results indicate that these adaptive techniques will be required for tokamak fluid-based simulations involving the diverted tokamak SOL modeling and MHD simulations problems related to the highest priority ITER relevant issues.

Adaptive algorithms are particularly attractive for the ITER tokamak SOL and MHD problems. In both cases, the problem domain is quite large compared to the fine-scale features of interest, even though details of the small features may have enormous impact on the whole of the solution profiles. However, magnetically diverted plasmas lead to multiply-connected domains and disparate time-scales that can complicate traditional, time-explicit, adaptive schemes. The workshop agenda and setting were conducive to spirited discussion over a number of such implementation issues. Among these were the benefits and disadvantages of structured gridding, fixed accuracy approximations, moving meshes, object-oriented programming in Fortran 90 and C++, and the lack of adequate benchmark problem specifications. Also discussed was the lack of funding for research directed solely for code and algorithm development.

The following is a summary of the invited review talks and participant presentations. Also included is a summary of the predominant issues discussed informally among the participants during the workshop.

Summary of Invited Review Talks

The three invited talks were oriented generally toward the details of algorithm implementation, with a focus on the constraints necessary to incorporate the relevant physics problem. The speakers were Monoj Prasad (LLNL), David Bacon (SAIC), and Phil Colella (UC Berkeley/LLNL-CCSE).

Manoj Prasad presented detailed features of the ICF3D hydrodynamics code used for inertial fusion simulations. This code is intended to be a state-of-the-art upgrade of the well-known fluid code, LASNEX. ICF3D employs discontinuous finite elements on a discrete unstructured mesh consisting of a variety of 3D polyhedra including tetrahedra, prisms, and hexahedra. Prasad discussed details of how the Roe-averaged second-order convection was applied on the discrete elements, and how the C++ coding interface has helped to simplify implementing the many physics and numerics modules within the code package. Prasad emphasized the virtues of object-oriented design in large scale projects such as ICF3D.

David Bacon presented an invited review talk on the Omega code, used for weather simulation and the modeling of aerosol transport through the atmosphere. Omega employs a 3D mesh of wedge shaped elements (triangles when viewed from above) that adapt with time. Because wedges are laid out in layers of triangular elements, the scheme can utilize structured storage and differencing techniques along the elevation coordinate, and is thus a hybrid of structured and unstructured methods. Bacon illustrated the utility of adaptive gridding in his model near geographic features such as coastlines, where material properties change discontinuously. Temporal adaptivity was used additionally to track moving internal fronts, such as clouds of aerosol contaminants. Bacon also discussed limitations specific to his problem, including manipulation of huge data bases and fixed turn-around times. In practice, the latter requires a carefully tuned optimization between accuracy and computation speed.

A structured approach to adaptivity was described in an invited review talk by Phil Colella. Colella described the hyperbolic and parabolic applications of the Automatic Mesh Refinement (AMR) algorithms of M. Berger (CIMS/NYU). Adaptivity is achieved by overlaying finer grids only in areas flagged by a generalized error criterion. Colella discussed some of the issues involved in abutting disparate-resolution grids, and demonstrated that suitable algorithms exist for dissipative as well as hyperbolic systems. Most of the complex AMR grid hierarchy is

implemented in C++, but the underlying rectangular array operations are carried out in Fortran for efficiency on modern compilers. By combining higher-order convection schemes with AMR, the group can perform large 3D calculations that were otherwise impossible with structured schemes.

Summary of Participant Presentations

The nine participant presentations covered a wide range of plasma applications, from heliosphere and magnetospheric work through tokamak MHD and SOL calculations. These presentations were again geared toward the details of adaptive scheme application.

Hank Strauss of CIMS/NYU described FEMHD, an adaptive mesh code for RMHD (reduced MHD), which uses an unstructured triangular mesh in 2D and wedge shaped mesh elements in 3D. There is also a version of his code for modeling the coupled neutral and charged species at the edge of a deverted tokamak. Strauss also has an effort underway with Wonchull Park of PPPL, to incorporate the unstructured mesh software into MH3DK, a full MHD-particle code.

Jim Wiley of Texas, described general "hp" finite element methods and adaptive grids. The work was based on that of Oden and collaborators at Texas. The term "hp" refers to the method where refinement is done not only in space (h) but in the order of polynomials used for the finite element discretization (p). Working with finite elements, the method seems to not have particular difficulty handling abutted grids of disparate resolution. His neutral fluid code is written in C++ to cope with the elaborate data structures.

Andrew Kuprat of LANL discussed unstructured grids for application to transport in the tokamak edge SOL. Kuprat has developed a new metric with which to judge element elongation and resolution requirements. Using this method, Kuprat applies a standard moving finite element technique to advance the SOL equations while inserting/deleting dynamically nodes that violate an elongation criterion. In a tokamak plasma, Kuprat's method achieves a more uniform accuracy, and results in highly stretched triangular finite elements, except near separatrix X-point where transport is more isotropic.

Donald Burton of LLNL described FLAG, a 3D adaptive free-Lagrange method for unstructured grids. The grid elements were 3D polygons, which move with the flow, and are refined or reconnected as necessary to achieve uniform accuracy. Burton stressed that they were able to construct

a 3D hydro version of the code in 3 months using an object-oriented FORTRAN approach.

Dalton Schnack of SAIC described the MHD code, TRIM which uses a finite volume discretization of the MHD equations on an unstructured adaptive grid of triangles in the poloidal plane. The toroidal direction is treated by a pseudospectral method. Care was taken to center variables appropriately on the mesh and to construct a self adjoint diffusion operator for cell centered variables.

Alice Koniges of LLNL described the new T3D parallel computer at NERSC. The adaptive mesh ICF3D code described above is one of the current applications being ported and developed for use on the T3D. David Kershaw of LLNL stressed that the development environment and tools available on the parallel computer is similar to any planned for the future including networks of workstations.

Dennis Hewitt described a method for treating curved boundaries with a rectangular mesh discretization. Special difference operators were constructed to approximate numerical zones split by the domain boundary; the operators are particularly simple for his rectangular mesh. Hewitt demonstrated that his simple numerical approach, Dynamic Alternating Direction Implicit, turned out to be considerably more efficient than more complex grid-adaptive algorithms that he tried in the past.

Daniel Swift of the University of Alaska described magnetosphere particle simulations, and Paulette Liewer of JPL described heliosphere fluid simulations. They both used single level, structured, but curvilinear 2D meshes. They packed the coordinate system more closely in regions, such as the bow shock near the earths magnetosphere, that required higher resolution.

Summary of Predominant Informal Discussions

Of the many informal discussions between participants during the workshop there were five recurring topics of discussion: structured vs. unstructured gridding, lack of funding ear-marked specifically for code or algorithm development, lack of standard benchmark test problems to encourage the development of new algorithms, object-oriented design, and the attractiveness of a class library repository for fusion-related fluid computations.

One the primary decisions in developing a grid-adaptive algorithm is whether to use structured or unstructured gridding. Structured data allows organized solution techniques, incorporation of a well-developed field of numerical hydrodynamics and relatively direct vectorization of algorithms on modern computer hardware. Unstructured storage conversely provides a wealth of flexibility in adaptive refinement schemes and the ability to incorporate complex domain geometries. Representatives from SAIC's Omega weather simulation group and the LLNL ICF3D code development group demonstrated the power and flexibility of unstructured meshes; whereas LLNL's CCSE group demonstrated the corresponding strengths of an organized grid approach with examples from the AMR work.

Lack of funding was cited as one possible explanation of the relatively few developed dynamically adaptive codes in fusion-related fluid calculations. Due to decreasing budgets, many of the funded projects are based solely on exercising previously developed codes---this was recognized as short-sighted in light of the possible improvements that adaptive methodologies have to offer.

Object-oriented design was hailed as the solution for rapid prototyping of the complex dynamically adaptive algorithms, and was being used by both the structured and unstructured camps. Object-oriented design is implementable via C++ or Fortran 90. Some groups, notably the CCSE AMR group still use Fortran 77 as the underlying code for the computation intensive parts of the algorithm.

A benchmark problem was developed at the workshop, and then in detail by Tom Rognlien of LLNL, to contain a minimal set of the physics necessary to test a new code for it appropriateness to the tokamak edge SOL problem. This problem was to be the first in a series of progressively more difficult tests. Rognlien will communicate with other interested workshop attendees via electronic mail to finalize all the parameters of this test problem, and ensure its applicability.

Finally, it was the consensus of the group that adaptive methods tend to involve complex programming. In order to minimize the development efforts involved by having many disjoint code development projects, it was suggested that the NERSC possibly maintain an evolving library of various class and graphics libraries.

Conclusion

The workshop was successful in its objectives of showing fusion researchers the state-of-the-art in modern CFD. At the same time, it was clear that fusion scientists have made progress in introducing adaptive mesh methods into MHD and edge modeling. These methods are required in computational problems which include the presence of a divertor, such as MHD ELM simulations and radiative divertor modeling, and deserve firm, unwavering support. In addition to developing the adaptive mesh methods, there should also be an effort made to make adaptive mesh code packages which could be integrated into other codes to decrease the development time of future codes and algorithms. Object oriented languages such as C++ and Fortran 90 are well-suited for such a library development.

Finally, we would like to thank Debbie Lofrisco and Terry Burch for secretarial and organizational support.

Alice Koniges, NERSC

Dalton Schnack, SAIC

H. R. Strauss, NYU

Gary Craddock, NERSC

Marc Day, NERSC

ADAPTIVE GRID METHODS FOR FUSION PLASMAS

DECEMBER 8-9, 1994

List of Attendees	Affiliation
Allen, Darrel	University of California, Davis
Aydemir, Ahmet	University of Texas, Austin
Bacon, David	Science Applications International Corporation
Bradley, Michael	Lawrence Livermore National Laboratory
Brown, Peter	Lawrence Livermore National Laboratory
Burton, Donald	Lawrence Livermore National Laboratory
Charlton, Lowell	Oak Ridge National Laboratory
Colella, Phil	University of California, Berkeley
Craddock, Gary	Lawrence Livermore National Laboratory
Day, Marc	University of California, San Diego
Dimits, Andris	Lawrence Livermore National Laboratory
Dorr, Milo	Lawrence Livermore National Laboratory
Glasser, Alan	Los Alamos National Laboratory
Hewett, Dennis	Lawrence Livermore National Laboratory
Hughes, Michael	Grumman Corporation
Kershaw, David	Lawrence Livermore National Laboratory
Koniges, Alice	Lawrence Livermore National Laboratory
Kuprat, Andrew	Los Alamos National Laboratory
Liewer, Paulette	Jet Propulsion Laboratory
Longcope, Dana	University of California, Berkeley
Marcus, Dan	Lawrence Livermore National Laboratory

Miller, Doug	Lawrence Livermore National Laboratory
Milovich, Jose	Lawrence Livermore National Laboratory
Modi, Bijal	University of California, Berkeley
Murty, Susarla	Lawrence Livermore National Laboratory
Nebel, Rick	Los Alamos National Laboratory
Pace, John	Lawrence Livermore National Laboratory
Painter, Jeff	Lawrence Livermore National Laboratory
Park, Wonchull	Princeton Plasma Physics Laboratory
Prasad, Manoj	Lawrence Livermore National Laboratory
Riddle, Alan	Lawrence Livermore National Laboratory
Rodrigue, Garry	University of California, Davis
Rognlien, Tom	Lawrence Livermore National Laboratory
Schnack, Dalton	Science Applications International Corporation
Sheehey, Pete	Los Alamos National Laboratory
Shestakov, Alek	Lawrence Livermore National Laboratory
Smith, Gary	Lawrence Livermore National Laboratory
Strauss, Hank	New York University
Swift, Daniel	University of Alaska
Vesey, Roger	Princeton Plasma Physics Laboratory
Wake, Dan	University of California, Davis
Wang, Joseph	Jet Propulsion Laboratory
Wiley, Jim	University of Texas, Austin
White, Dan	University of California, Davis

Operational
Multiscale
Environment Model with
Grid
Adaptivity

OMEGA:
The Operational Multiscale Environment model with Grid Adaptivity

David P Bacon
Science Applications International Corporation

December 8, 1994

OMEGA Team

D. Bacon	Y-L. Ho	S. Peckham
P. Boris	T. Lee	P. Satyanarayana
Z. Boybeyi	I. Lottati	R. Sarma
T. Dunn	M. McCorcle	S. Young
M. Hall	R. McNally	J. Zack

This effort is supported by DNA under contract DNA001-92-C-0076.
The Technical Monitor is Lt. Col. J. Hodge

SAIC Computational Physics Division
An Employee-Owned Company
Science Applications International Corporation

Program Objectives

- Build a State-of-the-Art Atmospheric Forecast Model with an Embedded Atmospheric Transport and Diffusion Capability to Address the Following Missions:
  - Provide Real Time Predictions of the Dispersal of Nuclear, Biological, and Chemical Hazards in Response to Incidents Anywhere in the World
  - Provide a Highly Accurate Predictive Model for Use by Mission Planners in Assessing NBC Weapons Effects or the Collateral Effects Caused by Damaging NBC Facilities
- Build on Lessons Learned from DESERT STORM

Problem Overview

- Aerosol Dispersal Is Inexorably Linked to the Free Tropospheric Conditions:
  - Wind
  - Convection
  - Precipitation
  - Turbulence
- Surface Characteristics Determine the Fluid Motions in the Planetary Boundary Layer (PBL)
  - Orography
  - Sea Breeze / Land Breeze Circulations
  - Urban / Canopy Effects
  - Soil Moisture
- Problems Range from Microscale to Hemispheric Scale

Winds are Key

- World Wide Wind Data is Sparse
  - NA Surface Data Spacing: ~ 50 km
  - NA Upper Altitude Spacing: ~ 250 km
- Surface Orography Modifies Wind Field
  - Mass Consistency
- Surface Processes Modify Local & Larger Scale Circulations
  - Non-Uniform Surface Heating
    - » Inhomogeneous Albedo
    - » Urban Heat Island
    - » Land / Water Boundary
  - Evapotranspiration
  - Surface Roughness / Canopy Effects
- **Simulation can Fill the Data Void**

North America WMO Surface Observations

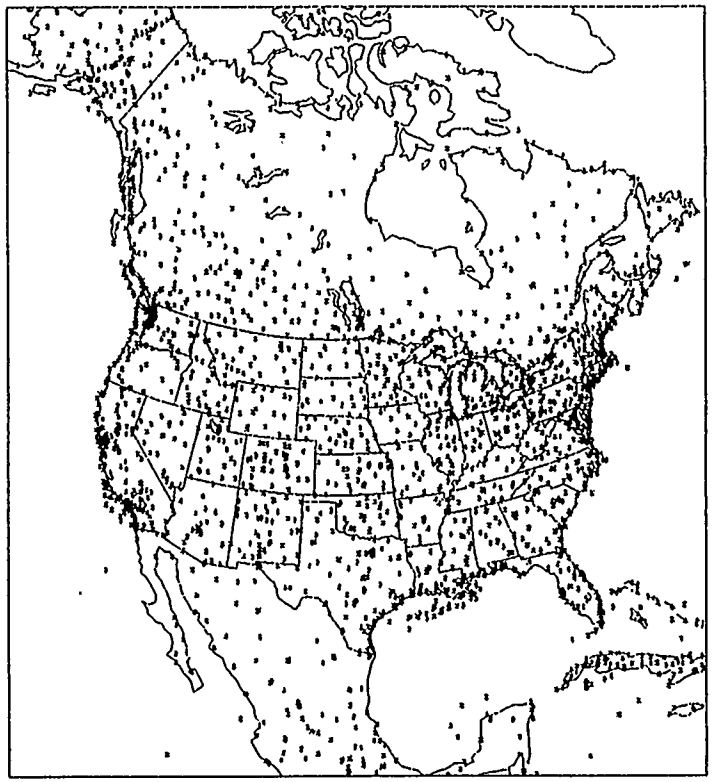

North America WMO Upper Air Stations

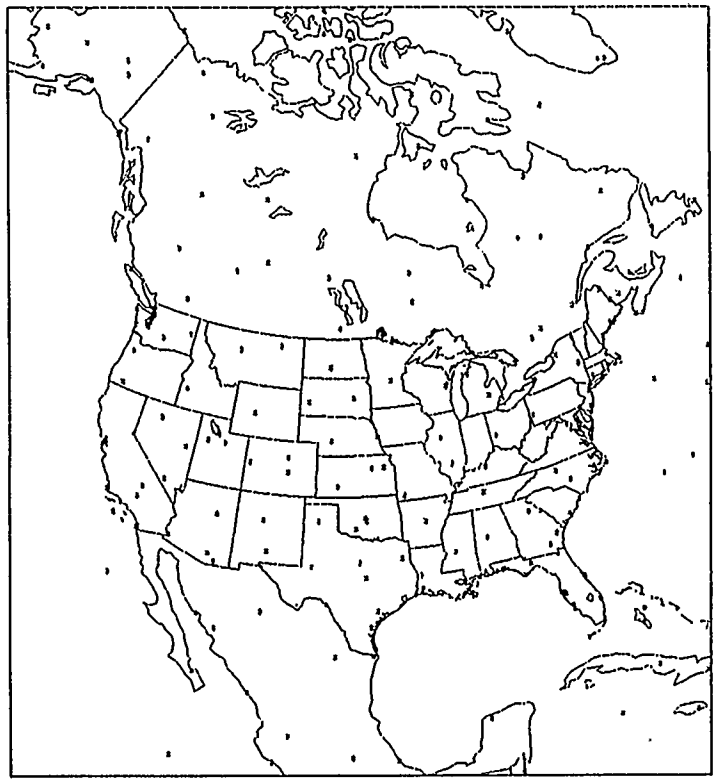

PBL Physics is Critical

- Non-Uniform Surface Heating is Key to Local Circulations
  - Inhomogeneous Albedo Leads to Differential Heating
  - Urban Centers are Localized Heat Sources
  - Difference in Heat Capacity of Soil and Water Leads to Sea Breeze / Land Breeze Circulations
  - Evapotranspiration Provides Localized Cooling
  - Surface Roughness / Canopy Drag the Flow Field
- Surface Processes Lead to Non-Classical Mesoscale Circulations
  - Low Level Jet
  - Boundary Layer Convection
  - Which Can Lead to Severe Weather

- These Modifications are Important for Aerosol Transport in the PBL

Urban heat islands, sea/land breeze circulations, orographic separation and low level jets are examples of PBL driven phenomena.

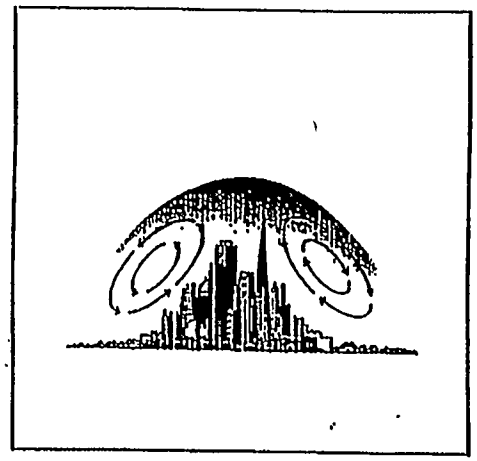

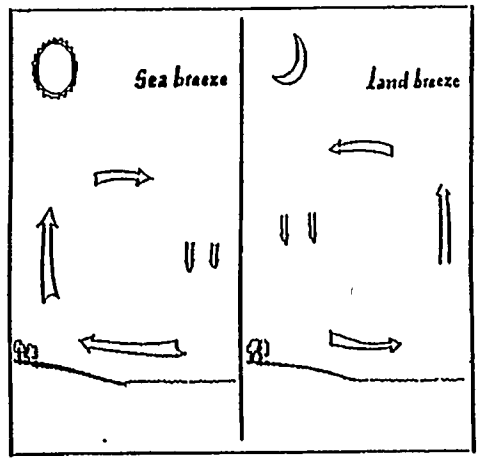

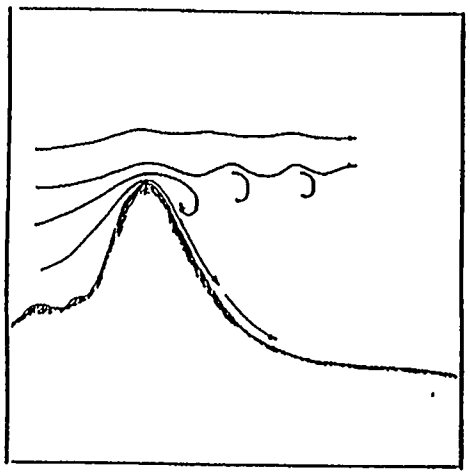

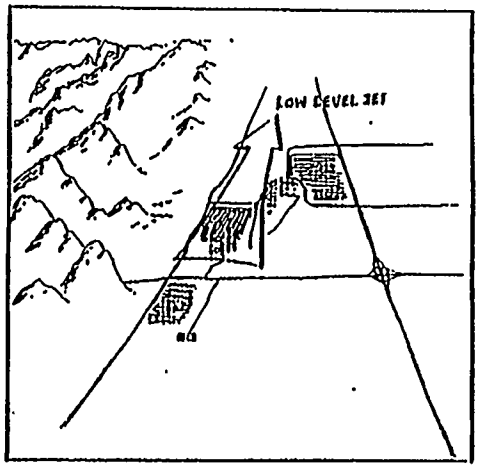

The terrain surrounding Bhopal, the urban heat island effect, and the lake effect all contributed to the magnitude of the disaster.

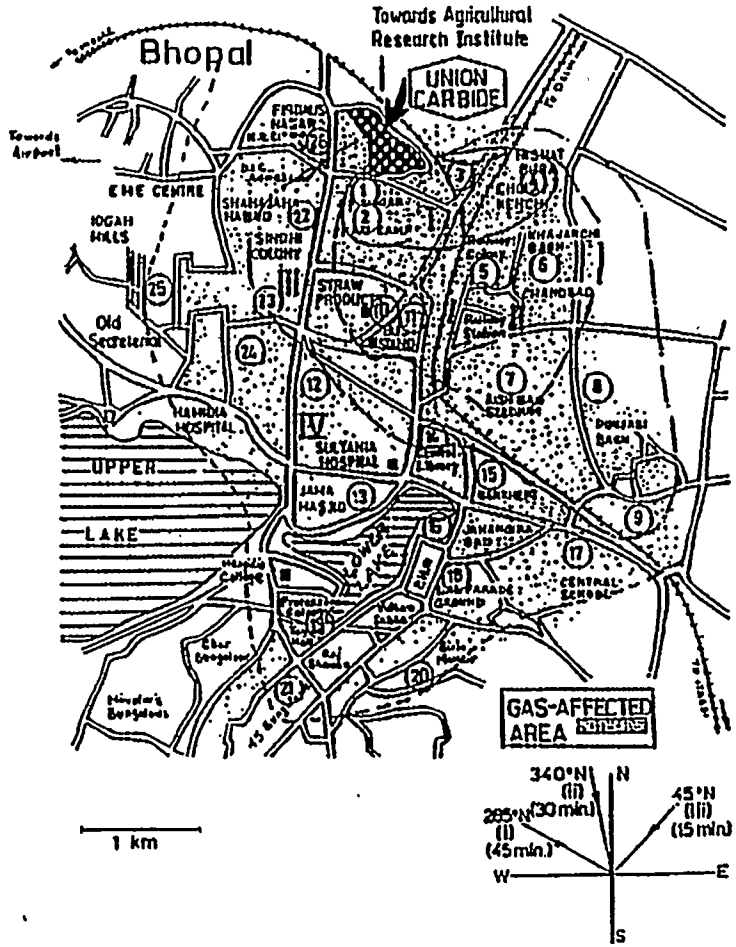

MASS: Simulated Surface Winds at 0900 LST

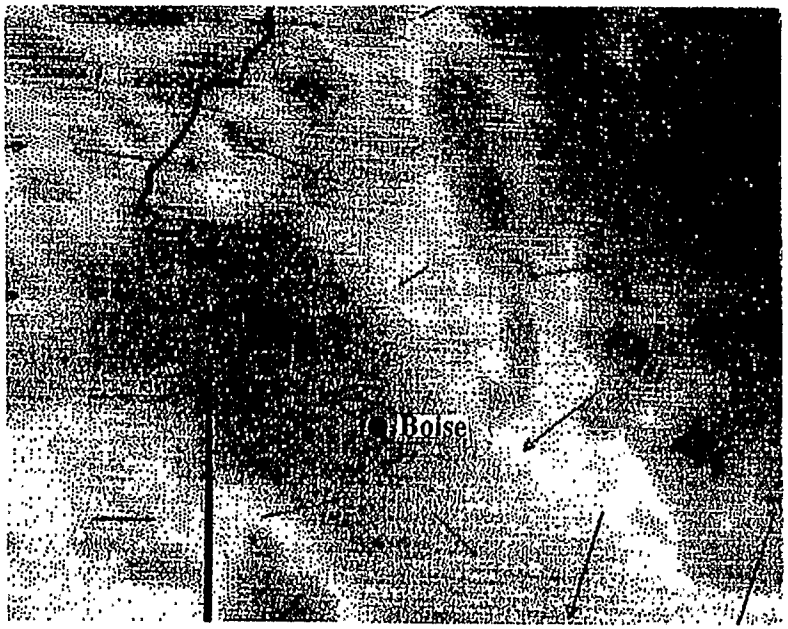

45 km Resolution 15 km

Mission Requirements

- World Wide Operability
  - For Pre-determined Fixed Sites
  - For Arbitrary Locations
  - *Including Regions of Complex Terrain*
- Fast Turn-Around Time
- High Resolution
- All Weather Capability

World Wide Operability

- World Wide Surface Datasets
- Requires Flexible Data Assimilation
  - Full Global & Local Data where Available
    - » Large Scale Simulation Output
      - NA (NMC/FNOC) & Europe (ECMWF) at 100 km
      - Remainder of Earth at 300 ± km
    - » Local Met Station & Rawinsonde Releases

Fast Turn-around Time

- Requires Rapid Data Assimilation & Model Execution (Including Post-Processing)
  - Fixed Site
  - Arbitrary Site
- Maximum Automation
  - System Execution Including Adaptation

Weather Products Timelines

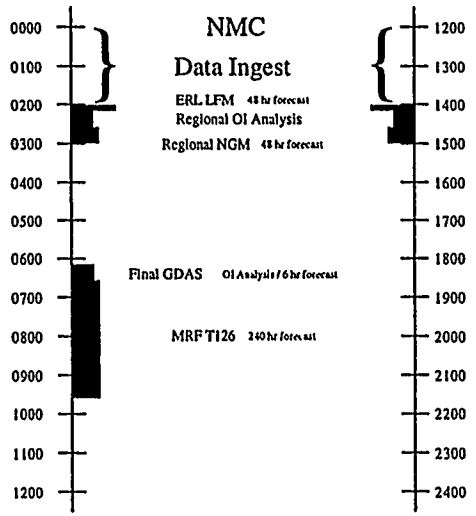

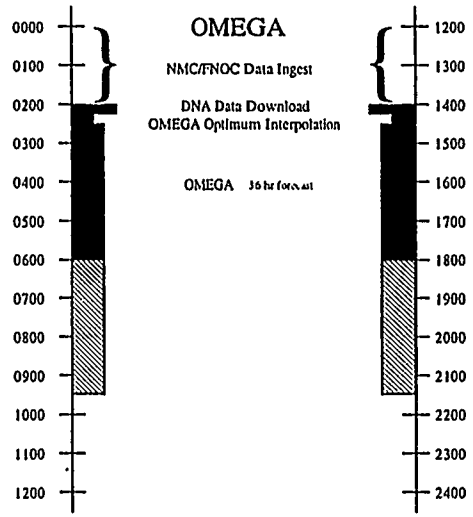

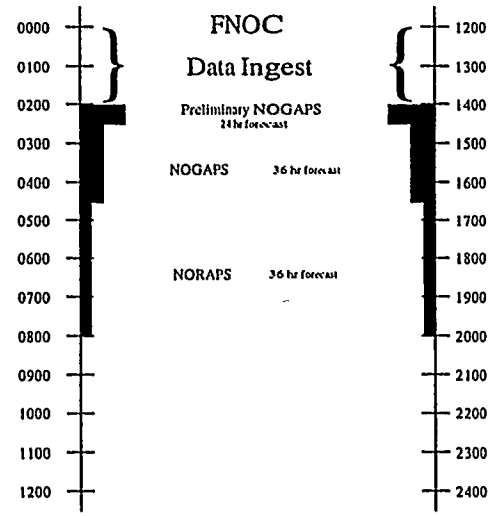

High Resolution

- Spatial Scales Down to 1 km for Winds
  - Requires Nesting or Continuous Adaptive Grid
- Spatial Scales Down to 100 m for Aerosol Transport
  - Requires Lagrangian Transport Scheme

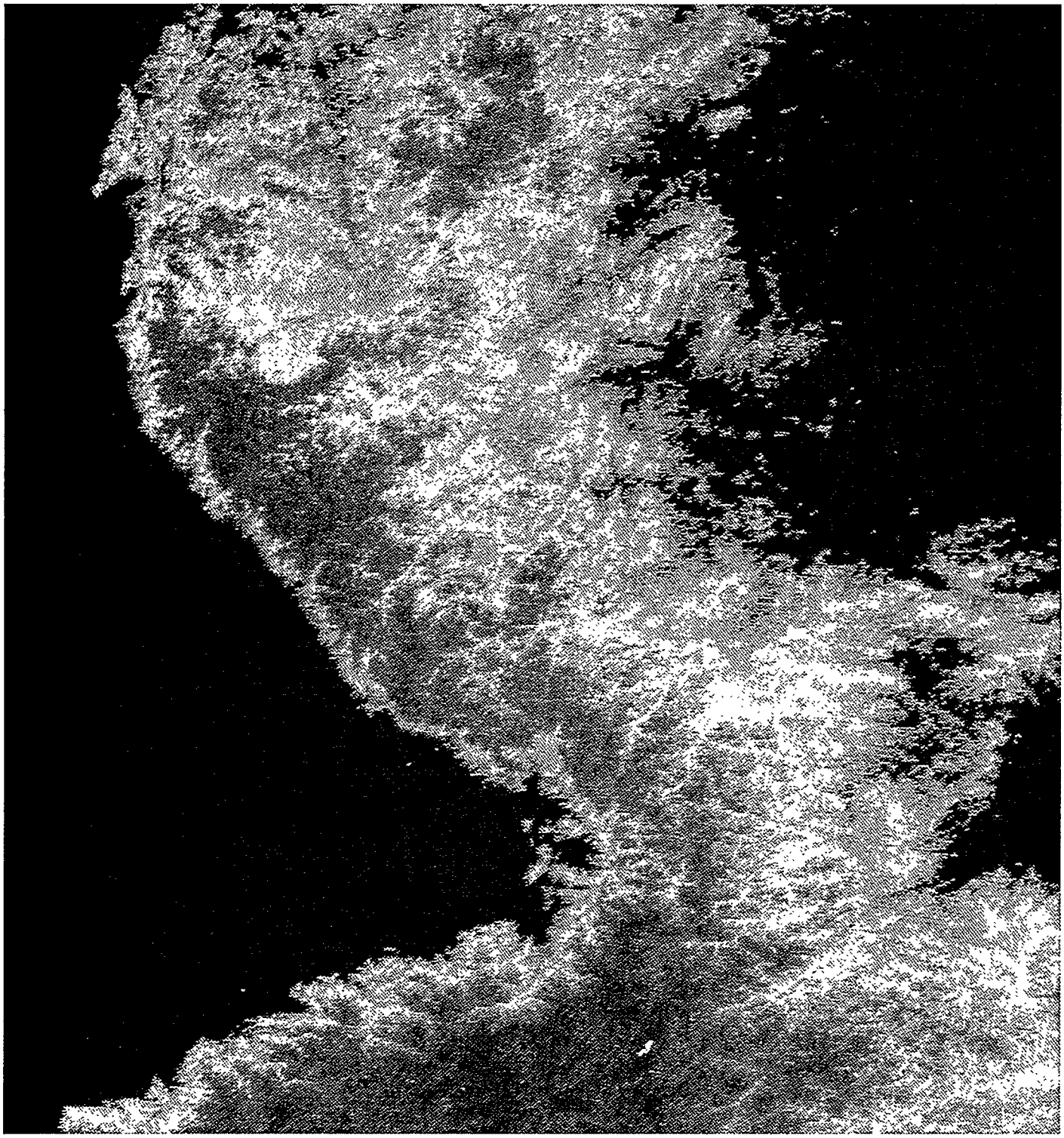

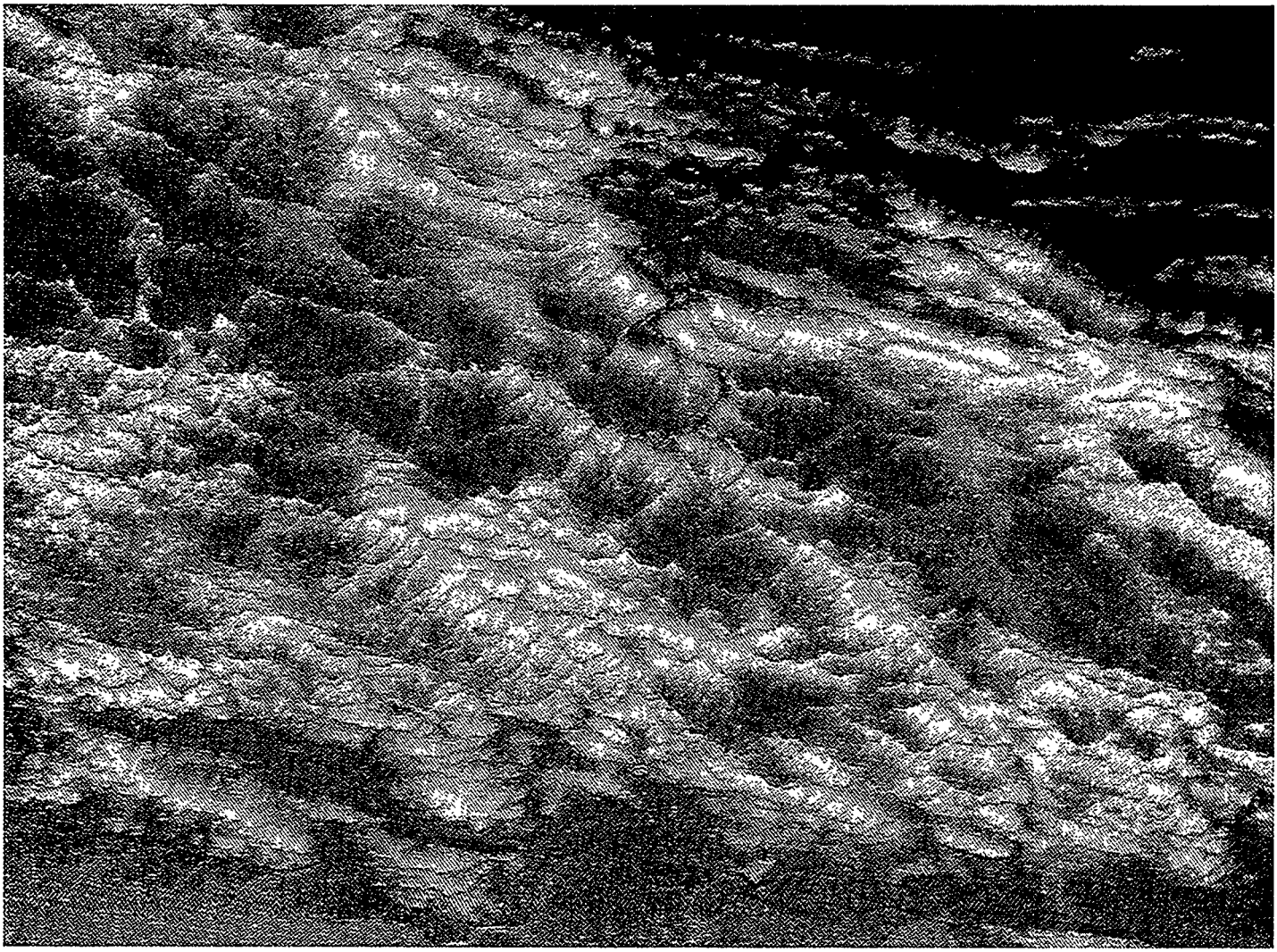

All Weather Capability

- Non-Hydrostatic Model to Treat:
  - Frontal Activity
  - Convective Activity
- Adaptive (Manual or Automatic) Grid to Treat:
  - Evolving Weather
  - Moving Aerosols

OMEGA is a Synthesis of Advanced Physics and State-of-the-Art Numerical Methods

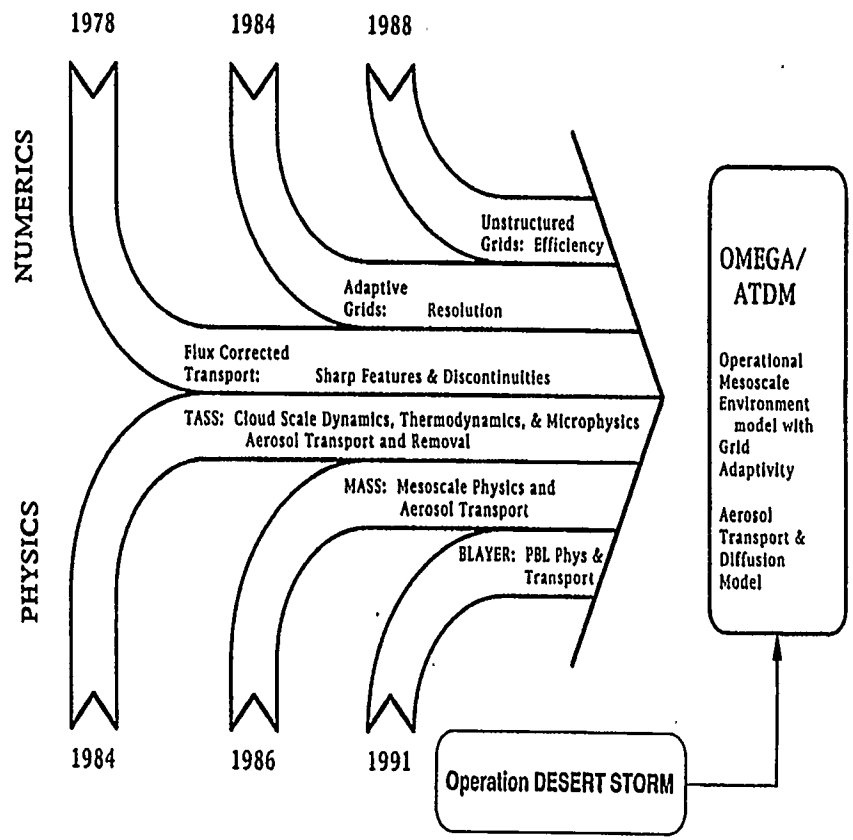

OMEGA Overview - I

Governing equations	Fully non-hydrostatic equation set
Dimensionality	3D
Grid structure	Unstructured and adaptive triangular prisms
Coordinate system	Rotating Cartesian coordinate framework
Numeric	Finite volume based upon Smolarkiewicz (1983)
Horizontal Resolution	1 - 100 km
Vertical Resolution	20 - 1000 m

OMEGA Overview - II

Surface roughness	Specified over land, predicted over water (Charnock, 1955)
Soil surface	Based on the force-restore rate method (Deardorff, 1978)
PBL	Planetary boundary layer is treated separately as viscous sublayer (Deardorff, 1974), surface layer (Businger et al., 1971), and transition layer
Turbulence closure	First order closure: For unstable conditions - O'Brien K-profile (O'Brien, 1970); Blackadar local K-profile for stable conditions (Blackadar, 1979) 1.5 order closure: Based on turbulent kinetic energy and its dissipation

OMEGA Overview - III

Cumulus parameterization	Modified Kuo scheme (Kuo, 1965; Anthes, 1977)
Microphysics	Extensive bulk-water microphysics (Lin et al., 1983)
Radiation	Shortwave absorption by water vapor and longwave emissivities of water vapor and carbon dioxide and computationally efficient technique of Sasamori (1972)
Initialization	Based on 4D data assimilation

OMEGA Overview - IV

Transport and diffusion	**Embedded Eulerian and Lagrangian aerosol transport algorithms**
Operational Status	**Real-time Operational Configuration (Research Mode also Supported)**

OMEGA Data Requirements

- OMEGA Utilizes High Spatial Resolution Surface Data
  - 1 km: Terrain Elevation, Land / Water, Albedo, Land Use
  - 4 km: Soil Texture
- OMEGA Utilizes Time Varying Surface Conditions
  - Vegetation, Snow / Ice Coverage, Soil Moisture
- OMEGA will Assimilate both Traditional & Non-Traditional Data
  - Surface Observations, Rawinsonde Observations, Soil Moisture
  - Satellite Derived Temperature & Wind Profiles
  - Profilers, Doppler Radar, Special Dropsonde / Rawinsonde Obs
- OMEGA Ingests Gridded Data
- OMEGA will be Capable of both Static & Dynamic Initialization

Data Requirements - Fixed Data

• Elevation (DTED)	
– Height (~1 km)	1300 MB
– Standard Dev (~1 km)	1300 MB
• Land Use (~1 km)	650 MB
• Land / Water (~1 km)	81 MB
• Soil Type / Global (~ 4 km)	41 MB
• Soil Type / NA (~1 km)	12 MB
» TOTAL	3.5 GB

Data Requirements - Time Varying Data

Seasonal:	• NDVI / Global (~18 km)	16	MB
	• NDVI / NA (~1 km)	100	MB
	• Surface Albedo (~1 km)	2600	MB
2 Week Cycle:	• NDVI / Global (~4 km)	81	MB
	• Surface Albedo (~1 km)	650	MB
Daily Cycle:	• Snow / Ice Depth (~4 km)	41	MB
	• Surface Moisture (~4 km)	41	MB
	• NMC-MRF	15	MB
12 Hour Cycle:	• Upper Air Stations (983)	0.5	MB
	• FNOC - Gridded Data	13	MB
	• NMC-NGM Grids	14	MB
Hourly Cycle:	• Surface Observations	0.5	MB
	– TOTAL	4.3	GB

OMEGA Development - Need for Balance

- Physics
  - Advection
  - Diffusion
  - Turbulence
  - Thermodynamics
  - Cloud Microphysics
  - Radiation Transport
  - Surface Physics
  - Atmospheric Chemistry
  - Particle Physics

- Numerical Simulation
  - Completeness
  - Order of Accuracy
  - Data Requirements
  - Stability & Robustness
  - Computational Requirements

- Operational Constraints
  - Hardware Available
  - Communications Bandwidth
  - Time

Model Equations

- Conservation of Mass Equations for
  - Air
  - Water Vapor
  - Non-precipitating hydrometeors
    - » Cloud droplets & Ice crystals,
  - Precipitating hydrometeors
    - » Raindrops & Snow
- Conservation of Momentum Equation
- Thermodynamic Energy Equation
- Equation of State

OMEGA Microphysics

Microphysics: The collection of processes that transfer mass between the several forms of water in a cloud.

- Explicit
  - Bulk-water Microphysical Parameterization
- Sub-grid scale
  - Convective Parameterization

OMEGA includes mass conservation equations for five water species:

Water Vapor

Cloud Droplets Cloud Ice

Raindrops Snow

Microphysical Processes

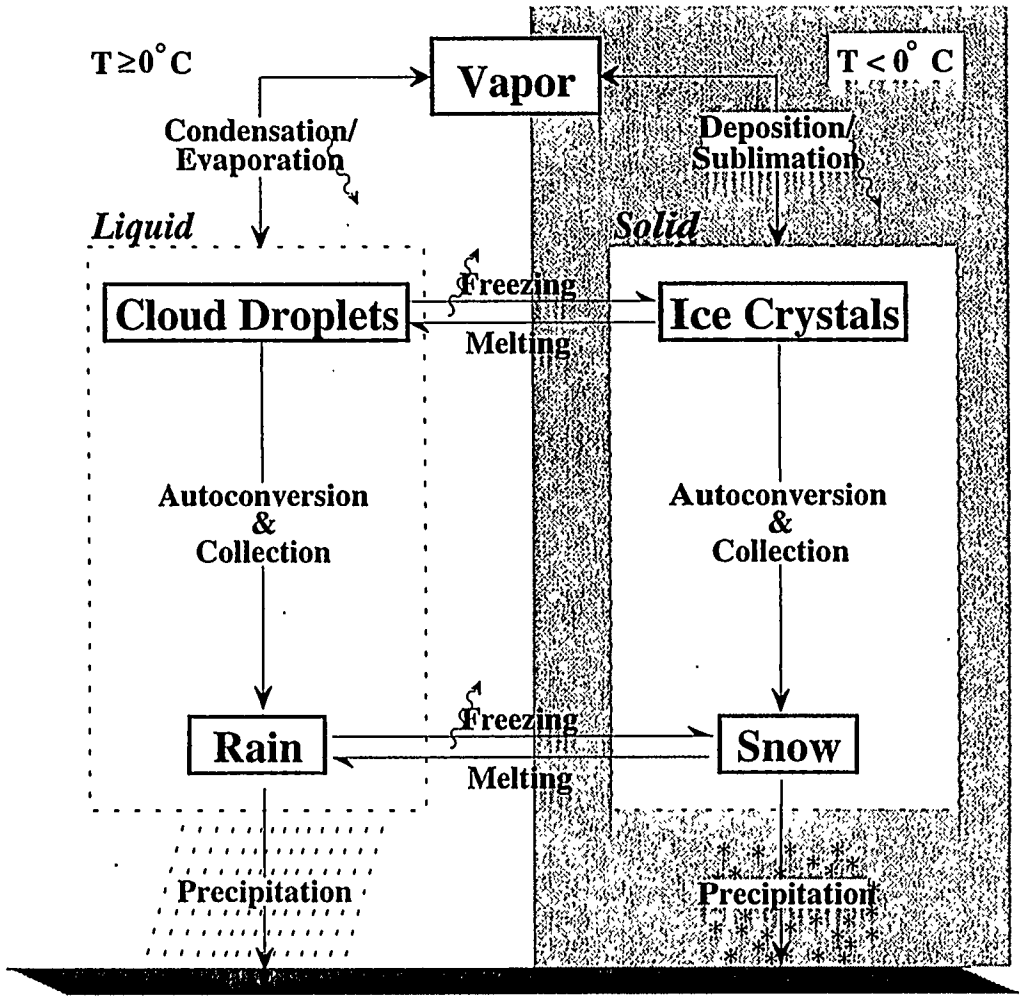

OMEGA Grid Element

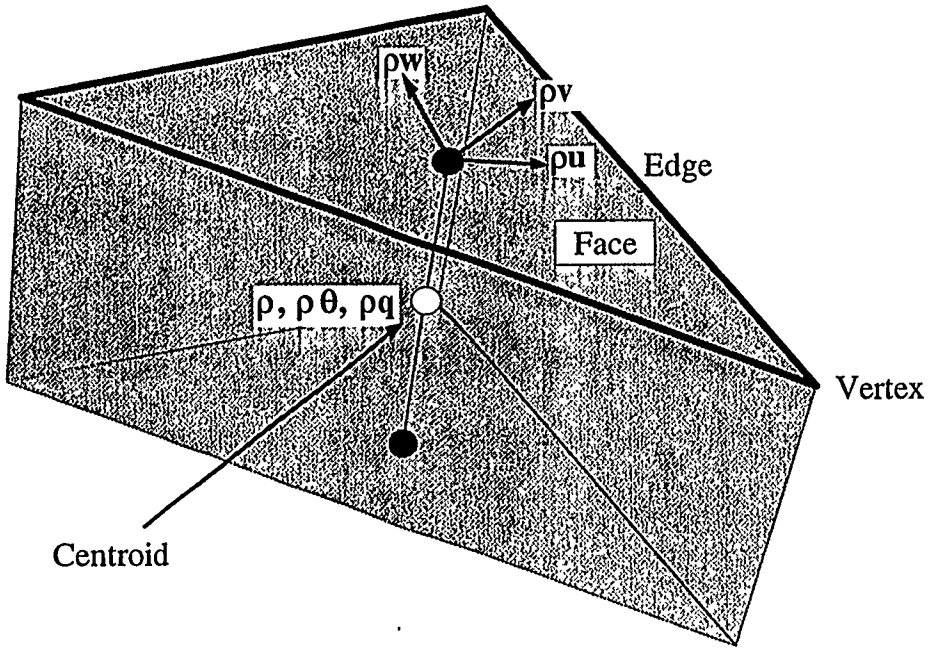

- **Triangles are Best Suited to Adapt to Surface and Atmospheric Features**
- **Triangular Prisms Most Closely Match Atmospheric Characteristics which are Highly Decorrelated in the Horizontal, but Correlated Vertically**

OMEGA Computational Domain

- Grid is unstructured in the horizontal.
- It is stuctured but non-uniform in the vertical.
- Each computational cell is a truncated triangular prism.
- Computations are done in a Cartesian reference frame with origin at the center of the Earth.

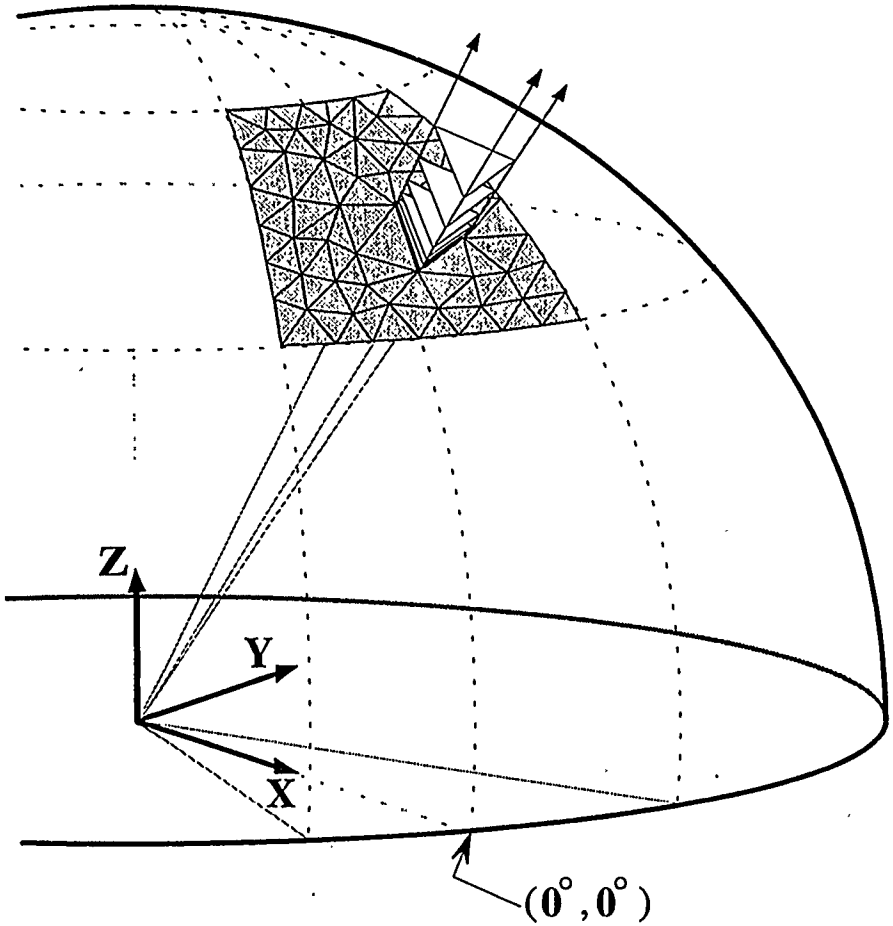

Vertex Addition and Reconnection

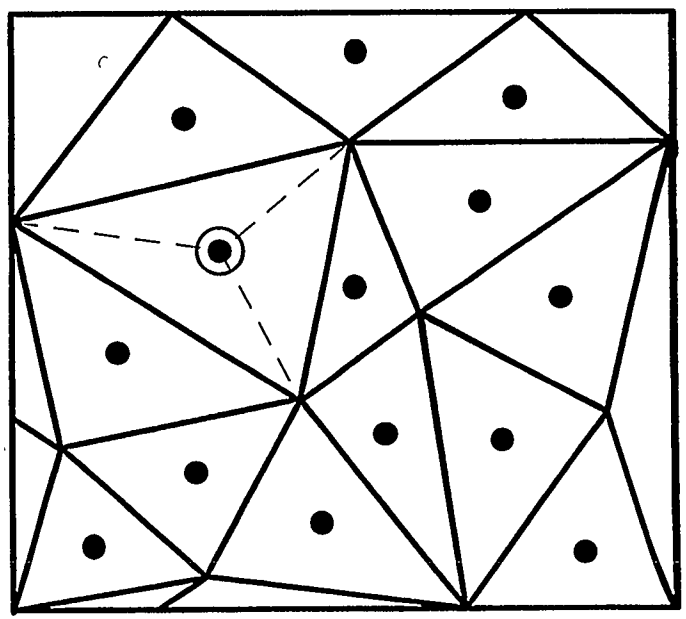

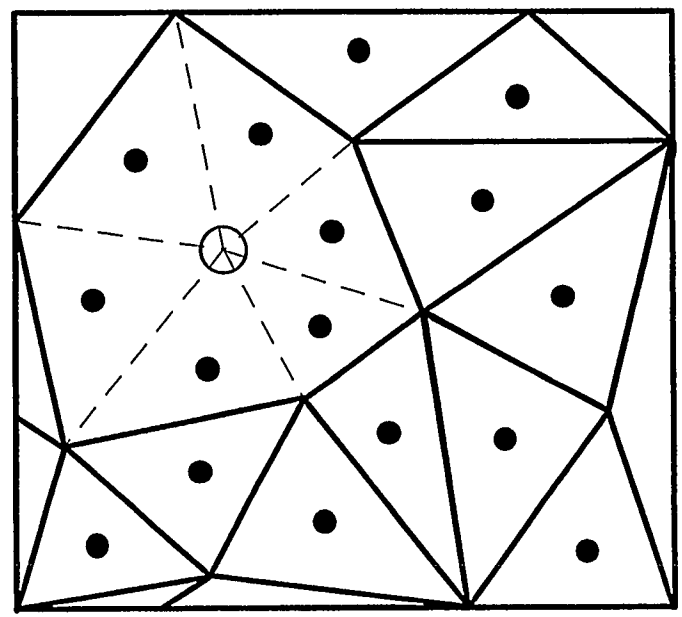

Vertex Deletion and Reconnection

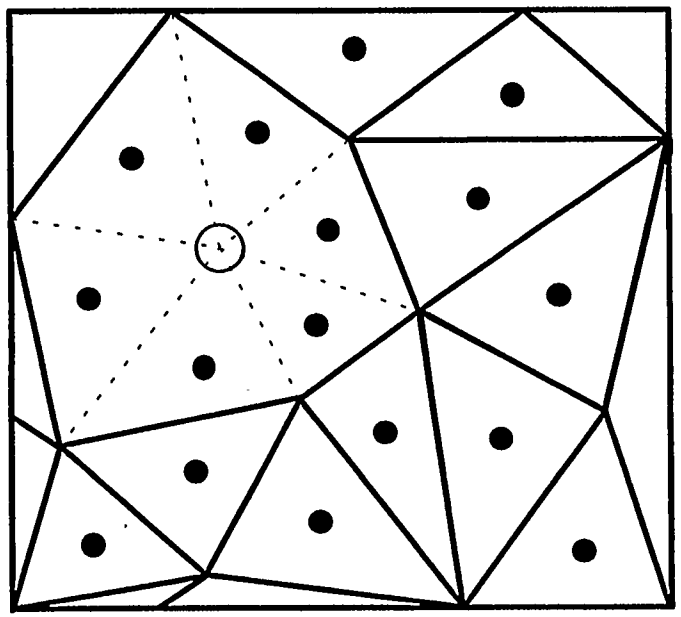

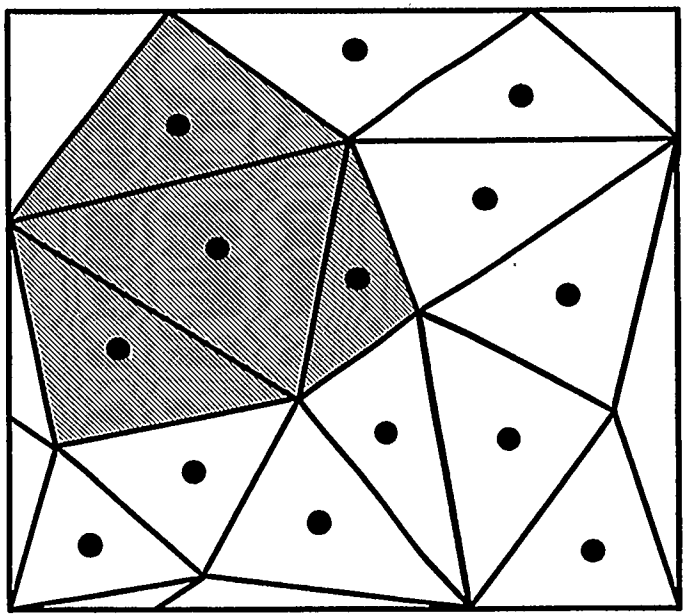

Grid Relaxation and Edge Bifurcation

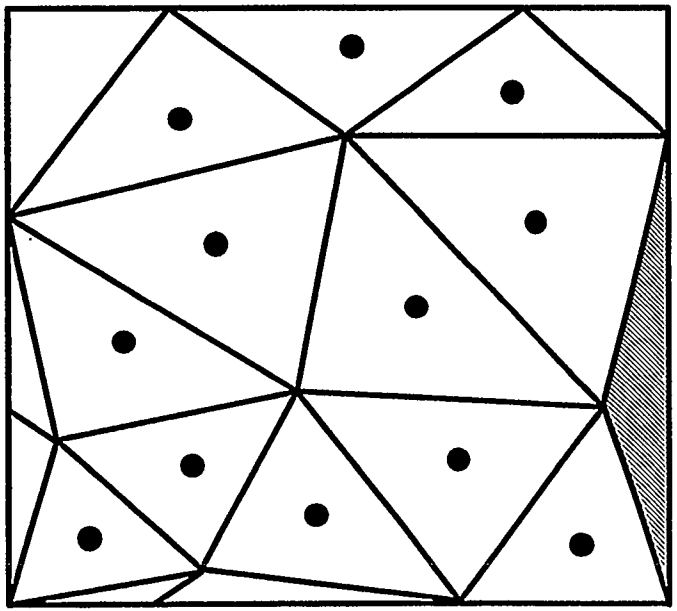

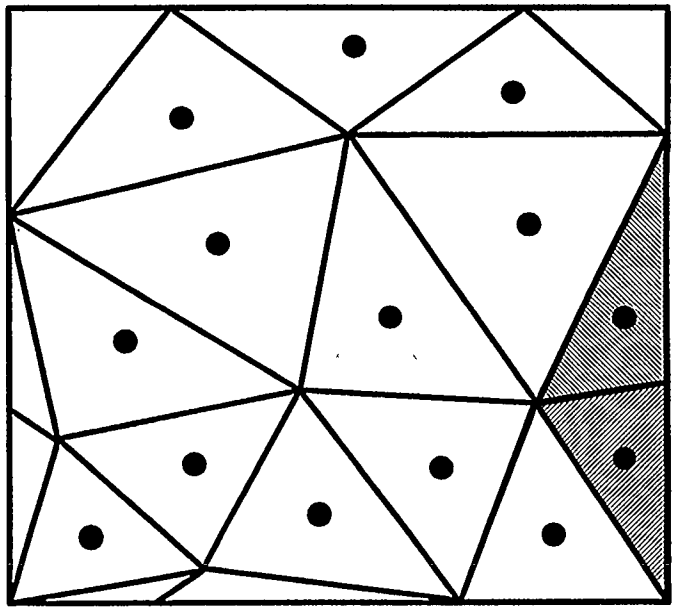

OMEGA Nor'easter Grid Adaptation

The OMEGA grid can adapt to virtually any criteria.

- Terrain. The grid is adapting to gradients in the elevation. This provides additional resolution in regions of complex terrain.
- Coastal or Land / Water Boundary. By establishing a dataset for which land is given an index of 1 and water an index of 0, adaptation to the land / water boundary can be accomplished by using the gradient of the index.
- Weather. Numerous weather variables are suitable as criteria for adaptation. In this example, the surface temperature (Frontal Boundary) was used to establish the criteria for grid adaptation.
- Composite. The Nor'easter of 1992. Setting all three adaptation criteria leads to this final grid which now has integrated the requirements to produce a grid with additional resolution for each criteria.
- NGM. The operational Nested Grid Model of the National Meteorological Center uses a regular 100 km grid. This captures the large scale structure and the upper level winds, but cannot resolve the important small-scale features, surface winds, or the details of the precipitation.

OMEGA Grid Generation
Adaptation to Topography

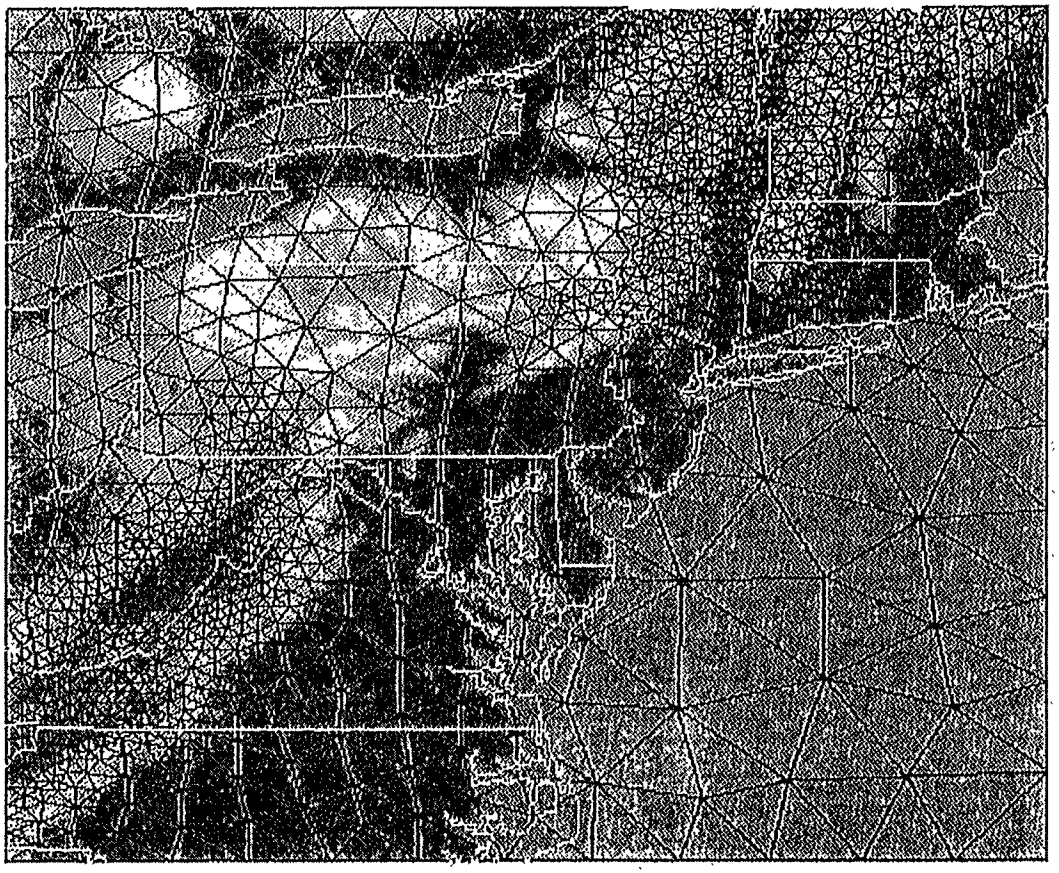

OMEGA Grid Generation
Adaptation to Land / Water Boundary

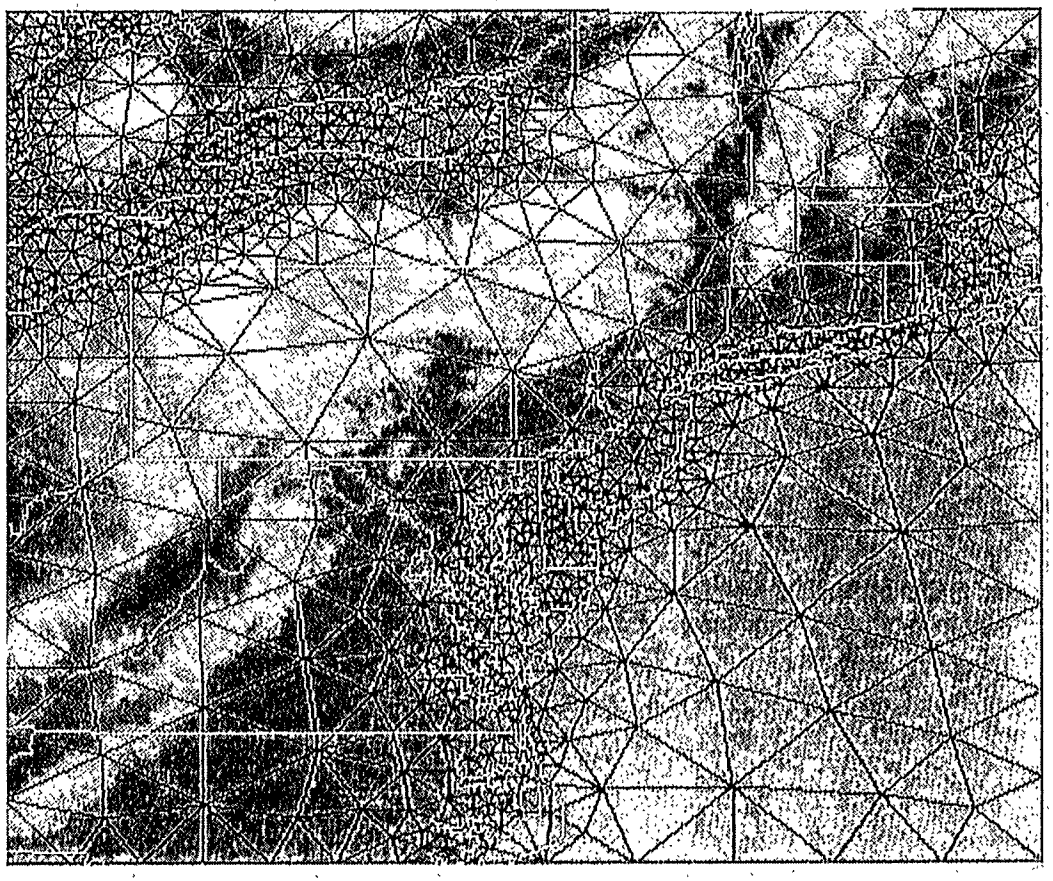

OMEGA Grid Generation
Adaptation to Existing Weather

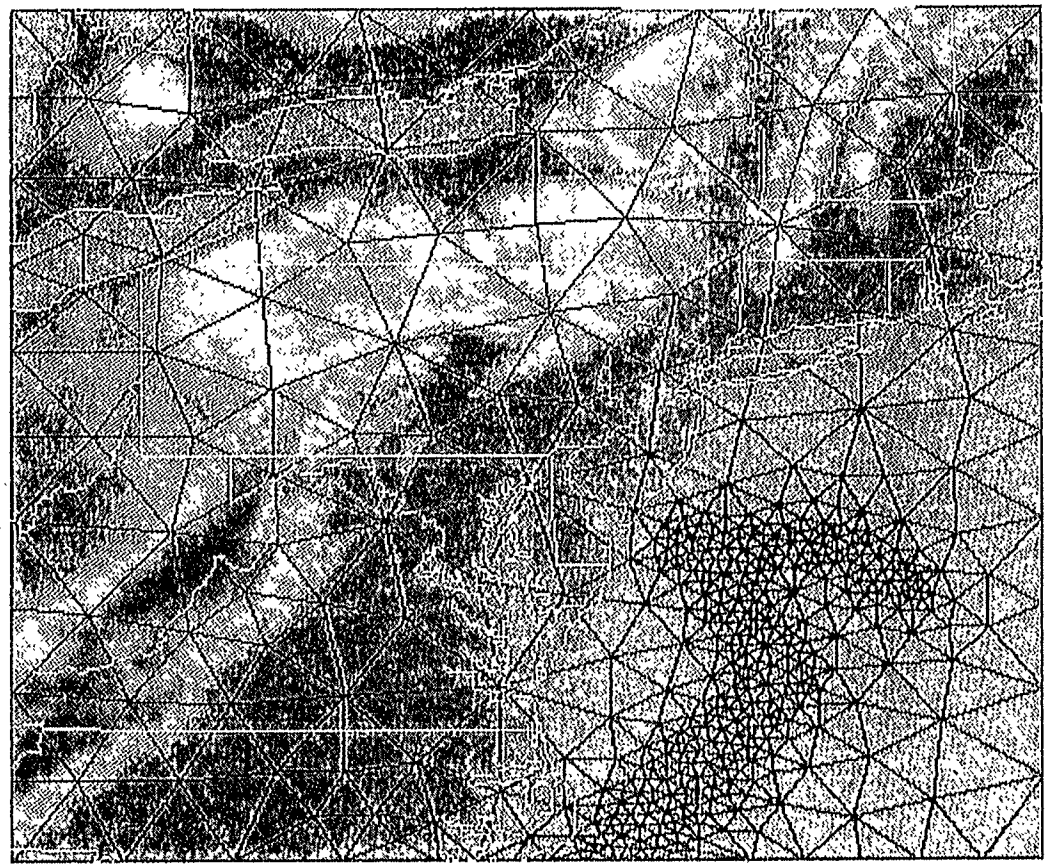

OMEGA Grid Generation
The Nor'Easter of 1992

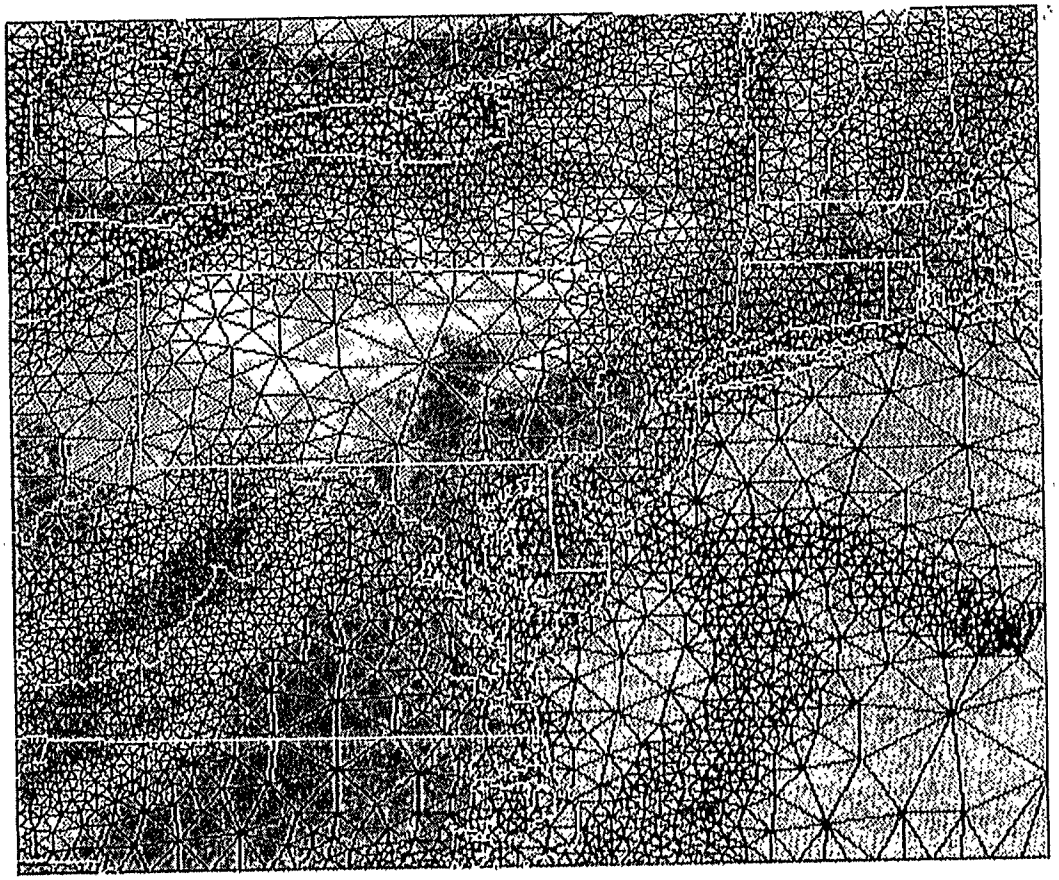

NGM Captures

- Large-Scale Structure
- Upper-Altitude Winds

NGM Misses

- Small-Scale Features
- Surface Winds
- Precipitation Details

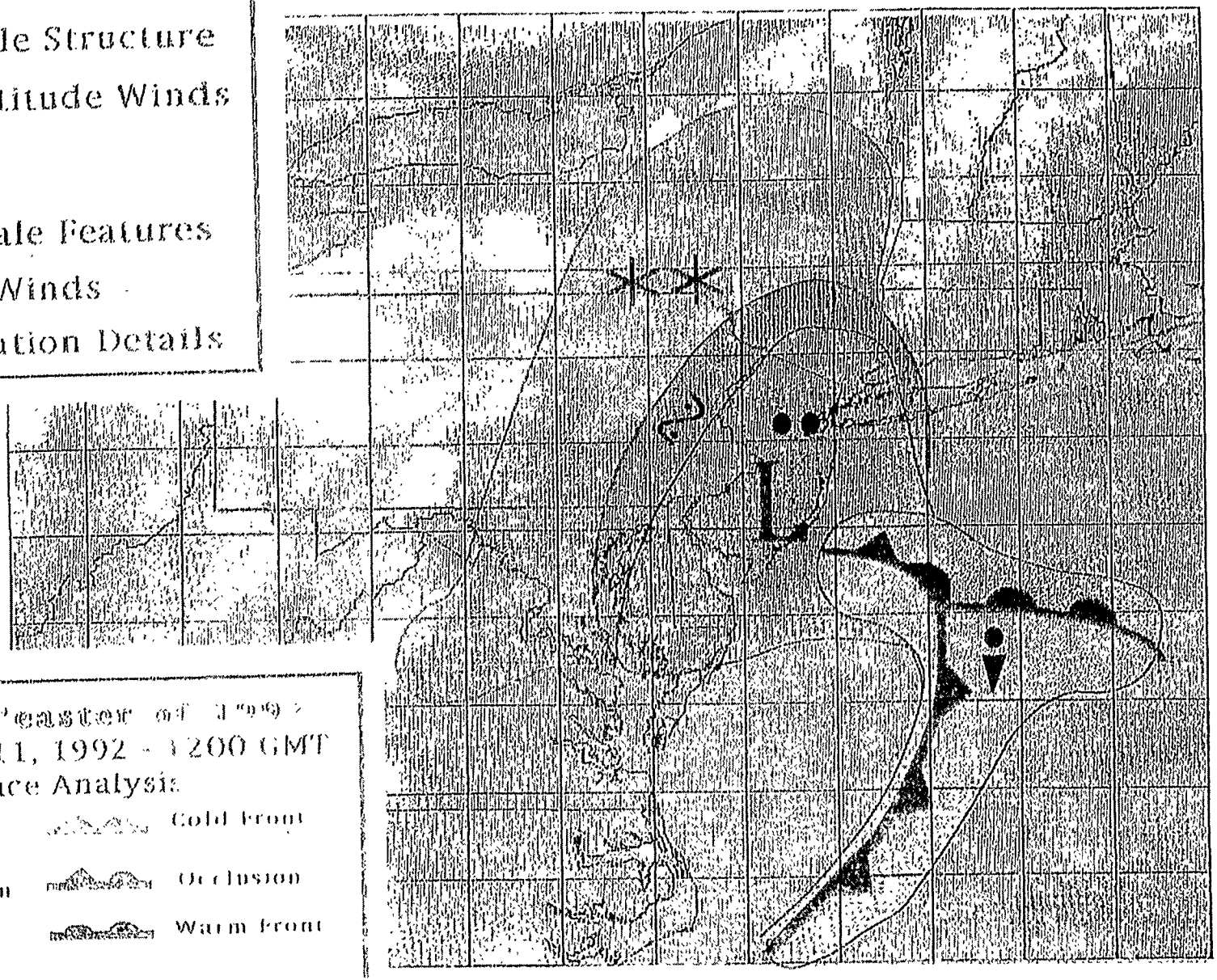

The Nor'easter of 1992
December 11, 1992 - 1200 GMT
Surface Analysis

Snow
Sleet
Freezing Rain
Rain
Showers
Cold Front
Occlusion
Warm Front

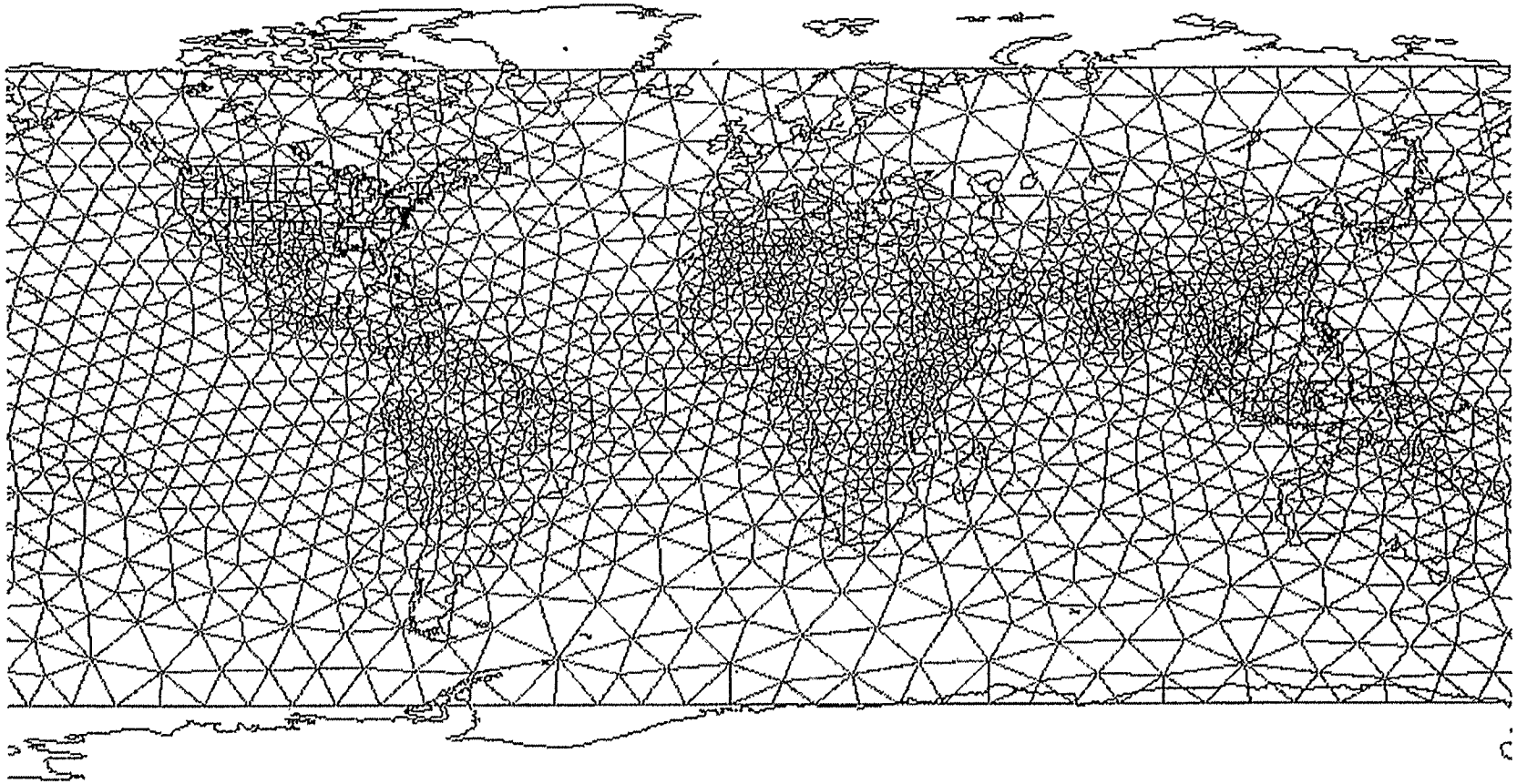

Out Year (1997+) Goal

<u>Ω (OMEGA)</u>

Operational on a TFLOP (Sustained) Class Machine with Gbit/s Communications

- **Memory Requirements**
  - **Hemispheric Coverage (100 km res)** — **3.25 Megacells (Mcells)**
  - **Regional (5000 x 2500 km; 10 km res)** — **12.5 Mcells**
  - **Convective Region (500 x 500 km; 1 km res)** — **25 Mcells**

TOTAL: 40,000,000 cells x Overhead of 100 Words/cell = 4 Gigawords

<u>ω (omega)</u>

OMEGA on a workstation (IBM R/S 6000)

Simulation of Transport in a Florida Sea Breeze using OMEGA

- Simulation Initialized at 7 am local time, Ends at 7 pm local
- Computational Domain: 600 x 700 km x 6.5 km
  - Horizontal Resolution: 4 - 20 km
  - Vertical Resolution: 20 - 1000 m
- Total Number of Computational Cells: ~ 90,000
  - Rectangular Grid with 4 km Resolution: ~ 600,000
- Climatological Uniform Wind assumed: 6 m/s SW
- No Microphysics
- Test of PBL and Clear Sky Radiative Transfer
- Both Eulerian and Lagrangian Transport Enabled
  - Continuous Releases at 3 sites

Florida Sea Breeze
Grid & Initial Wind

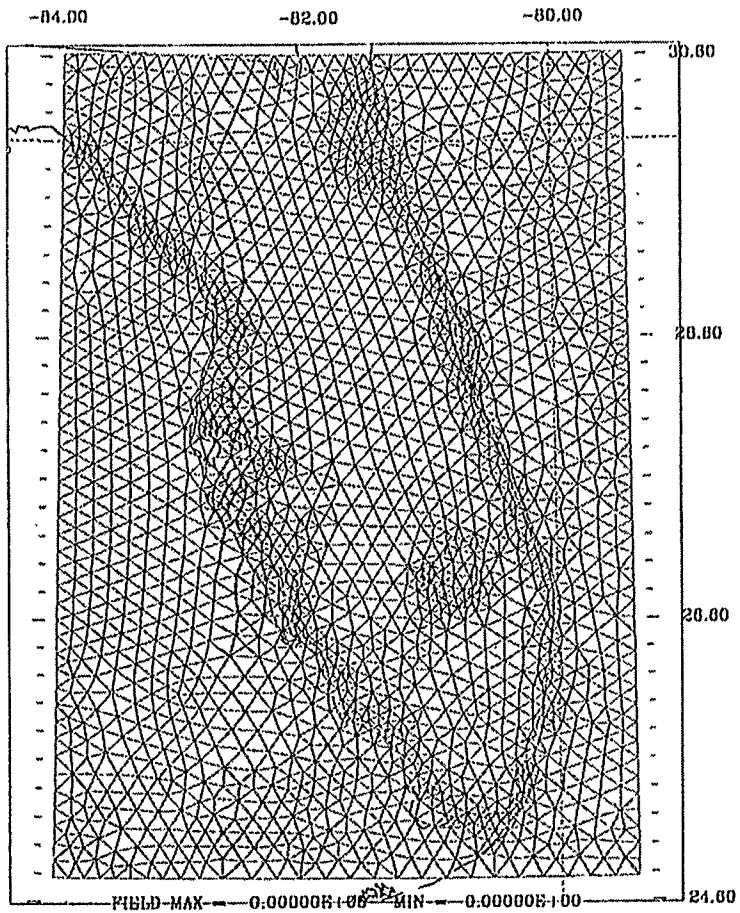

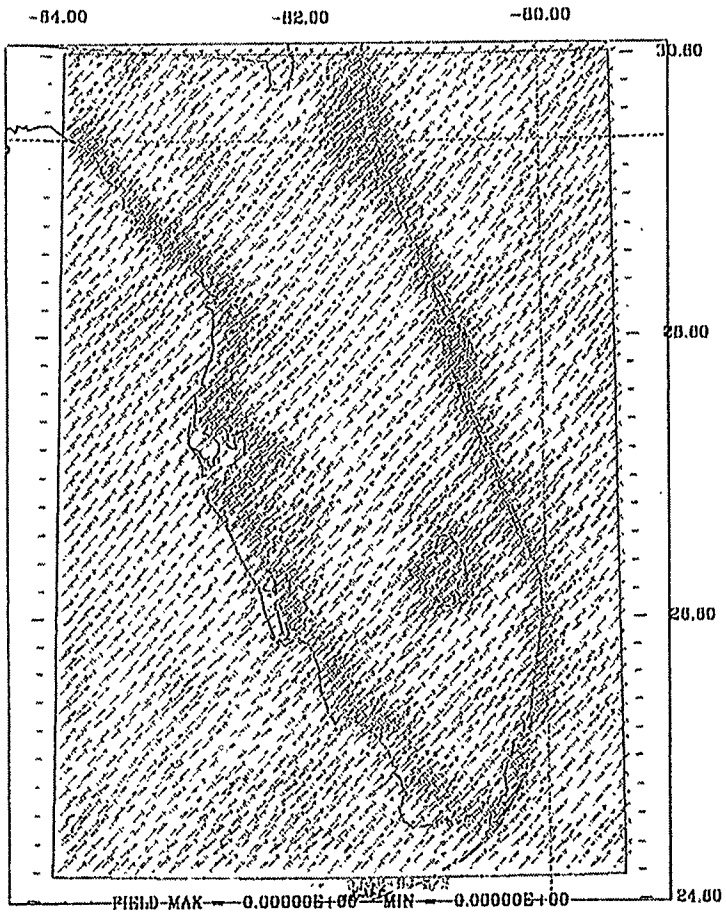

Florida Sea Breeze
10 am & 1 pm

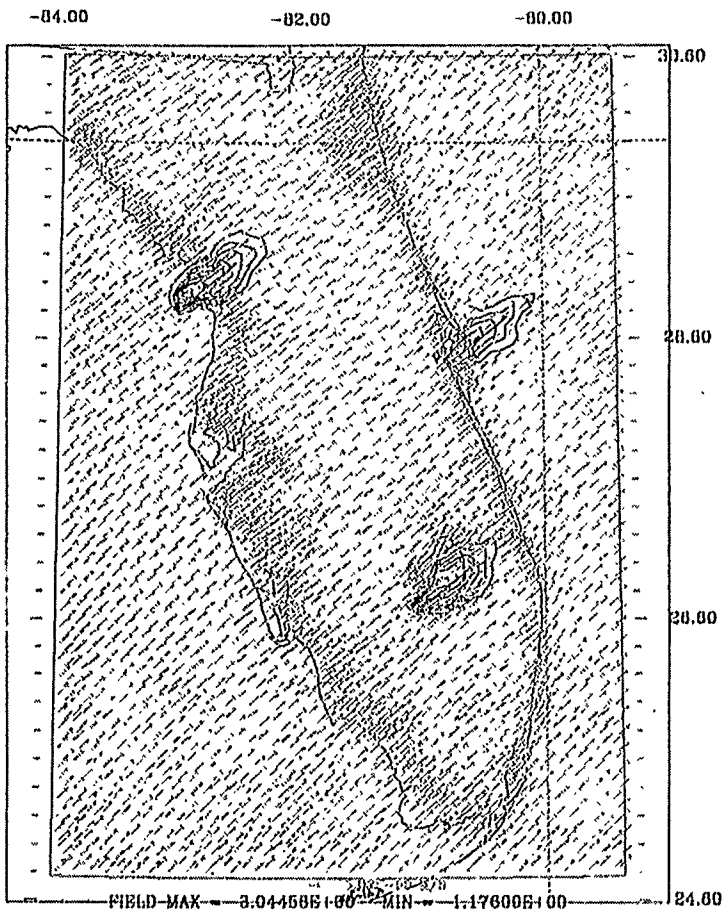

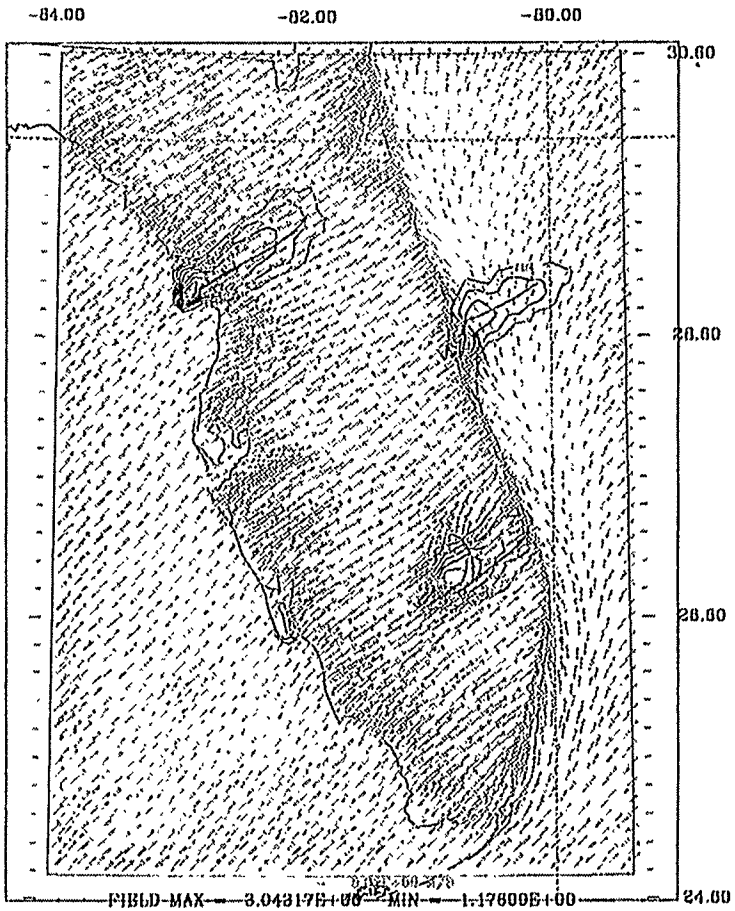

Florida Sea Breeze
4 pm & 7 pm

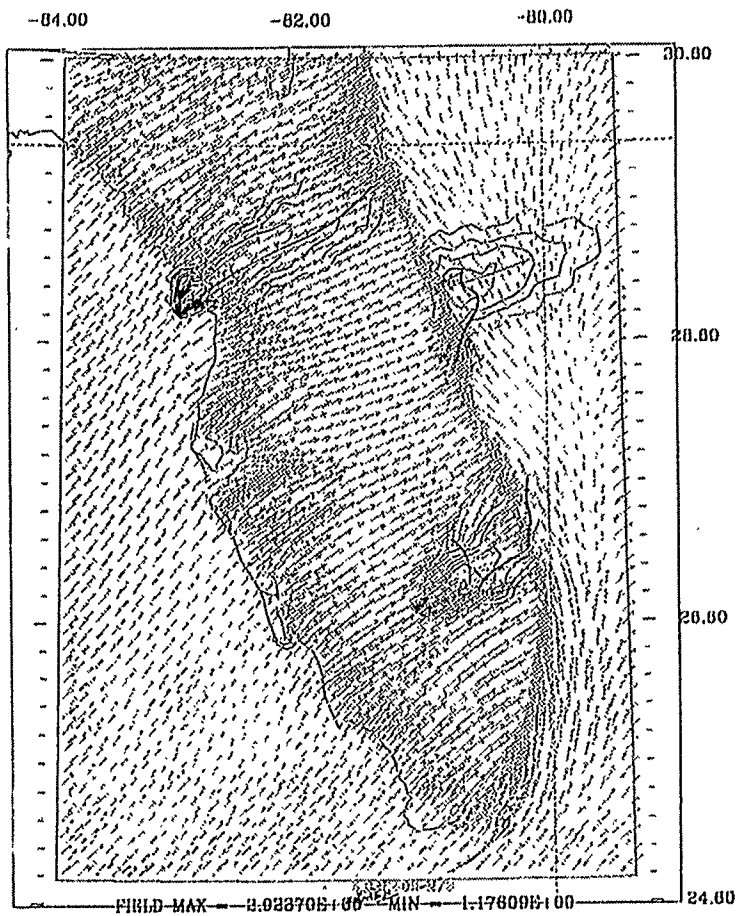

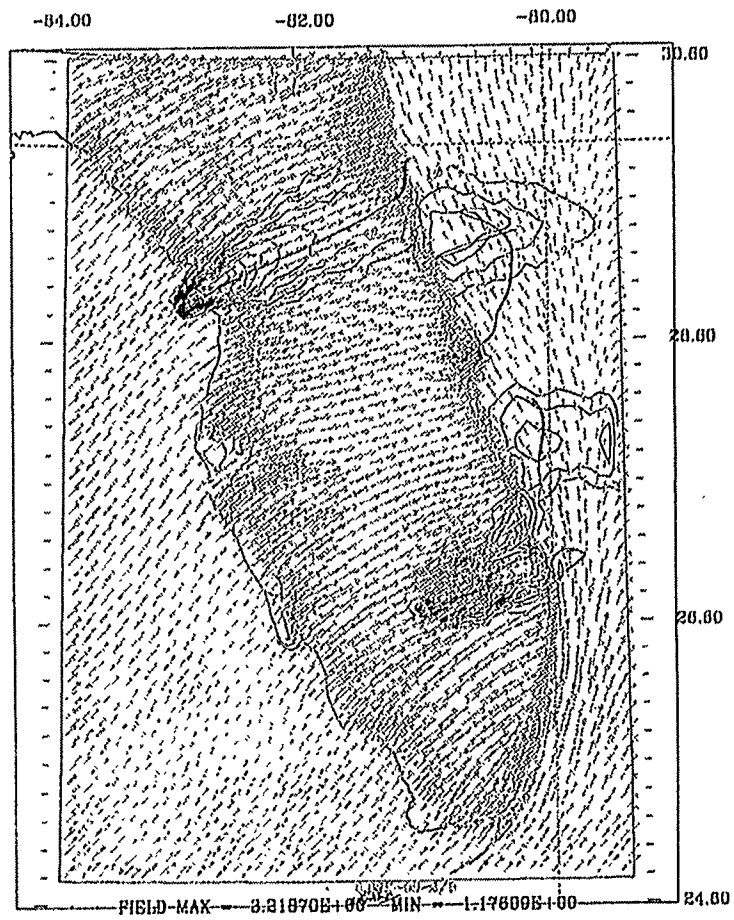

Simulation of Transport on Korean Peninsula

- Simulation Initialized at 8 am local time, Ends at 8 pm local
- Computational Domain: 600 x 700 km x 13 km
  - Horizontal Resolution: 5 - 50 km
  - Vertical Resolution: 20 - 1000 m
- Total Number of Computational Cells: ~ 44,000
  - Rectangular Grid with 5 km Resolution: ~ 440,000
- May 1994 Simulation
- Both Eulerian and Lagrangian Transport Enabled
  - Continuous Releases at 3 sites

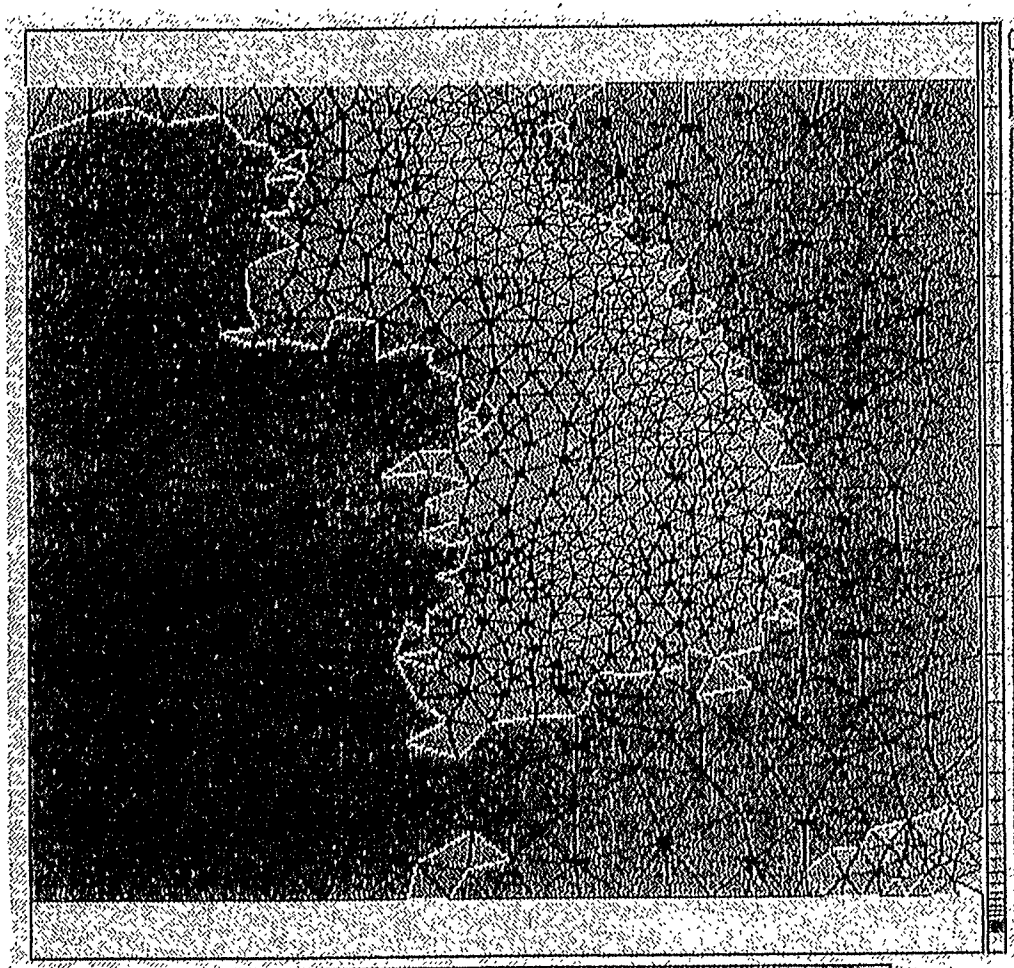

CELL #	LVL #	LAT/LON	TIME	ITER #
962	2	36,50	1	1

DOMAIN STATISTICS

# of cells: 1509; # of vertices: 799
# of edges: 2307; # of bndry edges: 87
# of levels: 29
Largest cell : 379, area = 2371.44 km^2
Smallest cell: 588, area = 29.41 km^2
Longest edge : 636, length = 85.46 km
belongs to cell : 407
Shortest edge: 243, length = 6.82 km
belongs to cell 588
Best cell : 92, Asp. ratio = 0.991
Worst cell: 796, Asp. ratio = 0.327

0.000e+00 | Terrain | 1.045e+03

Grid-F | Grid | Data-F | Redraw | ZOOM | VEL | ATDM | STAT | FIELD | LAYER | LATSCT | LONSCT | SKEWT | QUIT

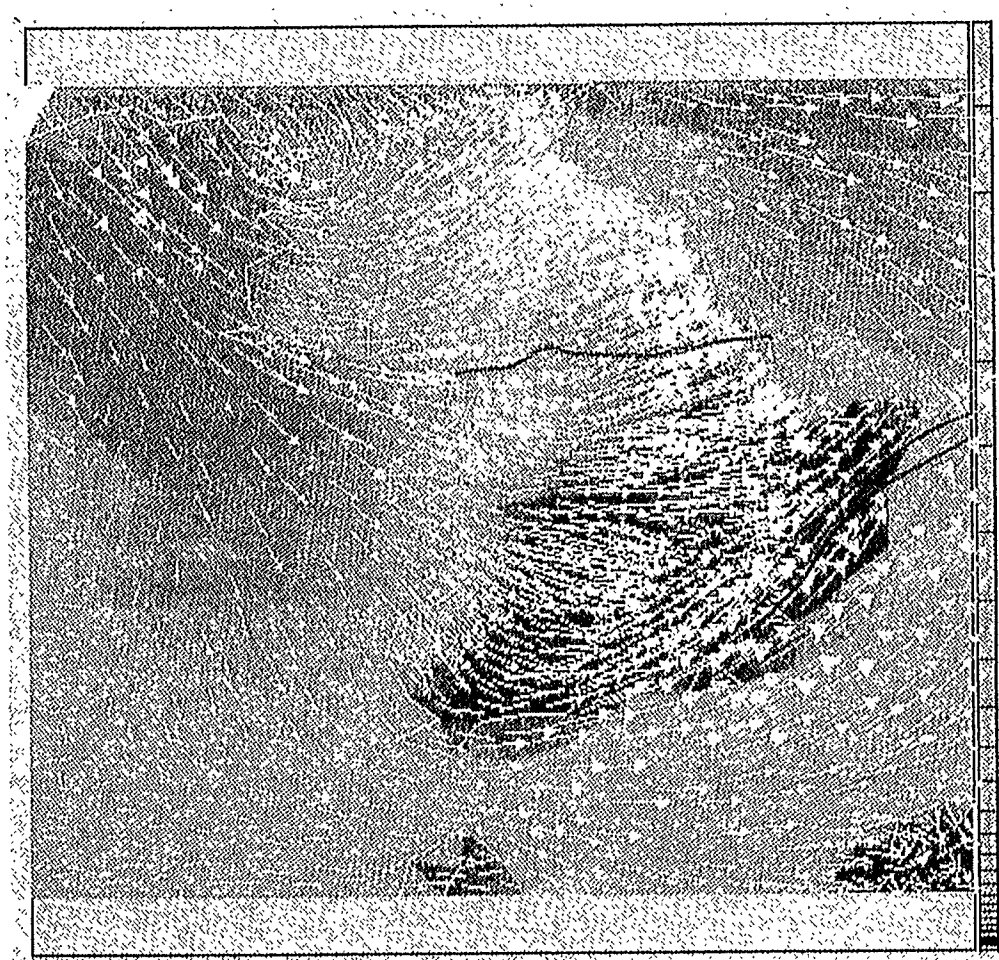

CELL #	LVL #	LAT/LON	TIME	ITER #
1251	4	36.50	09:08:18.73	2280

Location: (39.844, 123.090)
Vertices: 390, 225, 226
Edges: 2237, 616, -1650
Edge Lengths: 22.952, 51.867, 56.750 (km)
Avg Altitude: 174.330 (m)
Cell Area: 595.23 (km^2)

Pres0 : 982.568 mb; Rho0: 1.202e+00 kg/m^3
Pr Pert: 9.486 mb; Rho : 1.207e+00 kg/m^3
Press : 992.054 mb; Theta: 287.153 K
Temp : 286.499 ; Dew Pt : 267.679 C
X-vel: -4.732e+00 ; U-vel: 3.521e+00 m/s
Y-vel: 8.120e-01 ; V-vel: -5.131e+00 m/s
Z-vel: -3.959e+00 ; W-vel: -3.072e-02 m/s
K-M : 1.803e+01 ; K-H : 4.599e+01 m^2/s
Drop : 0.000e+00 ; ICE : 0.000e+00 kg/kg
Rain : 0.000e+00 ; SNOW: 0.000e+00 kg/kg
Vapor: 3.071e-03 kg/kg; SRATIO: 0.000e+00
Utrc1: 0.000e+00 ; Utrc2: 0.000e+00 kg/kg
Utrc3: 0.000e+00 kg/kg

2.850e+02 | Theta | 2.950e+02

Grid-F | Grid | Data-F | Redraw | ZOOM | VEL | ATDM | STAT | FIELD | LAYER | LATSCT | LONSCT | SKEWT | QUIT

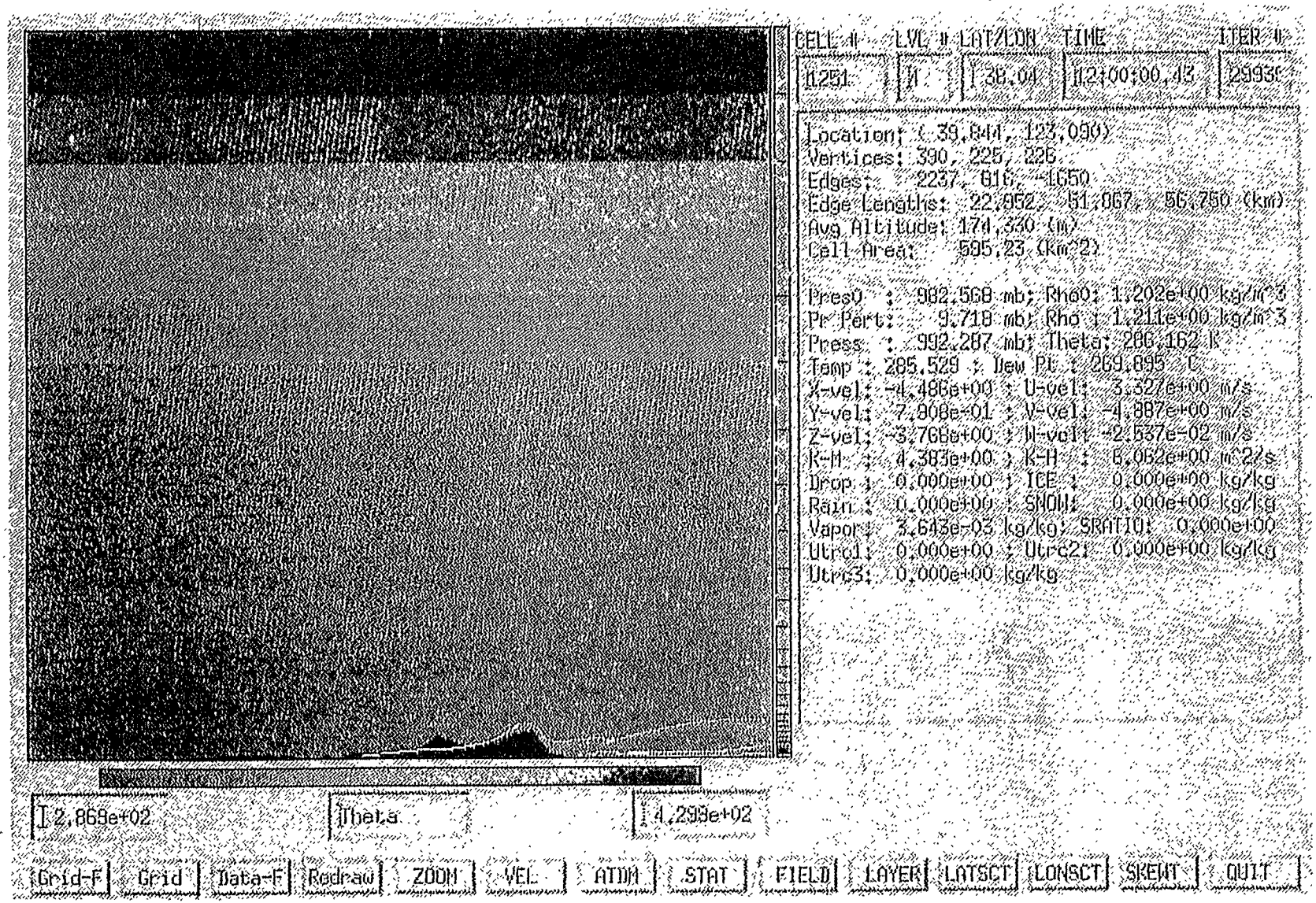
CELL # LVL # LAT/LON TIME ITER #
1251 1 38.04 12:00:00.43 29939
Location: (39.844, 123.090)
Vertices: 390, 225, 226
Edges: 2237, 616, -1650
Edge Lengths: 22.052, 51.067, 56.750 (km)
Avg Altitude: 174.330 (m)
Cell Area: 595.23 (km^2)
Pres0 : 982.568 mb; Rho0: 1.202e+00 kg/m^3
Pr Pert: 9.718 mb; Rho : 1.211e+00 kg/m^3
Press : 992.287 mb; Theta: 286.162 K
Temp : 285.529 ; Dew Pt : 269.895 C
X-vel: -4.486e+00 ; U-vel: 3.327e+00 m/s
Y-vel: 7.808e-01 ; V-vel: -4.887e+00 m/s
Z-vel: -3.768e+00 ; W-vel: -2.537e-02 m/s
K-M : 4.383e+00 ; K-H : 6.062e+00 m^2/s
Drop : 0.000e+00 ; ICE : 0.000e+00 kg/kg
Rain : 0.000e+00 ; SNOW: 0.000e+00 kg/kg
Vapor : 3.643e-03 kg/kg; SRATIO: 0.000e+00
Utrc1: 0.000e+00 ; Utrc2: 0.000e+00 kg/kg
Utrc3: 0.000e+00 kg/kg
I 2.869e+02
Theta
I 4.299e+02
Grid-F
Grid
Data-F
Redraw
ZOOM
VEL
ATDM
STAT
FIELD
LAYER
LATSCT
LONSCT
SKEWT
QUIT

Southern India – Grid and Terrain

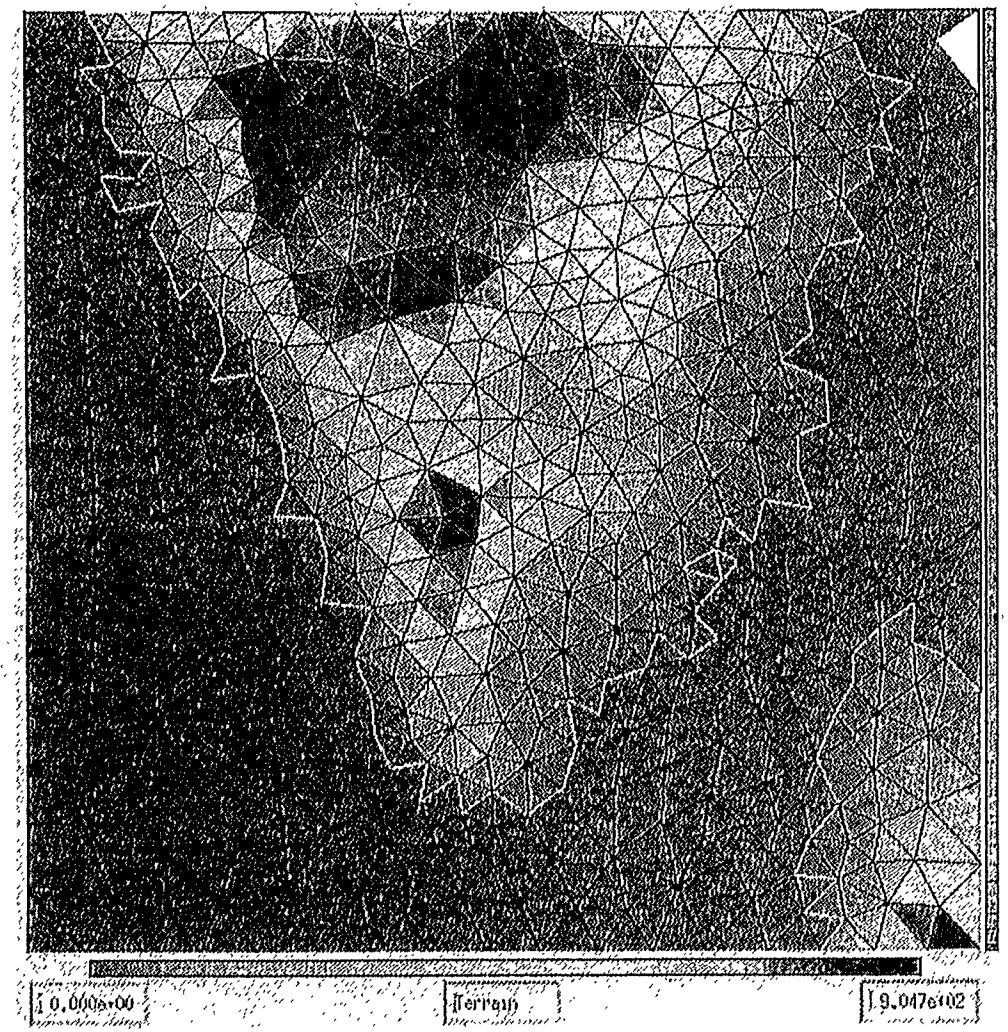

- No. of triangles: 950
- No. of layers: 26
- Initialization time: 1 Nov 94, 00Z
- Simulation period: 12 hours

Southern India –Winds at 50 m AGL at 00Z

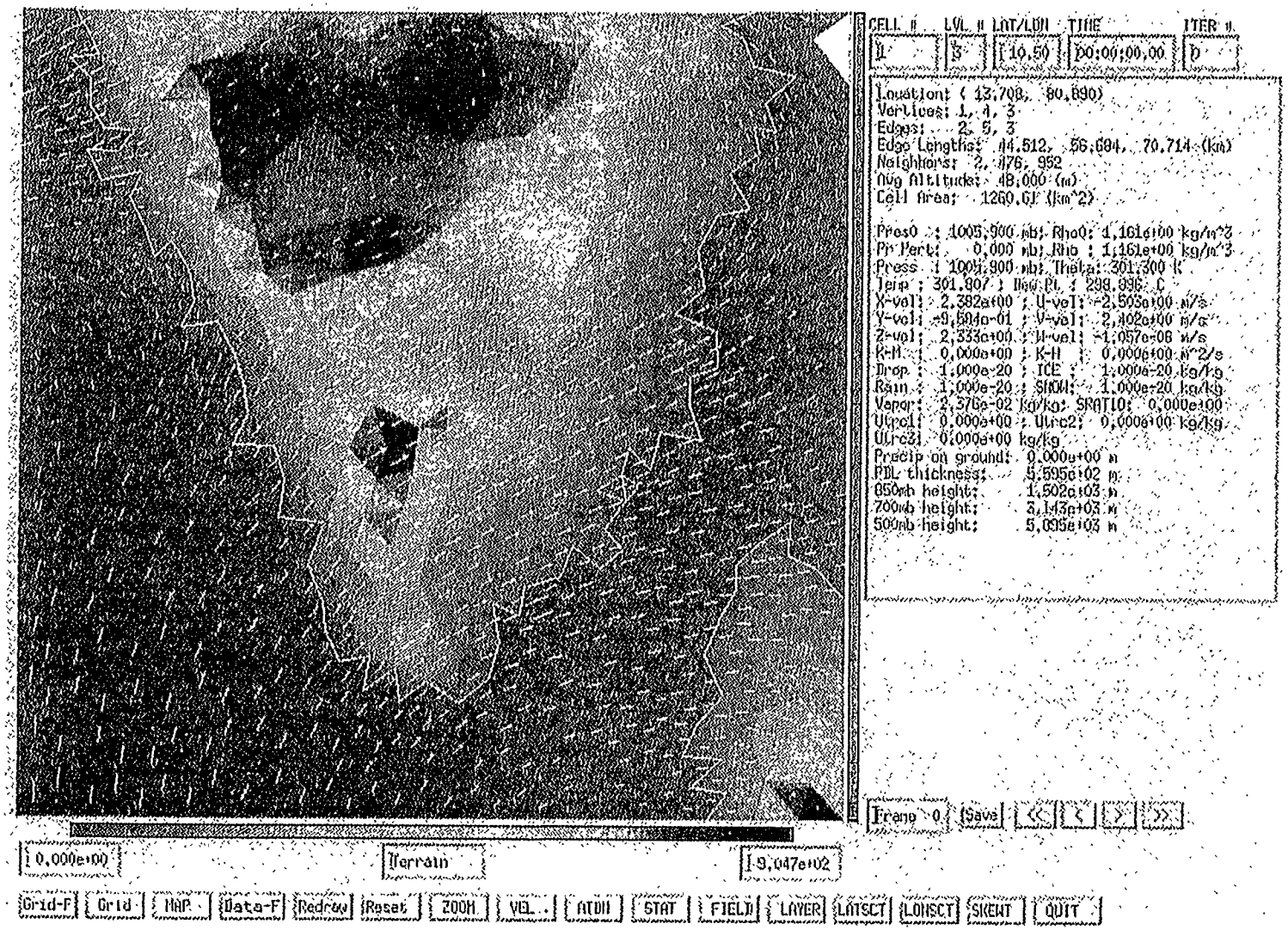

Computational Physics Division

SAIC © An Employee-Owned Company
Science Applications International Corporation

Southern India – Winds at 50 m AGL at 06Z

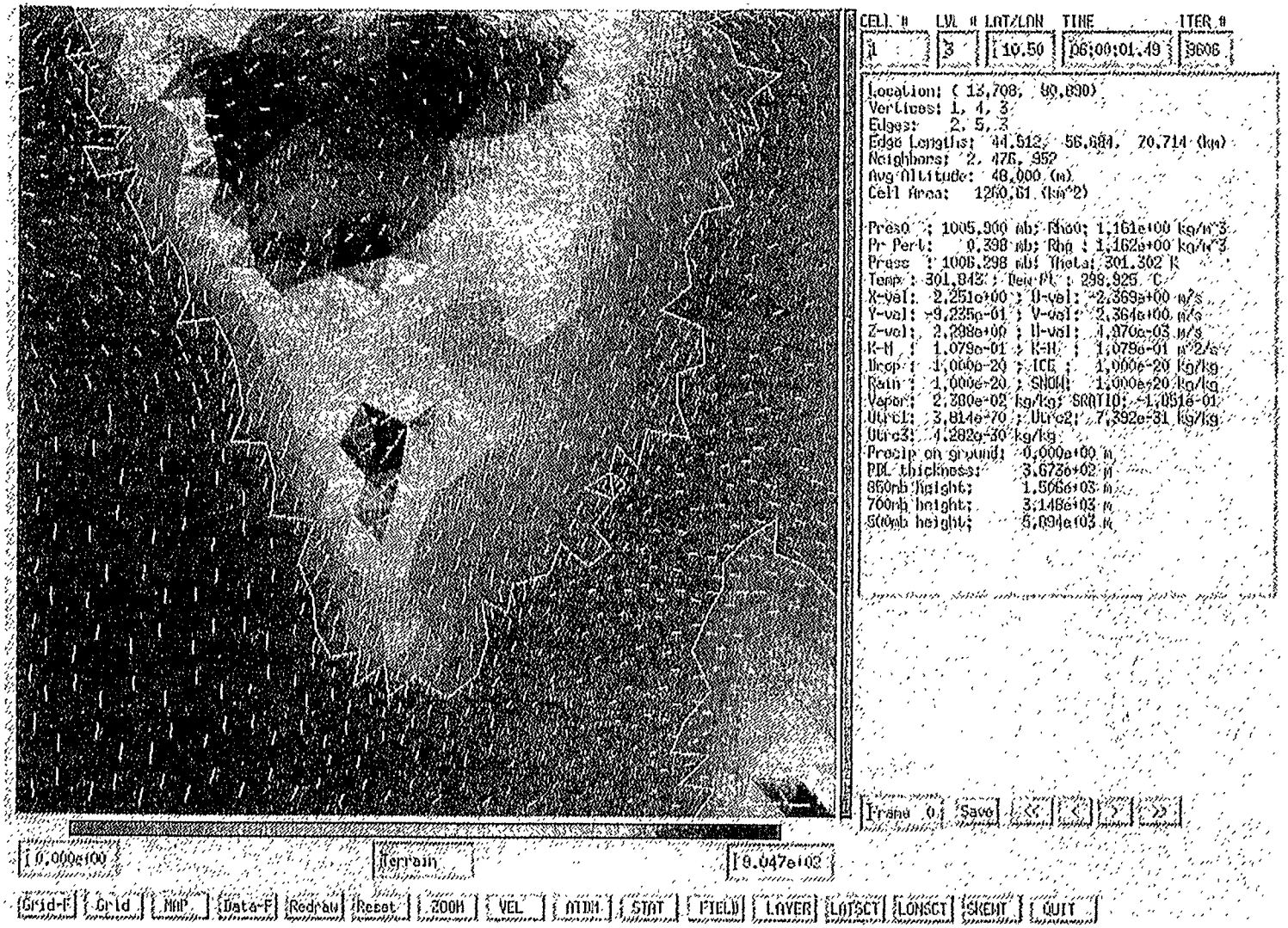

Computational Physics Division

SAIC® An Employee-Owned Company

Science Applications International Corporation

Southern India – Tracer fields at 12 Z

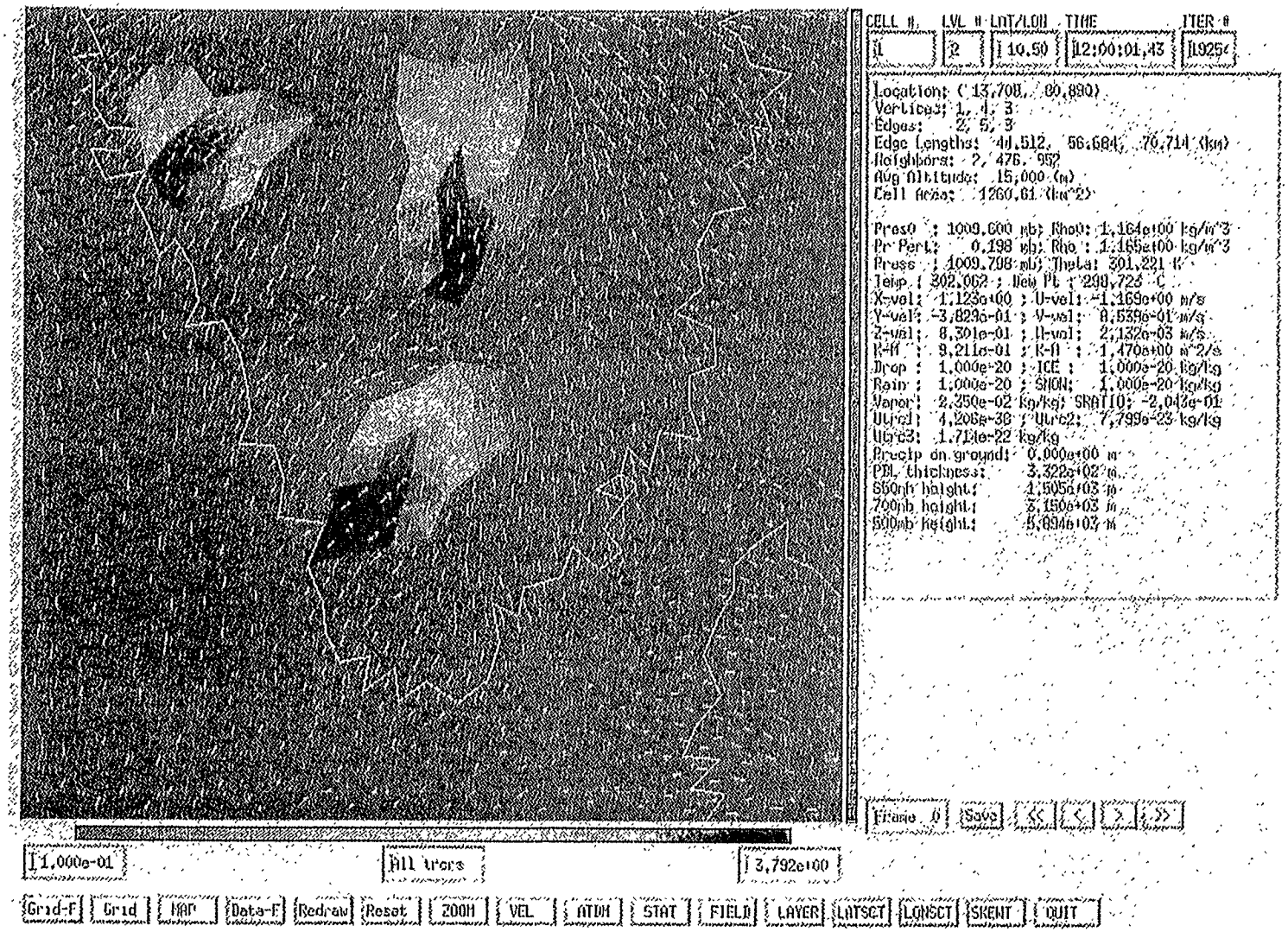

Computational Physics Division

SAIC © An Employee-Owned Company

Science Applications International Corporation

Malaysia – Grid and Winds

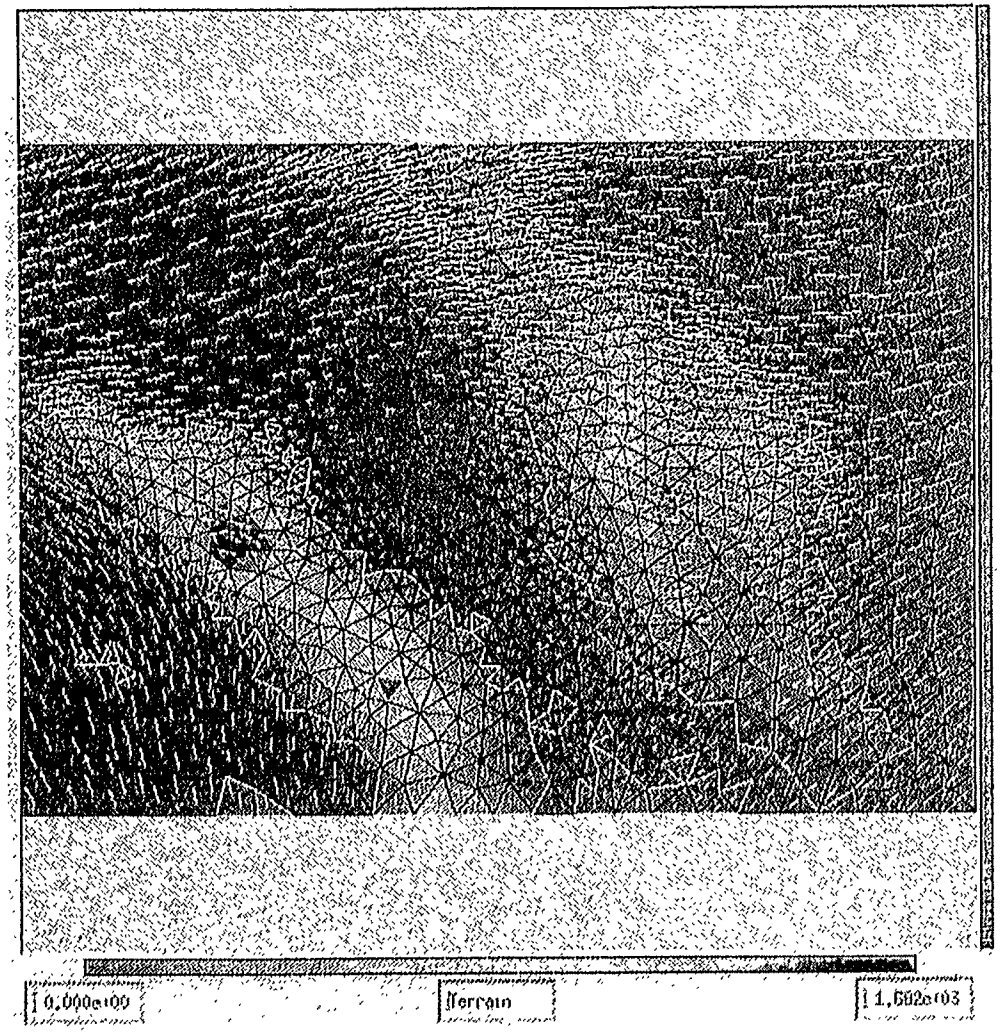

- No. of triangles: 950
- No. of layers: 26
- Initialization time: 1 Nov 94, 00Z

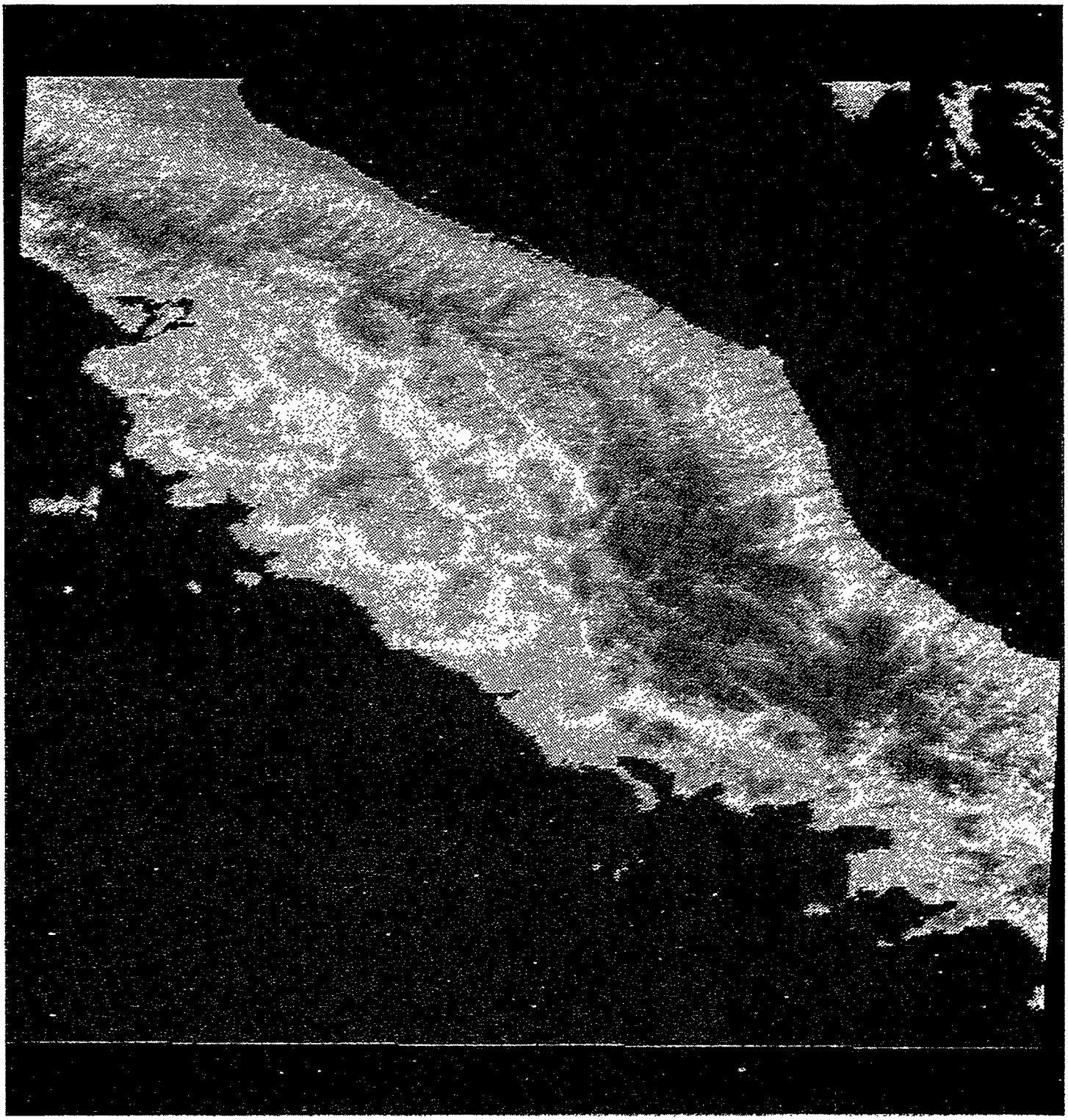

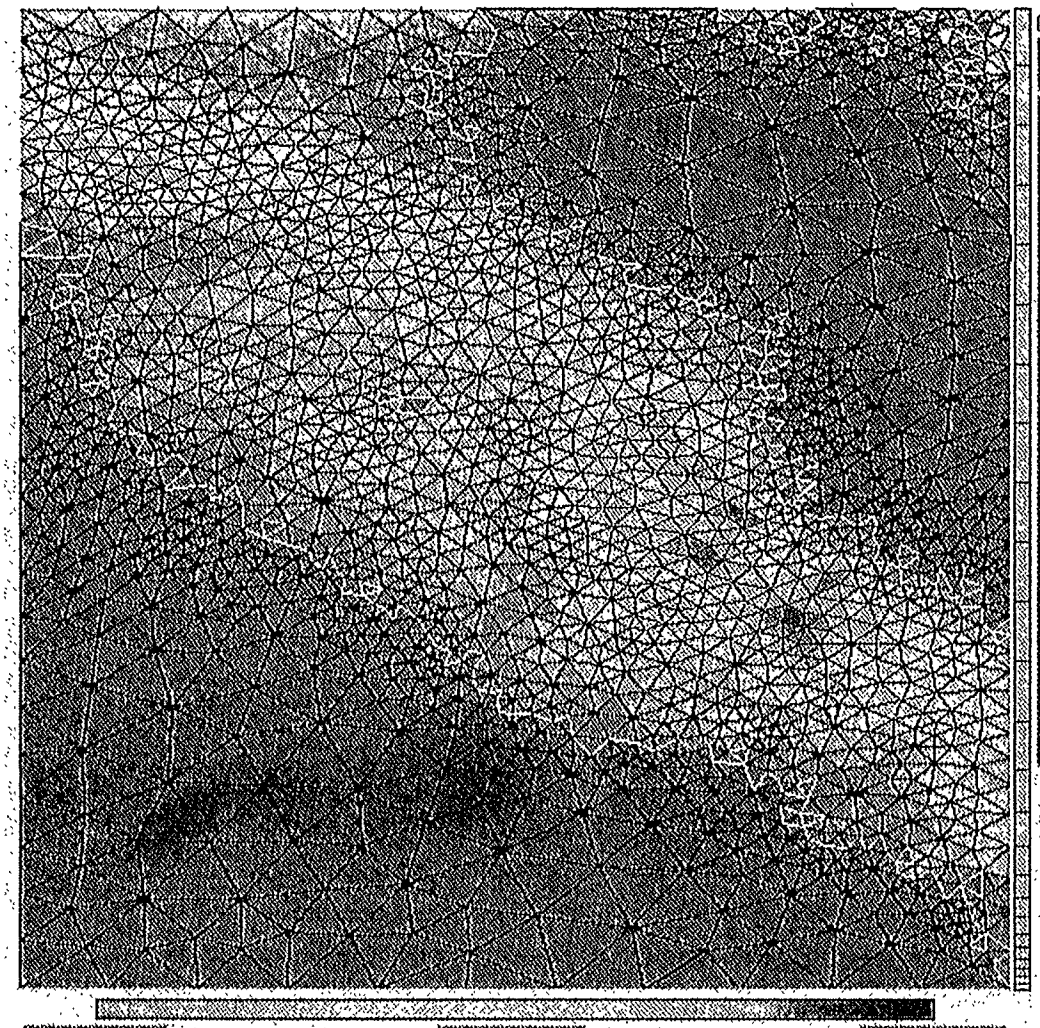

CELL #	LVL #	LAT/LON	TIME	ITER #
856	2	42,50	1	1

DOMAIN STATISTICS

```
# of cells:   3275; # of vertices:      1689
# of edges:   4963; # of bndry edges:    101
# of levels; 26
Largest cell :   444, area =    826.66 km^2
Smallest cell;  1582, area =     11.24 km^2
Longest edge :   171, length =   48.09 km
   belongs to cell   103
Shortest edge;  4639, length =    4.06 km
   belongs to cell  1582
Best cell :  1660, Asp. ratio = 0.997
Worst cell;  1914, Asp. ratio = 0.278
```

0.000e+00 | Terrain | 1.820e+03

Grid-F | Grid | MAP | Data-F | Redraw | ZOOM | VEL | ATDM | CHEMB | STAT | FIELD | LAYER | LATSCT | LONSCT | SKEWT | QUIT

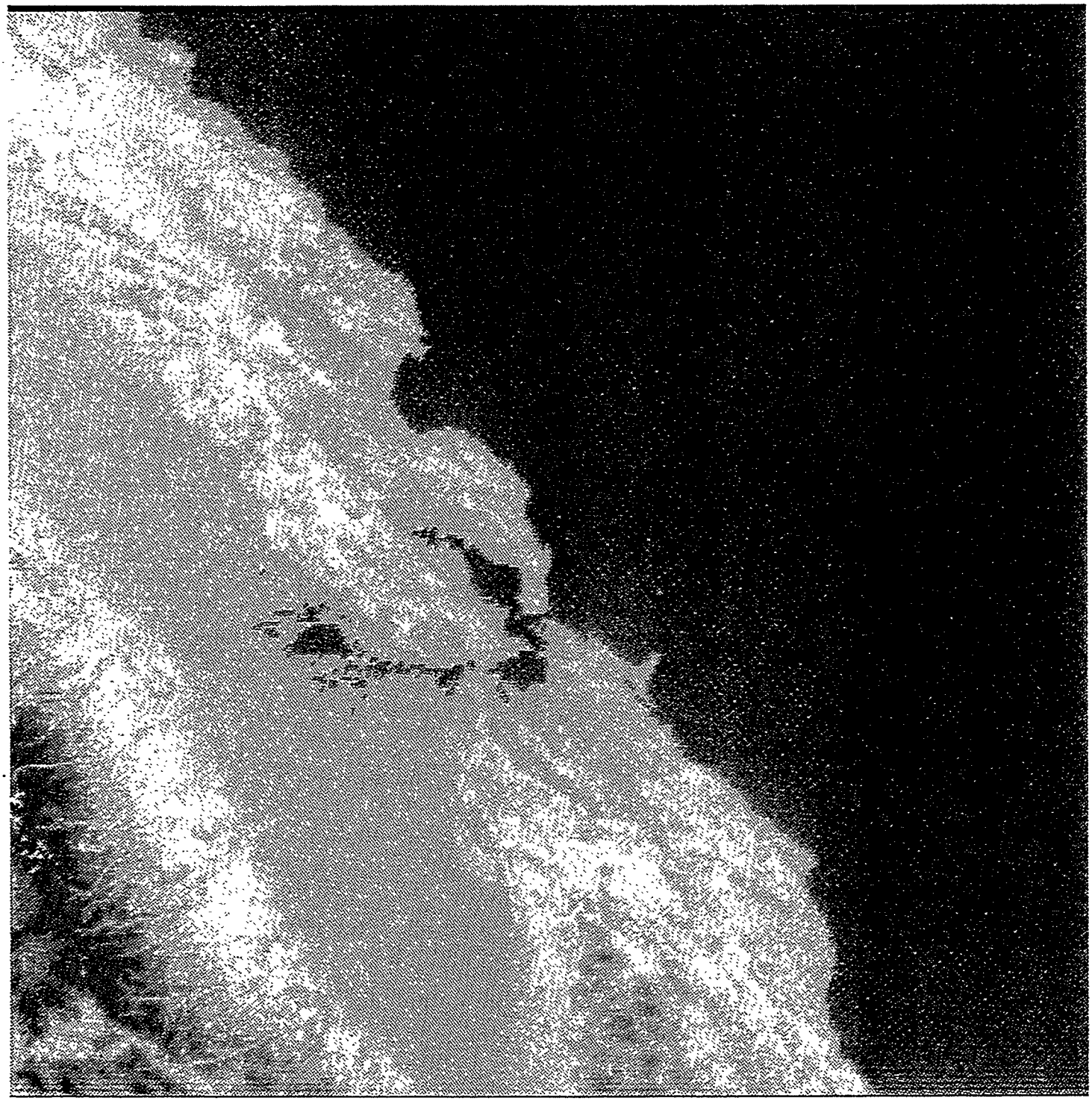

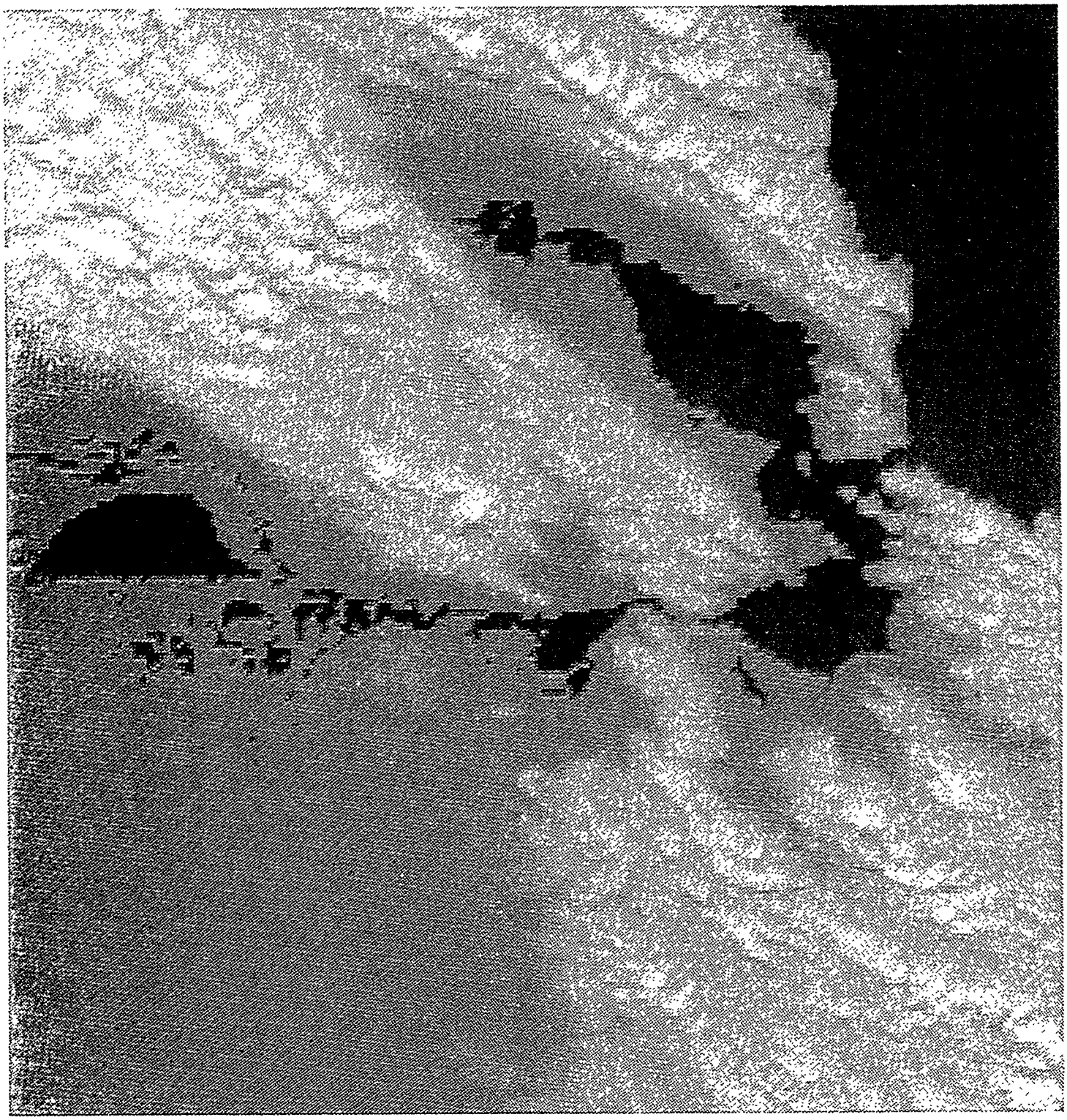

Southern India – Winds at 50 m AGL at 12Z

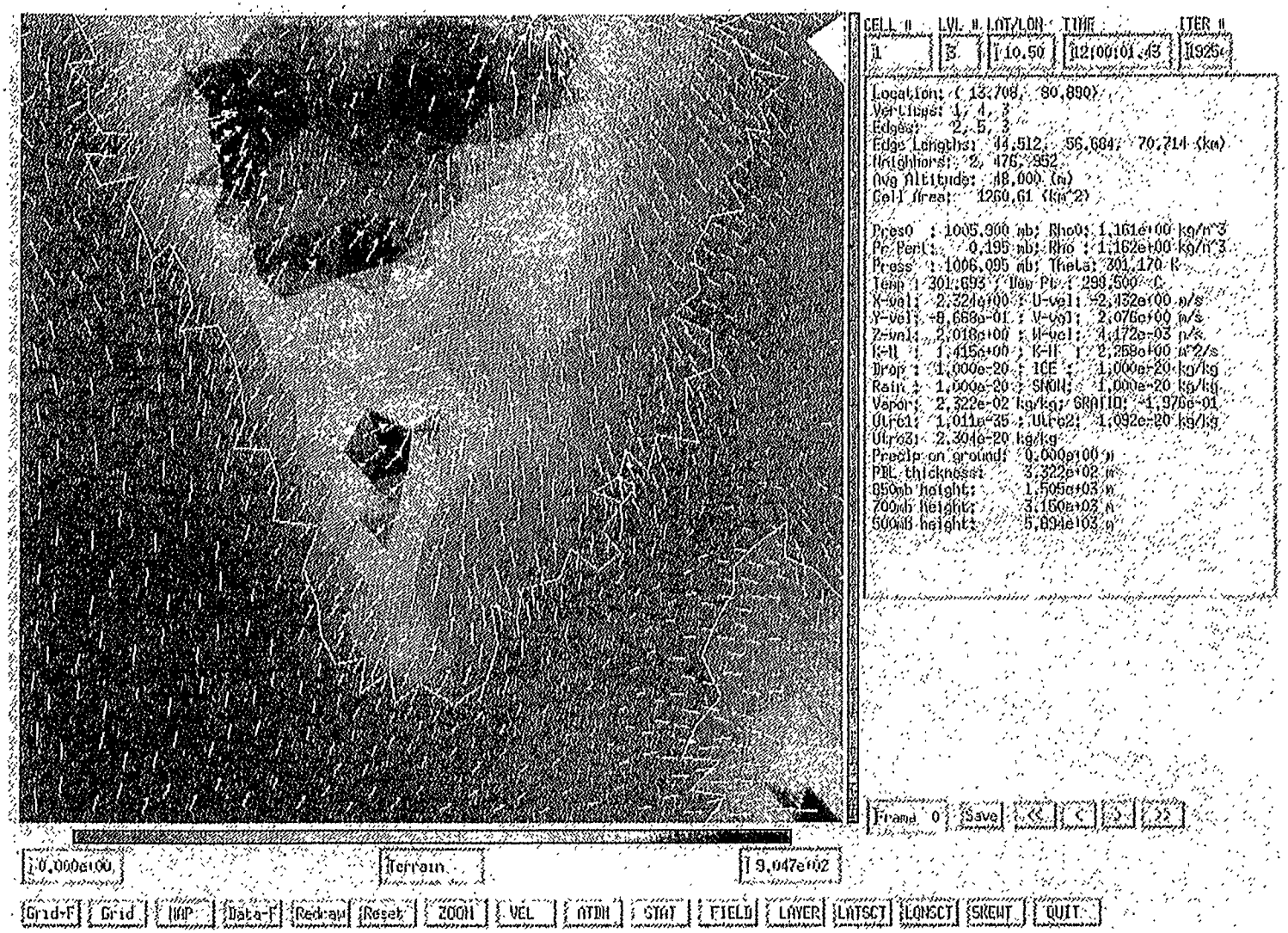

Computational Physics Division

SAIC® An Employee-Owned Company
Science Applications International Corporation

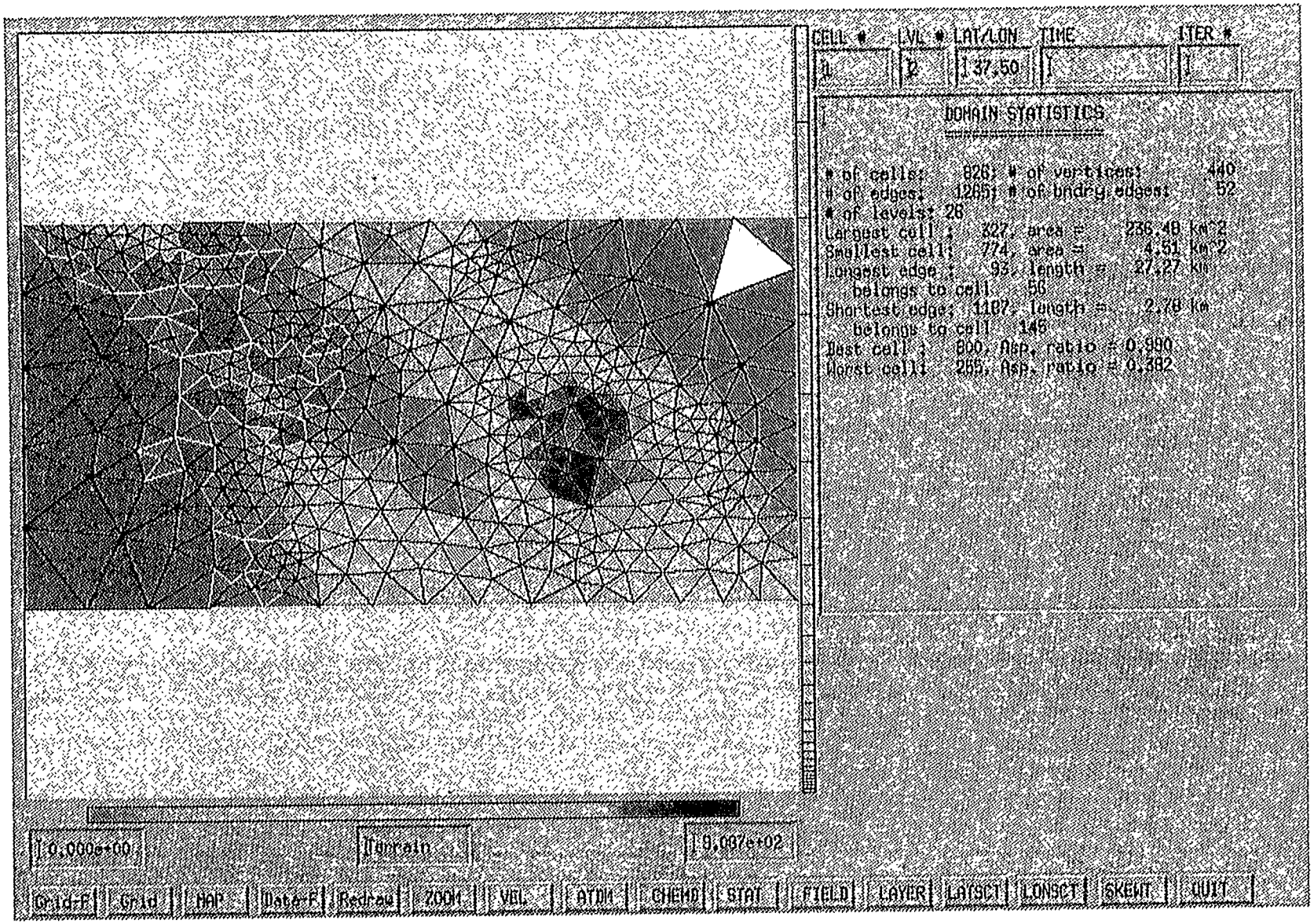
CELL #
LVL #
LAT/LON
TIME
ITER #
1
2
37.50
1
1
DOMAIN STATISTICS
# of cells: 826; # of vertices: 440
# of edges: 1265; # of bndry edges: 52
# of levels: 26
Largest cell : 327, area = 236.48 km^2
Smallest cell: 774, area = 4.51 km^2
Longest edge : 93, length = 27.27 km
belongs to cell 56
Shortest edge: 1187, length = 2.78 km
belongs to cell 146
Best cell : 800, Asp. ratio = 0.990
Worst cell: 265, Asp. ratio = 0.382
0.000e+00
Terrain
9.087e+02
Grid-F
Grid
MAP
Data-F
Redraw
ZOOM
VEL
ATDM
CHEMO
STAT
FIELD
LAYER
LATSCT
LONSCT
SKEWT
QUIT

FEMHD:

An adaptive finite element method for MHD and Edge Modelling

H. R. Strauss

Courant Institute of Mathematical Sciences

New York University

- FEMHD: Adaptive, Finite Element MHD
  - discretization
  - examples
- FEMH3D
- FEM Edge Plasma
- Merging FEMHD with MH3DK (PPPL)
- Further work

1 FEM Numerical Method

FEMHD (with Dana Longcope)

adaptive, finite element, unstructured mesh code.

Advantages-

- fit to irregular boundaries.
- allows the mesh cells to be aligned with magnetic field
- provides good resolution at the magnetic x point.
- Adaptive refinement to resolve solution features.

Meshpoints: vertices of triangles located at points $\vec{r}_i$.

2

1 RMHD Equations

$$\vec{b} = \nabla\psi \times \hat{z} + \hat{z} \tag{1}$$

$$\vec{v}_\perp = \nabla\phi \times \hat{z} \tag{2}$$

$$\frac{\partial\psi}{\partial t} = \nabla_\parallel\phi + \eta C \tag{3}$$

$$\frac{\partial\Omega}{\partial t} = -\vec{v}_\perp \cdot \nabla\Omega + \nabla_\parallel C \tag{4}$$

$$C = \nabla_\perp^2\psi \tag{5}$$

$$\nabla_\perp^2\phi = \Omega \tag{6}$$

Galerkin finite element discretization

Piecewise linear basis functions: $\lambda_i(\mathbf{x}_j) = \delta_{ij}$.

Mixed method, expand ψ, ϕ, Ω, C

$$\psi = \sum_i \psi_i \lambda^i.$$

Sparse matrix RMHD equations:

$$\begin{aligned}
M \cdot \Omega_t + P : \Phi\Omega &= P : \Psi C + \nu S \cdot \Omega \\
M \cdot \Psi_t + P : \Phi\Psi &= \eta S \cdot \Psi \\
S \cdot \Phi &= M \cdot \Omega \\
M \cdot C &= S \cdot \Psi
\end{aligned}$$

Matrices:

mass matrix M,

stiffness matrix S,

Poisson bracket matrix P,

$$
\begin{aligned}
M_{ij} &= \int \lambda^i \lambda^j d^2x \\
S_{ij} &= \int \nabla\lambda^i \cdot \nabla\lambda^j d^2x \\
P_{ijk} &= \int \lambda^i \nabla\lambda^j \times \nabla\lambda^k \cdot \hat{z} d^2x
\end{aligned}
$$

5

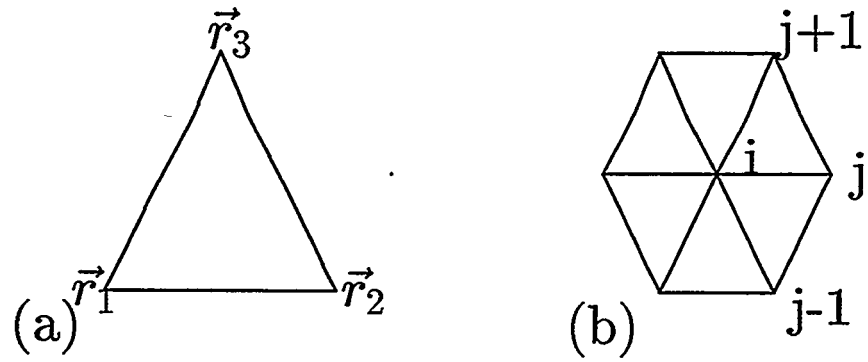

Figure 1: (a) triangle based vertex labels; (b) the support of basis function λ_i for matrix assembly

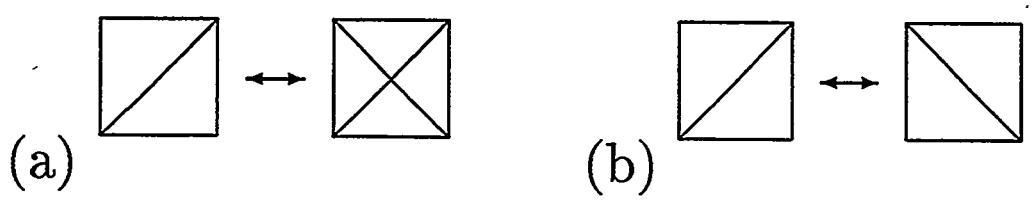

Figure 2: (a) splitting and unsplitting; (b) flipping

6

Algorithmic Notes: $\star$ explicit, leapfrog time differencing

$\star$ dissipative terms solved implicitly.

$\star$ stiffness and mass matrices inverted with Incomplete Cholesky Conjugate Gradient algorithm.

$\star$ refine / unrefine mesh criterion :$\delta C/C, \delta\rho/\rho$

Examples

- poloidal spinup (CRMHD)
  - x point mesh
- tilt mode
  - time dependent adaptive mesh

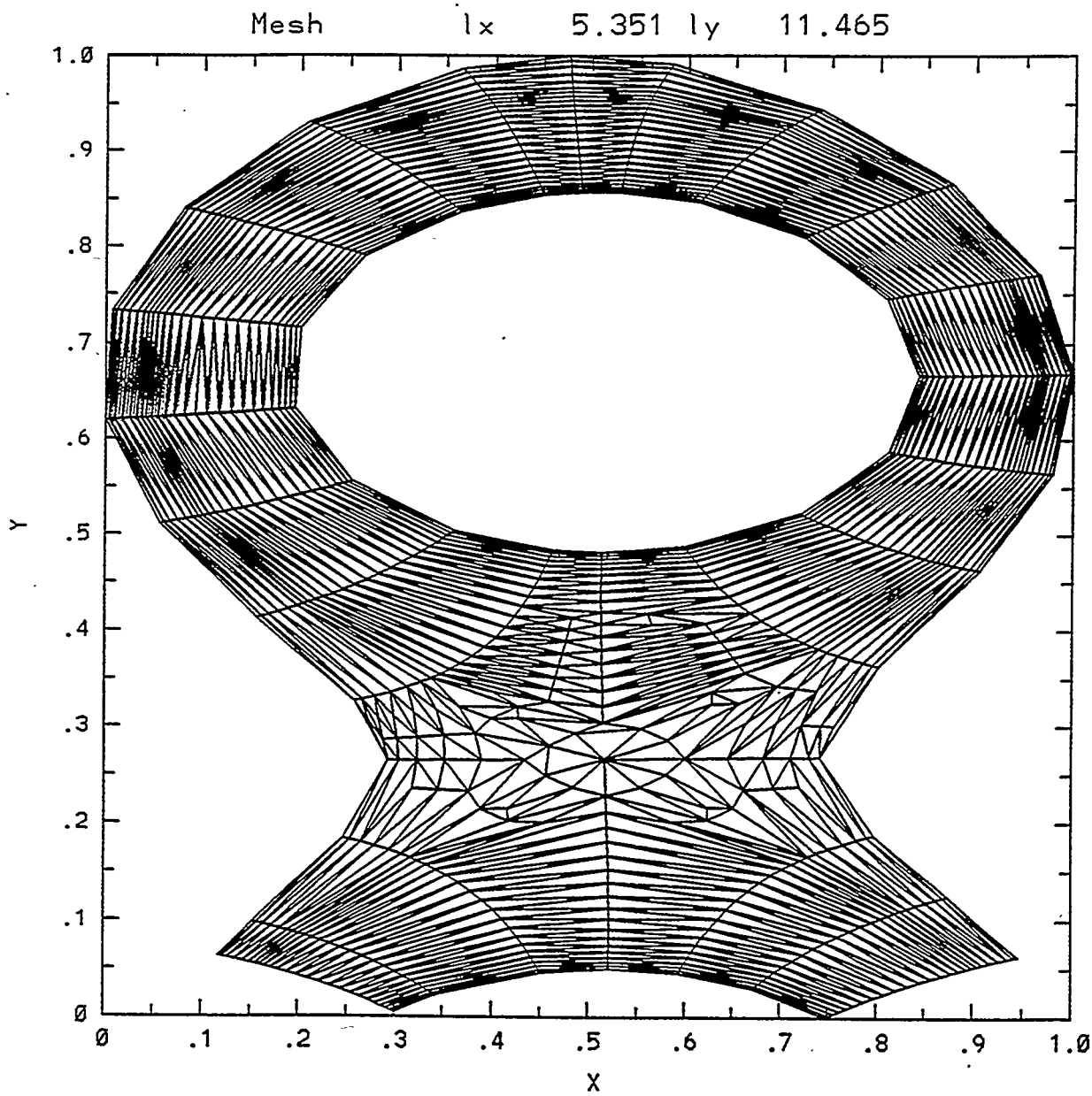

8

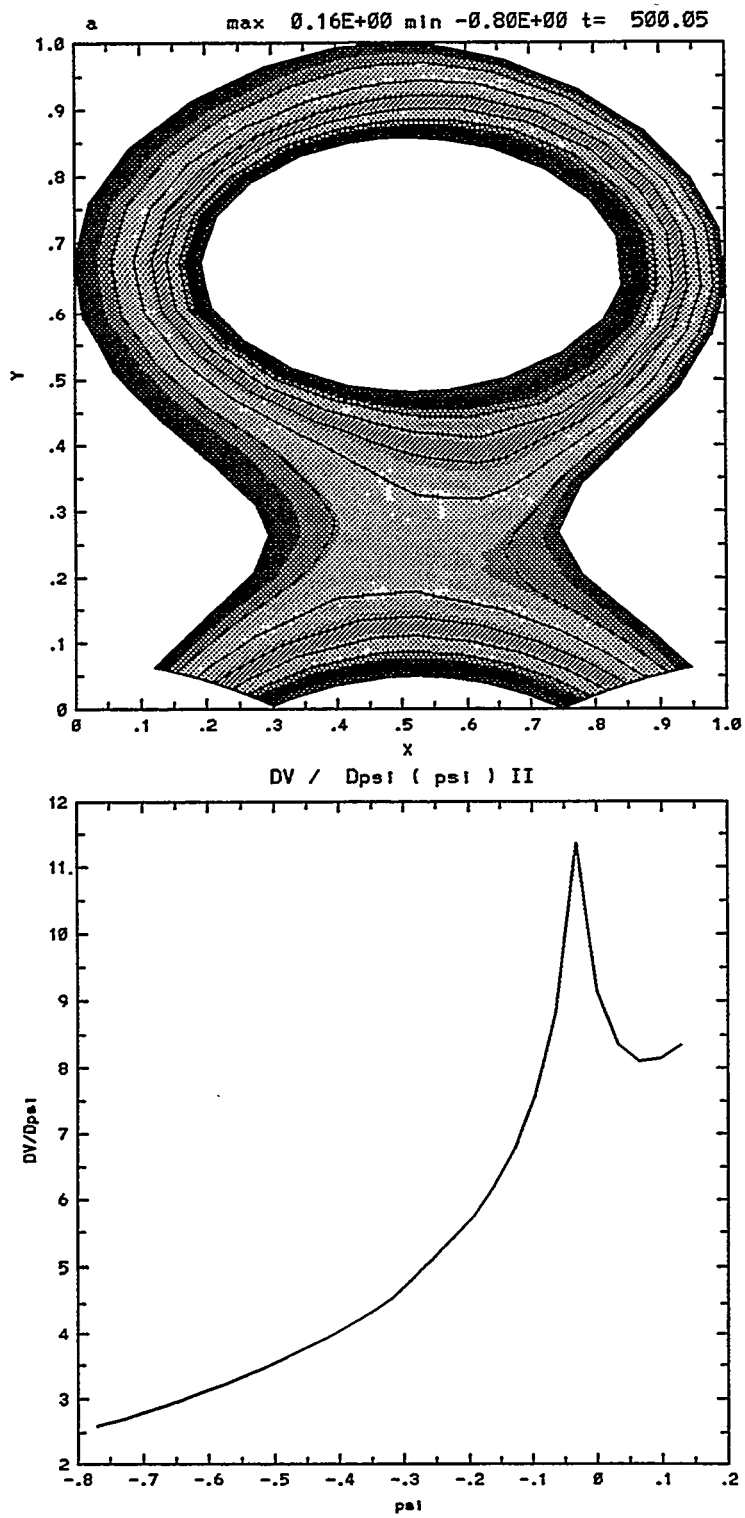

Figure 1: Magnetic flux ψ and rotational transform q.

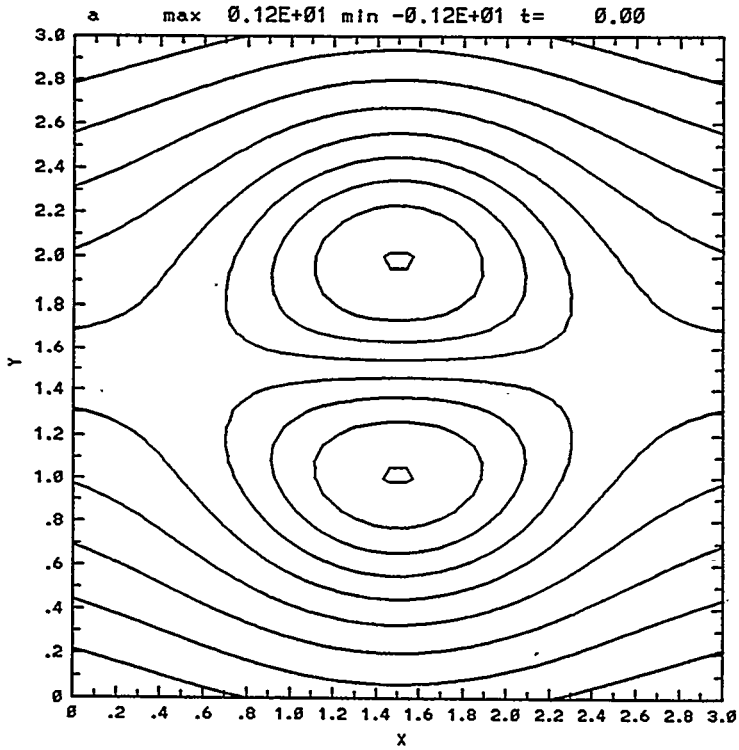

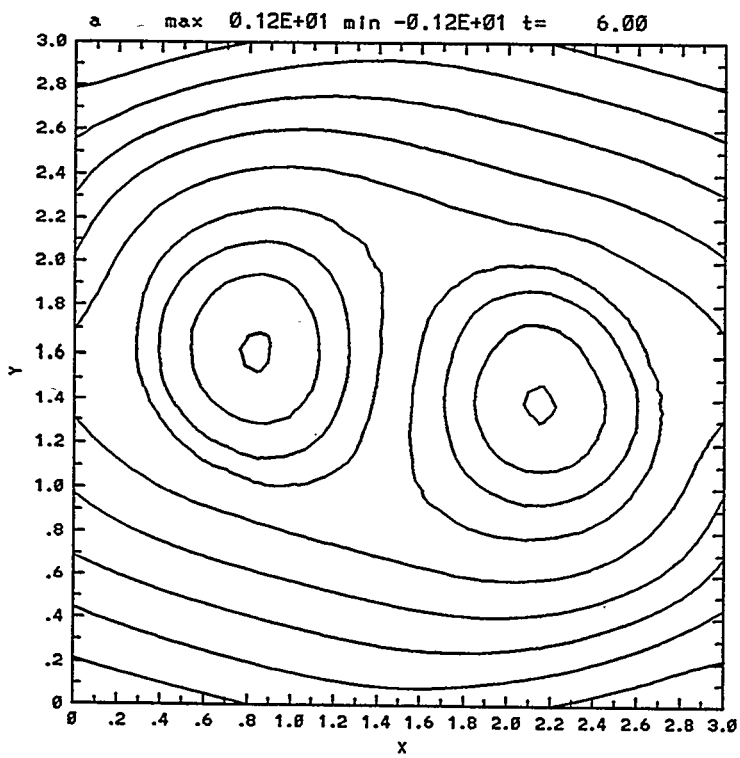

Figure 3: ψ at $t = 0$ and $t = 6$.

10

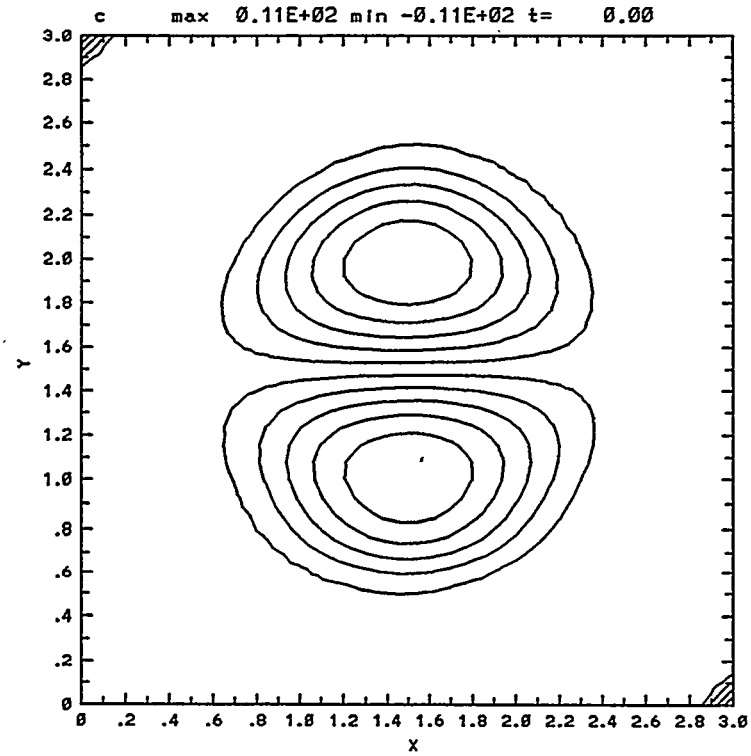

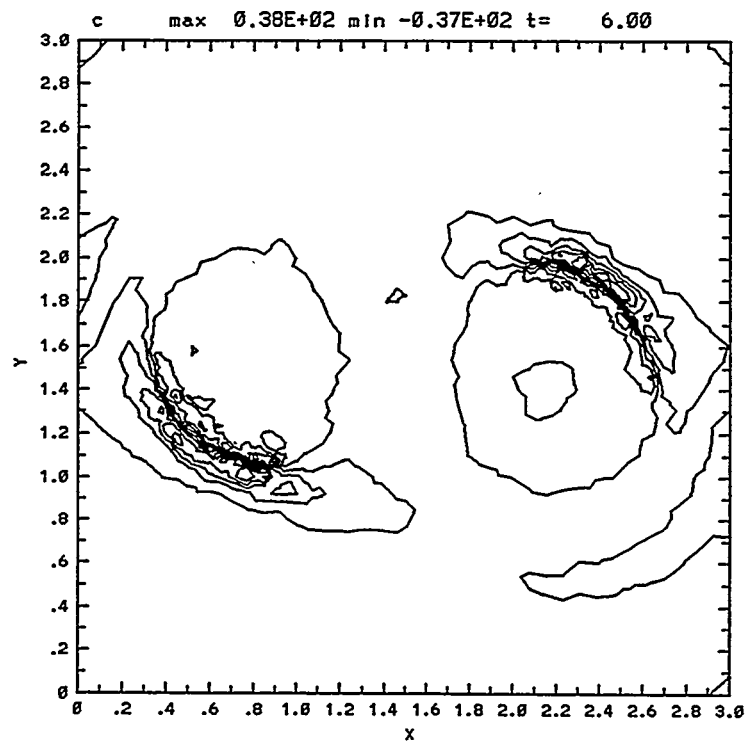

Figure 4: C at $t = 0$ and $t = 6$.

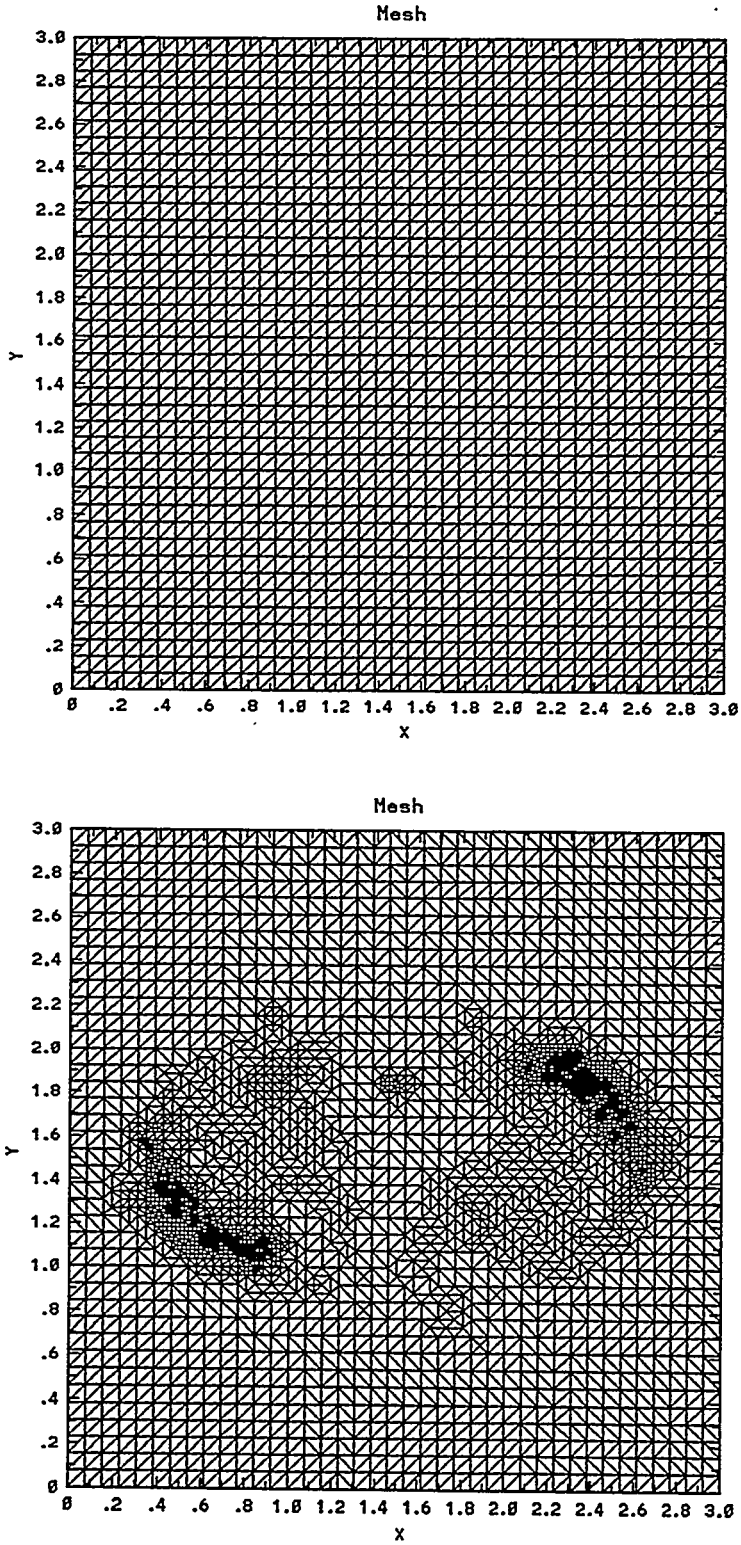

Figure 5: Mesh at $t = 0$ and $t = 6$.

12

FEMH3D

▷ Mesh is z - independent

▷ 3rd direction: staggered finite difference or Fourier series

Example:

▷ 3D resistive internal kink

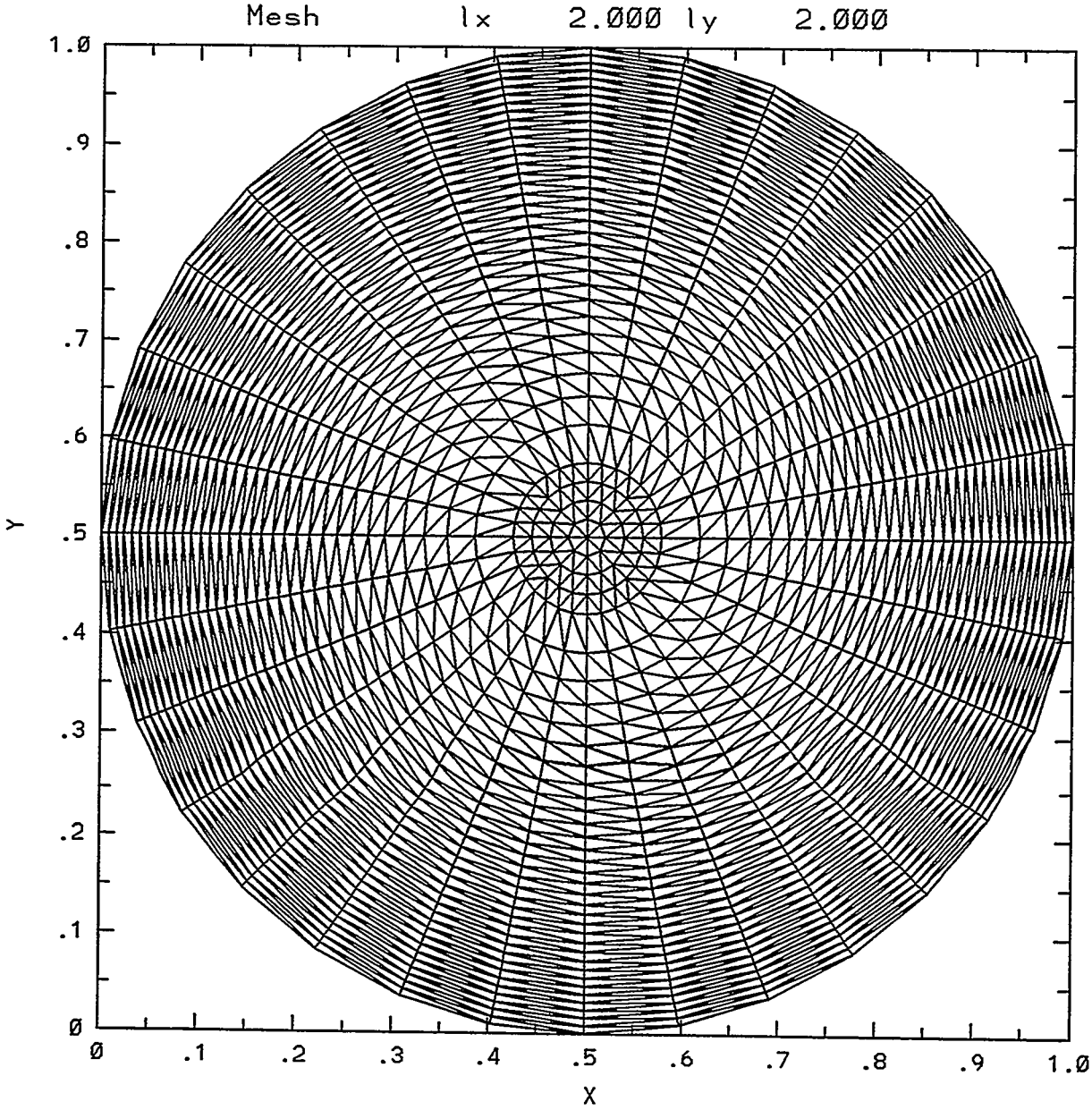
Mesh lx 2.000 ly 2.000
1.0
.9
.8
.7
.6
.5
.4
.3
.2
.1
0
Y
0
.1
.2
.3
.4
.5
.6
.7
.8
.9
1.0
X

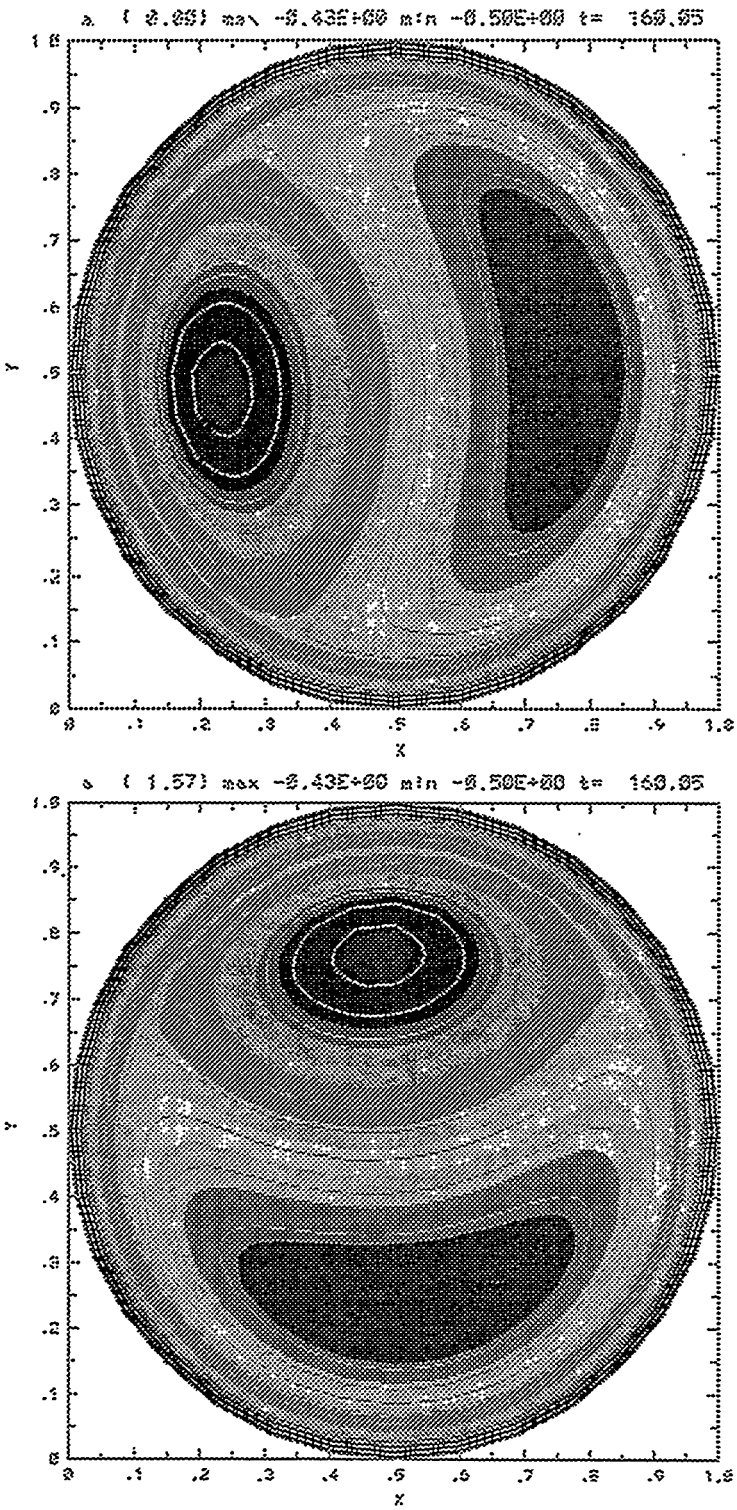

Figure 1: Nonlinear magnetic potential $\psi = A_z - r^2/2$ at $t = 120$ at toroidal angles $\zeta = 0, \pi/2$.

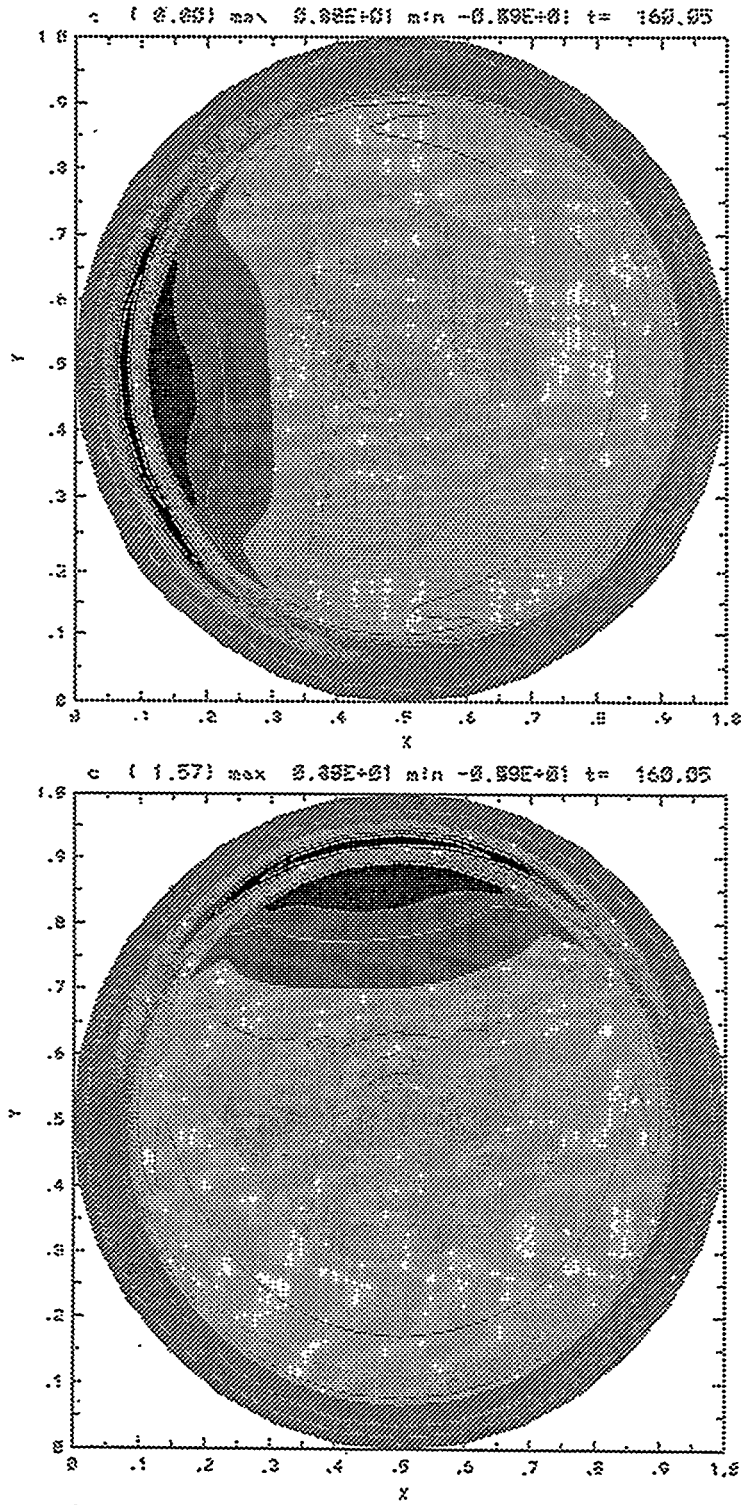

Figure 1: Nonlinear current J at $t = 120, \zeta = 0, \pi/2$.

FEMHD (Finite Element Method Hydro Dynamics) - Edge (with B. Braams, D. Rayevski)

for edge plasma problems

moving ionization fronts, shocks, and thermal collapse require adaptive mesh

version of FEMHD solves

- H ion continuity
- H neutral continuity
- H ion parallel momentum
- H neutral parallel momentum
- Electron temperature = ion temp. = neutral temp

Include nonlinear coupling:

- ionization
- charge exchange
- ionization radiation loss
- recycling model

16

Strauss - Box J06
11/23/94

run: gas16

```
gas16
          mesh:
        b2

nv, nt, nelm =   640  1152     0

gas16
-----
'n=10e14  b2rates, no visc heat, no bnd ionize
 500.,  50000.  100.  tfin, ntt, dtpl
 3*2.5E-2  mu, eta, chi
 0.5,  2*0.15  adt, a_x, montor
 0.1,  2*1.xcore, areamn, coreflx
 0.,  2.5E-2,  0.1mupar, mu0, eta0
'switches: +re  -a   -w
b2edge
11/22/94
  started from t = 0.
```

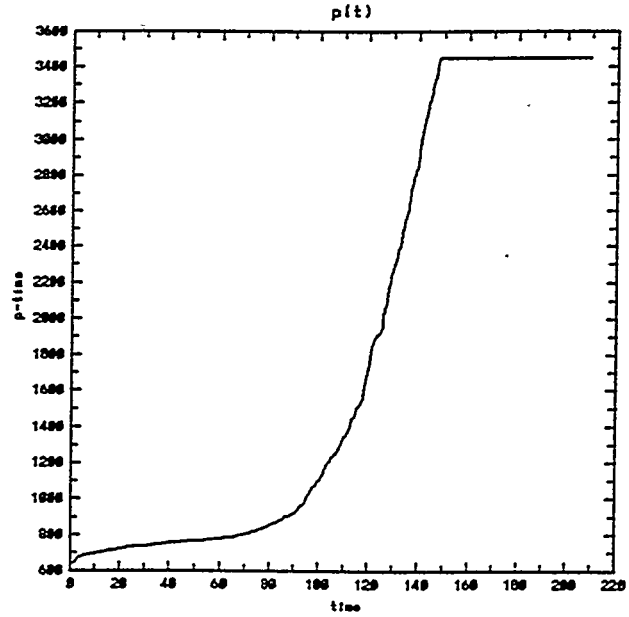

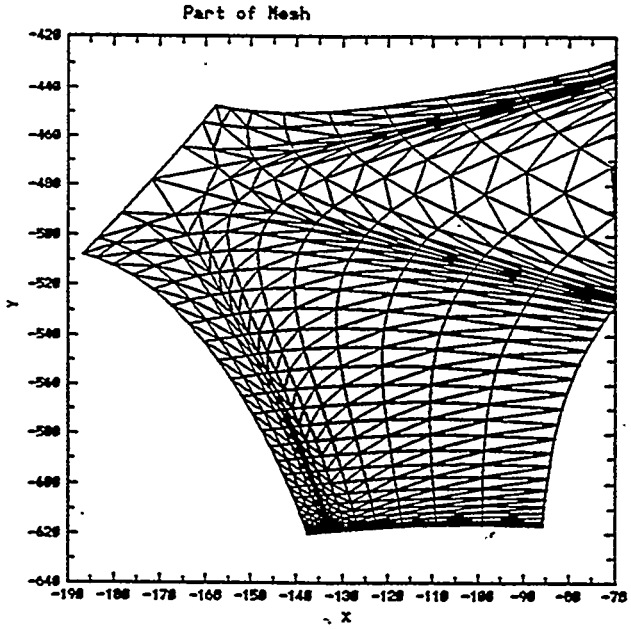

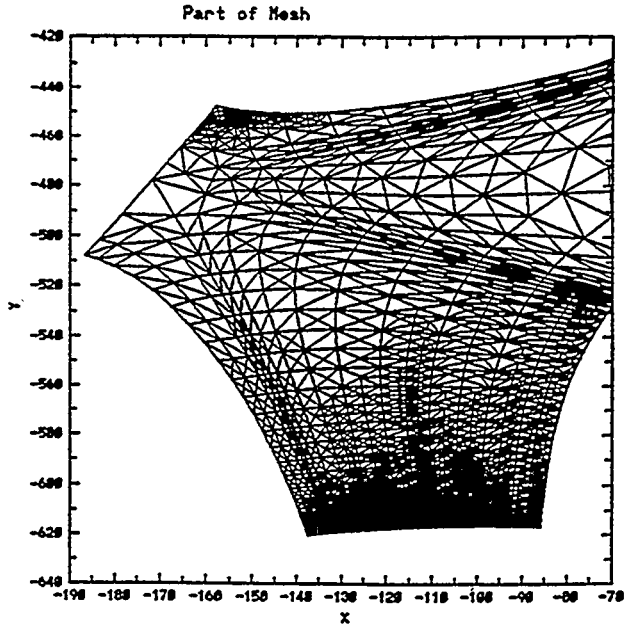

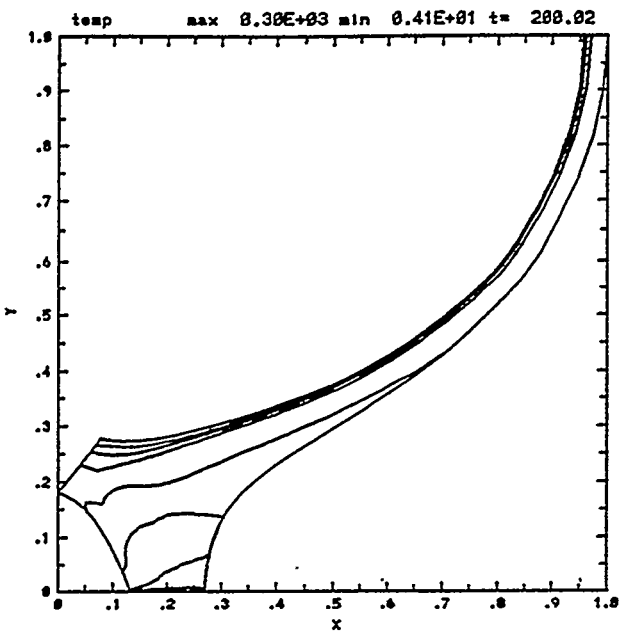
temp max 0.30E+03 min 0.41E+01 t= 200.02
Y
X

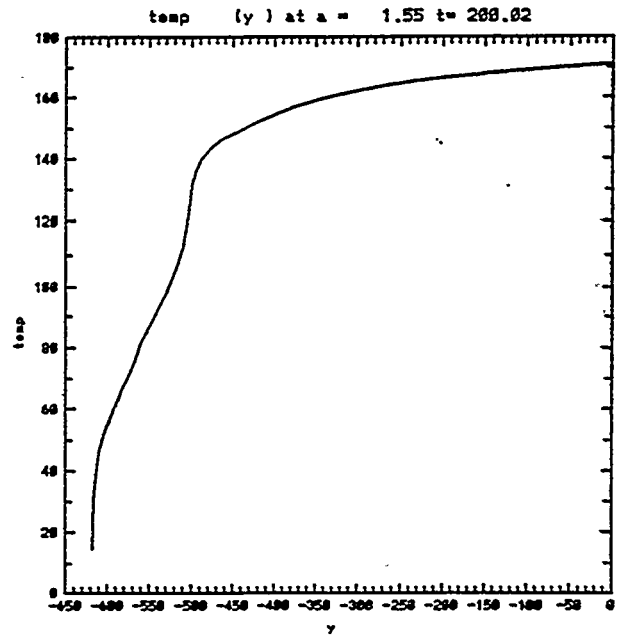
temp (y) at a = 1.55 t= 200.02
temp
y

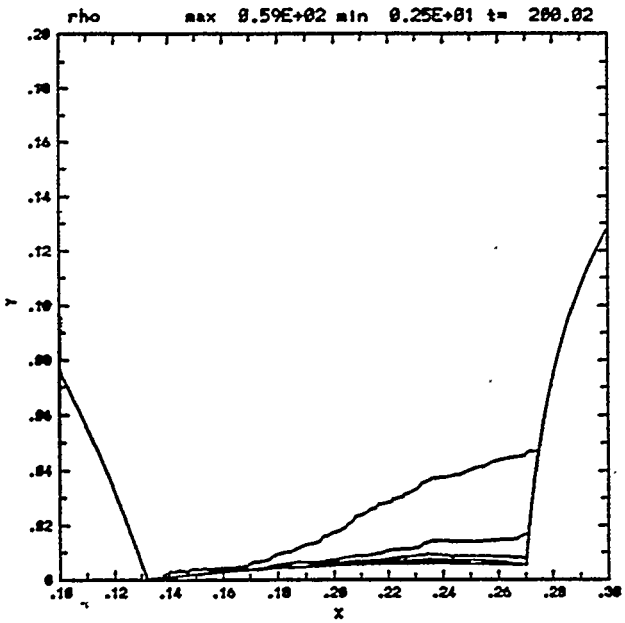
rho max 0.59E+02 min 0.25E+01 t= 200.02
Y
X

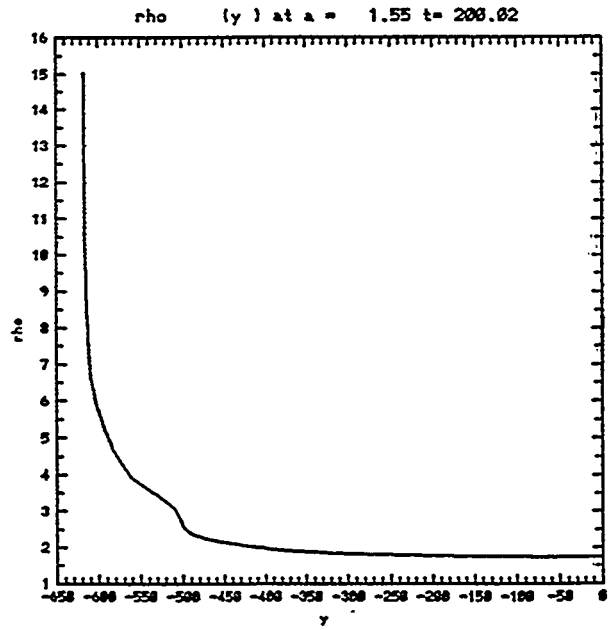
rho (y) at a = 1.55 t= 200.02
rho
y

Merging of FEMHD with MH3DK (with W. Park, PPPL)

Application to resistive wall modes with complex wall geometry.

FEMHD = 6,000 lines (unstructured mesh, RMHD)

MH3DK = 30,000 lines (structured mesh, full MHD + hot particles)

$FEMHD \cap MH3DK = 2,000 \text{lines}$

- Have to replace routines: Δ, Δ^{-1}, div, curl
- Fortran90 object - oriented features

Future: other discretizations

- primitive variables
  - "divergence cleaning" of $\nabla \cdot \vec{v}$, $\nabla \cdot \vec{B}$
- higher order elements
  - piecewise parabolic ψ
  - piecewise constant $C = \Delta\psi$

USE OF GENERALIZED CURVILINEAR COORDINATE SYSTEMS IN ELECTROMAGNETIC AND HYBRID CODES

by

Daniel W. Swift
Geophysical Institute
University of Alaska
Fairbanks, Alaska

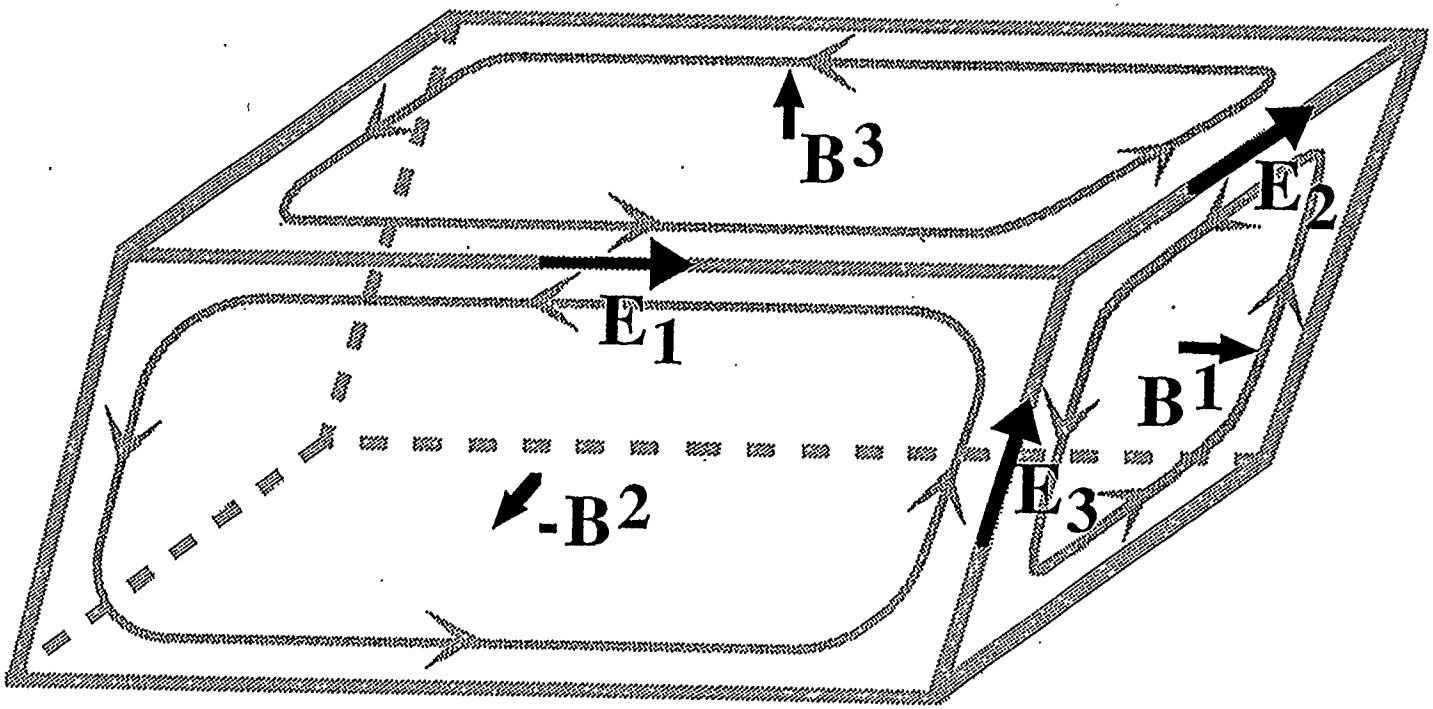
B3
E2
E1
B1
E3
-B2

Particle equations of motion in curvilinear coordinates

The field equations are updated without the necessity of explicitly differentiating metric coefficients. The particle velocities are in Cartesian components, so the particle equations of motion do not involve differentiation of metric coefficients. The particle positions serve as pointers to the field quantities, so they must be expressed in curvilinear components. For convenience, the topological distance between grid points is of unity.

The curvilinear position is advanced by

$$\left(q^i\right)^{n+1} = \left(q^i\right)^n + \Delta t \mathbf{M}^i \cdot \mathbf{v}^{n+\frac{1}{2}}$$

where $\mathbf{V}$ is in Cartesian components.

Exactly Conservative Calculation of the Current

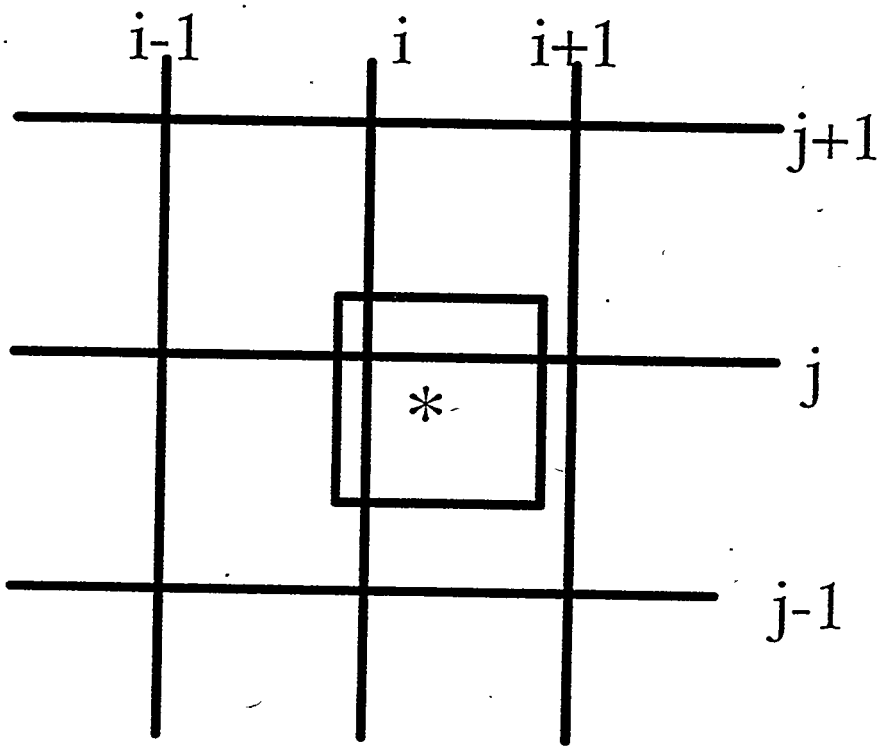

The grid has the topology of a cubic lattice. The coordinate variables are incremented in unit intervals between grid points. The particle is a finite element cube. The current is simply the amount of charge transported across a cell face per unit time. The rate of change of charge density at the dual cell is <u>exactly</u> the divergence of the current.

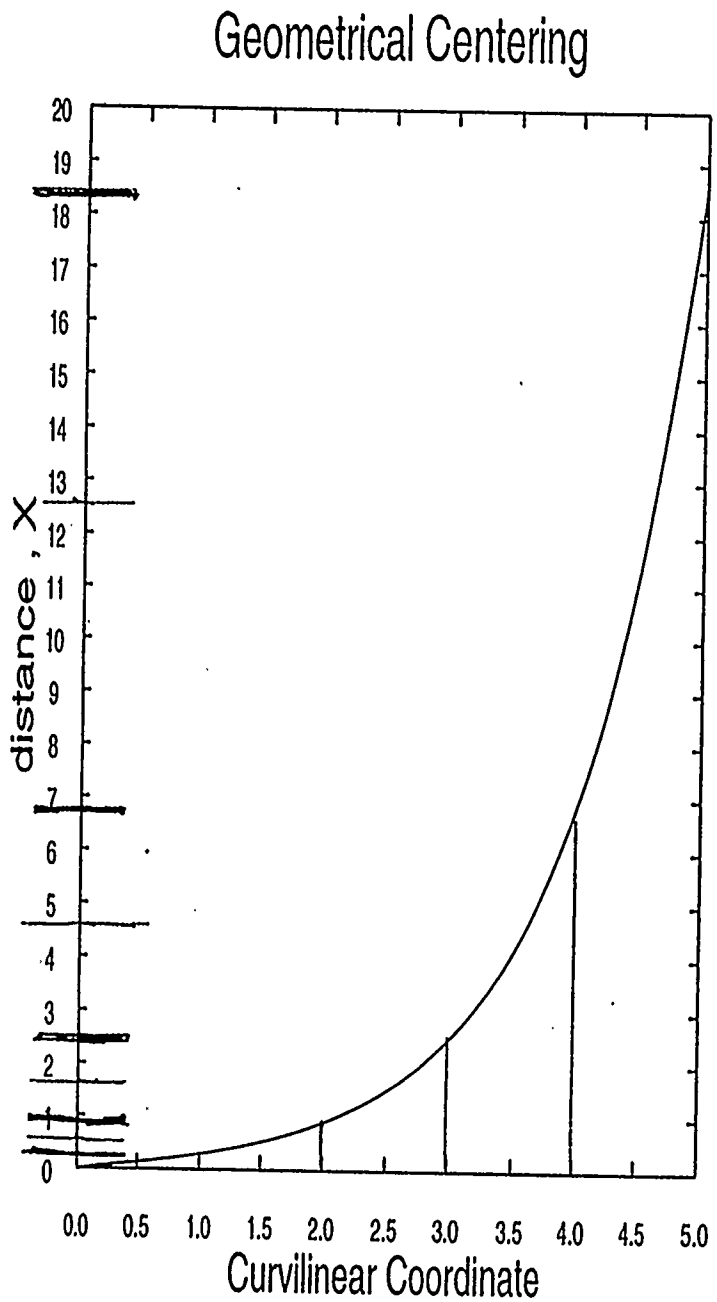
Geometrical Centering
distance , X
Curvilinear Coordinate
0.0 0.5 1.0 1.5 2.0 2.5 3.0 3.5 4.0 4.5 5.0
0 1 2 3 4 5 6 7 8 9 10 11 12 13 14 15 16 17 18 19 20

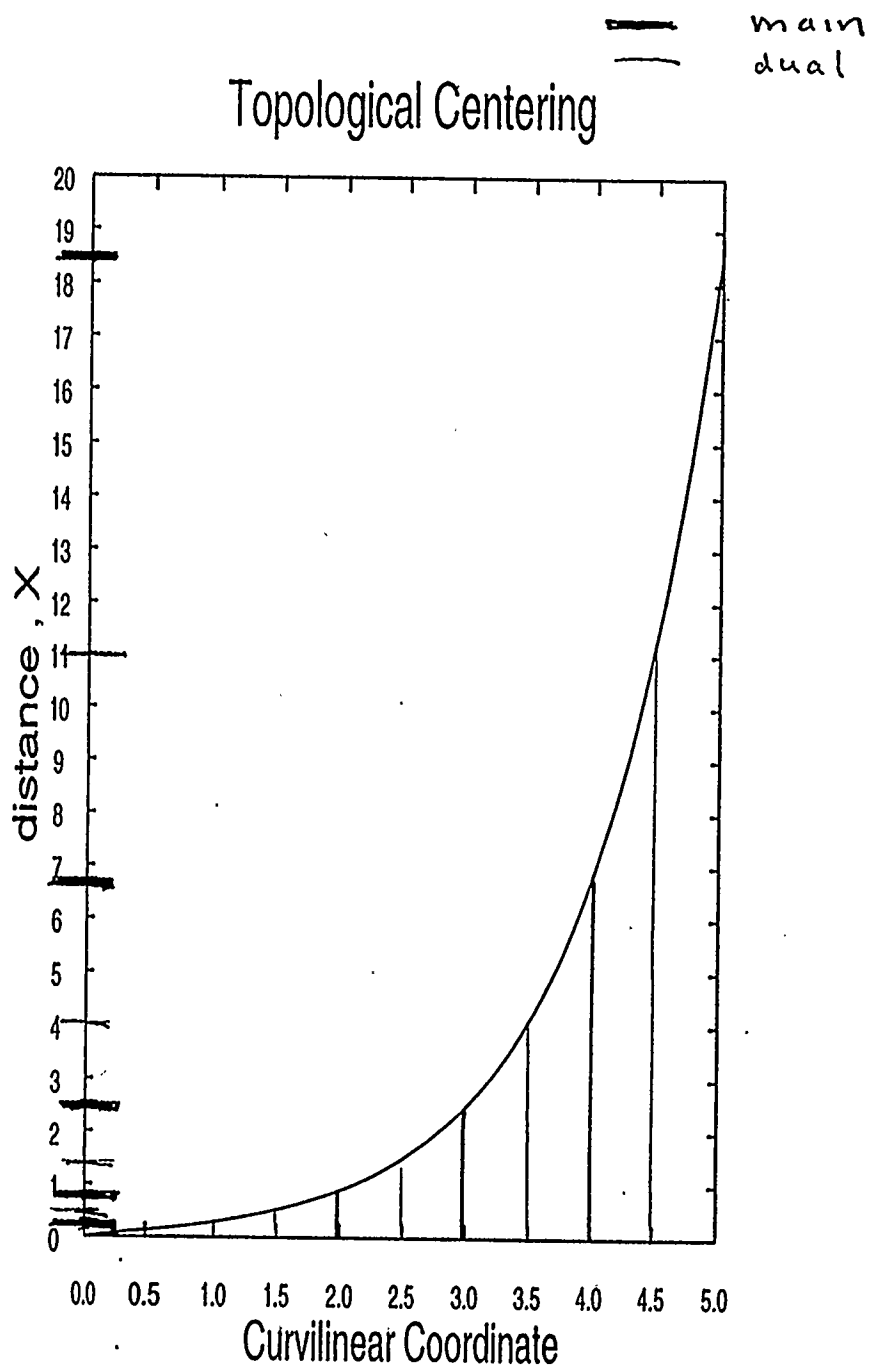
main
dual
Topological Centering
distance , X
Curvilinear Coordinate
0.0 0.5 1.0 1.5 2.0 2.5 3.0 3.5 4.0 4.5 5.0
0 1 2 3 4 5 6 7 8 9 10 11 12 13 14 15 16 17 18 19 20

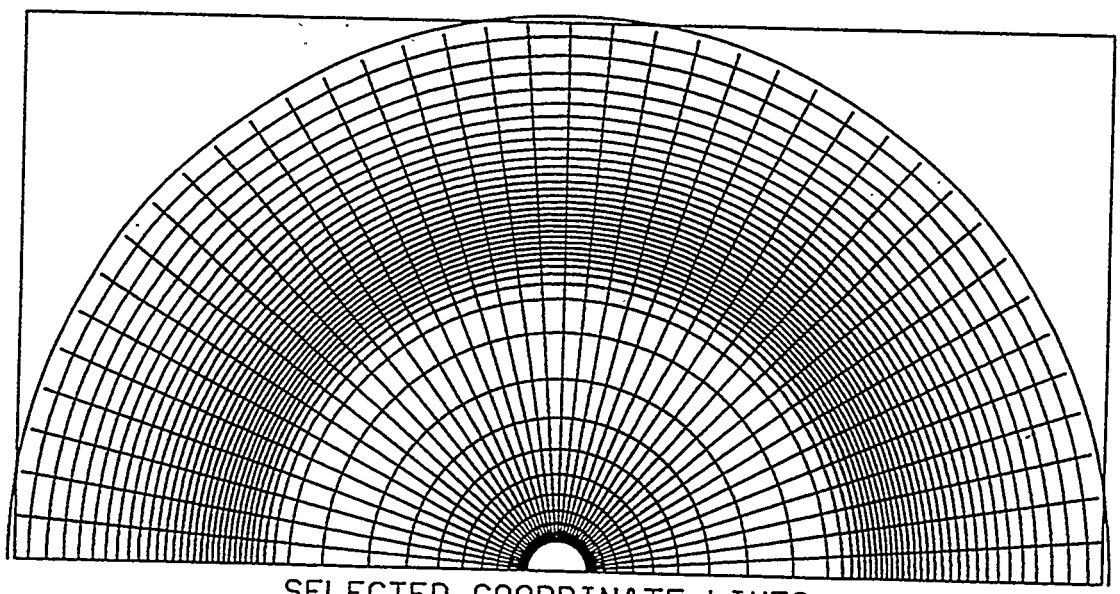

Figure 1 The coordinate system used in simulation of the magnetospheric noon meridian plane. The box extends toslightly more than $18R_E$ from the center of the Earth in the north, south and sunward directions. The region in te corners cot covered by the grid lines is outisde the simulaiton domain.

Tangent **B** and normal **E**

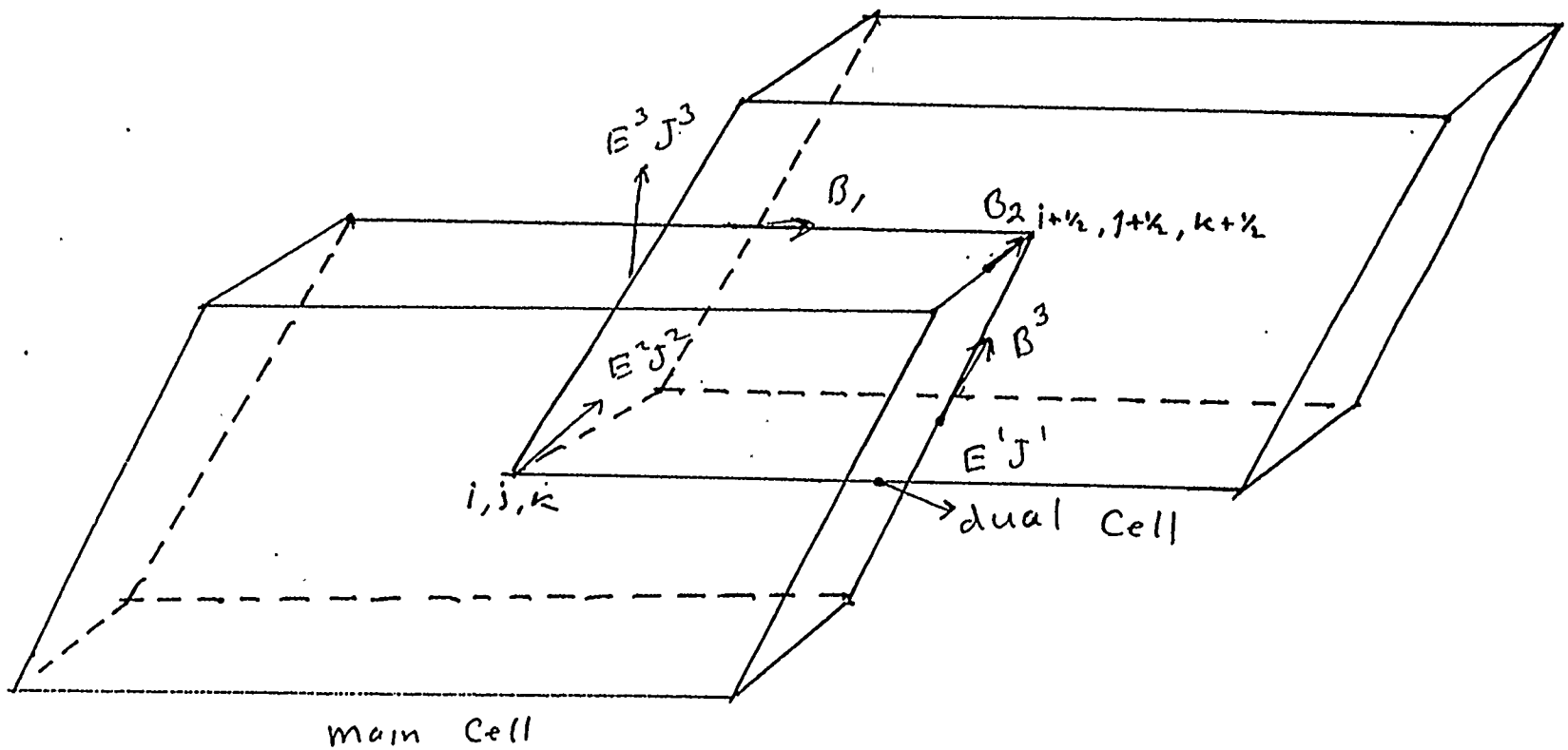

Update the magnetic field, using Stokes' law

$$\int \frac{\partial \mathbf{B}}{\partial t} \cdot d\mathbf{A} = -\oint \nabla \times \mathbf{E} \cdot d\boldsymbol{\ell}$$

$$\left[\frac{\left(B^1\right)^{n+1} - \left(B^1\right)^n}{\Delta t} A^1 \right]_{i+\frac{1}{2},j,k} =$$

$$\left(E_3^{n+\frac{1}{2}} l_3 \right)_{i+\frac{1}{2},j-\frac{1}{2},k} - \left(E_3^{n+\frac{1}{2}} l_3 \right)_{i+\frac{1}{2},j+\frac{1}{2},k} +$$

$$\left(E_2^{n+\frac{1}{2}} l_2 \right)_{i+\frac{1}{2},j,k+\frac{1}{2}} - \left(E_2^{n+\frac{1}{2}} l_2 \right)_{i+\frac{1}{2},j,k-\frac{1}{2}}$$

The tangent vectors are computed by taking difference between coordinate points. For example,

$$\left(\mathbf{l}_2\right)_{i+\frac{1}{2},j,k+\frac{1}{2}} = \mathbf{r}_{i+\frac{1}{2},j+\frac{1}{2},k+\frac{1}{2}} - \mathbf{r}_{i+\frac{1}{2},j-\frac{1}{2},k+\frac{1}{2}}$$

Tangent **E** and normal **B**

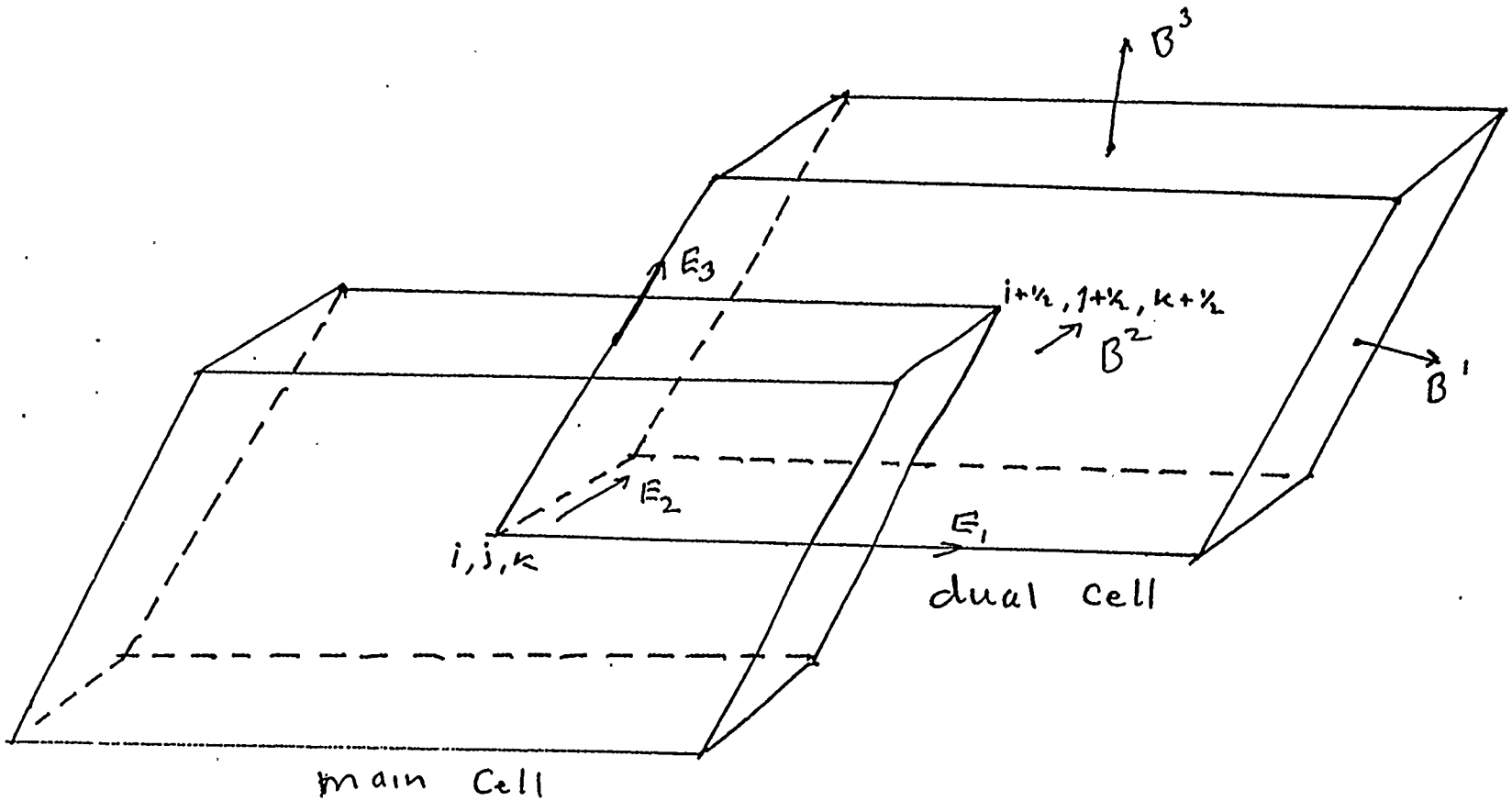

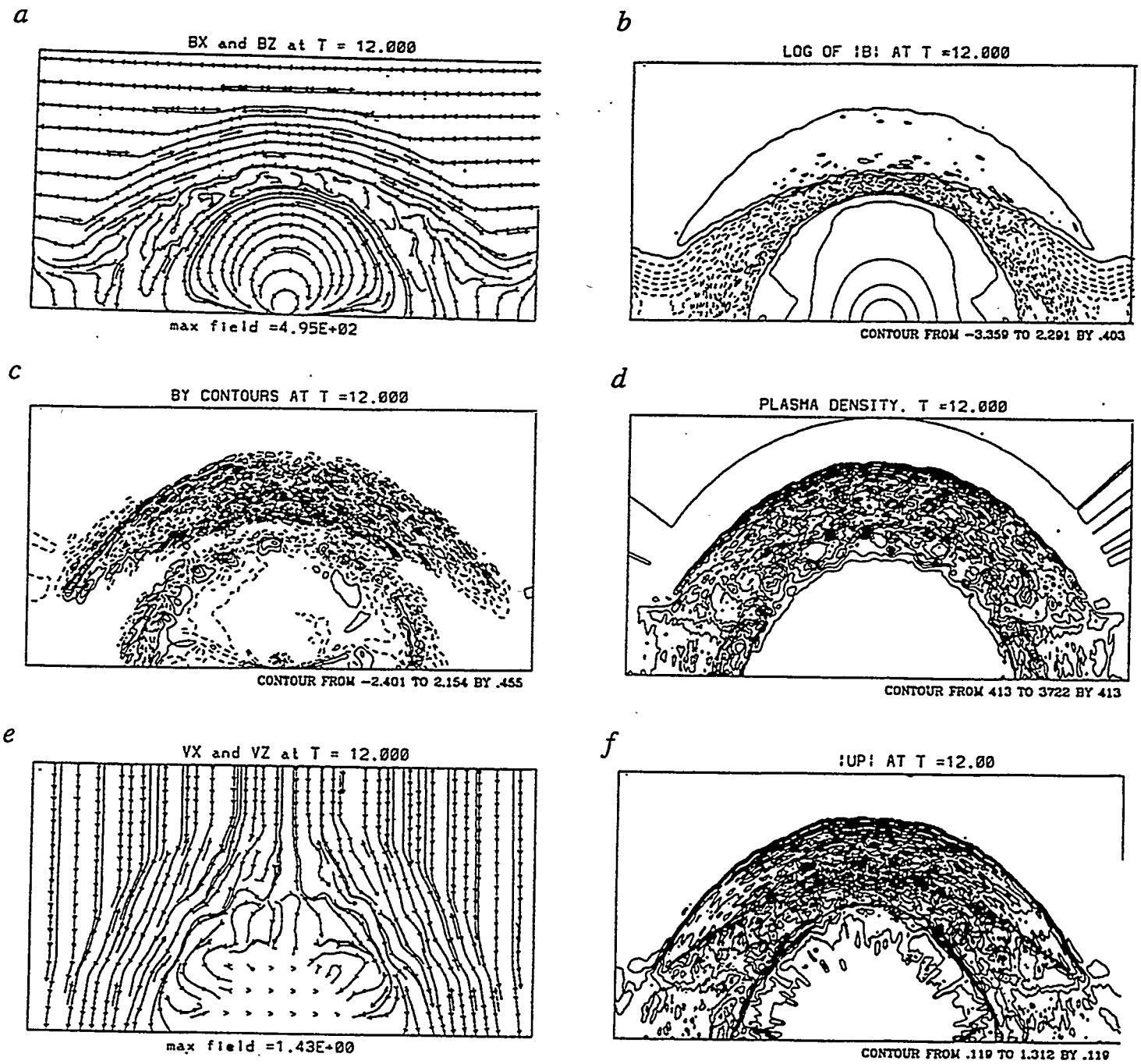

Figure 3. Magnetic field vectors (a), logarithm of the magnetic field intensity (b), the y-component of the magnetic field (c), the plasma density (d), the plasma flow vectors (e) and the magnitude of the plasma flow speed. (f)

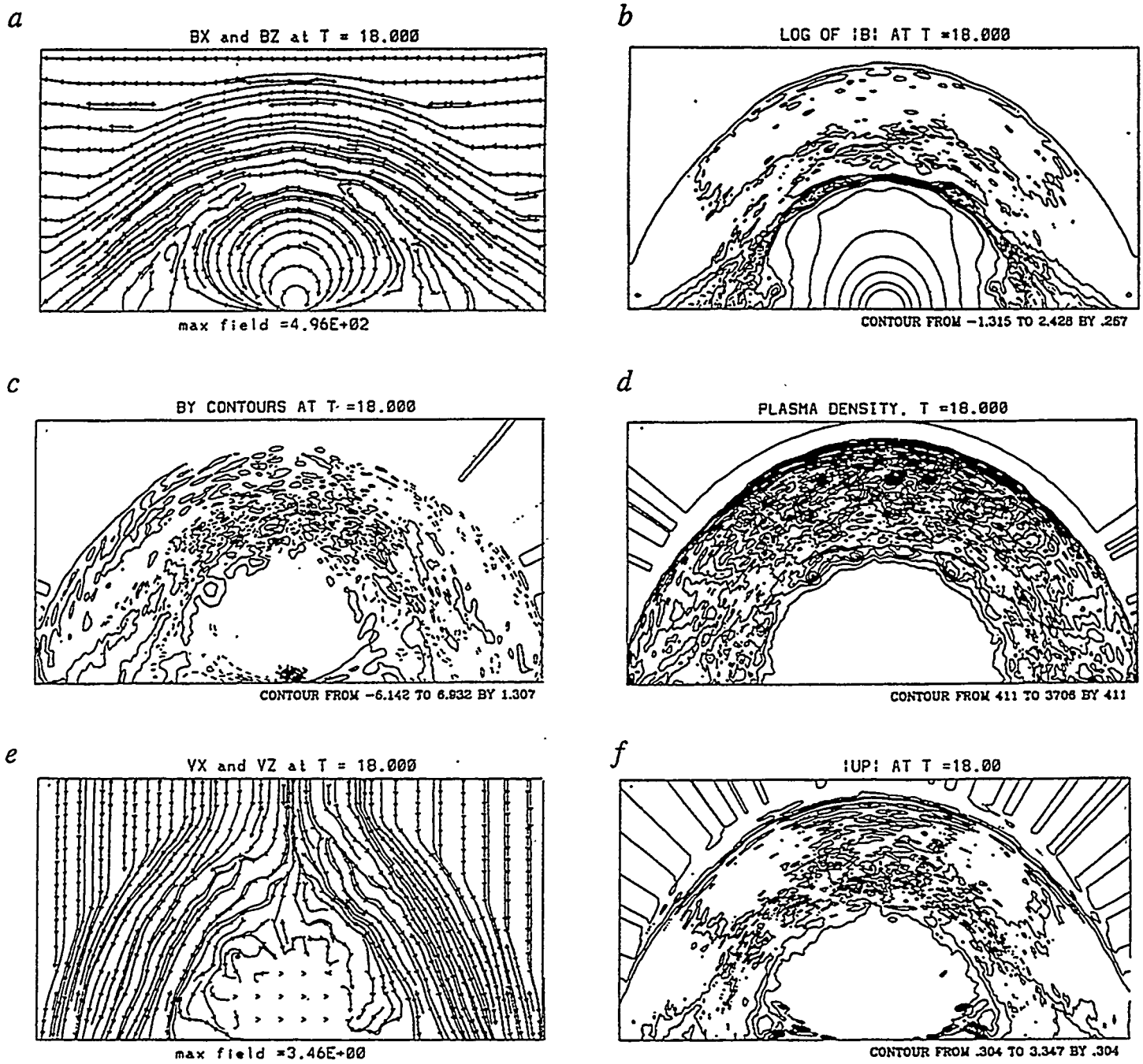

Figure 4 Same as Figure 3, except at the end of the run.

Workshop On Adaptive Grid Methods
For Fusion Plasmas

Pleasanton, CA
December 8-9, 1994

Adaptive hp Finite Element Methods

James C. Wiley

Fusion Research Center
University of Texas at Austin
Austin, Texas 78712

Acknowledgements:
J. T. Oden and L. Demkowicz
Yusheng Feng and Abani Patra
Andrzej Safjan

Adaptive hp Finite Element Methods

- Definition
- Motivation
- Finite Element Method
- Elements
- Example Meshes
- Challenges
- Hyperbolic example

Definition

Adaptive-hp methods use a refinement control strategy driven by a local *a posteriori* error estimate to locally modify the element size, h, and polynomial order, p to increase computational efficiency. The result is an unstructured mesh in which each node may be associated with a different polynomial order and each cell may have a different size.

Should be contrasted with the moving finite element method, which adaptively modifies the element shape.

Payoff

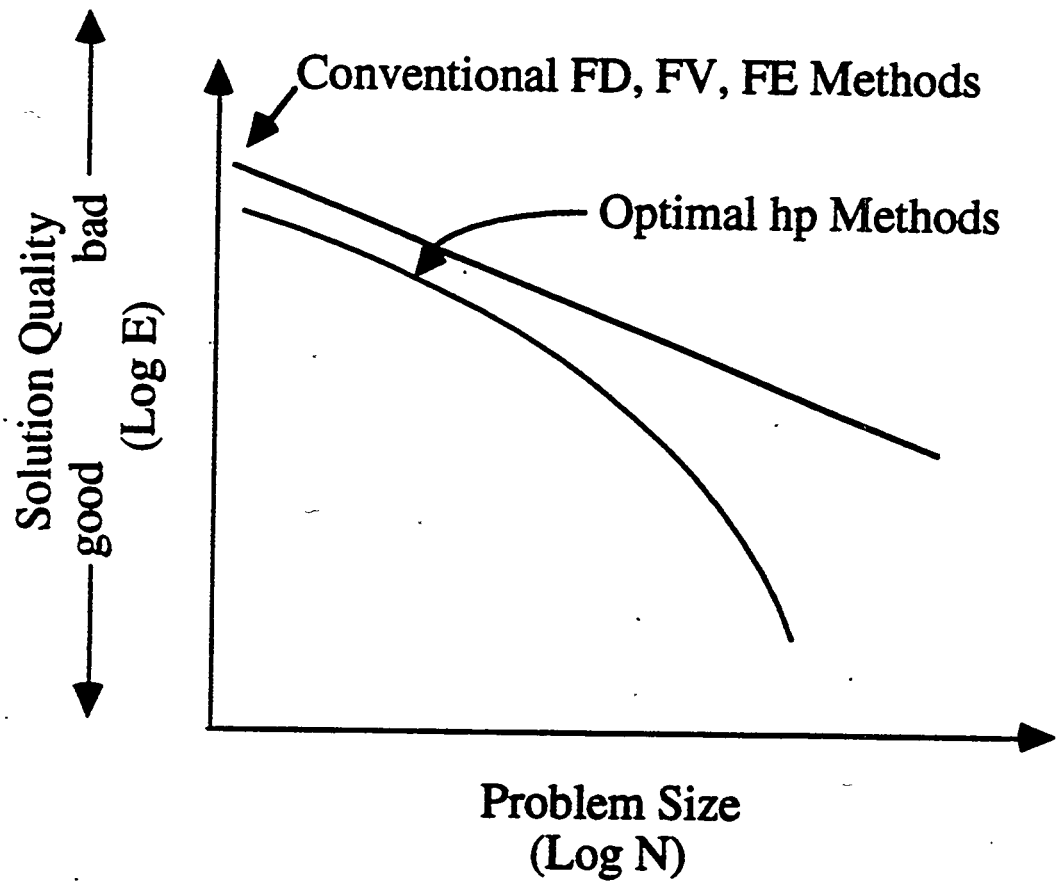
Conventional FD, FV, FE Methods
Optimal hp Methods
Solution Quality
bad
good
(Log E)
Problem Size
(Log N)

References

[1] I. Babuska and M. R. Dorr, "Error estimates for the combined h and p-version of the finite element method", Numer. Math. **37**, 257-277(1981).

[2] I. Babuska, Manil Suri, "The h-p Version of The Finite Element Method with Quasiuniform Meshes", RAIRO Math. Model Numerical Anal. **21**, 199-238, (1987).

[3] I. Babuska, Manil Suri, "The p- and h-p Versions of The Finite Element Method, An Overview", CMAME **80**, 5-26, (1990).

[4] L. Demkowicz, J. T. Oden, W. Rachowicz, and O. Hardy, "Toward A Univeral h-p Adaptive Finite Element Strategy, Part 1, Constrained Approximation and Data Structures", CMAME **77** 76-112 (1989).

[5] J. T. Oden, L. Demkowicz, W. Rachowicz, and T. A. Westermann, "Toward a Universal h-p Adaptive Finite Element Strategy, Part 2. A Posteriori Error Estimation",CMAME, 77, 113-180, (1989).

[6] W. Rachowicz, J. T. Oden and L. Demkowicz, "Part 3. Design of h-p Meshes", CMAME, 77, 181-212, (1989).

[7] Andrzej Safjan, "High-Order Taylor-Galerkin and Adaptive hp-Methods For Hyperbolic Systems with Applications to Structural Acoustics", Dissertation, Univ. of Texas at Austin, Dec. 1993.

[8] Kim Bey, "An hp-adaptive Discontinuous Galerkin Method For Hyperbolic Conservation Laws", Disseration, Univ. of Texas at Austin, May 1994.

[9] J. Tinsley Oden, "Optimal hp-Finite Element Methods", CMAME, **112**, 309-311,(1994).

[10] J. Tinsely Oden, Abani Patra, and Yusheng Feng, "An hp Adaptive Strategy", AMD,**157** Adaptive, Multilevel, and Hierarchical Computational Strategies, ASME, (1992).

[11] Michael S. Warren and John K. Salmon, "A Parallel Hashed Oct-Tree N-Body Algorithm", Proceedings of Supercomputing '93.

Model Finite Element Method Problem

Given an operator A

$$Au = f \qquad \text{in region} \qquad \Omega,$$

with BC

$$u=0 \quad \text{on } \Gamma_0\,, \qquad a\frac{\partial u}{\partial n} = b \qquad \text{on } \Gamma_1,$$

where A might be

$$Au = -\nabla[D\nabla u - Vu] + Cu.$$

We seek an approximate solution to the weak form of (1),

$$a(u^h, v^h) = l(v^h) \quad \forall v^h \in V^h(\Omega)$$

where

$$a(u,v) = \int_\Omega (\nabla v D \nabla u - \nabla v V u + v C u)\,dx$$

$$l(v) = \int_\Omega f\,v\,dx + \int_{\Gamma_1} b\,v\,ds,$$

and

$$u^h \in V^h(\Omega) = \left\{ v^h \in H^1(\Omega) \colon \gamma v = 0 \; on \; \Gamma_0 \right\}.$$

Divide region into elements

$$\Omega = \sum_e \Omega_e$$

Integrations become local over each element

$$a(u,v) = \sum_e \int_{\Omega_e} (\nabla v D \nabla u - \nabla v V u + v C u) dx$$

The approximation is expanded into local basis functions

$$u^h = \sum_e \sum_i u_i^e \phi^{e,i}$$

The result is a linear system for the coefficients

$$Au = b$$

The key practical problems are the selection of the approximating spaces and the efficient solution of the resulting linear system.

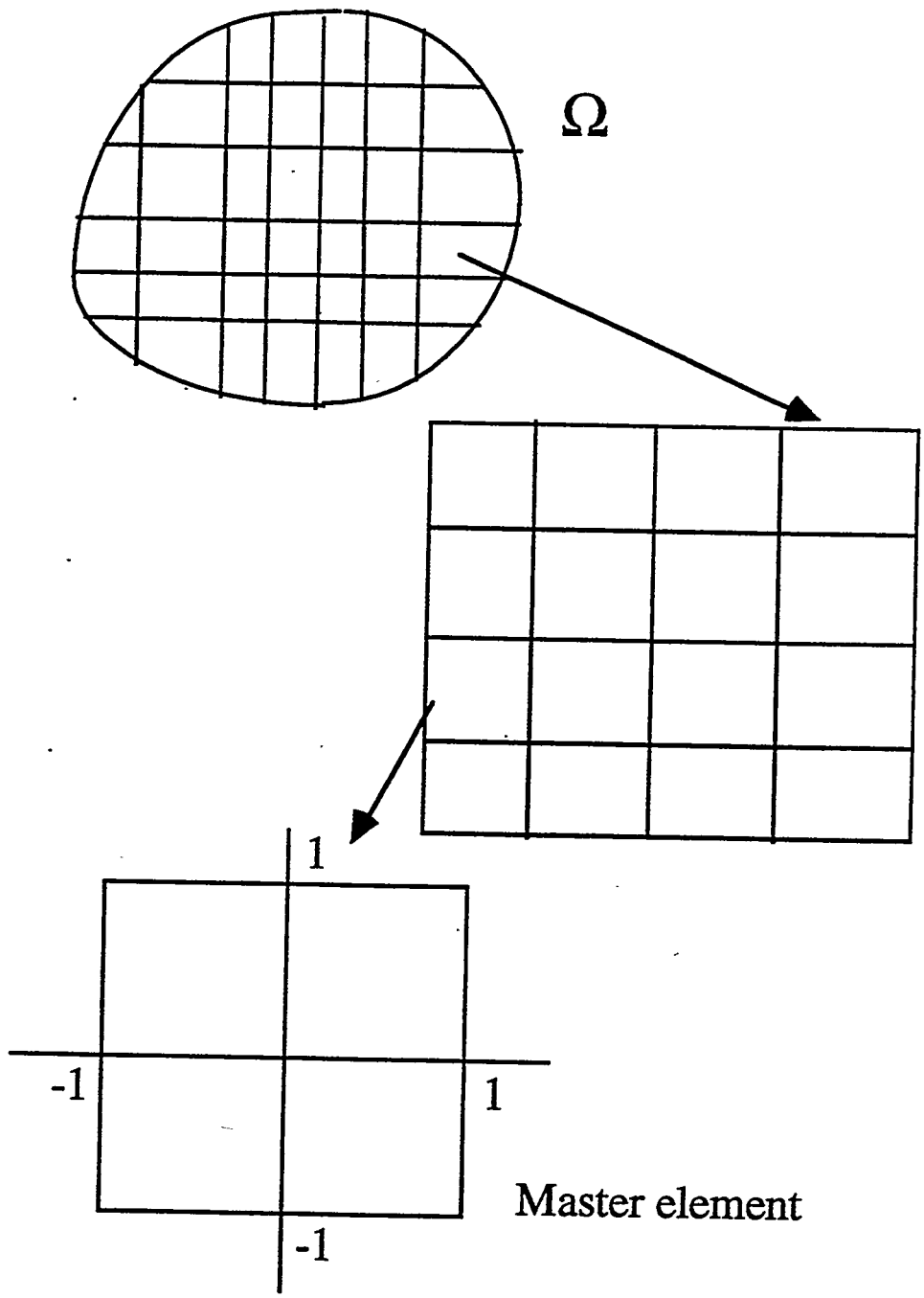
Ω
1
-1
1
-1
Master element

Typical quadrilateral master element

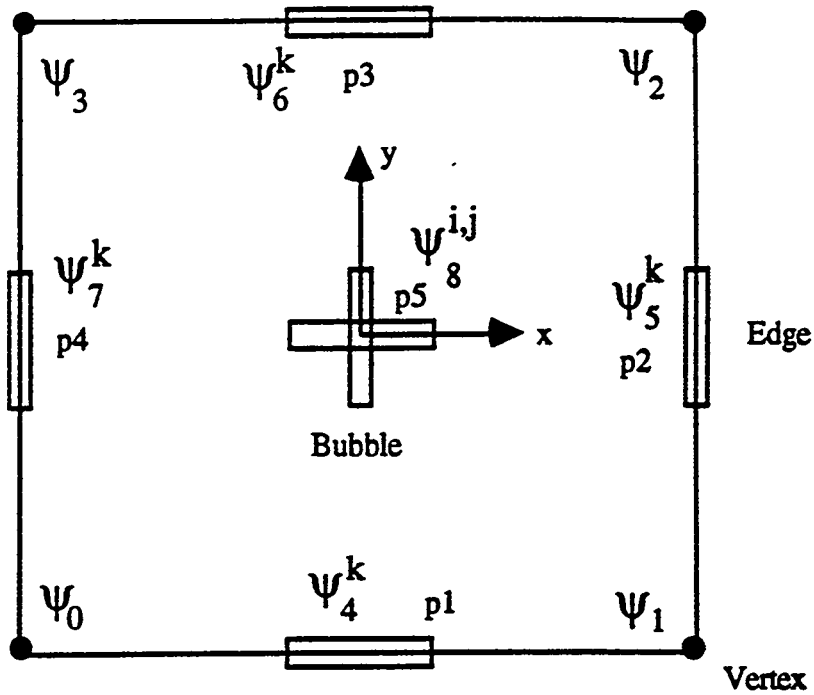

hierarchical polynomials

$$P_0(x) = (1-x)/2$$

$$P_1(x) = (1+x)/2$$

$$P_{2n}(x) = \frac{1}{2n!}x(x^{2n}-1)$$

$$P_{2n+1}(x) = \frac{1}{(2n+1)!}(x^{2n}-1)$$

node function

$$\Psi_0(x,y) = P_0(x)P_0(y)$$

edge function

$$\Psi_4^k(x,y) = P_k(x)P_0(y) \quad k = 2,\ldots,p_1$$

bubble function

$$\Psi_8^{i,j}(x,y) = P_i(x)P_j(y), \quad 2 \le i,j \le p_5$$

degrees of freedom

$$dof = 4 + \sum_{i=1}^{4}(p_i - 1) + (p_5 - 1)^2$$

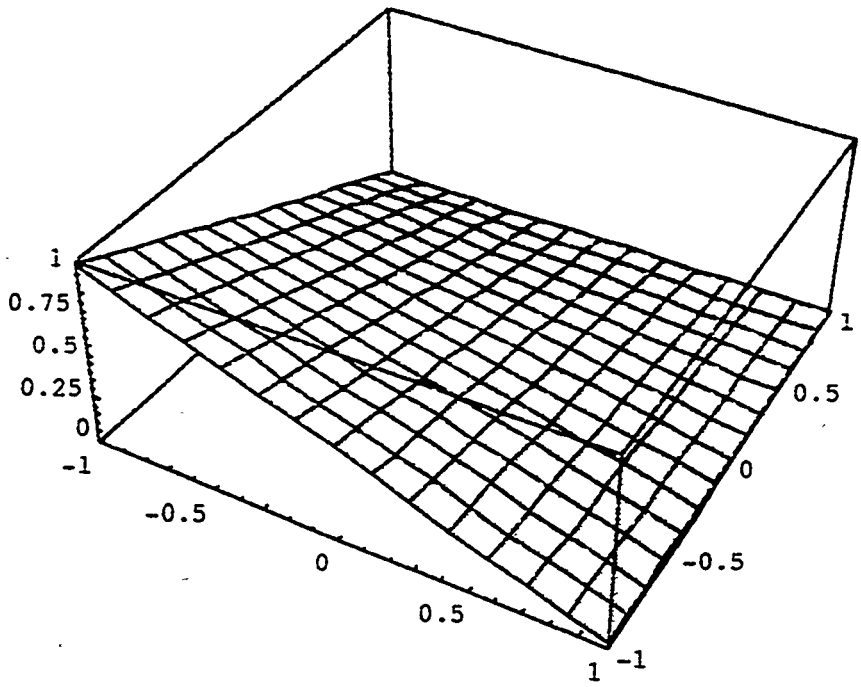

Typical vertex function.

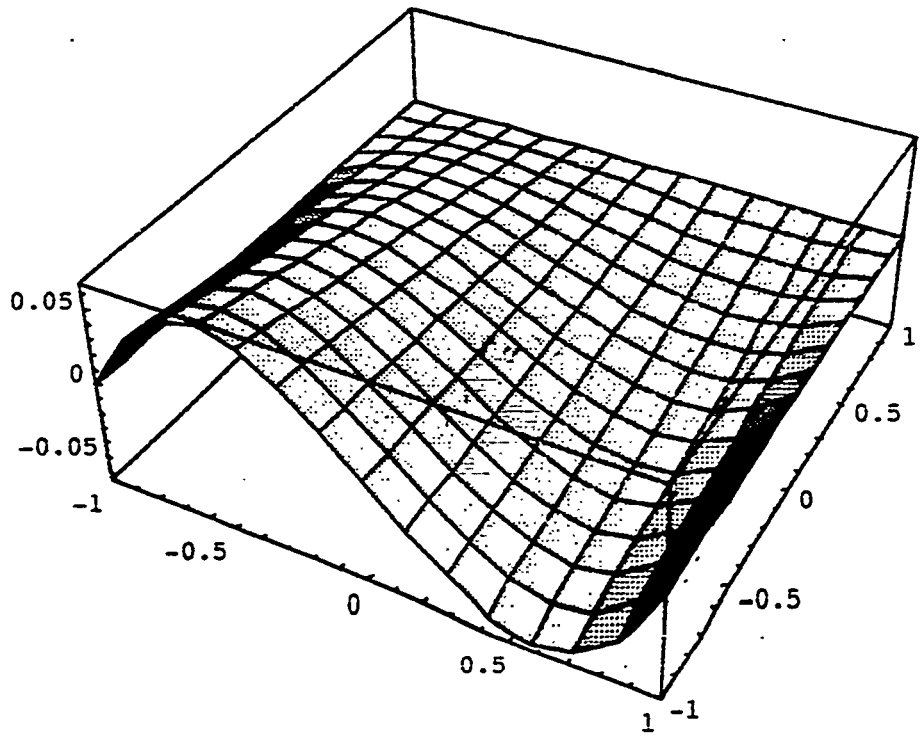

Edge function with p=3.

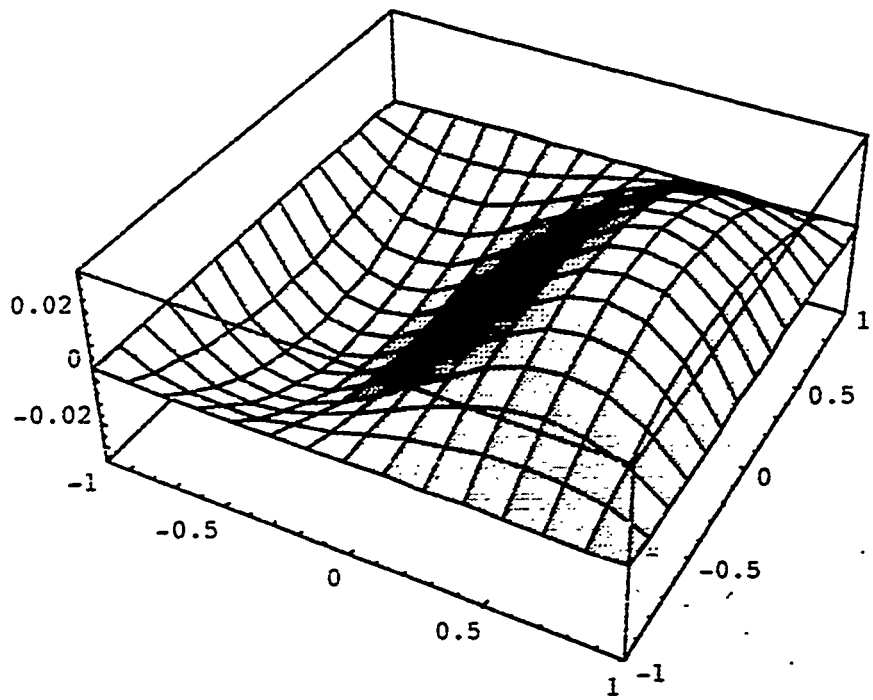

Typical bubble function, $\psi(x,y) = p_3(x)p_4(y)$

1-irregular grid

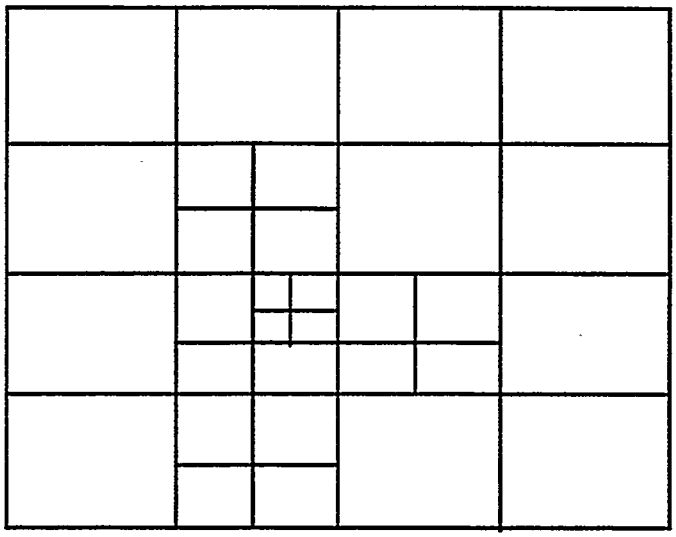

A node in the mesh is regular if it is a vertex for each neighbor element otherwise it is irregular. If the maximum number of irregular nodes on an element side is one then the mesh is 1-irregular.[2] A 1-irregular quadrilateral mesh is shown.

Continuity is not guaranteed where there is an irregular node. As can be seen in Fig. 8, the number of degrees of freedom along the edge from the right is greater than the number from the left, corresponding to different approximating spaces of functions.

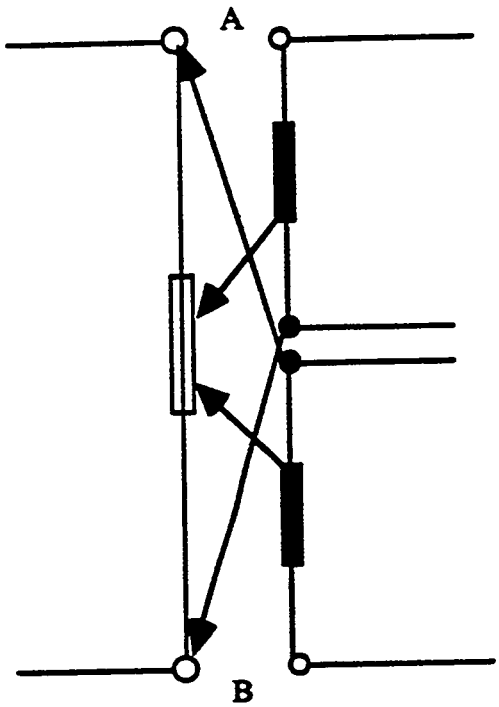

Figure 8. Typical 1-irregular interface between elements. The dark nodes must be constrained to insure continuity across the interface.

Additional constraints must be placed on the functions allowed along AB from the right. The three edge nodes are required to have the same order and are associated with the same degrees of freedom. The coefficients associated with the constrained nodes are replaced by the ones at the unconstrained nodes as shown by the arrows in the figure. The approximating function space is therefore reduce. The additional degrees of freedom from the right are used to modify basis functions along the constrained edge.

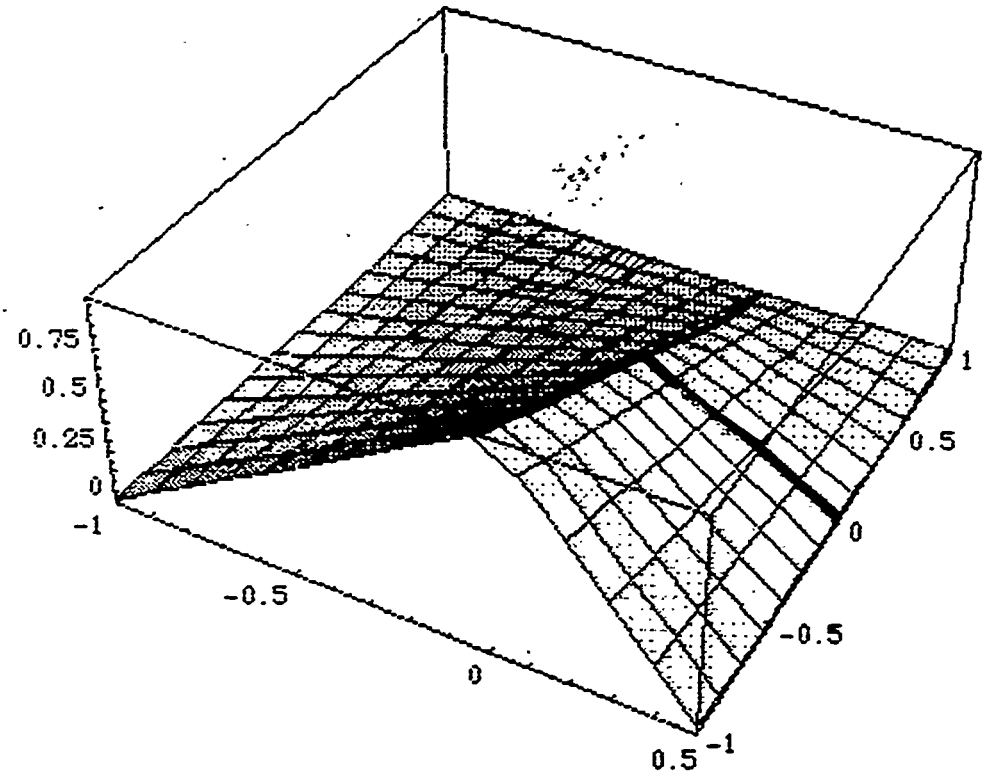

The constrained shape functions associated with B=1 in the configuration shown in Fig. 8.

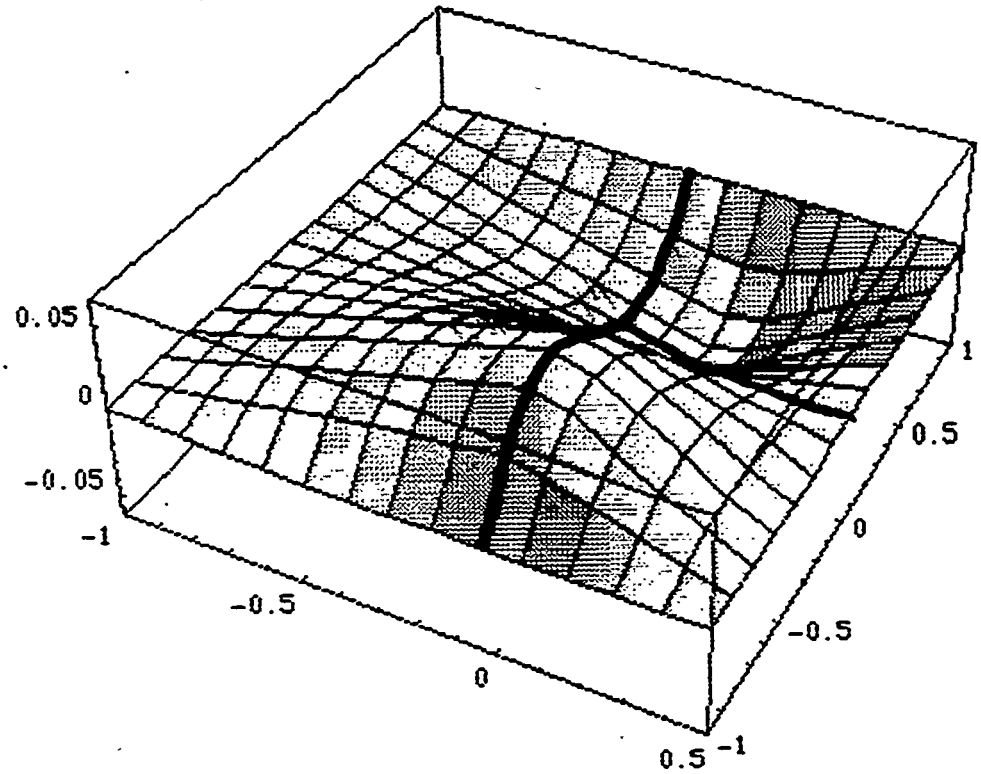

■ Two wire divertor model: original grid

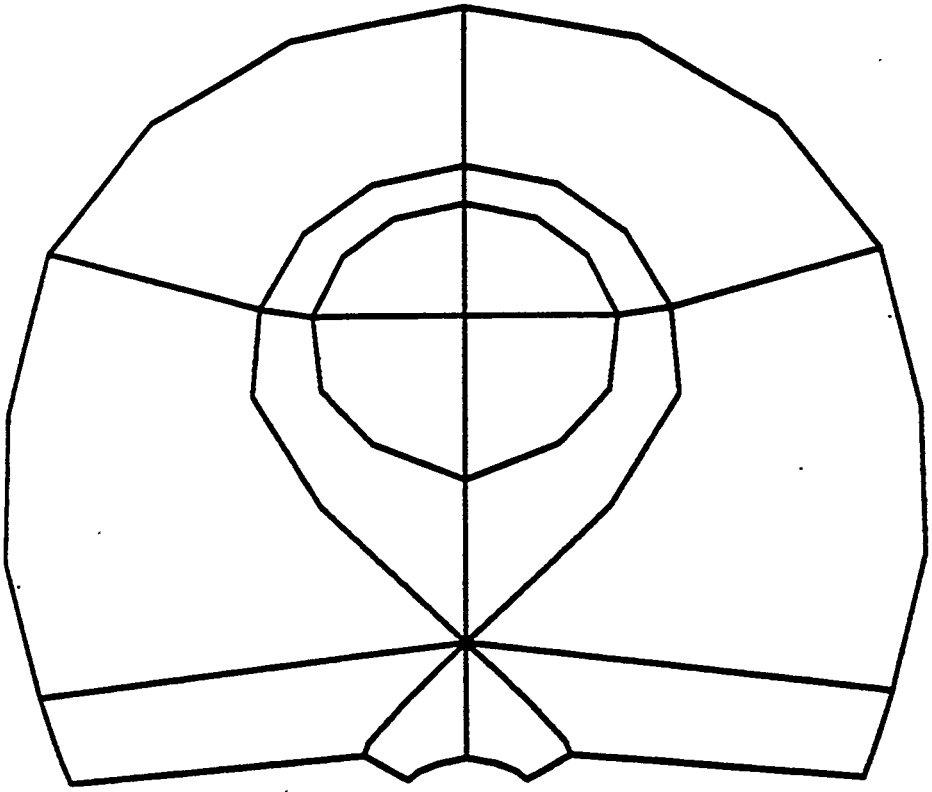

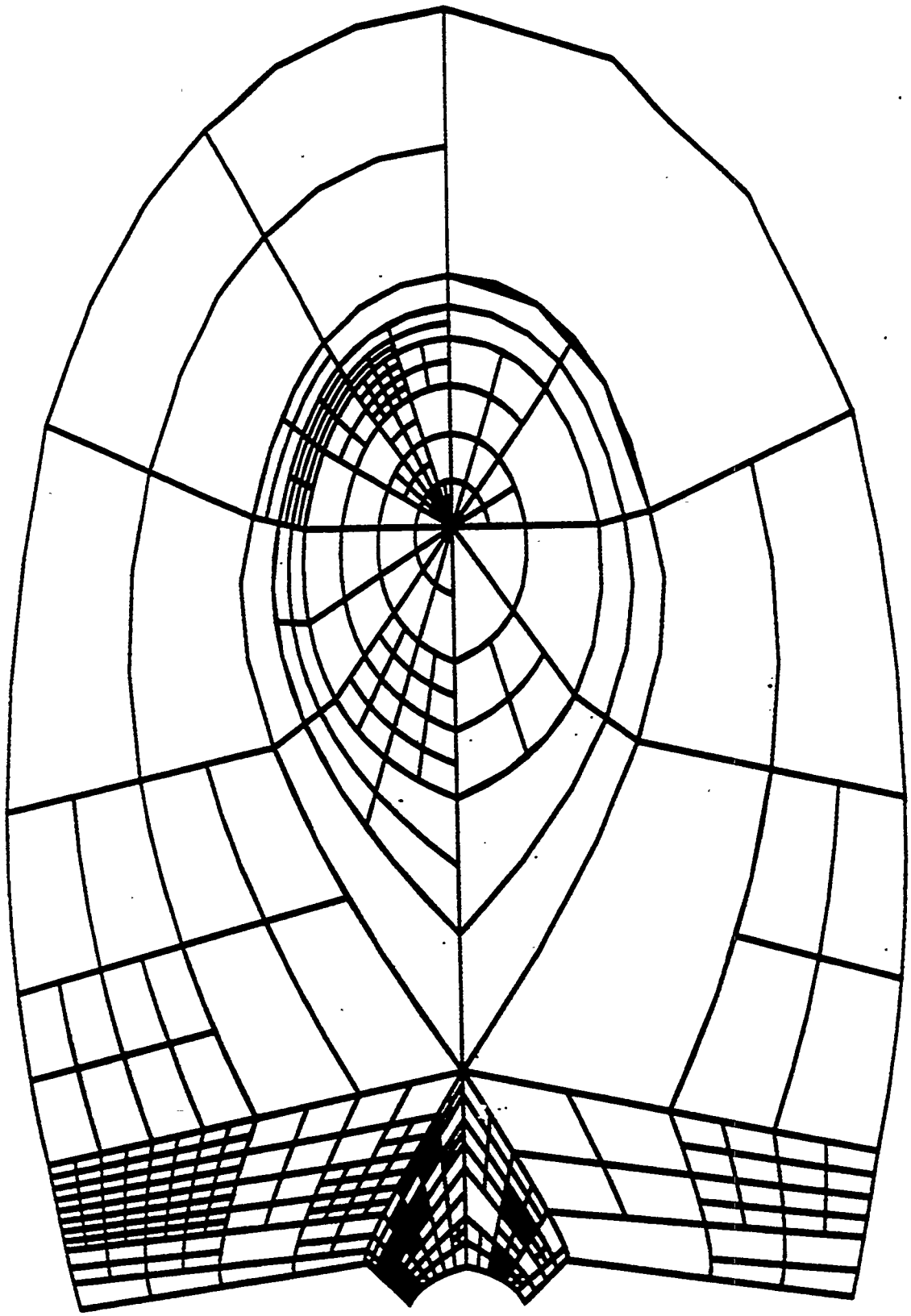

External Two Wire Problem
Approximation

uniform h and p-refinement

# Elements	dof	r	p	L_inf	‖u-v‖/‖v‖	
16	25	0	0	5.20E-02	4.77E-02	*
16	81	0	1	6.20E-03	5.41E-03	
16	169	0	2	2.90E-03	1.56E-03	
16	289	0	3	7.60E-04	2.39E-04	*
64	81	1	0	1.80E-02	1.09E-02	
64	289	1	1	2.20E-03	1.05E-03	
64	625	1	2	5.90E-04	1.24E-04	
64	1089	1	3	2.00E-04	2.99E-05	
256	289	2	0	6.70E-03	2.79E-03	
256	1089	2	1	7.40E-04	1.51E-04	
1024	1089	3	0	1.90E-03	7.10E-04	*

Approximation Error

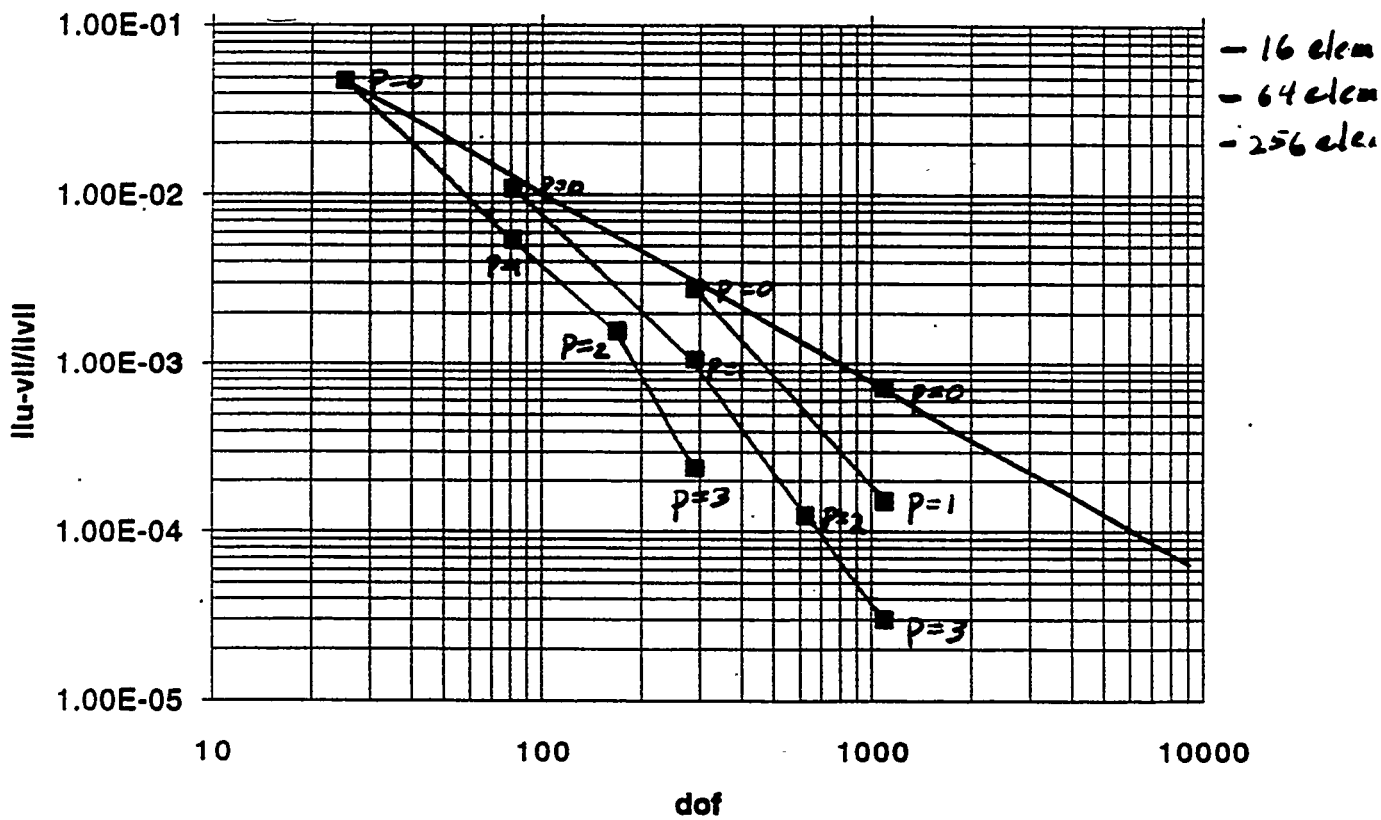

hp Finite Element Methods

- hp methods attempt to increase computational efficiency by adaptively modifying the mesh size, h, and the polynomial order, p.

The cost for this increase in efficiency is complexity:

- Locally refined h, implies irregular grids. Here we restrict the grid to a 1-irregular type.

- Varying p and irregular mesh, implies need for additional constraint equations to maintain C_0 approximation.

- To guide refinement, a posteriori error estimates (control variable) and refinement strategies (control algorithm) are needed.

- High polynomial orders can increase condition number of linear systems, requiring advanced preconditioners.

- Varying polynomial order, mesh spacing, and constraints require dynamic data structures.

- Need for significant computational resources suggest parallel execution, which adds complexity.

hp finite element calculation of the interaction of an acoustic fluid and a submerged elastic structure

by

A. Safjan

System

- Equations of linear acoustics
- Equations of elastodynamics
- Contact conditions
- Nonreflecting boundary conditions

Numerical solution

- Adaptive hp finite element method in space
- 2- stage 4th order Taylor-Galerkin

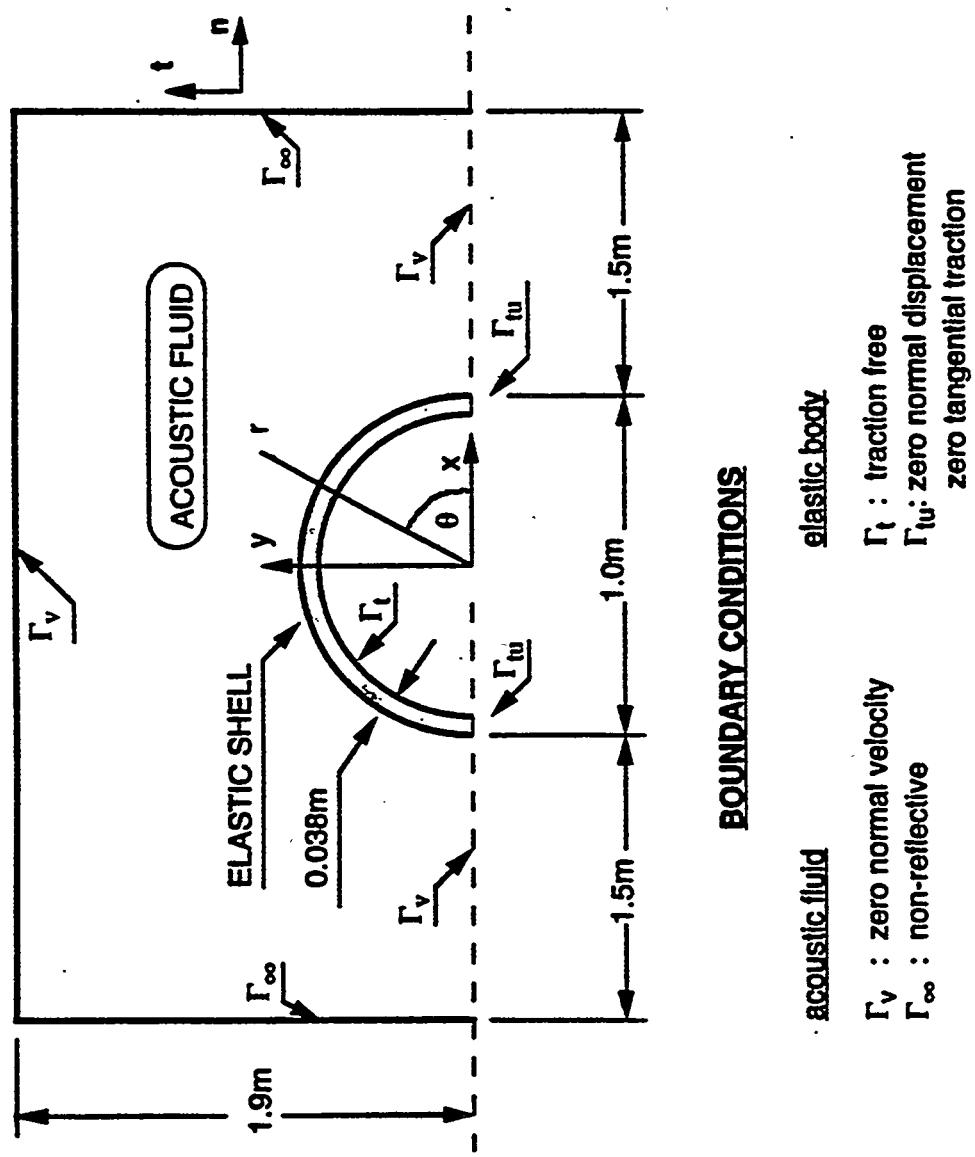

Fig. 78. Plane progressive wave impinging on a cylindrical elastic shell. Problem definition.

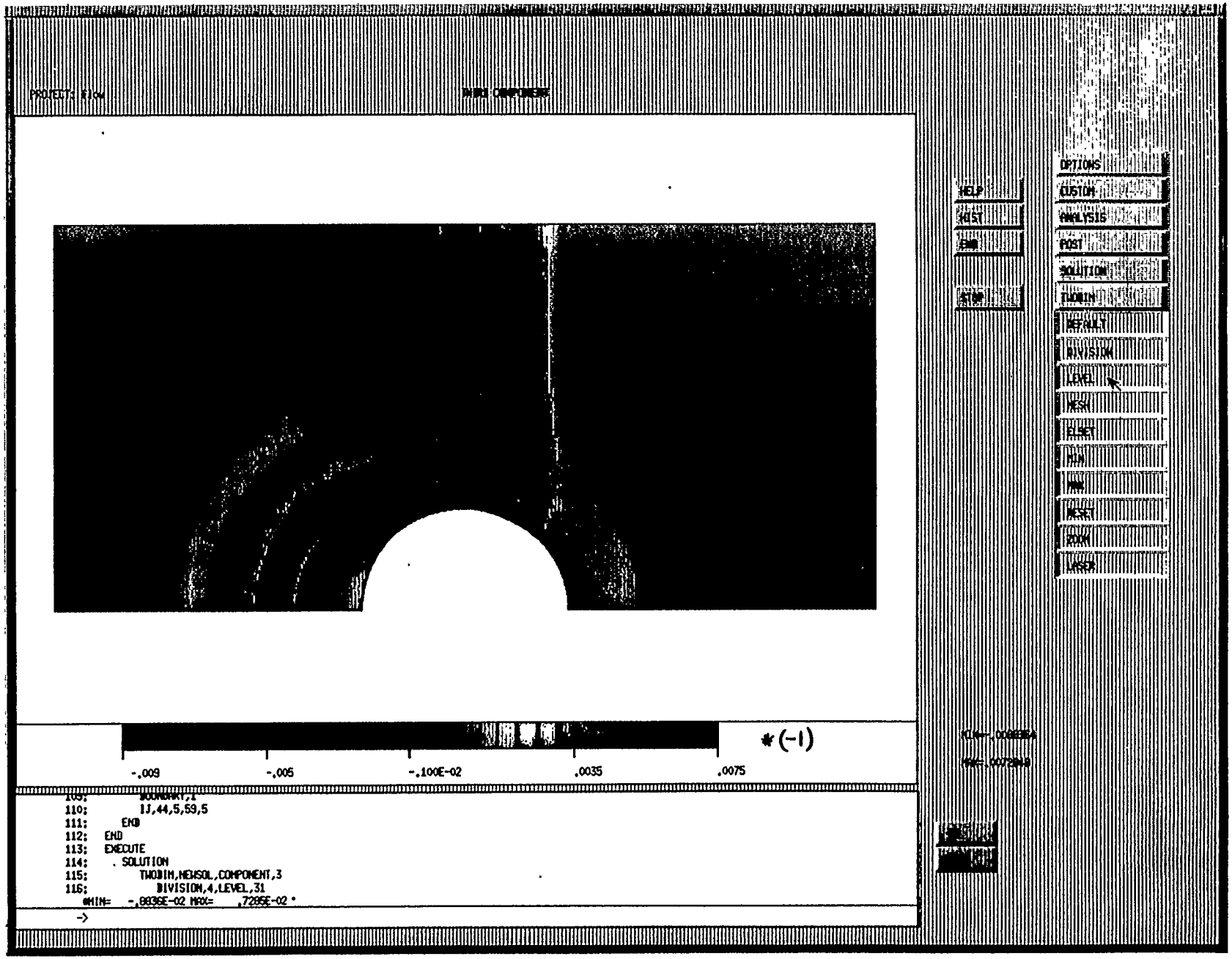
PROJECT: Flow
HELP
HIST
END
STOP
OPTIONS
CUSTOM
ANALYSIS
POST
SOLUTION
TWODIM
DEFAULT
DIVISION
LEVEL
MESH
ELSET
RUN
MAN
RESET
ZOOM
LASER
*(-1)
-.009
-.005
-.100E-02
.0035
.0075
110: IJ,44,5,59,5
111: END
112: END
113: EXECUTE
114: . SOLUTION
115: TWODIM,NEWSOL,COMPONENT,3
116: DIVISION,4,LEVEL,31
MIN= -.8836E-02 MAX= .7285E-02
->

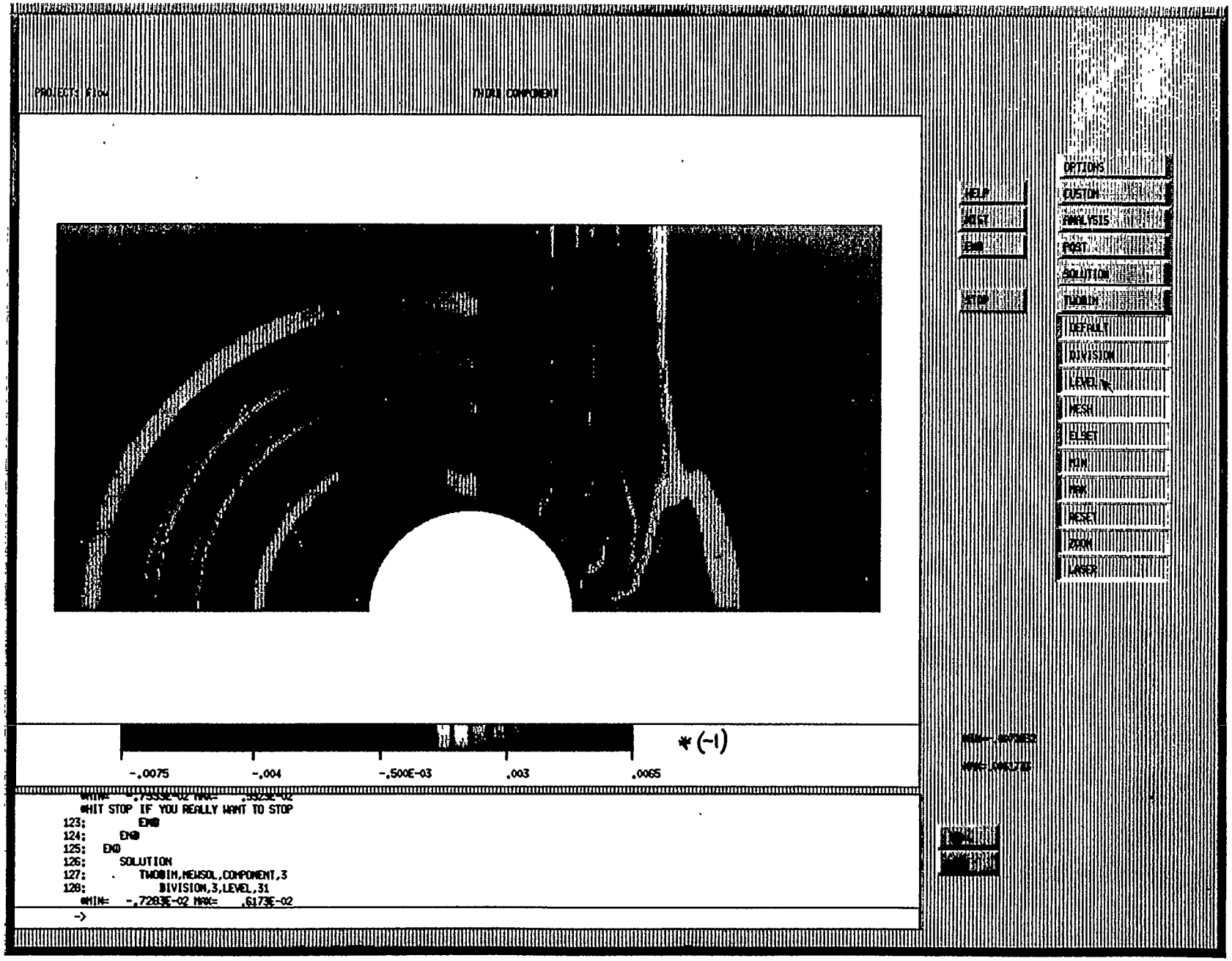

Fig. 7 Elastic scattering problem. Pressure p^* at time $t^* = 1.5$

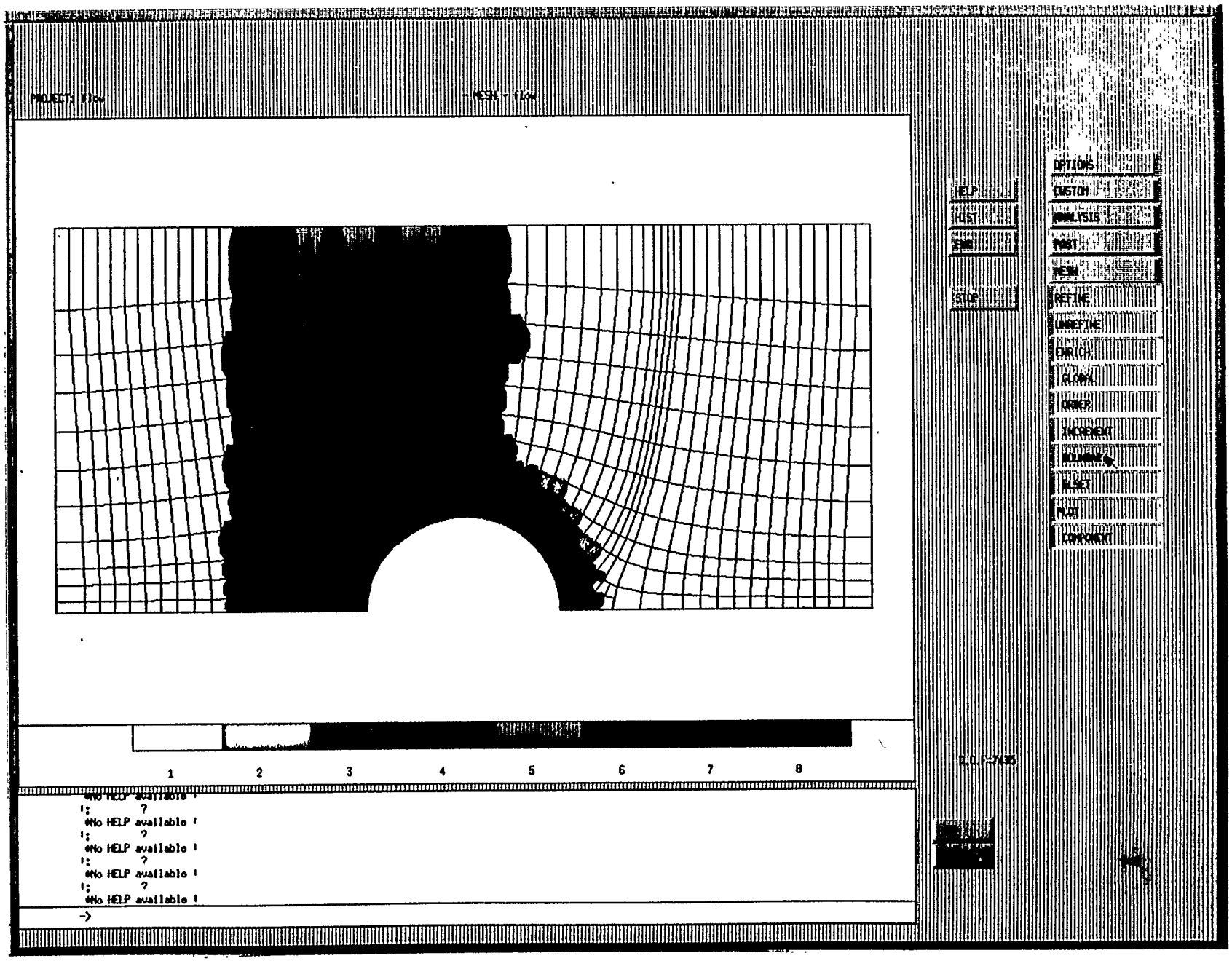

Fig. 23 Elastic scattering problem. An *h-p* adaptive finite element mesh at

ADAPTIVE NUMERICAL METHODS FOR PARTIAL DIFFERENTIAL EQUATIONS

PHILLIP COLELLA

MECHANICAL ENGINEERING, UC BERKELEY

AND

CENTER FOR COMPUTATIONAL SCIENCES AND ENGINEERING, LLNL

PART OF THE DOE HPCC GRAND CHALLENGE PROJECT IN COMPUTATIONAL FLUID DYNAMICS AND COMBUSTION DYNAMICS (LLNL, LANL, NYU, UCB)

PROBLEM DOMAIN: NUMERICAL SOLUTION OF PDE'S OF CLASSICAL TYPE (HYPERBOLIC, PARABOLIC, ELLIPTIC)

LARGE NUMBER OF PHYSICAL PROBLEMS CAN BE DESCRIBED USING COMBINATIONS OF SUCH EQUATIONS

- COMBUSTION
- SUBSURFACE FLOWS
- SOLID MECHANICS
- MATERIALS PROCESSING
- SEMICONDUCTORS

EXAMPLE

$$\frac{\partial \vec{u}}{\partial t} + (\vec{u}\cdot\nabla)\vec{u} + \frac{L}{\rho}\nabla p = \nu \Delta \vec{u}$$

PARABOLIC

HYPERBOLIC

ELLIPTIC

$$\nabla \cdot \vec{u} = 0$$

PREDICTOR-CORRECTOR METHODS TO ISOLATE AND TREAT SEPARATELY EACH DIFFERENT TERM.

DESIGN PRINCIPLES FOR UNDERLYING DISCRETIZATIONS

- FINITE DIFFERENCES ON (SMOOTH MAPPINGS OF) RECTANGULAR GRIDS – EASY TO CONSTRUCT ACCURATE DISCRETIZATIONS

$$\left.\frac{df}{dx}\right|_{jh} \approx \frac{f((j+1)h) - f((j-1)h)}{2h} + O(h^2)$$

(CANCELLATION OF TERMS IN TAYLOR EXPANSION)

- CONSERVATION FORM

$$\nabla\cdot\vec{F} \approx \frac{1}{h}\left(F^x_{i+\frac{1}{2},j} - F^x_{i-\frac{1}{2},j}\right) + \frac{1}{h}\left(F^y_{i,j+\frac{1}{2}} - F^y_{i,j-\frac{1}{2}}\right)$$

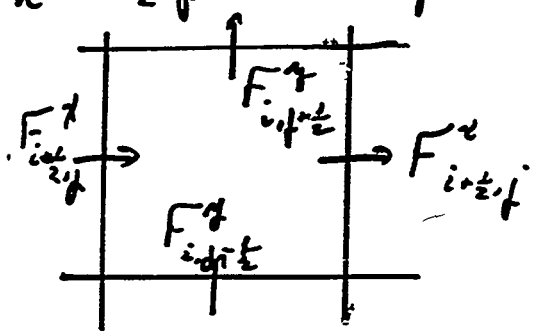

DISCRETE ANALOG OF INTEGRAL CONSERVATION LAWS (E.G. MASS, MOMENTUM, ENERGY) $\Longrightarrow$ CORRECT COMPUTATION OF DISCONTINUITI AS WEAK SOLUTIONS

SOLVABILITY FOR ELLIPTIC PROBLEMS:

$$\Delta\varphi = \nabla\cdot\vec{u} \quad \text{ON } \Omega$$
$$\frac{\partial\varphi}{\partial n} = 0 \quad \text{ON } \partial\Omega$$

$\vec{u}\cdot\hat{n} = 0$ ON $\partial\Omega \Longrightarrow \int \nabla\cdot\vec{u}\,dx = 0$ i.e. SOLVABILITY

DESIGN PRINCIPLES (CONT'D)

- USE OF UPWIND SCHEMES, LIMITERS FOR HYPERBOLIC TERMS

  DEGRADES GRACEFULLY IN UNDERRESOLVED REGIONS

  WELL-POSED BOUNDARY CONDITIONS FOR INITIAL / BOUNDARY VALUE PROBLEM BUILT IN.

  LOW PHASE ERROR PROPERTIES

MAY WANT TO RUN CALCULATIONS FOR WHICH LARGE PARTS OF THE DOMAIN ARE MARGINALLY RESOLVED: ROBUSTNESS, MACROSCOPIC CONSERVATION LAWS ESSENTIAL IN THAT SETTING.

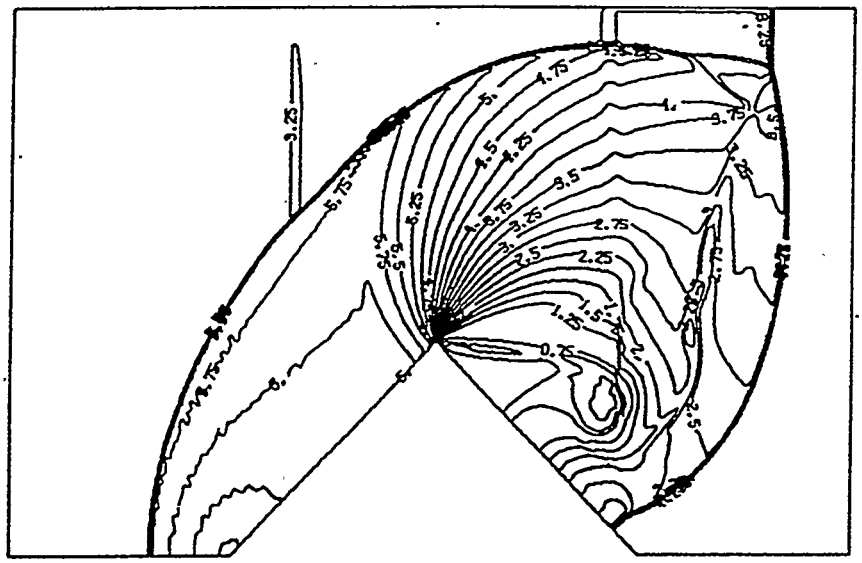

Density contours
440×220 grid

Experimental Interferogr
of Zhang and Glass

Fig.3. Comparison of numerical solution with experiment for shock diffraction over a half-diamond cyli
Shock Mach number is 2.45.

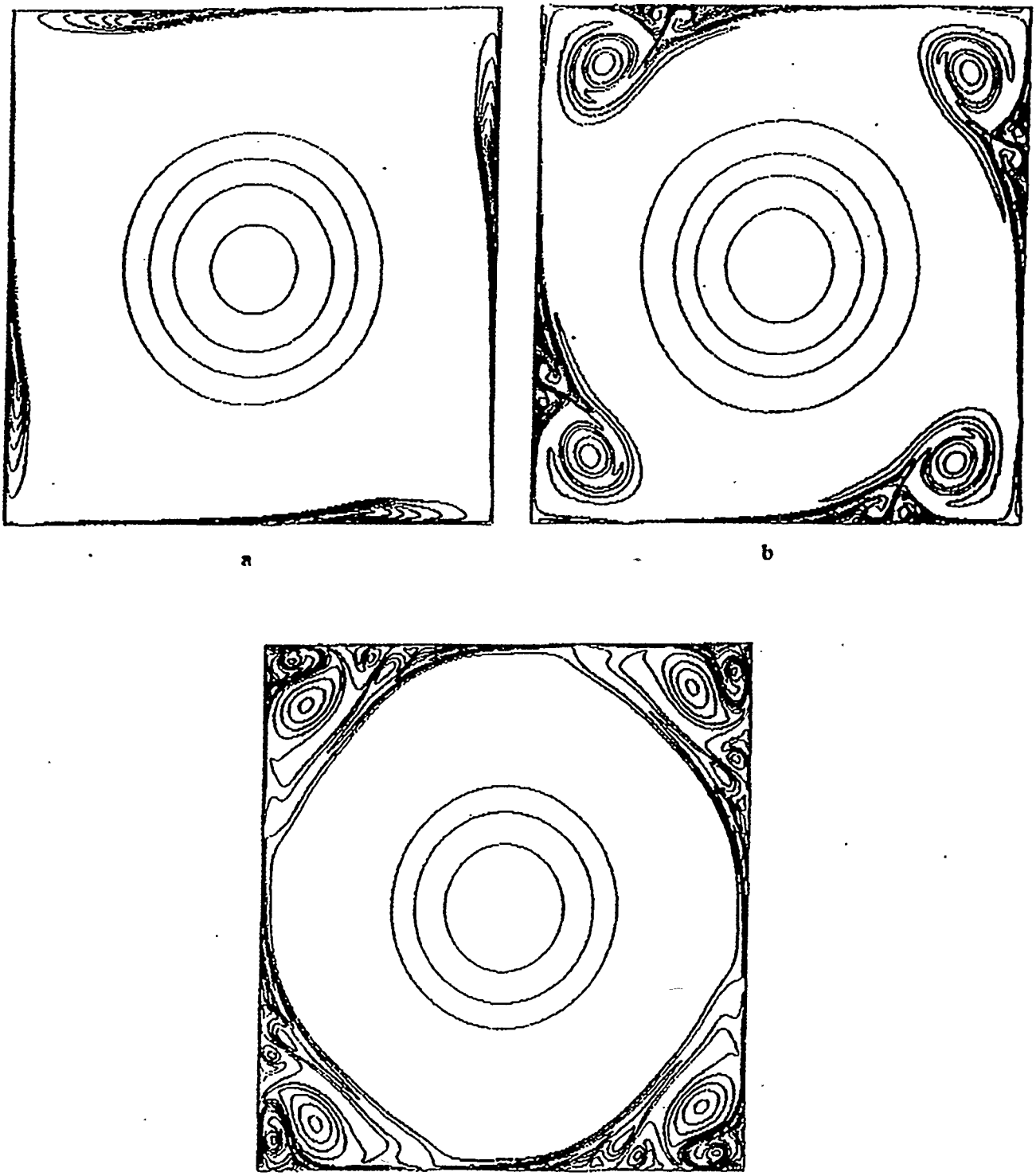

Figure 1. Spindown of a vortex in a box on a 256×256 grid. The maximum velocity in the initial data is .0686, and the length of the sides of the box is 1. Vorticity contours are shown at times 20 (a), 40 (b), and 60 (c). The total number of time steps taken is approximately 1100.

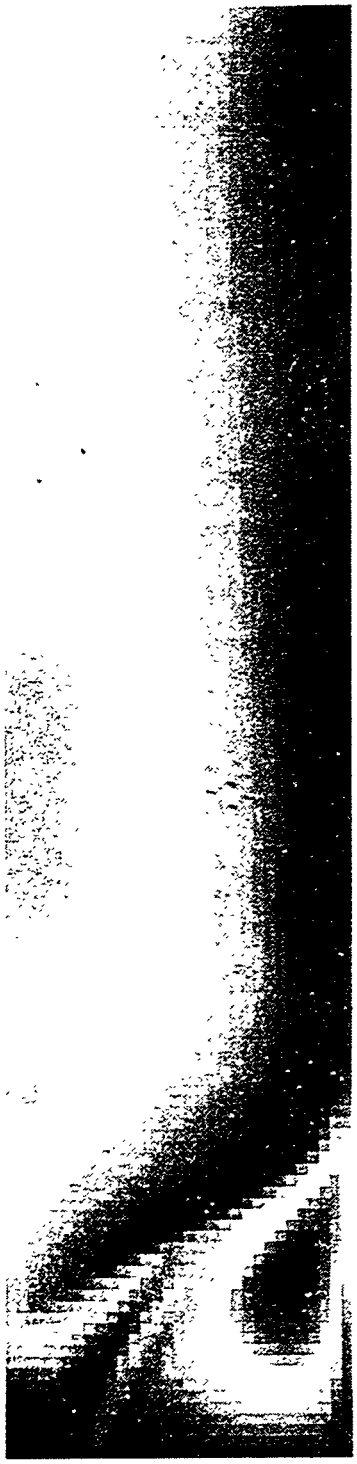

Turbulent viscosity

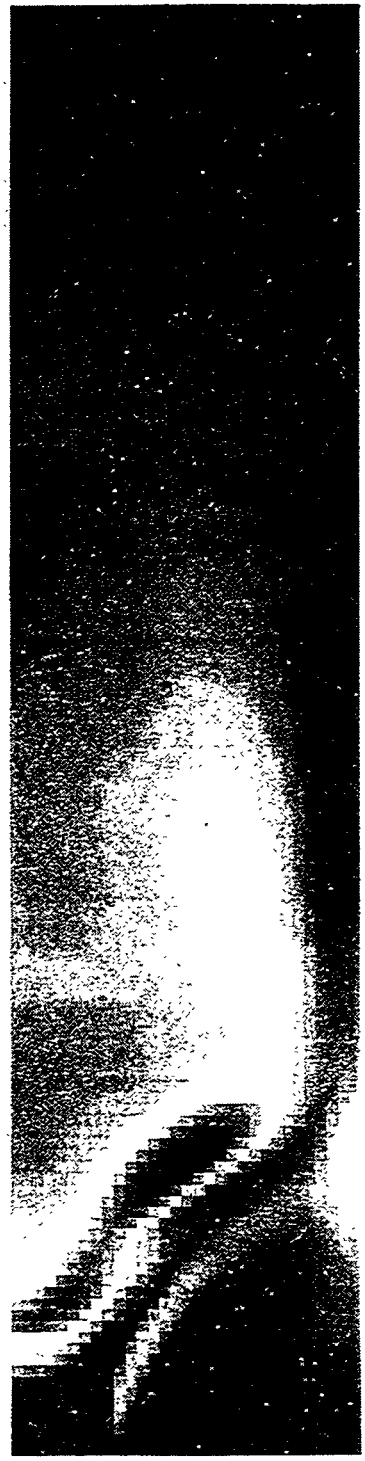

Turbulent kinetic energy

Turbulent dissipation rate

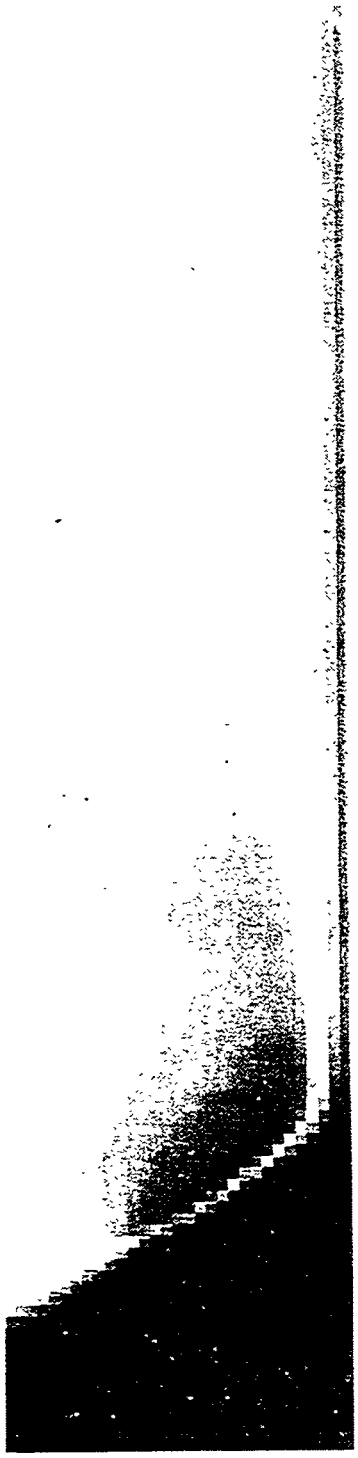

Temperature

Fuel

Product

ADAPTIVE MESH REFINEMENT (AMR) (BERGER + OLIGER, 1984)

CONCENTRATE COMPUTATIONAL EFFORT WHERE IT IS MOST NEEDED BY LOCALLY REFINING GRID.

- REFINEMENT IN BOTH SPACE AND TIME
- REFINED REGIONS CHANGE AS A FUNCTION OF TIME, IN RESPONSE TO CHANGING FEATURES IN THE SOLUTION.

BLOCK-STRUCTURED LOCAL REFINEMENT: REFINED REGIONS ARE ORGANIZED INTO RECTANGULAR BLOCKS THAT COVER THE REGION OF INTEREST (100'S - 1000'S PTS / BLOCK).

- OVERHEAD OF MANIPULATING IRREGULAR DATA STRUCTURE AMORTIZED OVER LARGE REGULAR CALCULATIONS.

- CLEAN SEPARATION OF FLOATING-POINT INTENSIVE WORK ON REGULAR ARRAYS AND MANIPULATION OF NON-ARRAY STRUCTURES.

- SOME FLOATING POINT WORK DONE ON IRREGULAR SUBSETS OF REGULAR DATA STRUCTURES, BUT SMALL FRACTION OF TOTAL CALCULATION.

Locally Refined Grid Structure

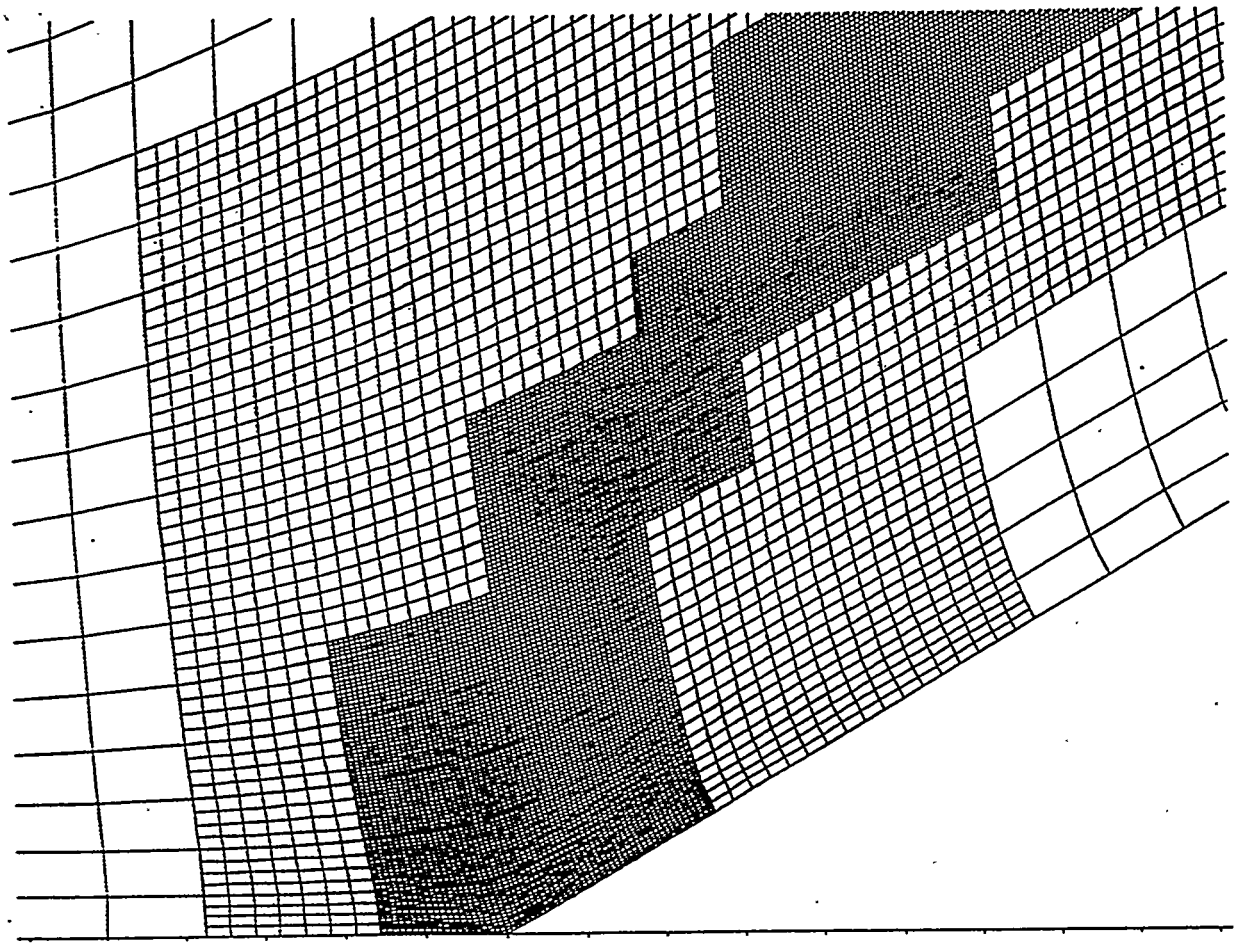

AMR TIME EVOLUTION - HYPERBOLIC CASE

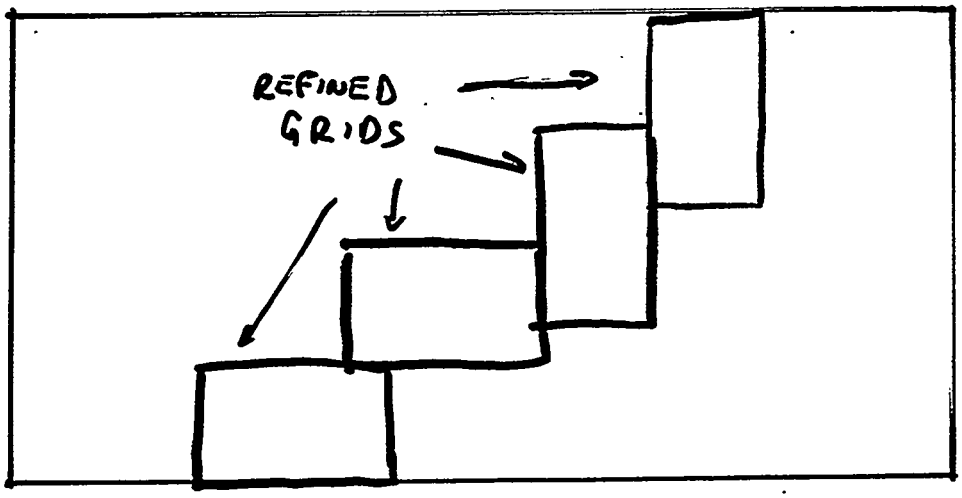

(1) ADVANCE COARSE GRID IN TIME (INCLUDING CELLS COVERED BY FINE GRID)

(2) ADVANCE FINE GRID IN TIME, INTERPOLATING VALUES FROM COARSE GRID FOR BOUNDARY CONDITIONS (n_{ref} TIMES)

(3) SYNCHRONIZE COARSE GRIDS WITH FINE GRIDS

- AVERAGE FINE GRID VALUES ONTO COARSE GRID
- ADJUST COARSE GRID VALUES ADJACENT TO FINE GRID SO THAT CONSERVATION HOLDS:

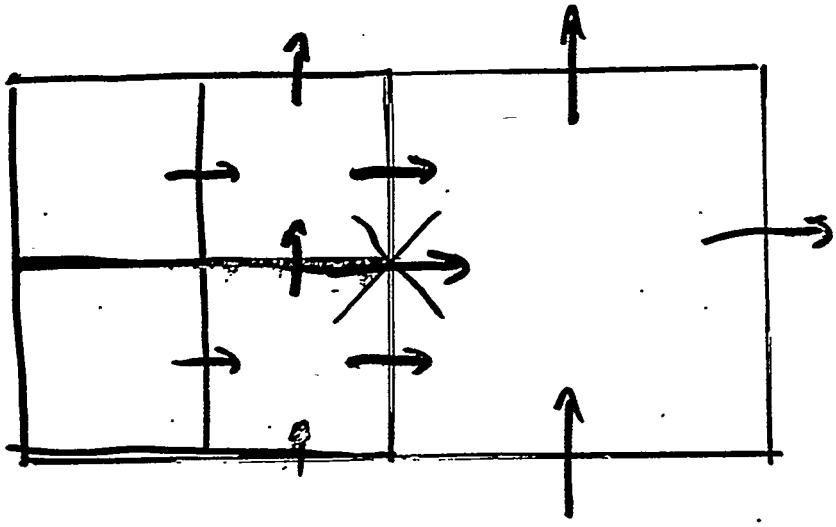

AMR FOR INCOMPRESSIBLE FLOW:

PRINCIPAL NEW ISSUE: WHAT ARE MATCHING CONDITIONS AT C/F INTERFACE FOR ELLIPTIC/PARABOLIC PROBLEMS?

ANSWER: INTERPOLATION AND FLUX MATCHING CONDITIONS (BOTH DIRICHLET AND NEUMANN DATA MUST MATCH)

— OTHERWISE, COARSE-GRID ERROR CONTAMINATES FINE-GRID PART OF SOL'N.

EXAMPLE: $\Delta^S \varphi = \rho$

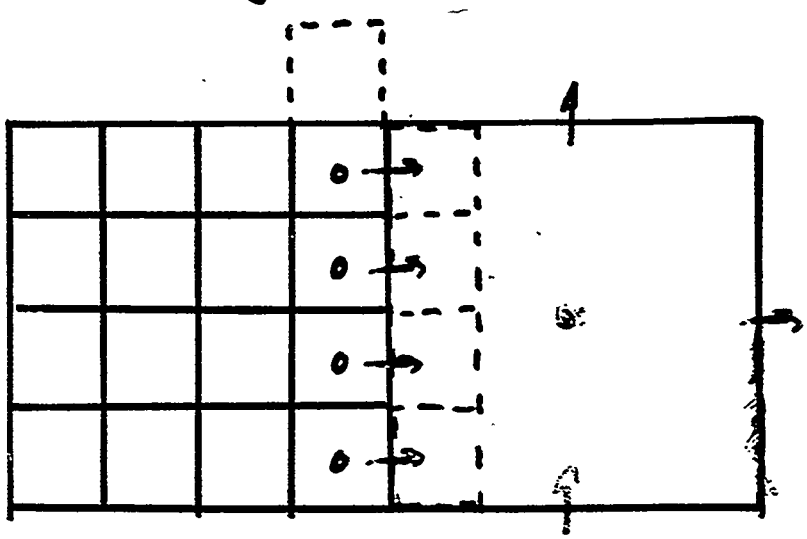

(1) TO COMPUTE $\Delta^S \varphi$ AT $\circ$, INTERPOLATE VALUES FROM COARSE GRID ONTO GHOST CELLS $\square$

(2) TO COMPUTE $\Delta^S \varphi$ AT $\bullet$, USE AVERAGE OF FINE GRID FLUXES $\left(\Delta\varphi = \nabla \cdot \vec{F}, \ \vec{F} = \left(\frac{\partial \varphi}{\partial x}, \frac{\partial \varphi}{\partial y} \right) \right)$ AS LEFT FLUX BOUNDARY CONDITION.

MULTIGRID USED TO SOLVE C/F EQUATIONS.

CONSERVATION FORM OF COMBINED OPERATOR <u>ESSENTIAL</u> — GUARANTEES SOLVABILITY AT EACH STEP.

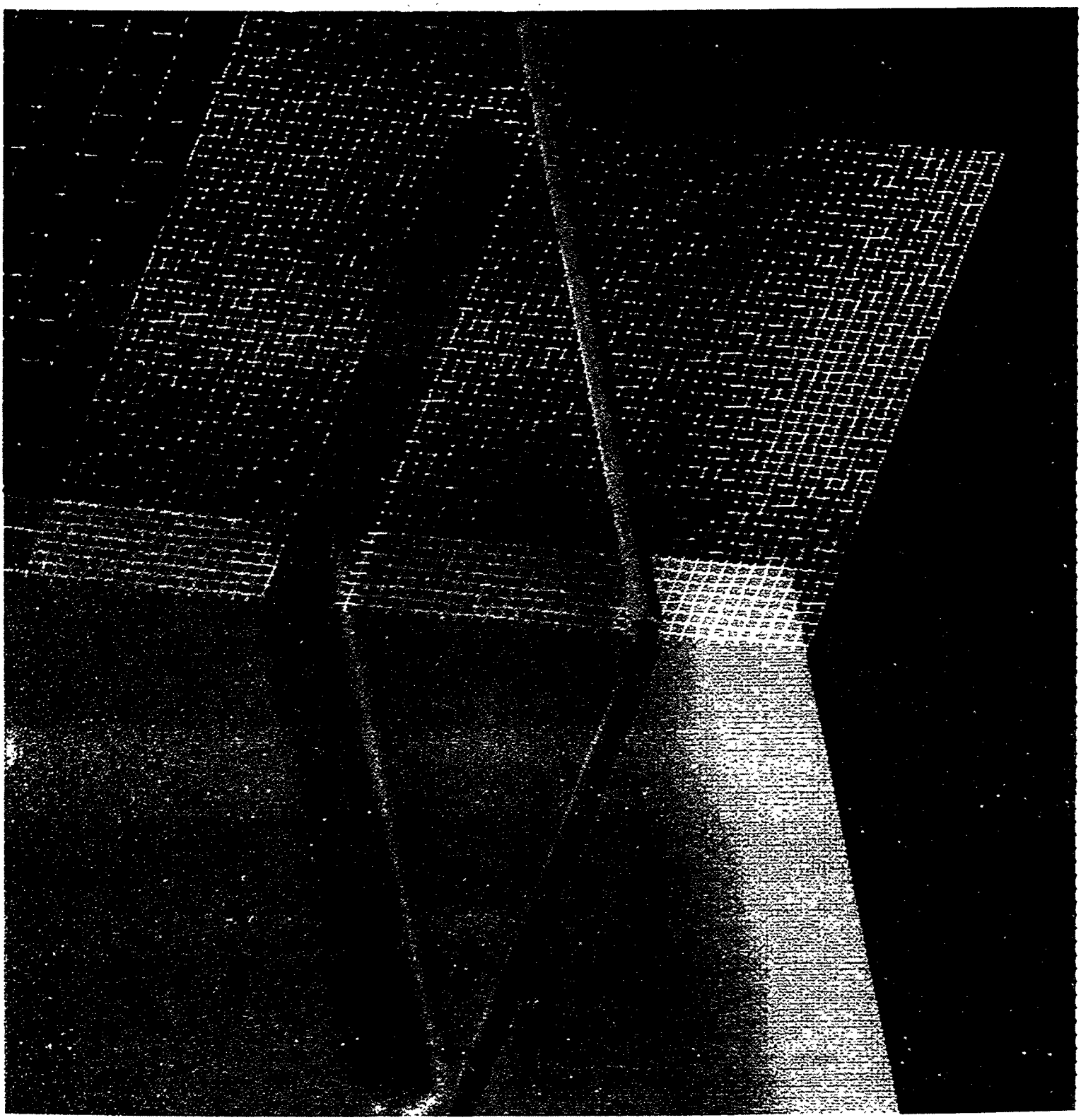

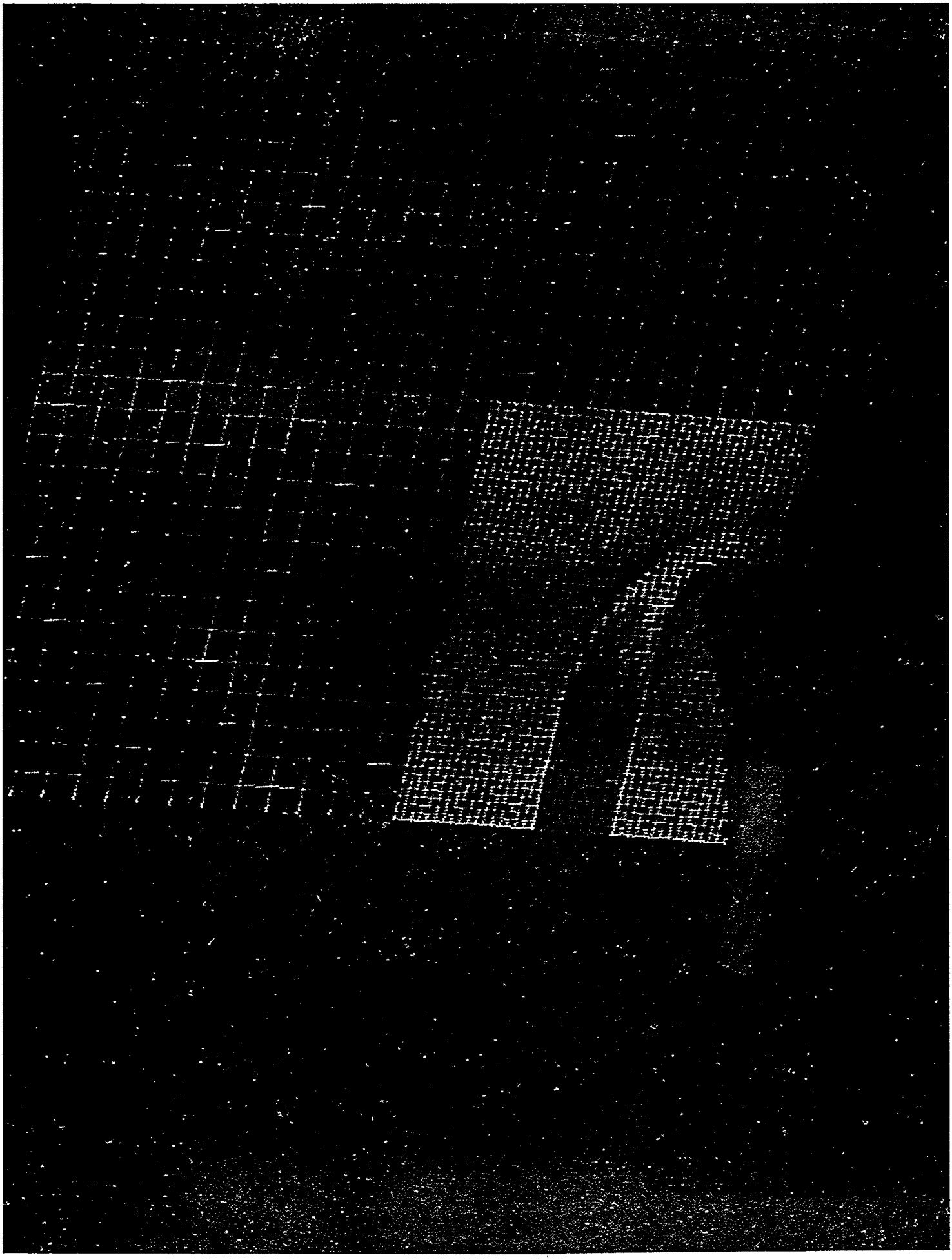

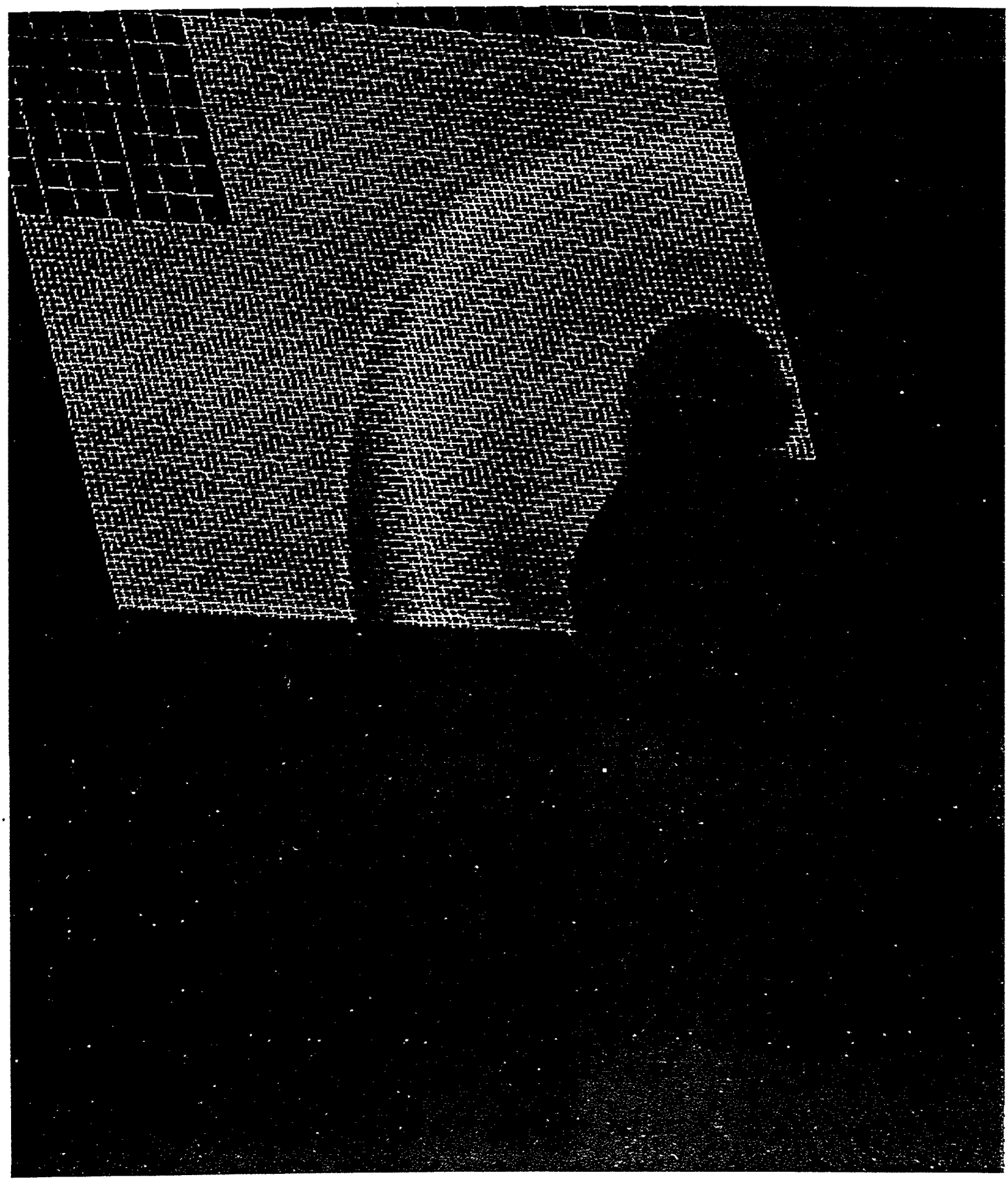

ALMGREN, BELL, COLELLA, HOWELL (1993)

Dynamics of an Inviscid Co-flowing Jet: Vorticity

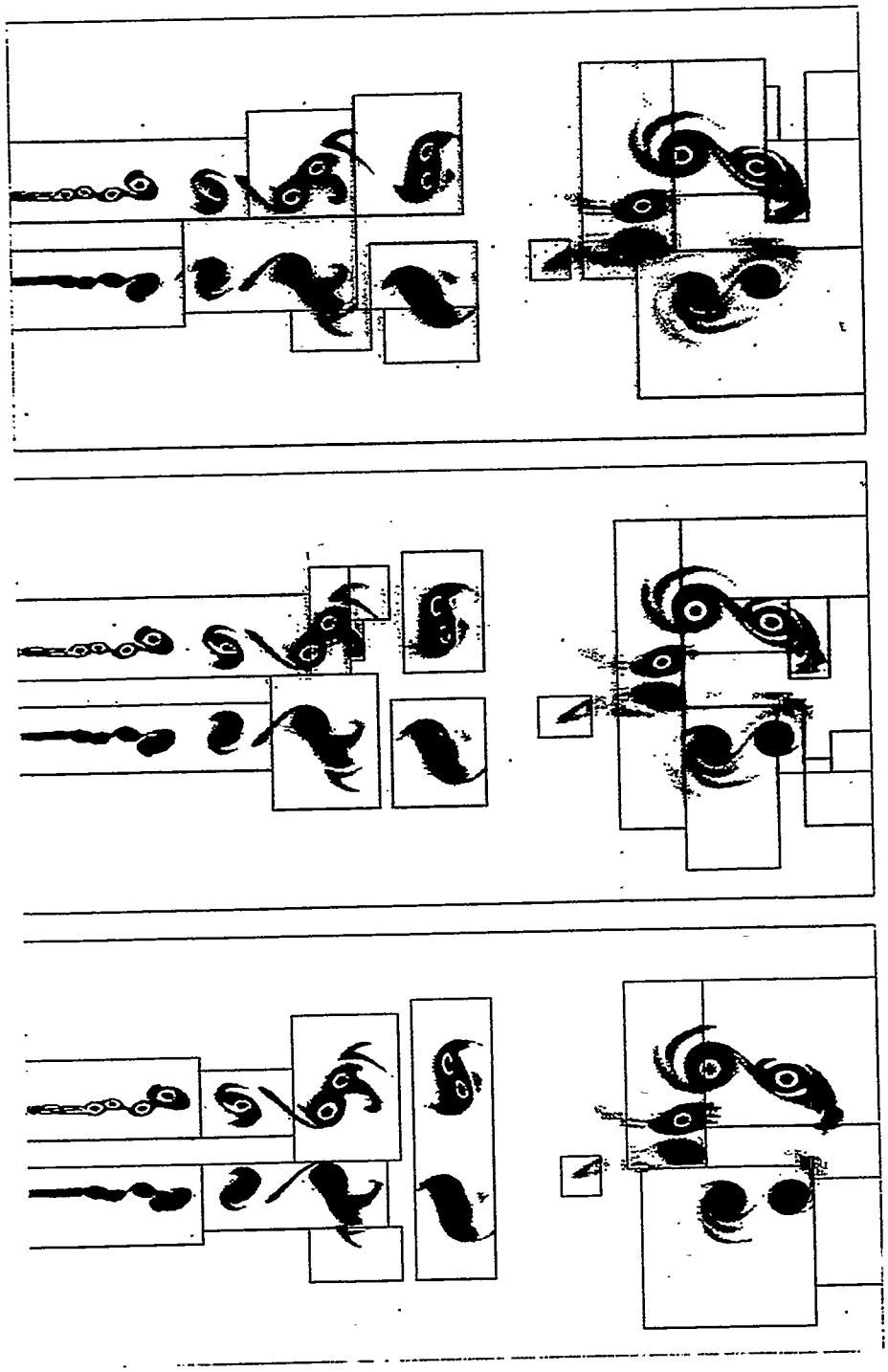

Anelastic Bubble Rise in an Adiabatic Atmosphere.

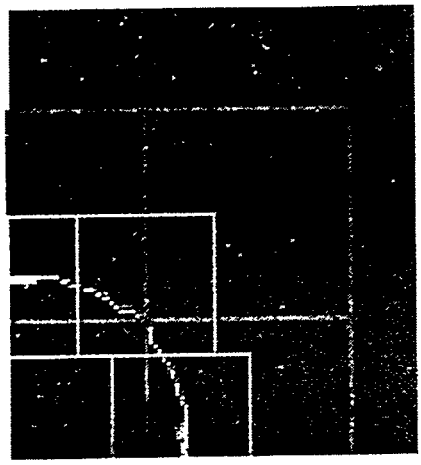

XY Slice

XZ Slice

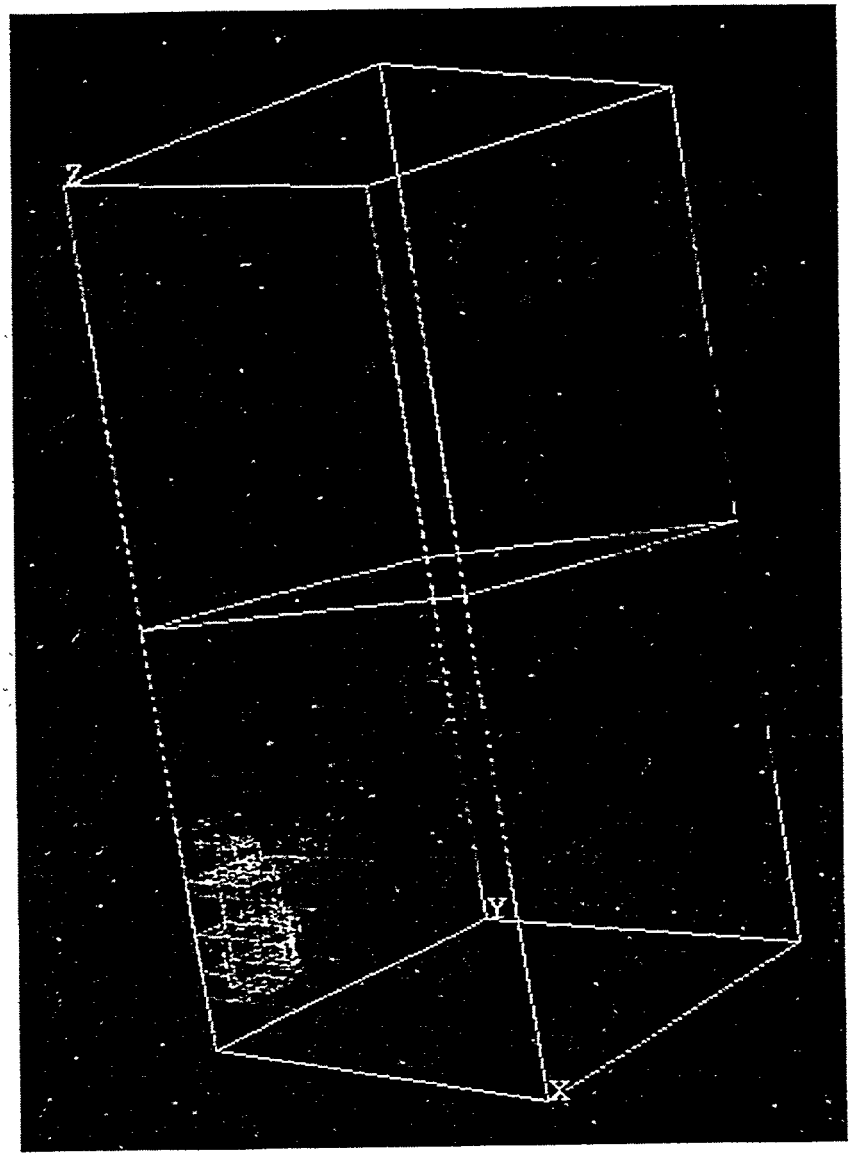

Grid Configutation

Density at Time = 6.75 Seconds

Anelastic Bubble Rise in an Adiabatic Atmosphere.

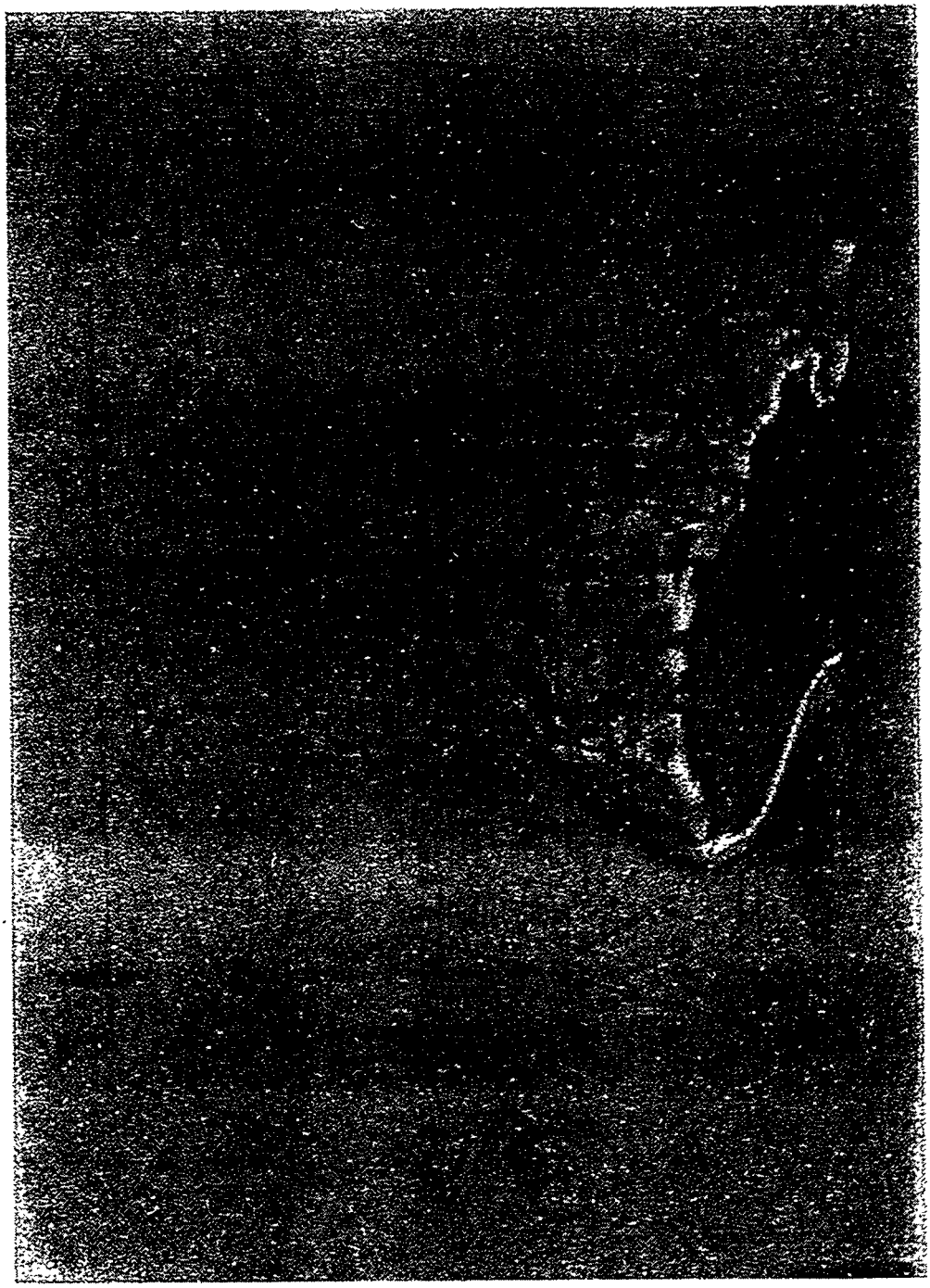

Bubble Tracer at Time = 6.75 Seconds

Anelastic Bubble Rise in an Adiabatic Atmosphere.

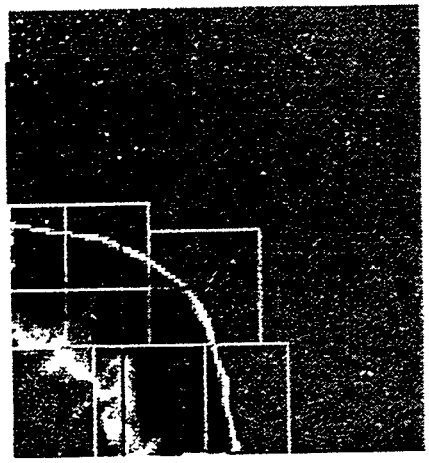

XY Slice

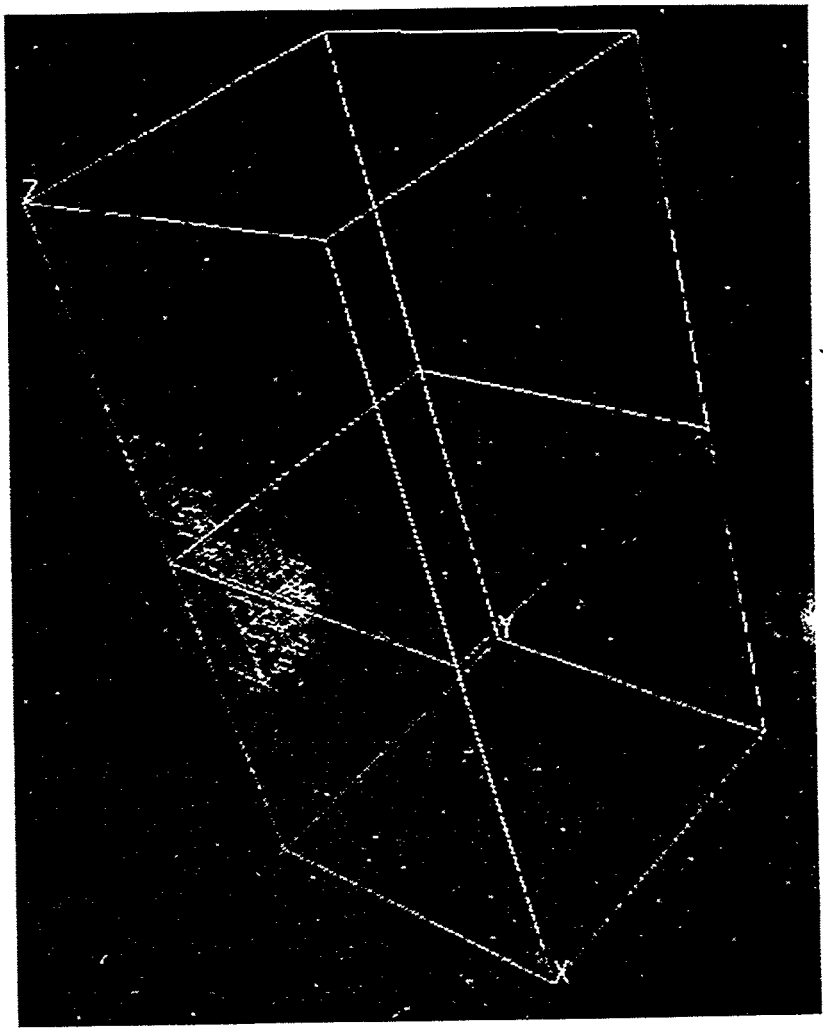

Grid Configutation

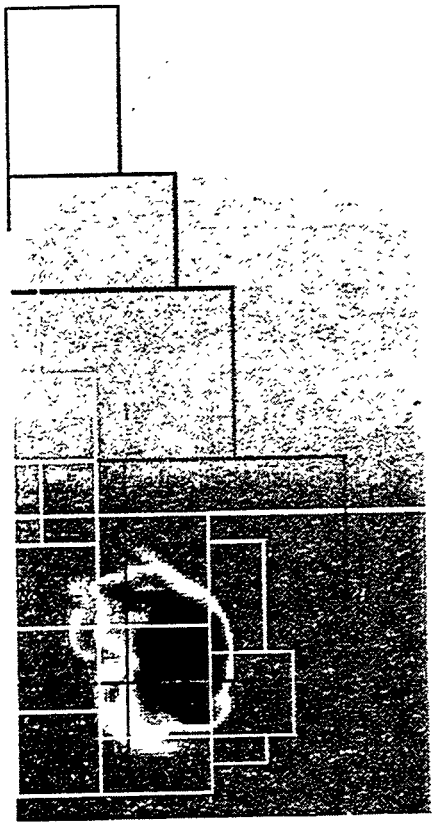

XZ Slice

Density at Time = 32.3 Seconds

Anelastic Bubble Rise in an Adiabatic Atmosphere.

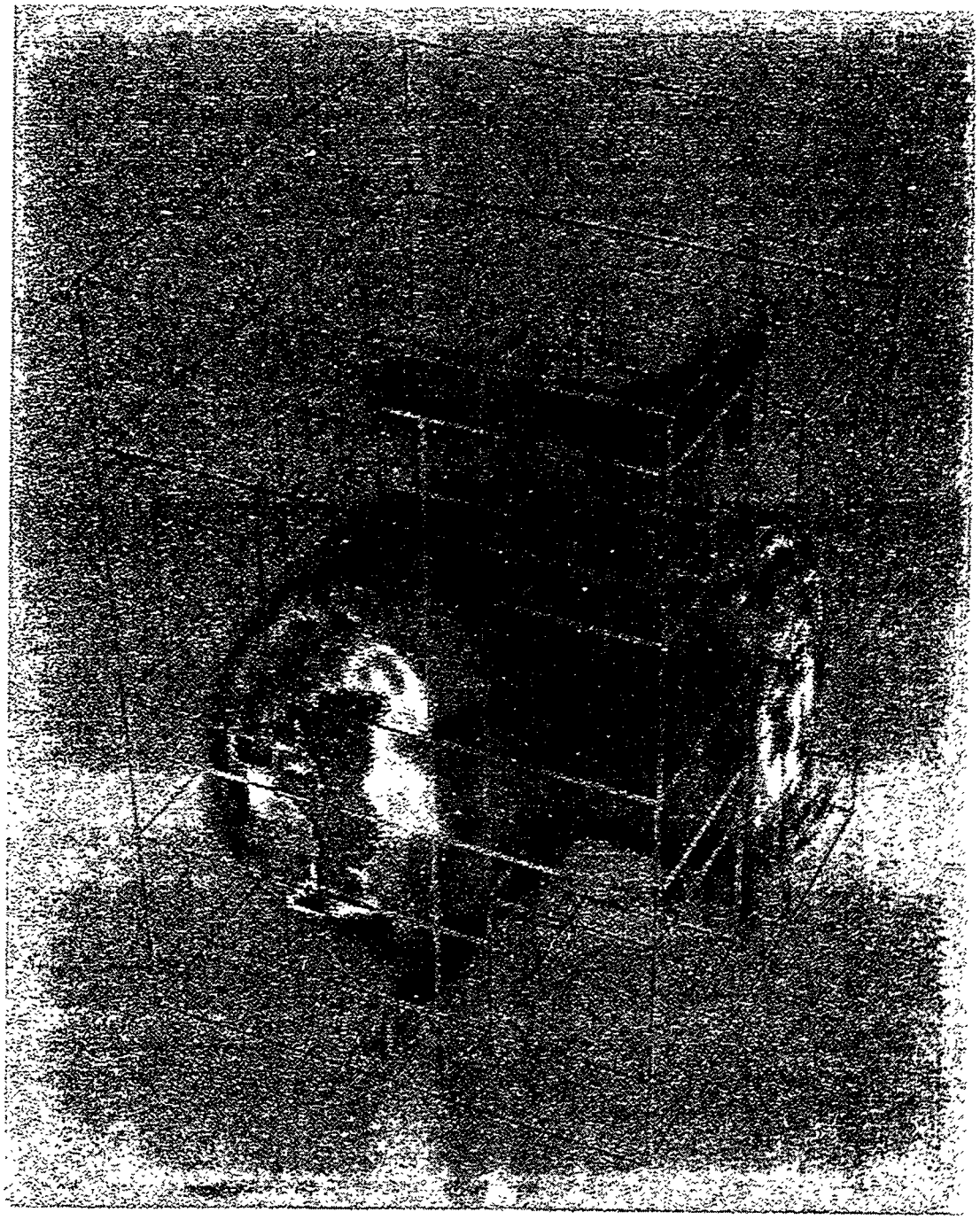

Bubble Tracer at Time = 32.3 Seconds

VOLUME-OF-FLUID REPRESENTATION OF MOVING BOUNDARIES

- FRONT REPRESENTED BY Λ^B, Λ^F, THE VOLUME OCCUPIED BY THE FLUID ON EITHER SIDE OF FRONT; AND U^B, U^F, VALUES OF SOLUTION ON EITHER SIDE OF FRONT.

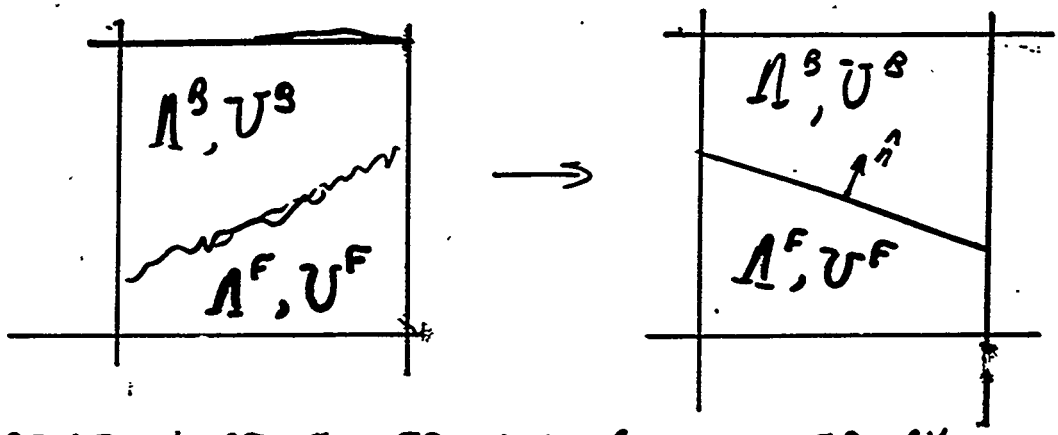

- LOCAL GEOMETRY OF THE FRONT IS CONSTRUCTED BY COMPUTING UNIT NORMALS IN EACH CELL. USING THIS INFORMATION, THE FRONT IS MOVED IN TIME BY TRANSPORTING Λ'S.

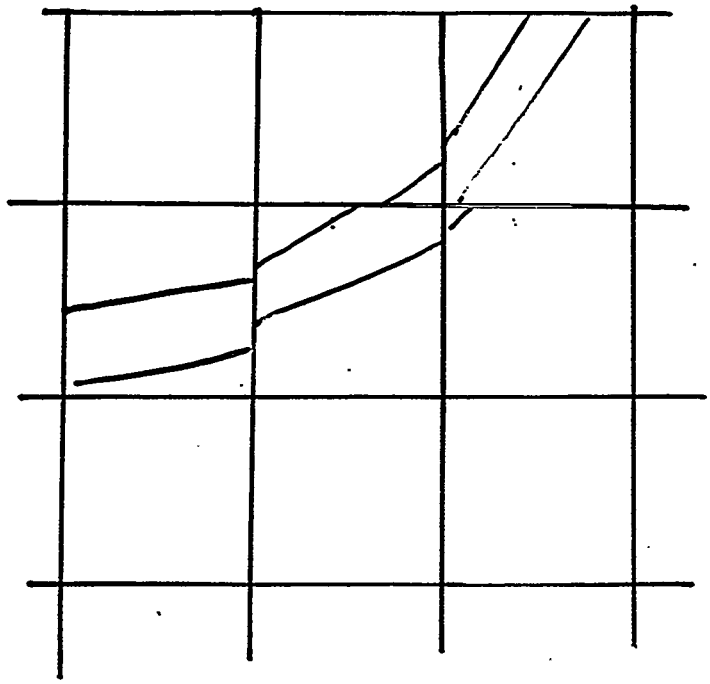

- U'S ARE UPDATED USING CONSERVATIVE, "FINITE VOLUME" DIFFERENCING.

PROPERTIES OF VOLUME-OF-FLUID REPRESENTATION

- CONSERVES VOLUME, MASS, ...
- AUTOMATICALLY HANDLES LARGE DEFORMATIONS, CHANGES IN TOPOLOGY
- STRAIGHTFORWARD TO COUPLE TO ADAPTIVE REFINEMENT
- EASILY EXTENDED TO 3D

FLUX DIFFERENCE REDISTRIBUTION

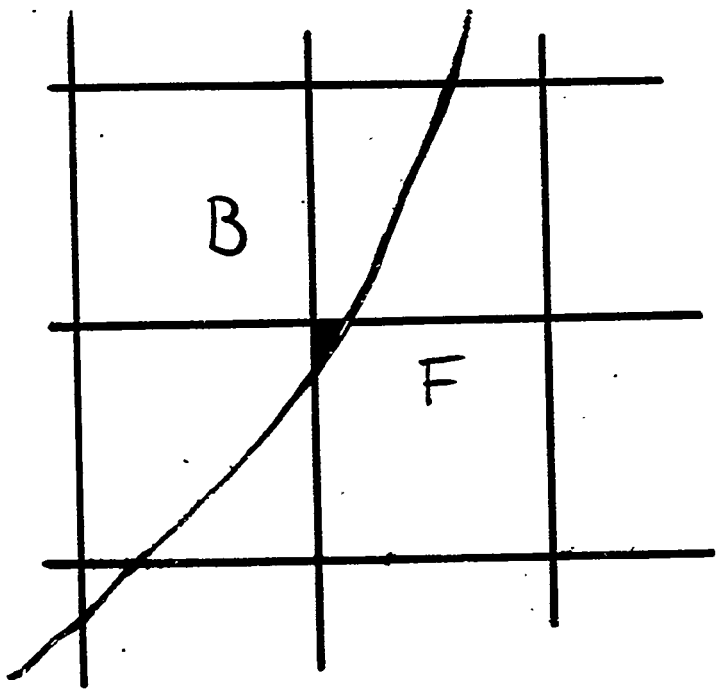

CONSERVATIVE DIFFERENCING:

$$U_B^{n+1} = U_B^n + \frac{\Delta t}{\Lambda} \sum l_s F_s$$

Λ = AREA OF CELL IN BACK OF DISCONTINUITY

UNSTABLE AS $\Lambda \to 0$

$$U_B^{n+1} = U_B^n + \frac{\Delta t}{\Delta x \Delta y} \sum l_s F_s$$

$$\delta M = (1-\eta)\, \Delta t \sum l_s F_s$$

B F

BELL, COLELLA, WELCOME (1991)

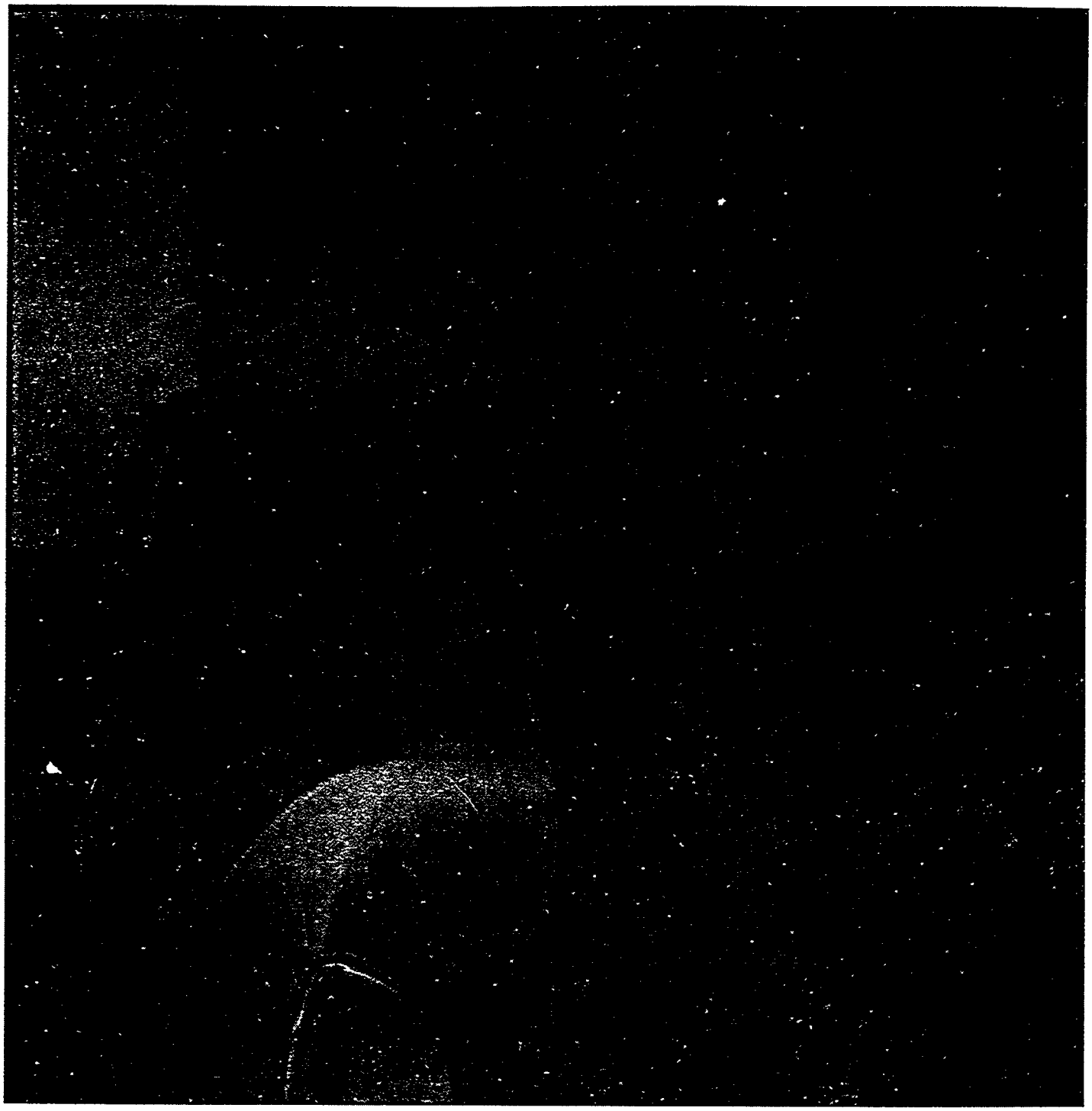

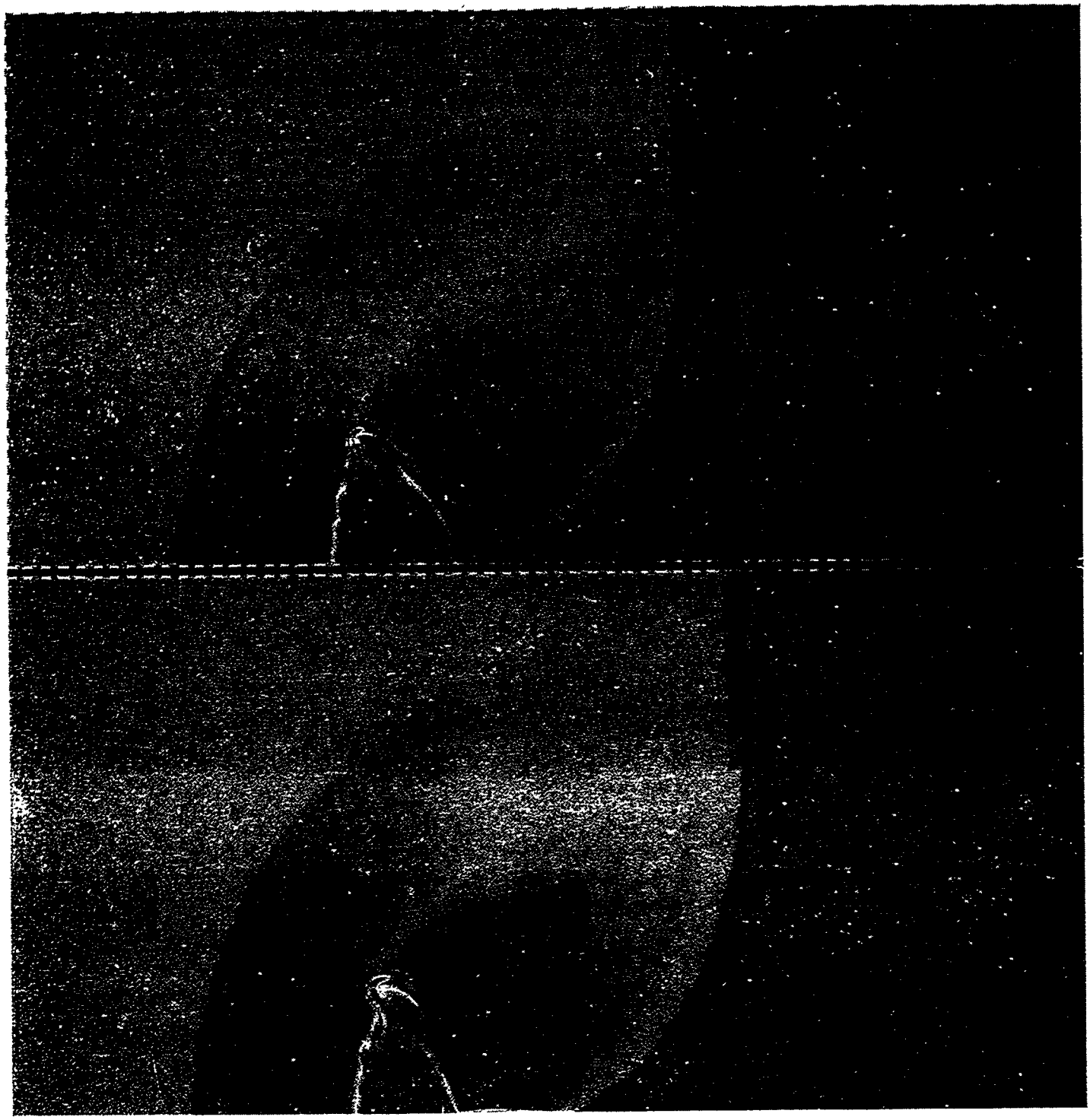

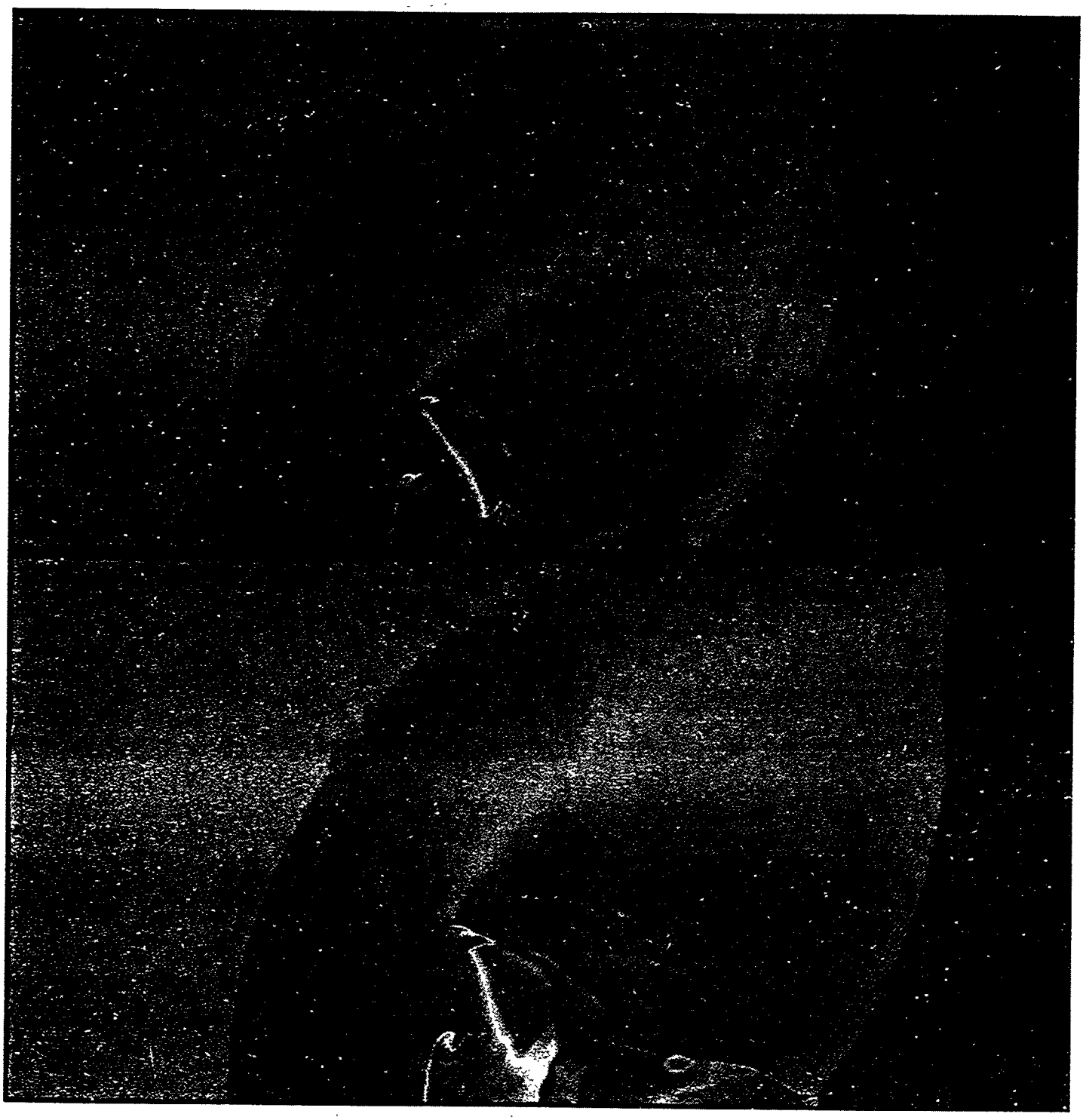

VOLUME-OF-FLUID REPRESENTATION OF FLUID INTERFACES

LOCAL GEOMETRY COMPUTED USING LOCAL LEAST-SQUARES FIT TO VOLUME FRACTIONS

ONLY THE THERMODYNAMIC VARIABLES ARE TRACKED (ρ, ε), WHILE VELOCITY IS SINGLE-VALUED IN CELL. REDISTRIBUTION IS ONLY DONE ON THERMODYNAMIC VARIABLES WITHIN A CELL, TO MAINTAIN PRESSURE CONTINUITY.

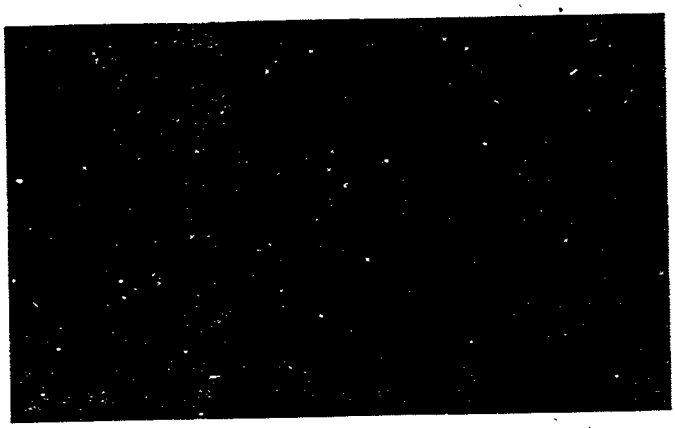

a) t = 0.0 microseconds

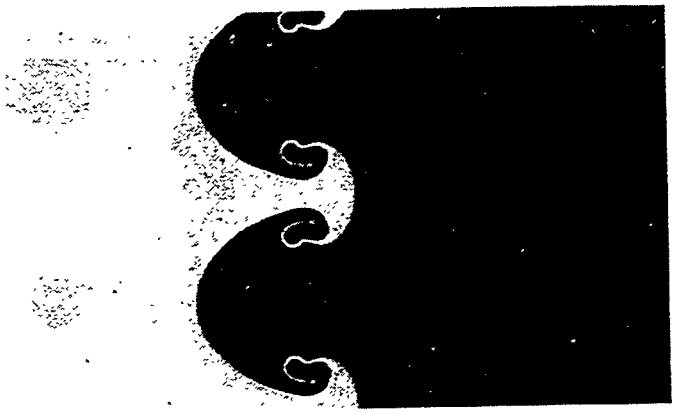

b) t = 213.3 microseconds

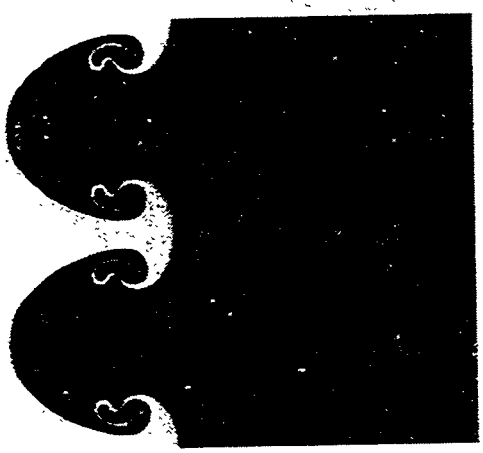

c) t = 230.1 microseconds

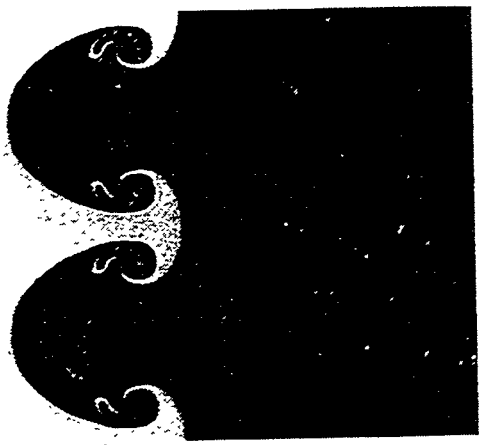

d) t = 245.8 microseconds

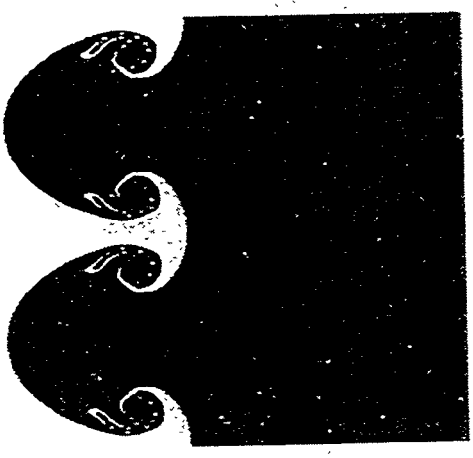

e) t = 268.9 microseconds

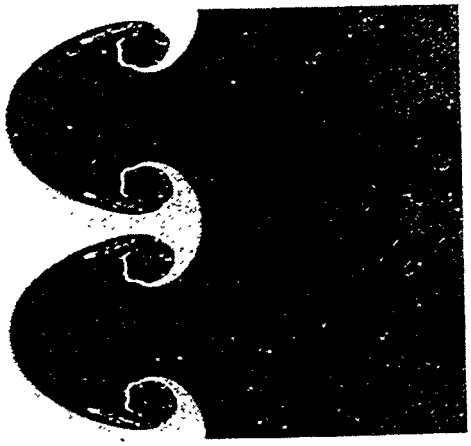

f) t = 300.0 microseconds

A Mach 3.45 shock in Argon strikes a sinusoidally perturbed interface between the Argon and Helium.

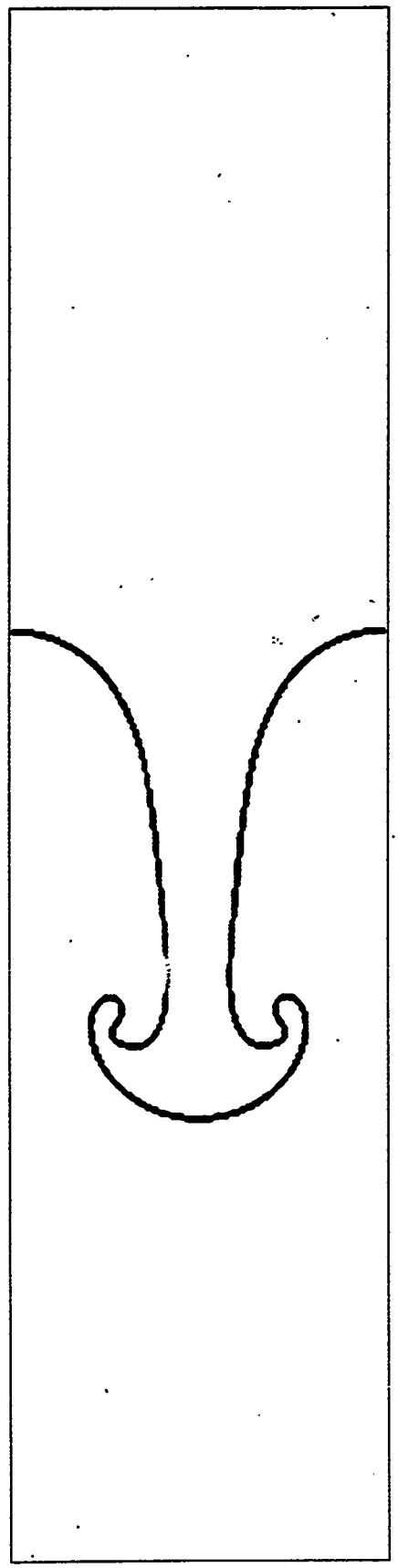

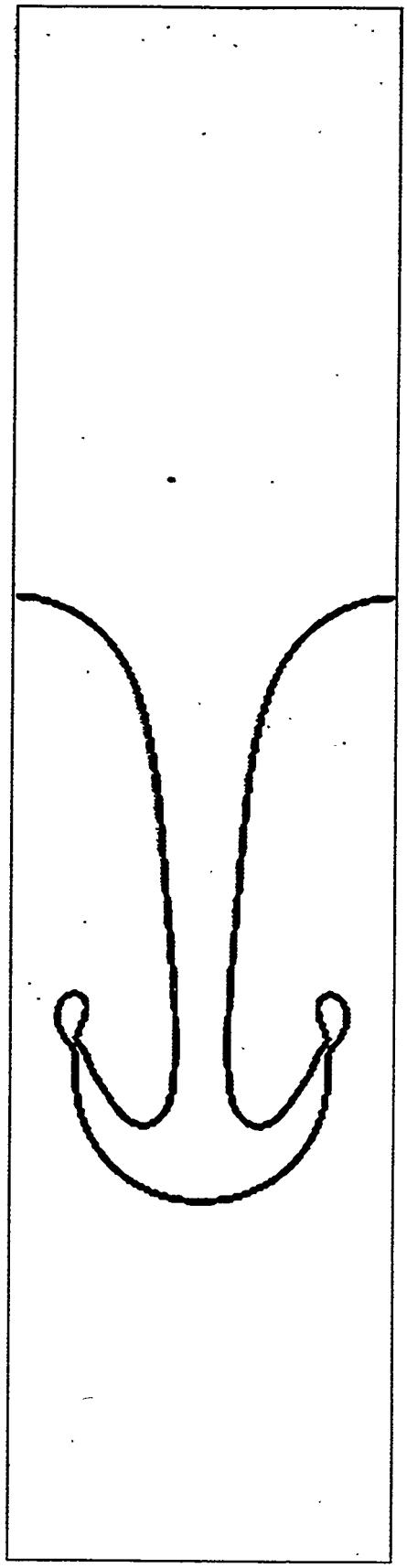

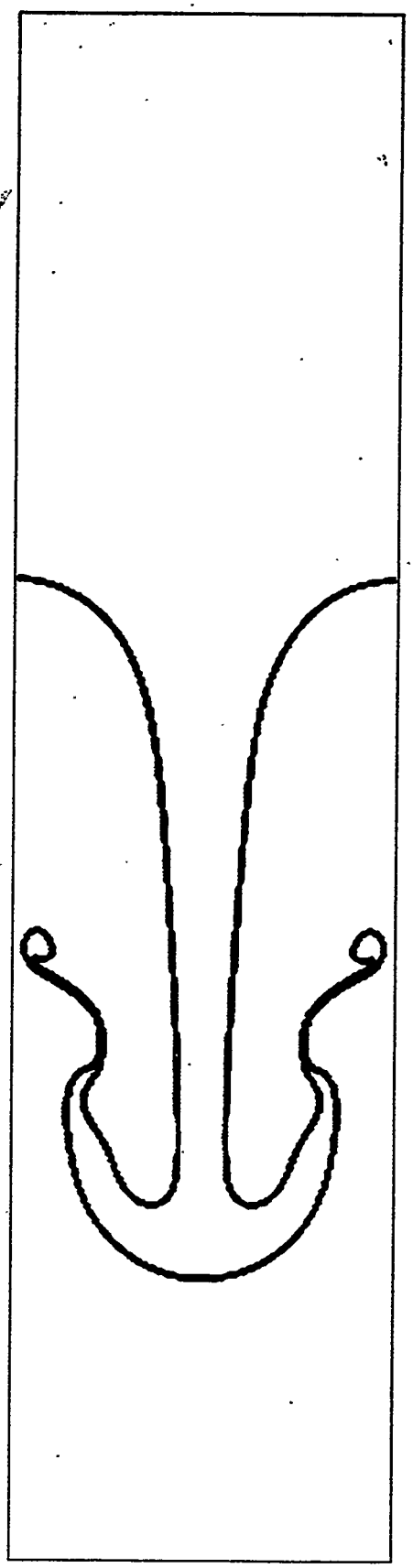

POCKETT, 1990

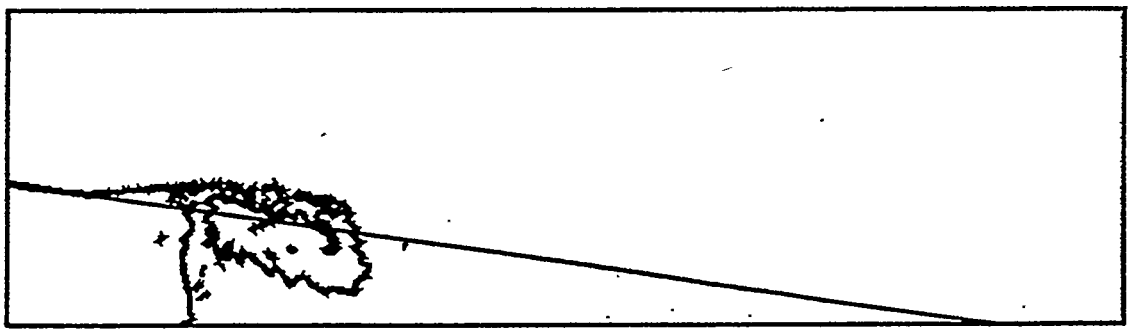

Fig. 8a The SLIC interface reconstruction algorithm

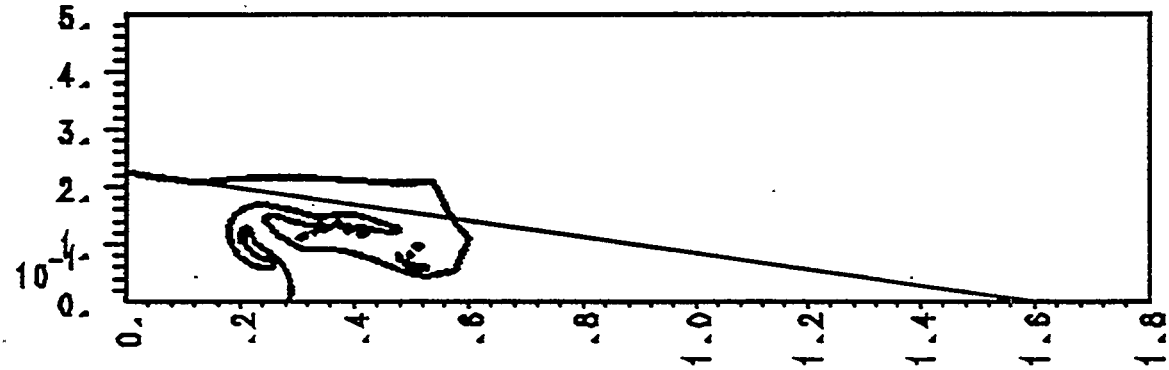

Fig. 8b The least squares interface recontruction algorithm

Fig. 8 A Mach 8 shock traveling from right to left striking an Ar / He interface inclined at an angle of 82 degrees (see Figs. 4 & 5). In these figures the contours of volume fraction are displayed at time t = 0.15. This is the best method for observing the interface. However the incident shock and other waves do not appear. The diagonal line that runs from upper left to lower right marks the location of the undisturbed interface at time t = 0.

CARTESIAN MESH REPRESENTATION OF GEOMETRY

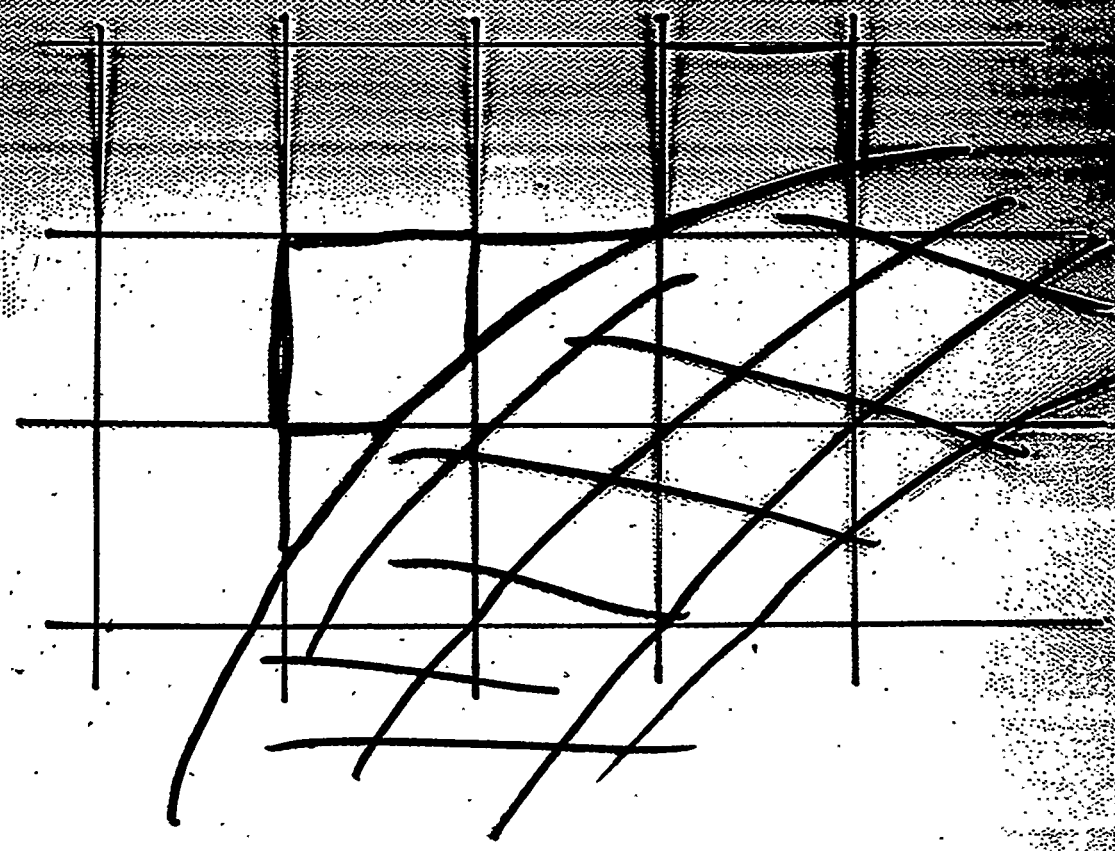

TREAT COMPLEX BOUNDARY AS "COOKIE CUTTER", CUTTING OUT IRREGULAR CELLS

FINITE VOLUME CONSERVATIVE DIFFERENCING ON IRREGULAR CELLS. CFL LIMITATIONS DUE TO SMALL CELLS AVOIDED USING REDISTRIBUTION, AS IN TRACKING CASE.

EASY TO REPRESENT VERY COMPLICATED GEOMETRIES

(a) Beginning of the injection phase: t = 0.200 ms.

(b) Jet just prior to collision with stagnation plate: t = 1.84 ms.

(c) Vortex ring formed by flow separation at the edge of the stagnation plate : t = 2.00 ms.

(d) Peak of injection phase: t = 4.07 ms.

ALMGREN, BELL, COLELLA, MARTHALER (1994)

Vortex Shedding Past a Half-Cylinder

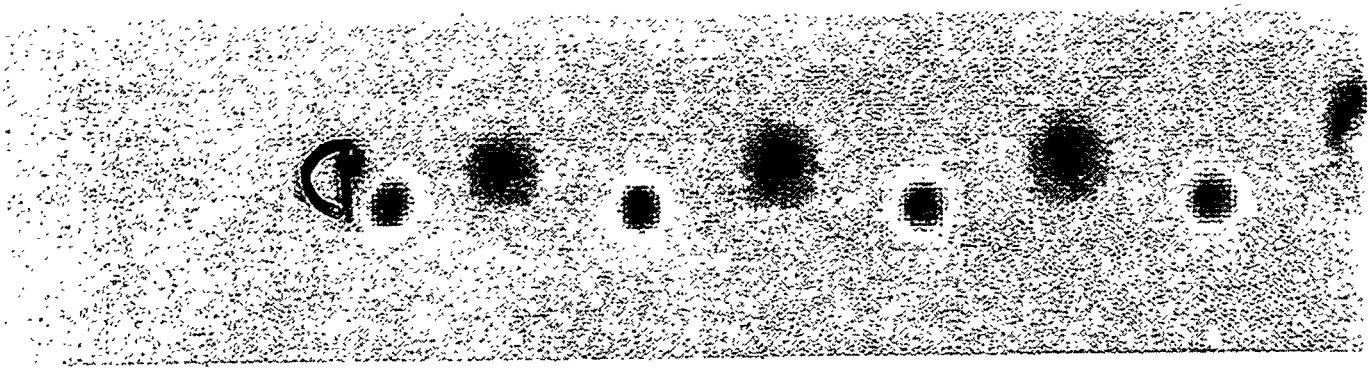

Vorticity

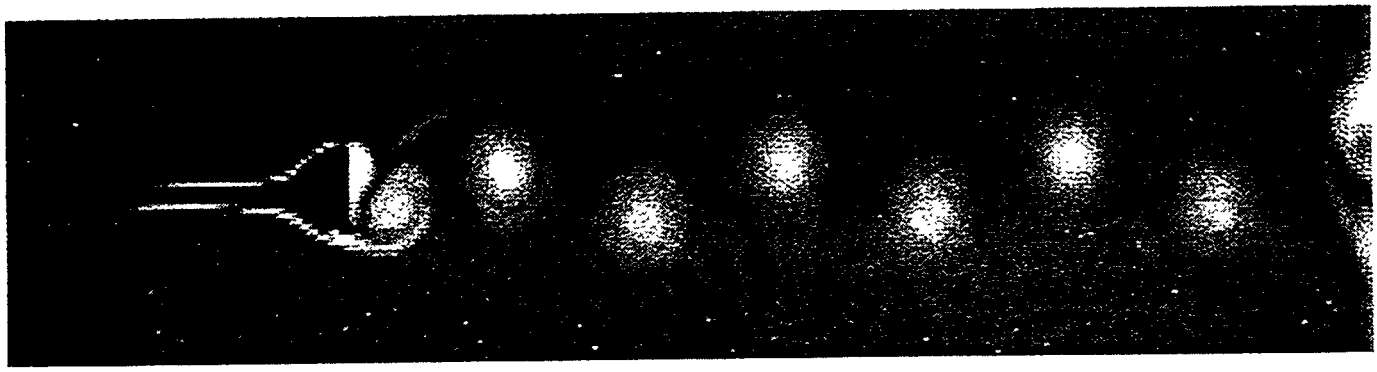

Passive Scalar

Incompressible Composite Grid Example

Vorticity

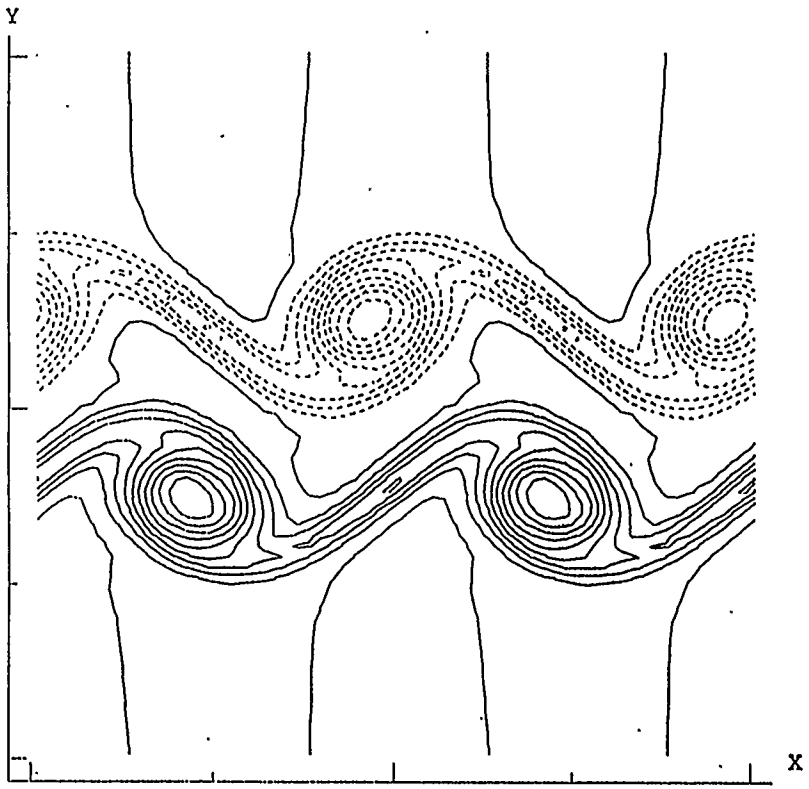

Single grid

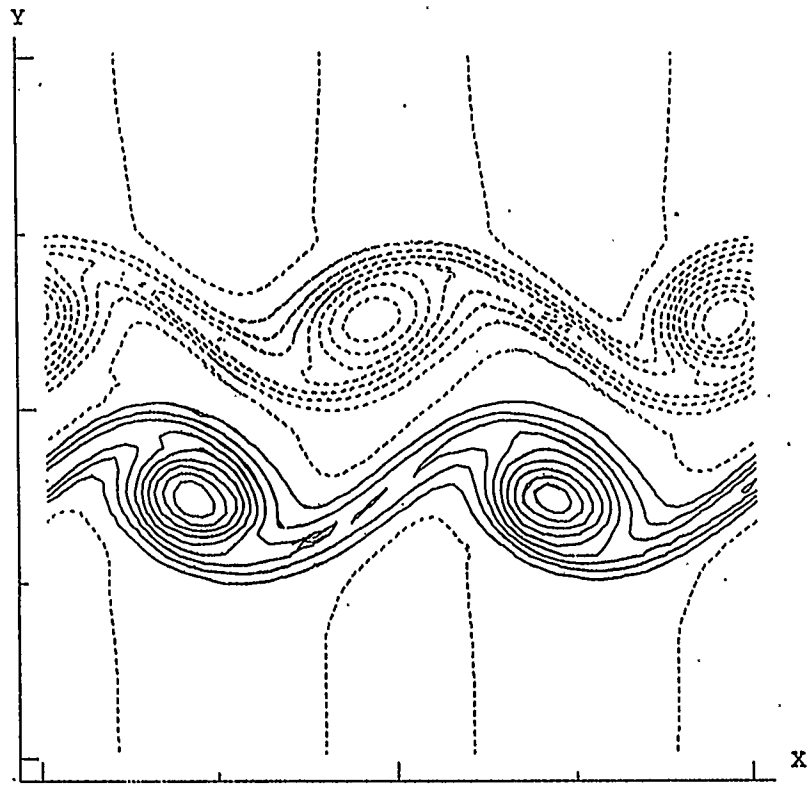

Composite grid

Incompressible Composite Grid

Grid Structure

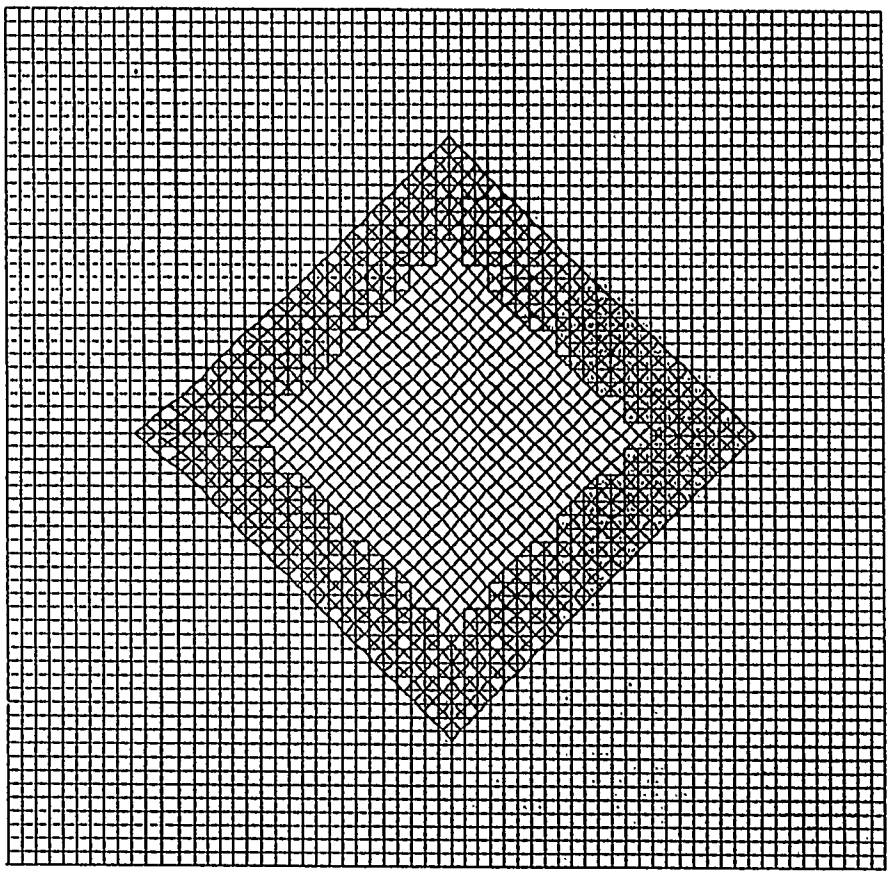

Composite Grids

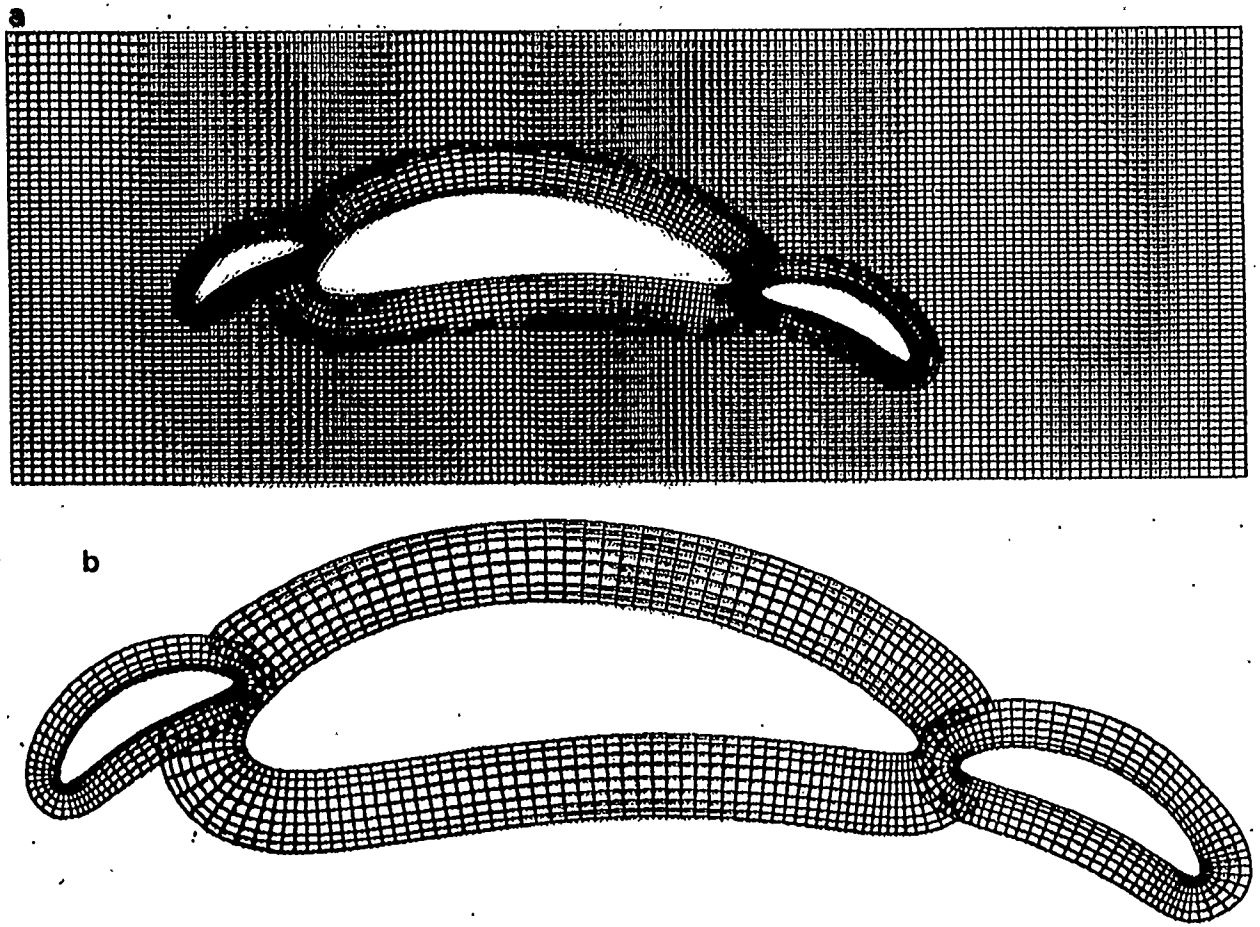

SOFTWARE INFRASTRUCTURE

HYBRID OF C++ / FORTRAN

- C++ TO MANIPULATE AMR DATA STRUCTURES
- FORTRAN TO PERFORM FLOATING POINT ON SINGLE RECTANGULAR GRID

LLNL BOXLIB

- C++ LIBRARY TO SUPPORT BLOCK-STRUCTURED GRID ALGORITHMS
- RECTANGULAR GRID INDEX SETS ("BOX") FUNDAMENTAL DATA TYPE
- UNWIELDY FOR SPARSE IMBEDDED DATA STRUCTURE

pointLib (UNDER DEVELOPMENT)

- BOX GENERALIZED TO pointDomain = ARBITRARY SUBSET OF $\mathbb{Z}^d$
- ARRAYS OF VALUES WITH pointDomain'S AS INDEX SETS

ADAPTIVE GRID FINITE ELEMENT MODEL OF THE TOKAMAK SCRAPEOFF LAYER

Andrew P. Kuprat and Alan H. Glasser
Los Alamos National Laboratory

Presented at the
Workshop on Adaptive Grid Methods
Pleasanton, CA, December 1994

Anisotropic Metric For Grid Generation

- In $\hat{\mathbf{B}}$ direction, diffusion dominated by $\chi_{\|}^{\mathbf{e}}$ (parallel electron thermal conductivity).
- Perpendicular to $\hat{\mathbf{B}}$, diffusion dominated by $\chi_{\perp}^{\mathbf{i}}$ (perpendicular ion thermal conductivity).
- $\chi_{\text{mesh gen.}} = \hat{\mathbf{B}}\hat{\mathbf{B}}\chi_{\|}^{\mathbf{e}} + (\mathbf{I} - \hat{\mathbf{B}}\hat{\mathbf{B}})\chi_{\perp}^{\mathbf{i}}$.
- Characteristic Length $\propto \sqrt{\chi}$.

  I.e. Characteristic length $\propto \sqrt{\chi_{\|}^{\mathbf{e}}}$ in $\|$ direction,

  I.e. Characteristic length $\propto \sqrt{\chi_{\perp}^{\mathbf{i}}}$ in $\perp$ direction.

Poloidal Plane

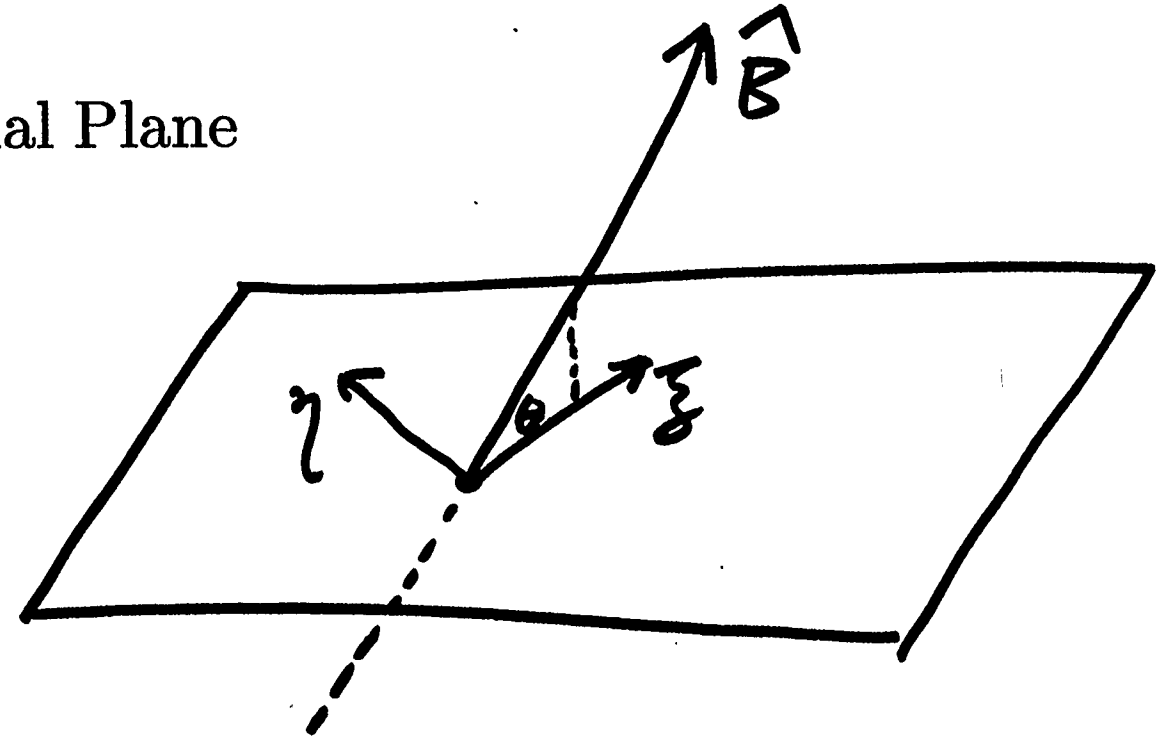

ξ, η are orthogonal unit vectors in Poloidal Plane.

θ is the angle $\hat{\mathbf{B}}$ makes with the plane.

$\eta \perp \hat{\mathbf{B}}$

ξ is projection of $\hat{\mathbf{B}}$ on the plane.

Anisotropic Metric For Grid Generation

- Vectors along η use characteristic length $\sqrt{\eta \cdot \chi \cdot \eta} = \sqrt{\chi_{\perp}^{i}}$.

- Vectors along ξ use characteristic length $\sqrt{\xi \cdot \chi \cdot \xi} = \sqrt{\chi_{\perp}^{i} \sin^2\theta + \chi_{\parallel}^{e} \cos^2\theta}$.

- If $\hat{\mathbf{B}}$ is in poloidal plane, anisotropy is $\sqrt{\frac{\chi_{\parallel}^{e}}{\chi_{\perp}^{i}}}$.

- If $\hat{\mathbf{B}}$ is perfectly normal to poloidal plane, length scales are isotropic. (Ie at **X** point.)

Riemann-Delaunay Triangulation

- Stretch factors in orthogonal directions induce a "Riemannian Metric": A continuously varying rule for the inner product $((\mathbf{v}, \mathbf{w}))$ of vectors at each point in space. So we have a rule for the **angles** between vectors.

- If we try to produce a "max min angle" triangulation (ie the **Delaunay Triangulation**) using this metric, we get an anisotropic grid aligned with $\hat{\mathbf{B}}$.

Quantitative Mesh Quality Measure

How successful are we at creating a properly anisotropic grid?

- A perfect equilateral triangulation has an average value of $\sin\alpha = \frac{\sqrt{3}}{2}$.

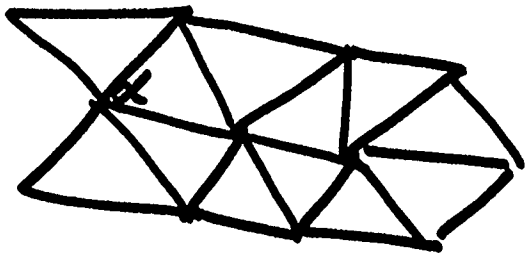

- Our anisotropic triangulation:

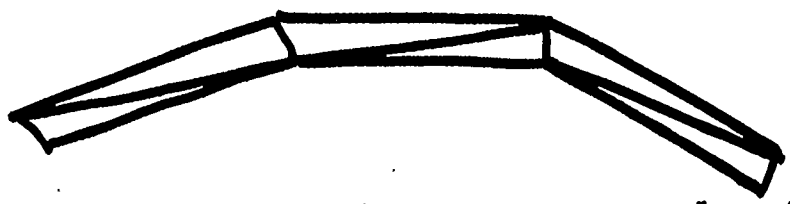

- Due to discretization and having to work with a highly curved domain, we can't attain a "perfect score" of "sin"$\alpha = \frac{\sqrt{3}}{2}$. We get "sin"$\alpha \approx 0.25$.
- More points would be needed to do a perfect job, but we're in the ballpark.

General Form of the Equations

$$\frac{\partial \mathbf{u}}{\partial t} + \nabla \cdot \mathbf{F} = \mathbf{S}$$

$$\mathbf{F} = \mathbf{C}(t, \mathbf{x}, \mathbf{u}) - \mathbf{D}(t, \mathbf{x}, \mathbf{u}) \cdot \nabla \mathbf{u}$$

$$\mathbf{S} = \mathbf{S}(t, \mathbf{x}, \mathbf{u}, \nabla \mathbf{u})$$

Variational Principle

$$L = \frac{1}{2} \int \left[\frac{\partial \mathbf{u}}{\partial t} + \nabla \cdot \mathbf{F} - \mathbf{S} \right]^2 w(t, \mathbf{x}, \mathbf{u}, \nabla \mathbf{u}) d\mathbf{x}$$

$$\frac{\delta L}{\delta(\partial \mathbf{u}/\partial t)} = 0$$

Thermodynamic vs. Conservative Variables

- We use thermodynamic variables $(n, T_e, T_i, v_{\|})$ rather than conservative variables $(n, nT_e, nT_i, \rho V_{\|})$ so that *computational* diffusion tensor is closer to diagonal.

$$\mathbf{u}_t + \nabla \cdot (\mathbf{C} - \mathbf{D}\nabla\mathbf{u}) = \mathbf{S}$$

  In the above equation, if $\mathbf{u}$ is a vector of thermodynamic variables, $\mathbf{D}$ will be more-nearly diagonal. Utilization of conservative variables led to negative eigenvalues for the diffusion tensor (and blowup) in the 1-D Moving Finite Elements code. (*Alan Glasser, JCP, 1989.*)

- Boundary conditions are more easily implemented, since they are usually Neumann or Dirichlet in the thermodynamic variable.

Equations for $n, T_e, T_i, v_{\|}$

To fit our equations into this form, fluxes and sources have to be rearranged so that all second order spatial derivative terms are due to the divergence of diffusive fluxes. We get:

$$\frac{\partial n}{\partial t} + \nabla \cdot (n\mathbf{v}) = 0$$

$$\frac{\partial T_e}{\partial t} + \nabla \cdot [\frac{2}{3}(T_e \mathbf{v}_e + \frac{\mathbf{q}_e}{n})] = \frac{2}{3}(\frac{Q_e}{n} - \frac{\mathbf{q}_e \cdot \nabla n}{n^2} - \frac{\mathbf{v}_e \cdot \nabla T_e}{2})$$

$$\frac{\partial T_i}{\partial t} + \nabla \cdot [\frac{2}{3}(T_i \mathbf{v} + \frac{\mathbf{q}_i}{n})] = \frac{2}{3}(\frac{Q_i}{n} - \frac{\mathbf{q}_i \cdot \nabla n}{n^2} - \frac{\mathbf{v} \cdot \nabla T_i}{2})$$

$$\frac{\partial v_{\|}}{\partial t} + \nabla \cdot (\frac{\pi \cdot \hat{\mathbf{B}}}{\rho}) = -\frac{\nabla n \cdot \pi \cdot \hat{\mathbf{B}}}{\rho n} - \mathbf{v} \cdot \nabla v_{\|} - \frac{\nabla_{\|} p}{\rho}$$

Some equation details

- Parallel to $\hat{\mathbf{B}}$, transport is flux-limited Braginskii.
- Flux limiting accomplished by reducing collision times:

$$\tau < \frac{\text{“1m”}}{v_{thermal}}.$$

  Use limited τ in expressions for Braginskii transport coefficients.
- Anomalous diffusion orthogonal to $\hat{\mathbf{B}}$. For example

  $\mathbf{v} = v_{\|}\hat{\mathbf{B}} + \mathbf{v}_{\perp}$, where
  $n\mathbf{v}_{\perp} = -D_a^n \nabla_{\perp} n$,
  $\nabla_{\perp} n = (\mathbf{I} - \hat{\mathbf{B}}\hat{\mathbf{B}})\nabla n$.
- Anomalous $\chi_{\perp}^{e}, \chi_{\perp}^{i}, \eta_2$ terms as well (these enter into the expressions for $\mathbf{q_e}, \mathbf{q_i}$, and π respectively.)

Initial Comparison with Other Code on Slab Geometry

- Looked at results of R. Vesey, Fusion Technology 1992.
- Comparison was approximate. Differences: Unlike our code, he
  - · has single species neutrals,
  - · uses Cartesian $\mathbf{x}, \mathbf{y}$ geometry,
  - · uses SUPG.
- Similar far field behaviour. Differences close to plate due to lack of neutrals.
- **Key Point:** Introduction of anisotropic, unstructured grid did not wreck solution, but **improved** it. Jaggedness due to computing with marginally high Peclet number disappeared.

Midplane

$\nabla n = 0$

$\nabla T_i = \nabla T_e = 0$

$u_{\parallel} = 0$

← .04m →

↑ 1m ↓

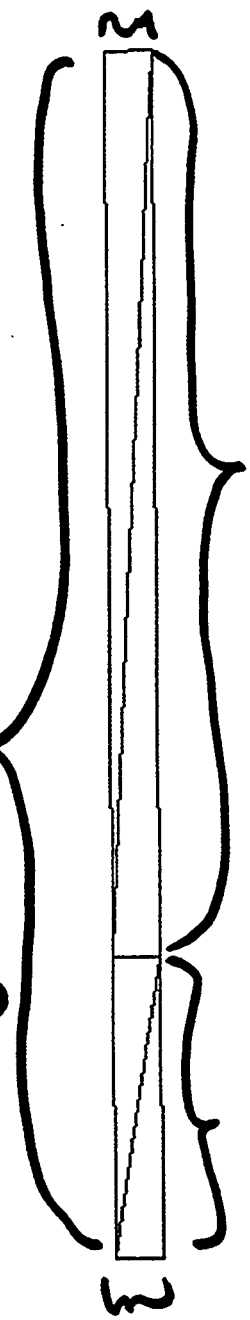

core

~~$T_i = T_e = 1.8 \times 10^{19}$~~

$T_i = T_e = 80\,eV$

$n = 1.8 \times 10^{19}$

$u_{\parallel} = 0$

SOL

$\nabla n = 0$

$\nabla u_{\parallel} = 0$

$\nabla T_i = \nabla T_e = 0$

Private Flux

$\nabla n = 0$

$\nabla u_{\parallel} = 0$

$\nabla T_i = \nabla T_e = 0$

Divertor

$$T_{\parallel} = \frac{\left(\frac{5}{2} - \delta\right) T n u_{\parallel}}{\chi_{\parallel}}$$

$\nabla n = 0$

$$u_{\parallel} = \pm\sqrt{\frac{T_e + T_i}{m_i}}$$

Jagged Solution on Structured Grid

(Parallel Velocity)

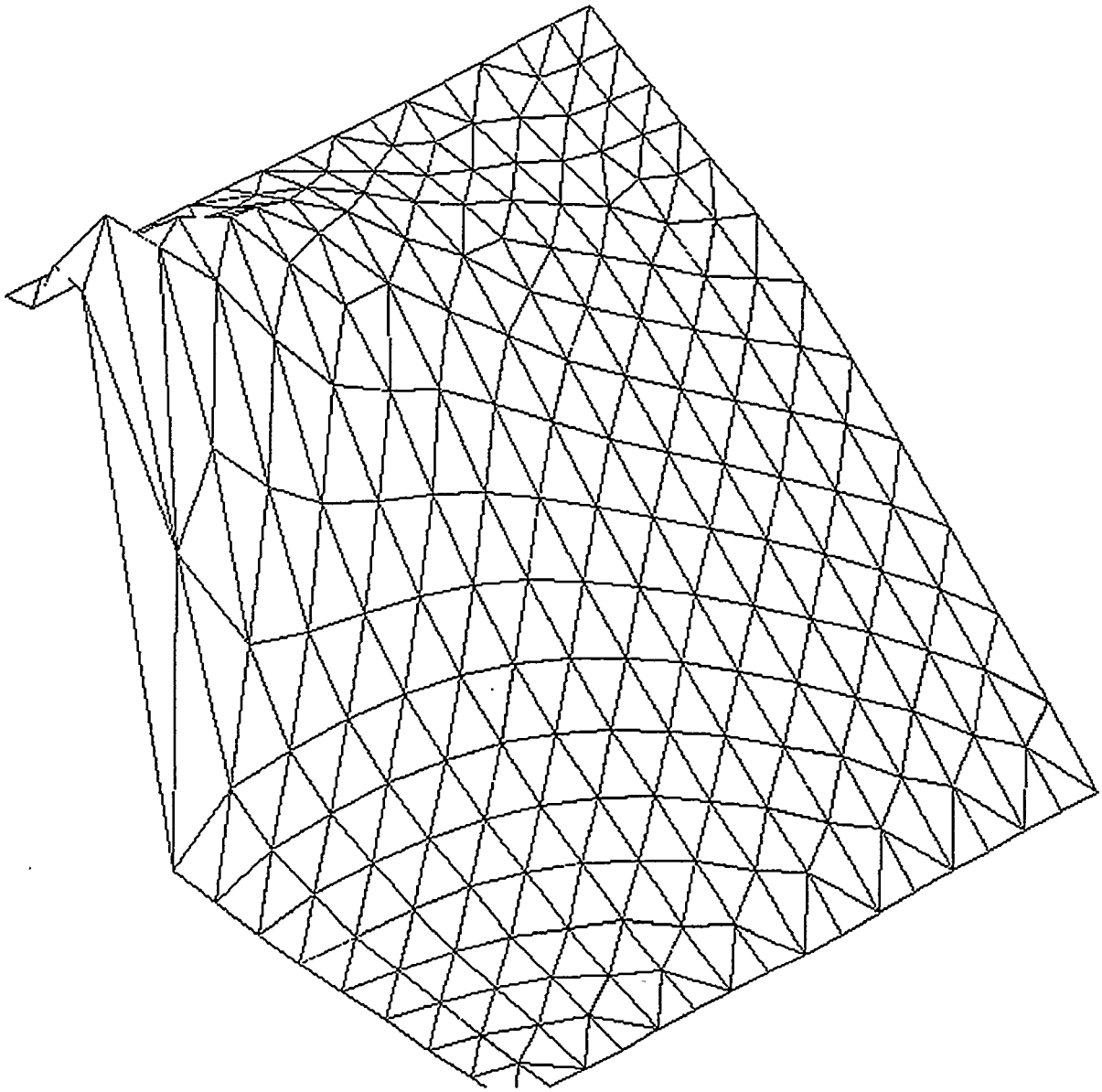

Smoother Solution on Adaptively Refined Unstructured Grid
(Parallel Velocity)

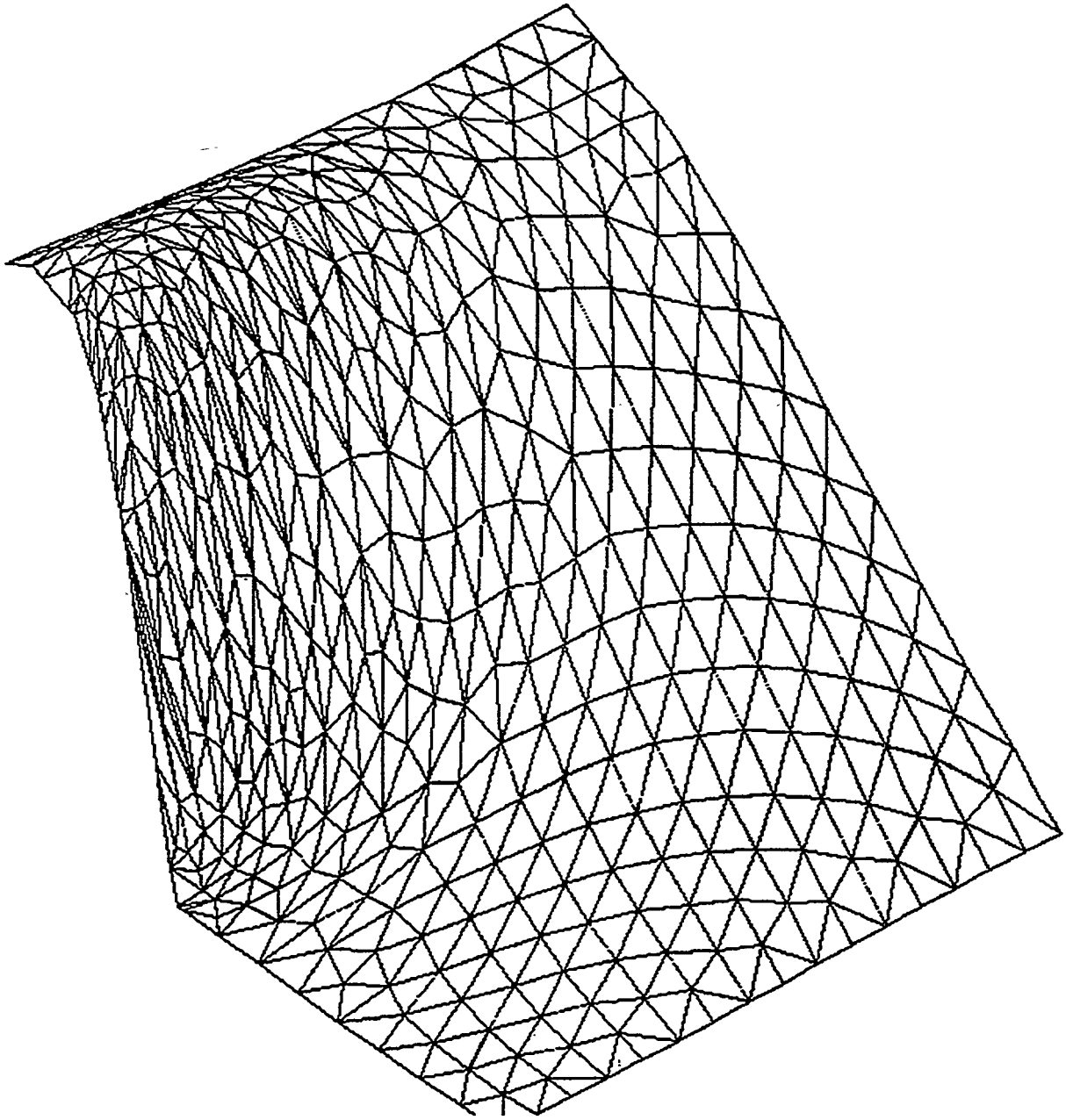

Neumann Boundary Conditions

- Easy to code up.
- Can lead to erratic results: Changed $v_{||}$ boundary condition on midplane from zero Dirichlet to zero Neumann. Result:
  · Large difference in steady-state $v_{||}$ value when triangle diagonals were all swapped on regular grid.
  · Total blow-up on unstructured grid.
- Flux boundary conditions are more physical and may be more important on an irregular domain. Any ideas?

Results on ITER-Like Domain

- Smooth solution along separatrix.
- Due to lack of neutrals, our plasma drains out.
- Need to put in neutrals recycling or get rid of sonic speed outflow boundary condition.
- Need to benchmark against another code to see how much grid prevents false perpendicular diffusion.

Frame 7/7, Topology 0/0, ieq=1, freeze=0

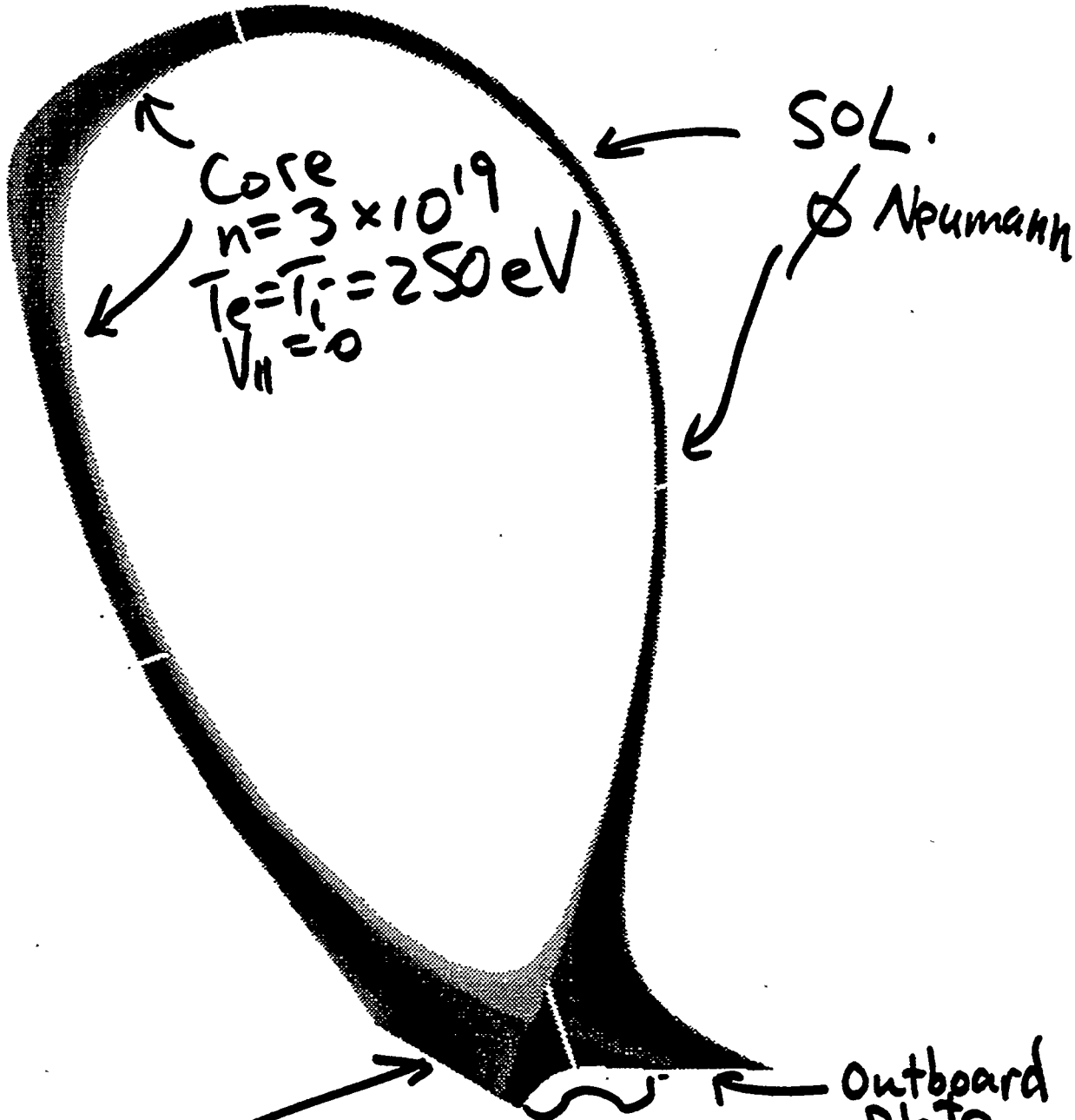

$$T_{\parallel} = \frac{(\frac{5}{2} - \delta) T_n V_{\parallel}}{\chi_{\parallel}}$$

$$V_{\parallel} = \pm \sqrt{\frac{T_e + T_i}{m_i}}$$

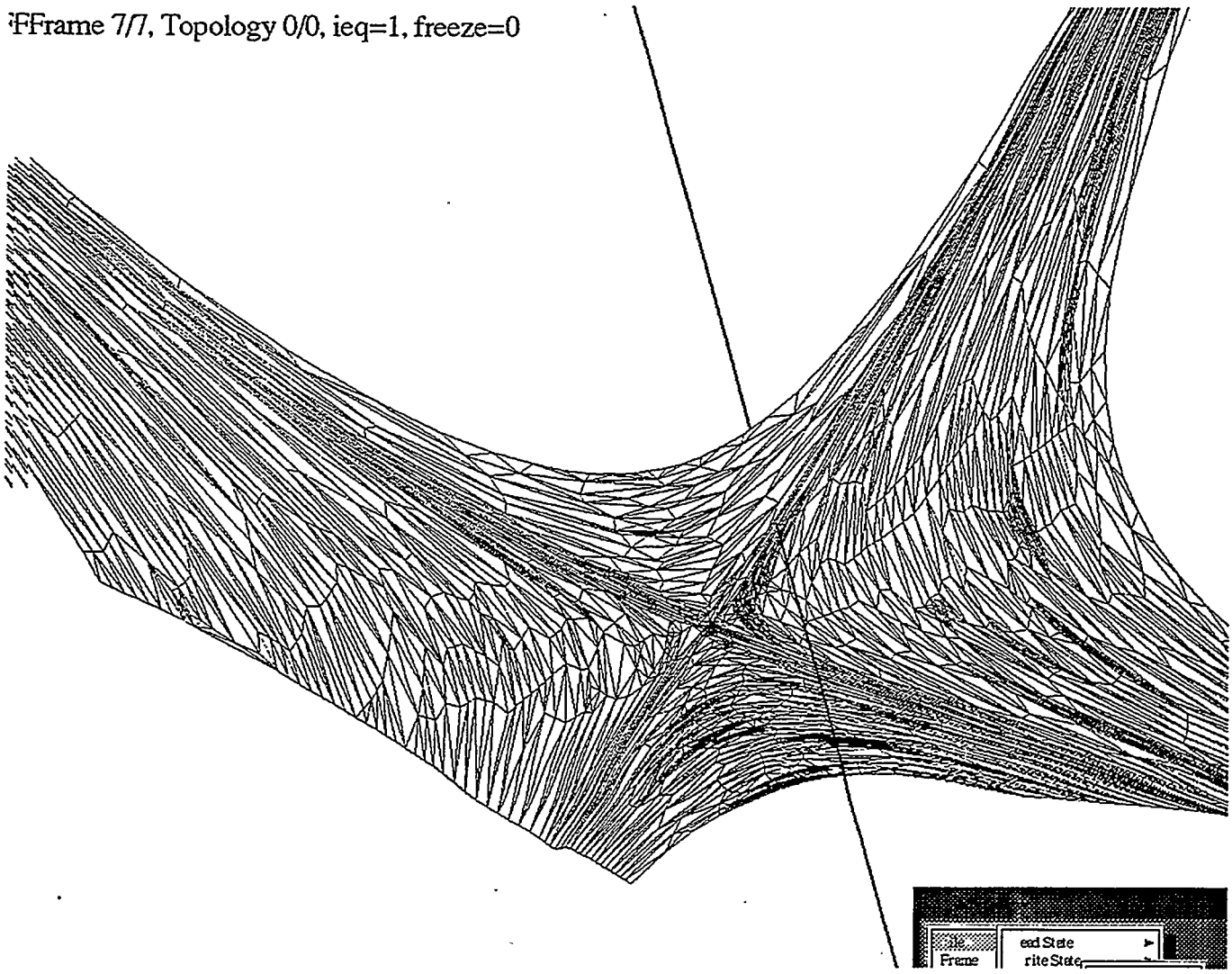

Grid based on anisotropic transport coefficients

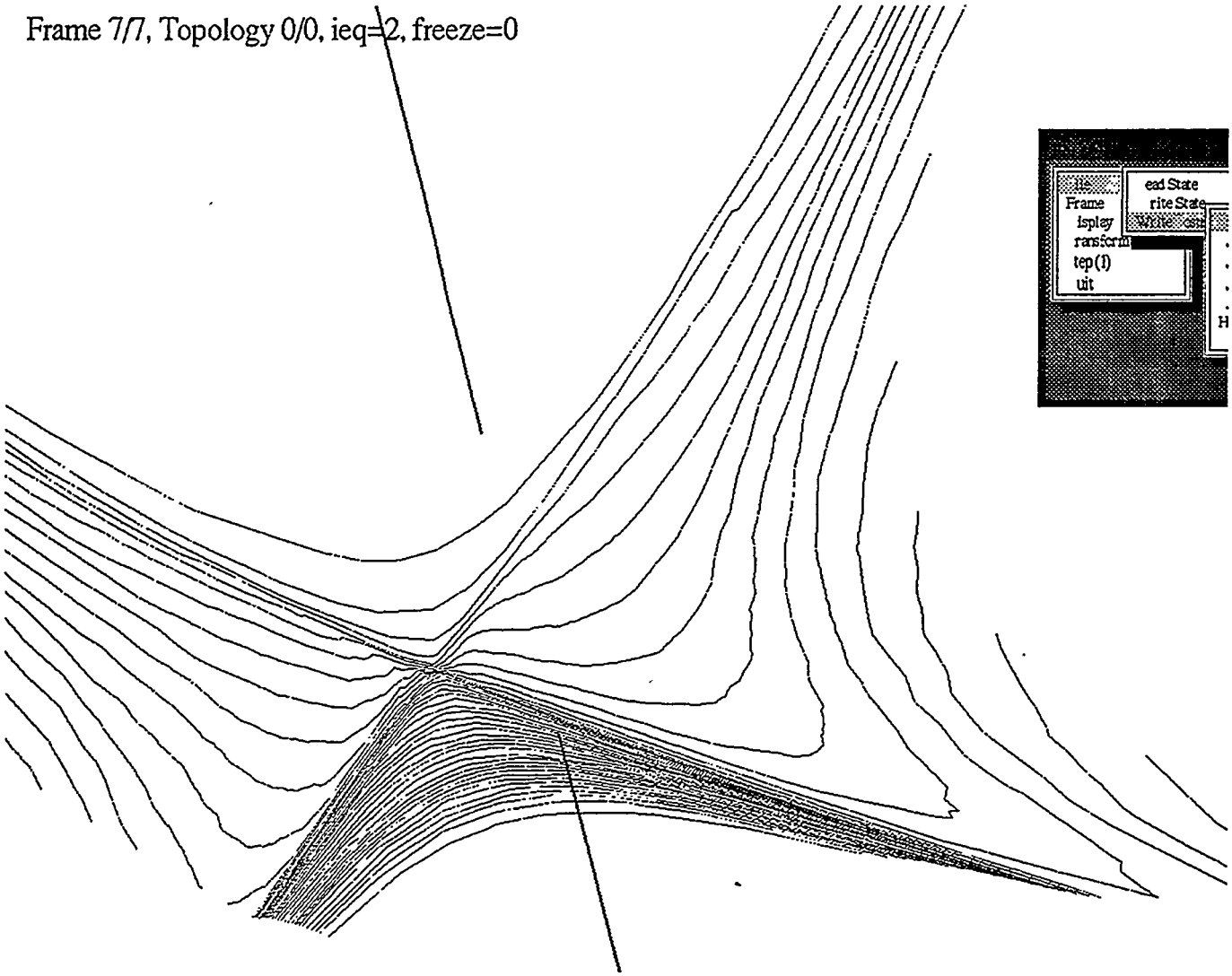

Smooth Solution (Te) on anisotropic grid

Frame 0/7, Topology 0/0, ieq=2, freeze=0

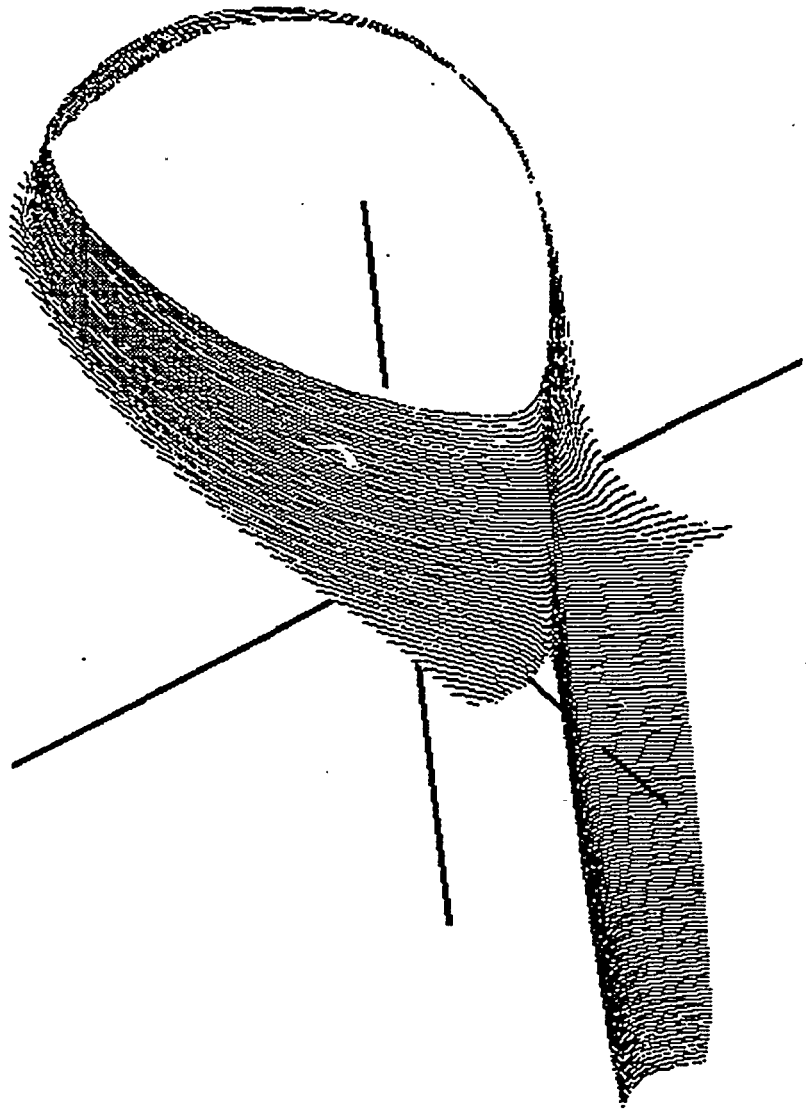

Perspective view of Te

Frame 8/22, Topology 1/1, ieq=1, freeze=1

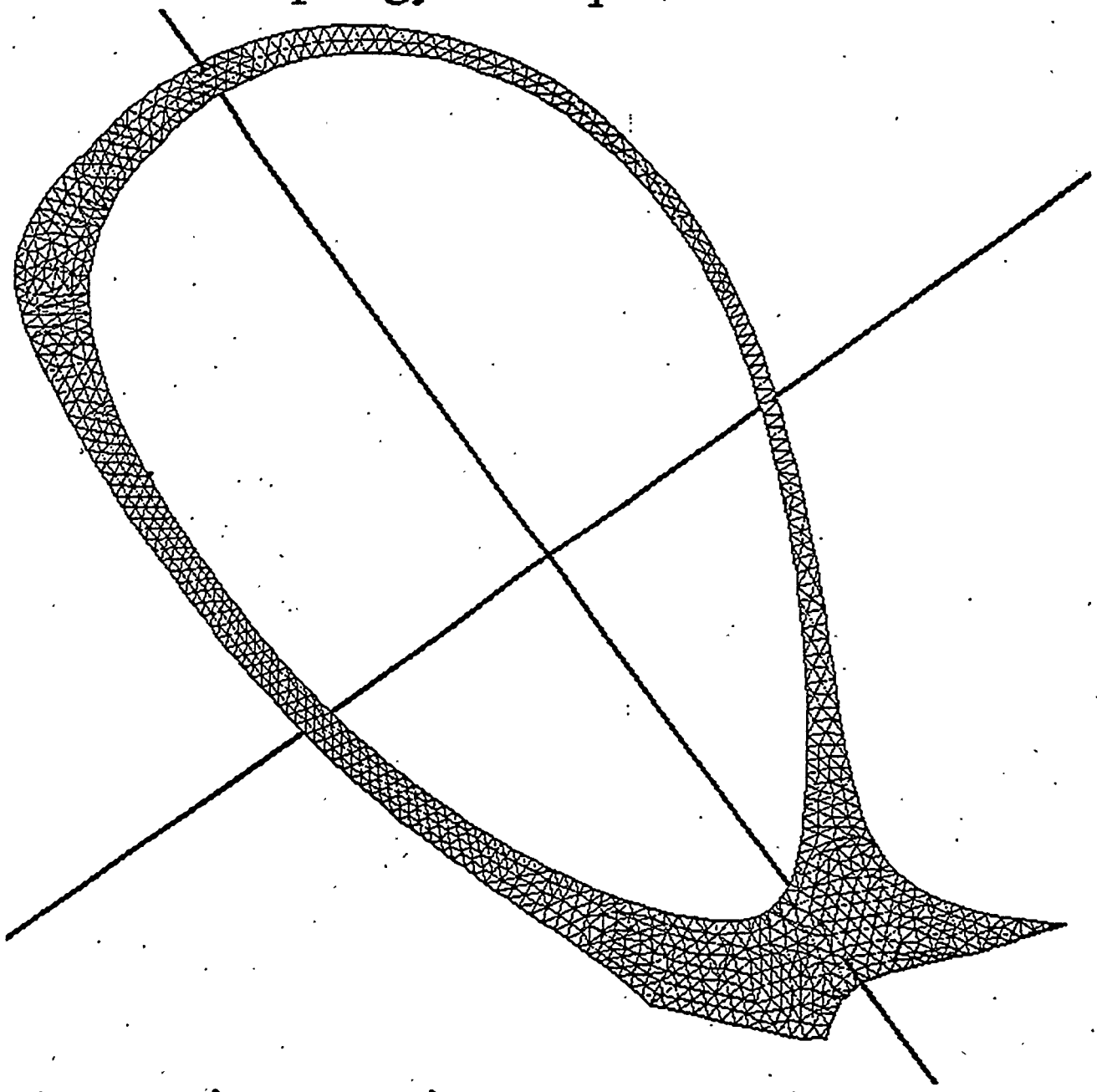

Let's try isotropic grid

Frame 8/22, Topology 1/1, ieq=1, freeze=1

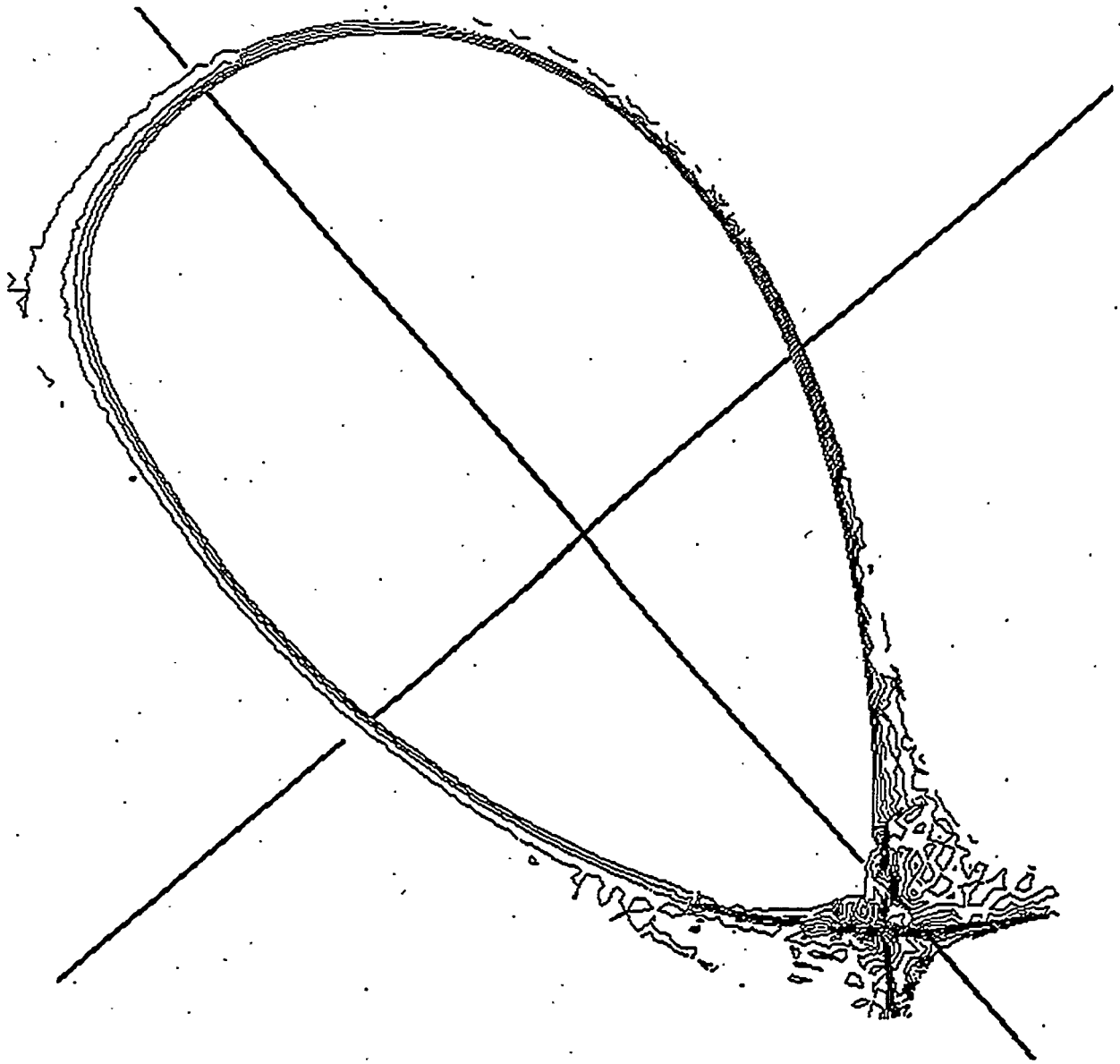

Poor solution (n_e) on isotropic grid

Remember Moving Finite Elements?

- Original formulation of MFE (K. Miller, UC Berkeley) treated space isotropically with respect to determining mesh motion.
- Alan Glasser changed code so that MFE recognized anisotropy *along a coordinate axis.*
- On slab problem, without this correction, nodes are "sucked into" Neumann SOL boundary.
- To handle spatially varying anisotropy (ITER problem), MFE code would have to be changed some more. When?
- MFE basically at its best with transient problems, not steady state.

Finite Volume Methods

- These curved anisotropic grids are not suitable for finite volume methods based on Voronoi control volumes. Reason: These methods require 'positive coupling coeffients' between all pairs of adjacent nodes, which implies that the triangulation has to be (nearly) nonobtuse. This is virtually impossible to achieve with *any* curved anisotropic grid.

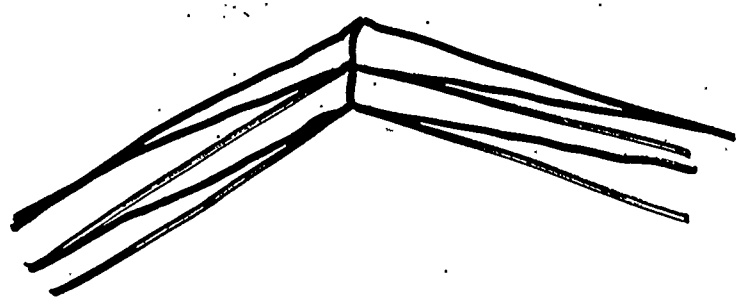

- These grids may be suitable for finite volume methods based on the median mesh. This method is lower order than the Voronoi method.

Conclusions

- For highly anisotropic transport phenomena, anisotropic grids are desirable to accurately resolve the gradients.
- Finite element methods can utilize these grids; many finite volume methods won't be able to compute with these grids.
- Triangular unstructured grids may be crucial for modeling realistic "ITER" divertor design.
- Our finite element method:
  - adapts on the gradients of the dependent variables, and
  - adapts on the actual anisotropy of solution transport processes.

Workshop on Adaptive Grid Methods
Pleasanton, CA.

A General Boundary Capability Embedded in an Orthogonal Mesh

Dennis W. Hewett and Yu-Jiuan Chen

December 8, 1994

Plasma Physics Research Institute
Lawrence Livermore National Laboratory

Curved boundaries are essential for realistic modeling

- In contrast to adaptive triangles, stairstep boundaries on orthogonal grids lead to straightforward data bases and are easy to solve

- Resulting solutions are "ok"
  more than "a couple" of cells away from the stairstep boundary
  but,
  many grid points are required to insure that the interesting physics is more than a few cells from the boundary.

- In some cases, (space-charge-limited emission, for example), the important physics is <u>right on</u> the boundary.

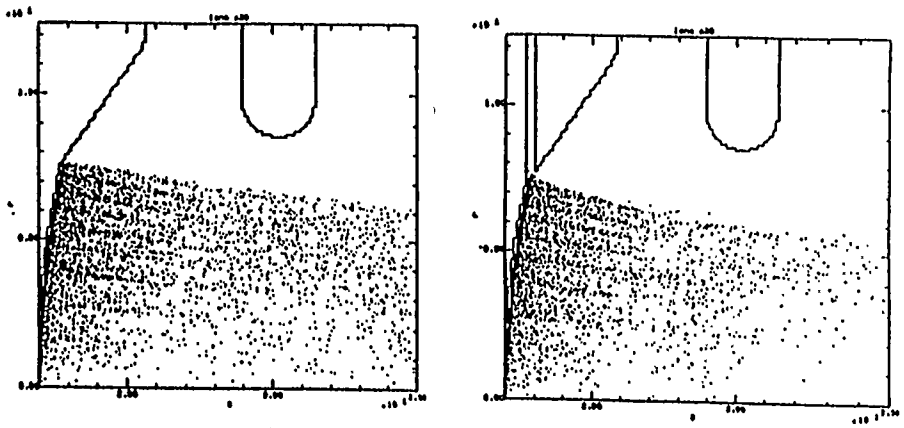

- Deformed grid elements offer an ideal solution....
  .....but
  1) lose "easy" second order accuracy
  2) lose "simple" data base
  3) lose "simple", fast solution techniques with small work arrays

Orthogonal meshes are great for ADI...which, for our problems, is too good to ignore

- We stubbornly hold onto orthoganal meshes because
  1) we can solve our physics with ADI methods
  2) ADI works well on orthogonal grids
  3) for us, ADI runs so*oo* much faster than other methods
     (~2000 X faster, 7 X less storage)

- We use a form of ADI, Dynamic ADI, that dynamically selects the "acceleration" parameter--works much better than Pieceman-Rachford ADI for the general problem. (Doss and Miller, SIAM J. Numer. Anal., 1979)

DADI advances the solution $\Phi(t)$ towards $\Phi(\infty)$ using a double Δt $\{\Phi(d)\}$, then two single Δt s $\{\Phi(2s)\}$. The ratio of the L2 norm between $\Phi(2s)$ & $\Phi(d)$, and the L2 norm between $\Phi(2s)$ & $\Phi(t)$ determines the next Δt.

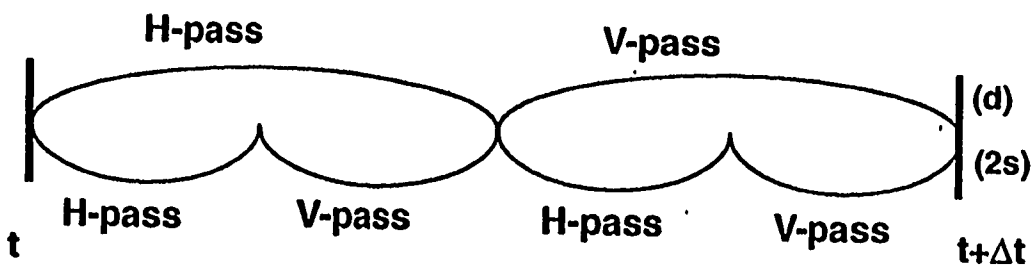

- We have used and extended this method to strongly coupled PDEs of interest in low-frequency EM simulation. (Hewett, Larson, and Doss, JCP 1992)

Our curved boundaries are embedded within the orthogonal mesh

- Starting with an analytic description of a "structure", we determine those grid points that lie just "inside".

- We find the intersection of the structure boundary and grid line & the boundary slope at this intercept...& store at the "corner" just inside.

- These intercepts and slopes define lines
  and
  the intersection of adjacent lines form the
  endpoints of a sequence of piecewise linear segments that are used as the structure definition in our simulations

- Simple examples

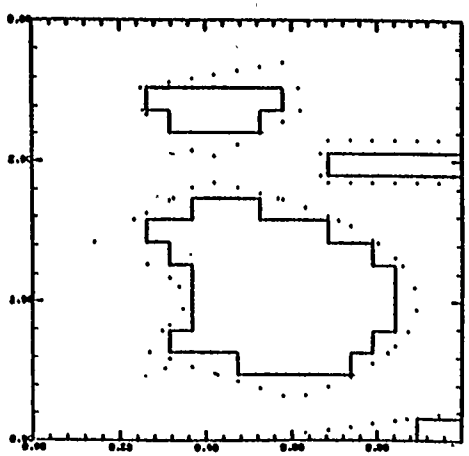

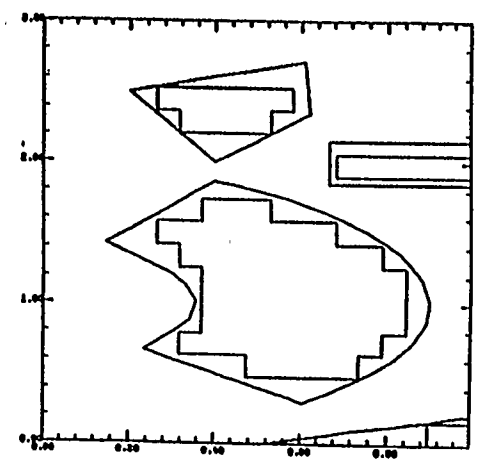

We build "smarter" finite-difference schemes in the vacinity of the piecewise-linear segments

Using the basic eqn.

$$\frac{1}{\Delta x}\left[\frac{(\phi_{i+1}-\phi_{i,j})}{\Delta x}-\frac{(\phi_{i,j}-\phi_{i-1})}{\Delta x}\right]+\frac{1}{\Delta z}\left[\frac{(\phi_{j+1}-\phi_{i,j})}{\Delta z}-\frac{(\phi_{i,j}-\phi_{j-1})}{\Delta z}\right]=-4\pi\rho$$

Dirichlet

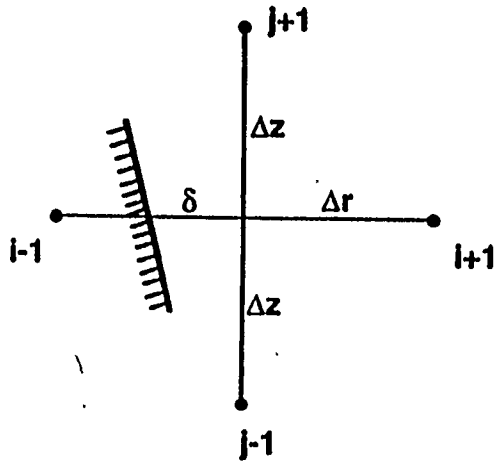

plus the constraint

$$\phi_D = (1-\delta)\phi_{i,j} + \delta\phi_{i-1}$$

to eliminate

$$\phi_{i-1}$$

Neumann

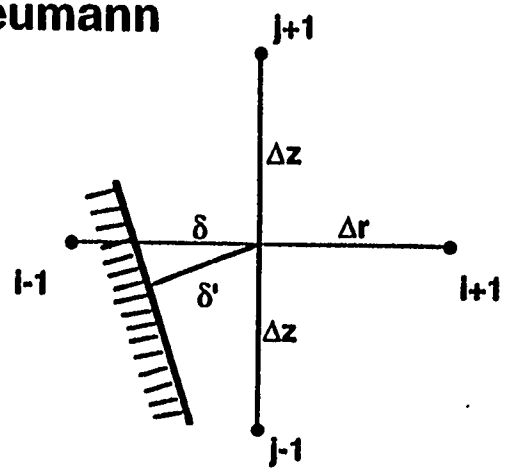

plus the constraint

$$\frac{(\phi_{i,j}-\phi_*)}{\delta'}=\sigma$$

where

$$\phi_* = (1-\delta)\phi_{i,j} + \delta\phi_{i-1}$$

to eliminate

$$\phi_{i-1}$$

The piecewise linear segments have become the real boundary

- A defect correction scheme is used so that these more expensive coefficients need be generated only once, stored, and used on successive iterations

- The remainder of the codes has evolved so that the piecewise linear segments are the real boundary....
  they just happen to be stored on an underlying "scaffold" which is the original orthogonal mesh.

- This underlying mesh need not be uniform...just orthogonal

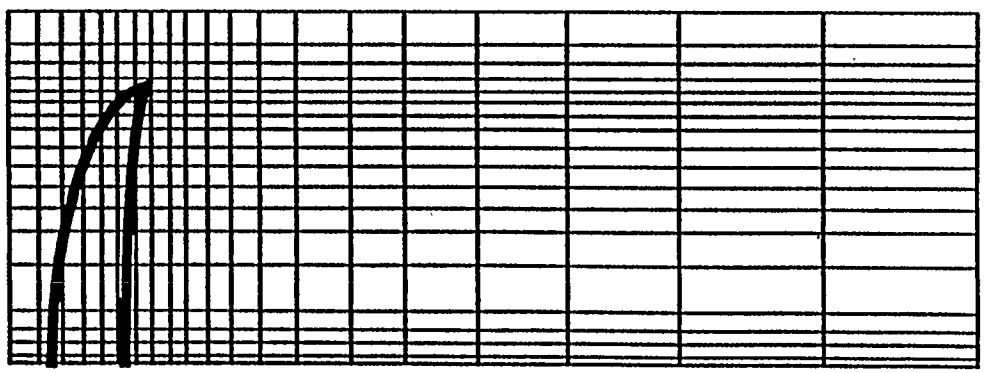

- Orthogonality will at best, waste some resolution...could also slow down with highly elongated cells.

We have been able to do some things quite well

A cone-shaped conductor illustrates some features

120X130

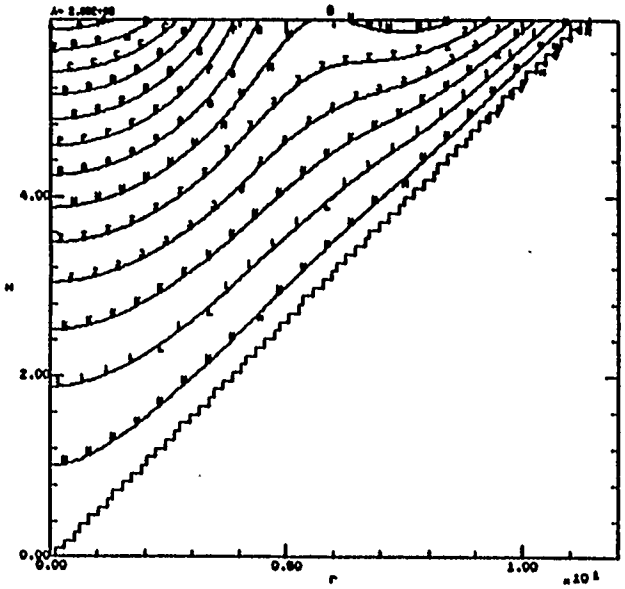

60X65

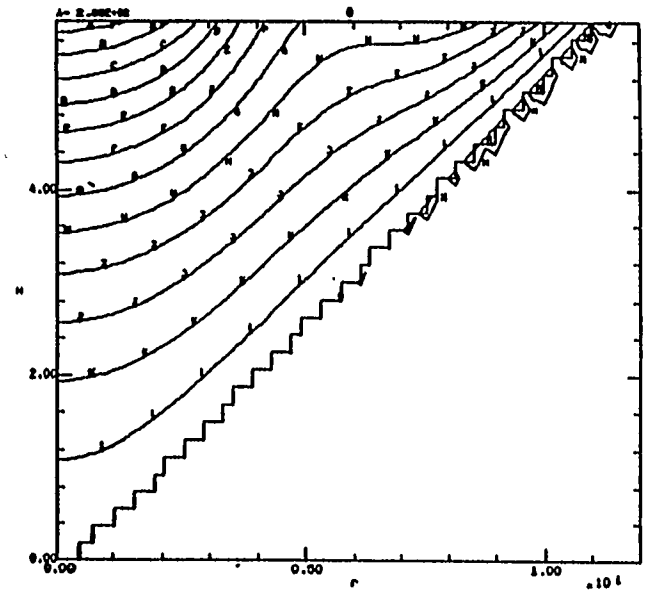

An enlargement of the upper right shows the "dribble" within the boundary needed to make the contour plotter work properly!

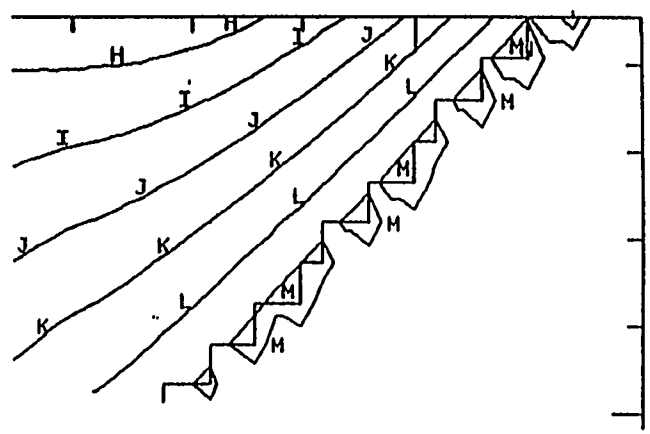

Some examples display the capabilities

This embedded boundary capability has been built into GYMNOS, a R-Z PIC/fluid/hybrid code used to test low-ω EM models. Consider an axisymetric "particle injector" for test cases.

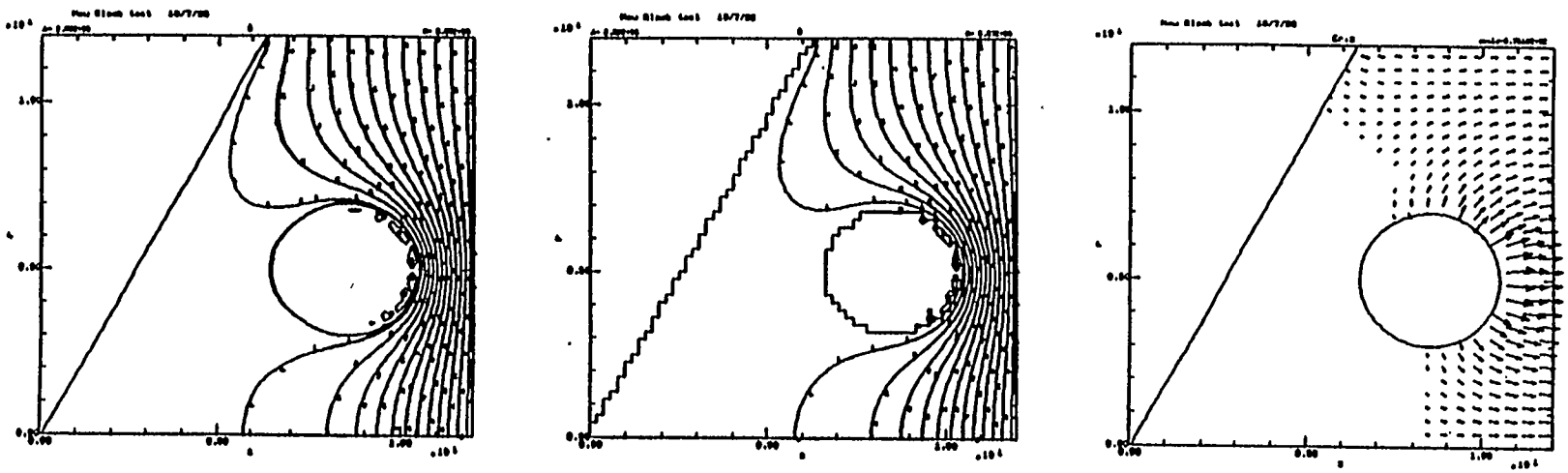

and, with more resolution,

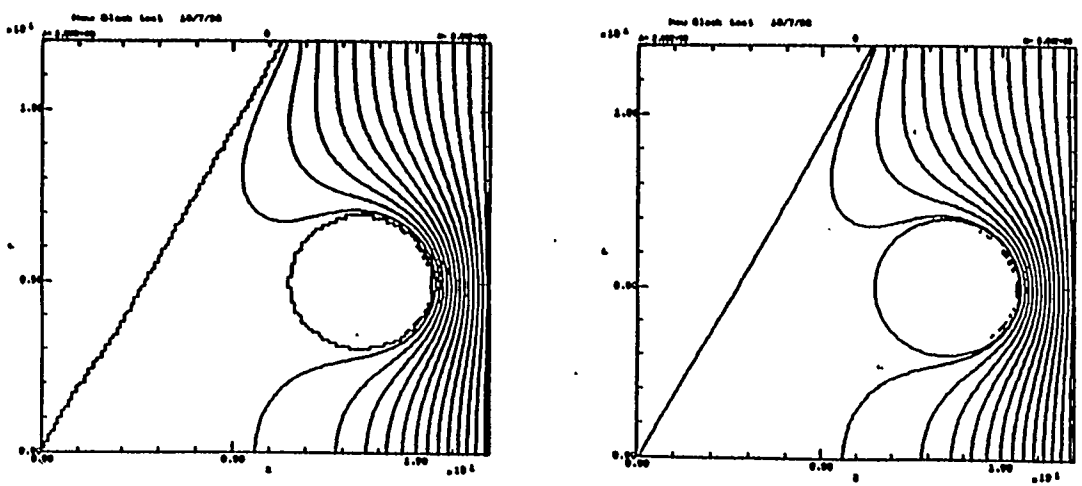

Neumann conditions enhance the applicability

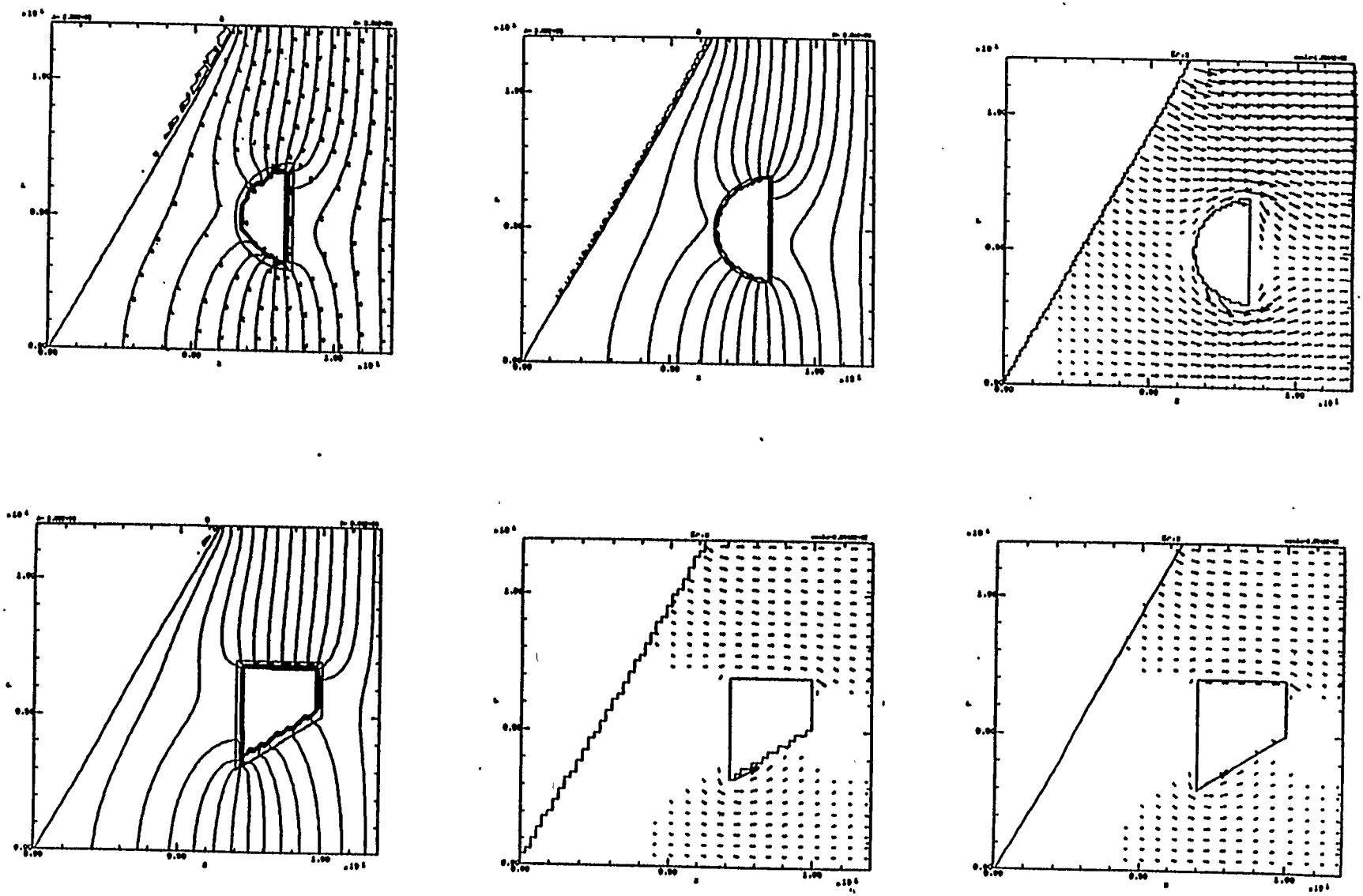

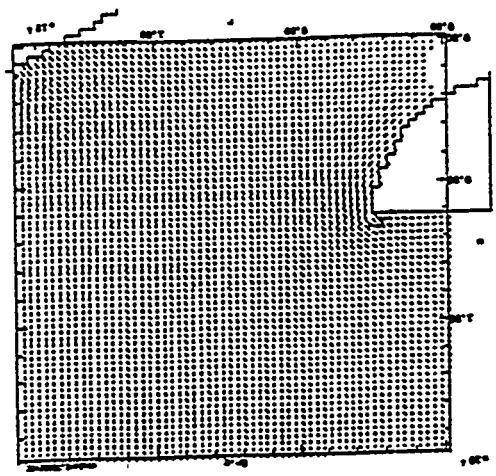

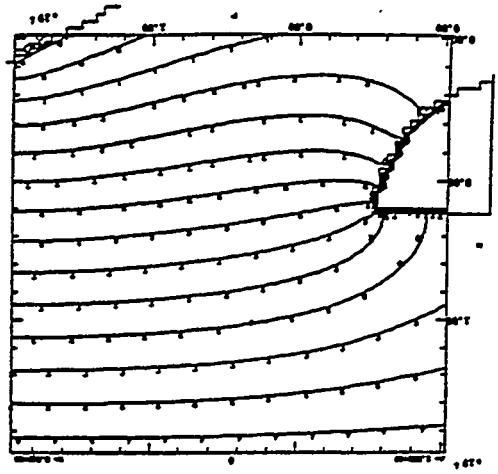

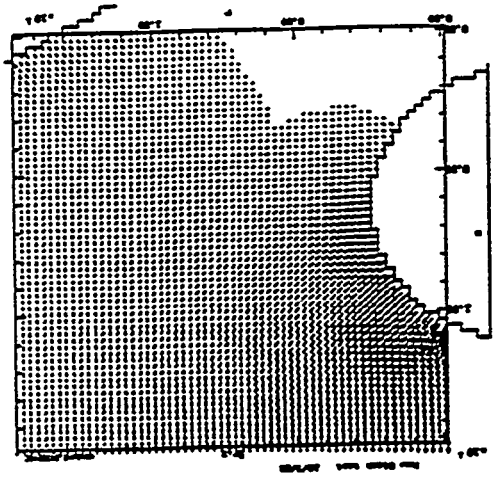

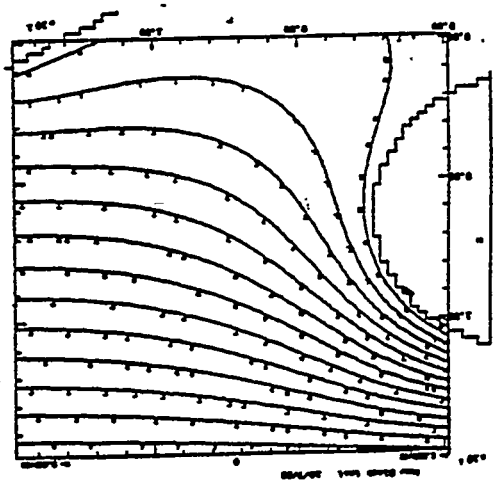

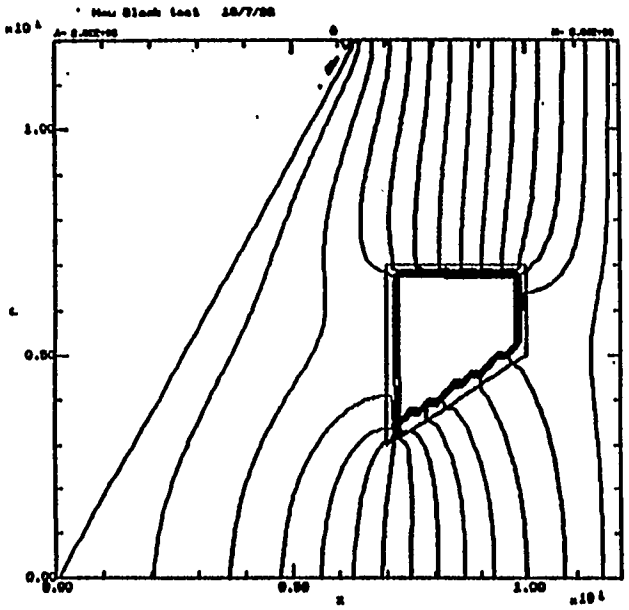
1.00
0.50
0.00
0.00
0.50
1.00
z

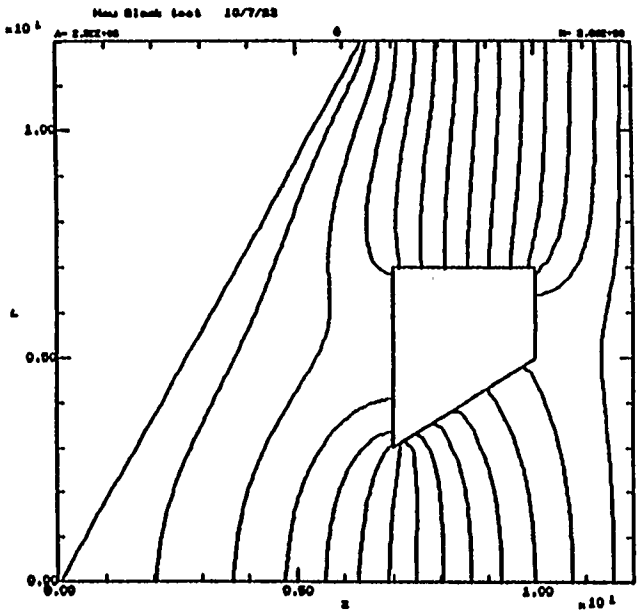
1.00
0.50
0.00
0.00
0.50
1.00
z

More work needed for space-charge-limited emission

Pure Stairstep

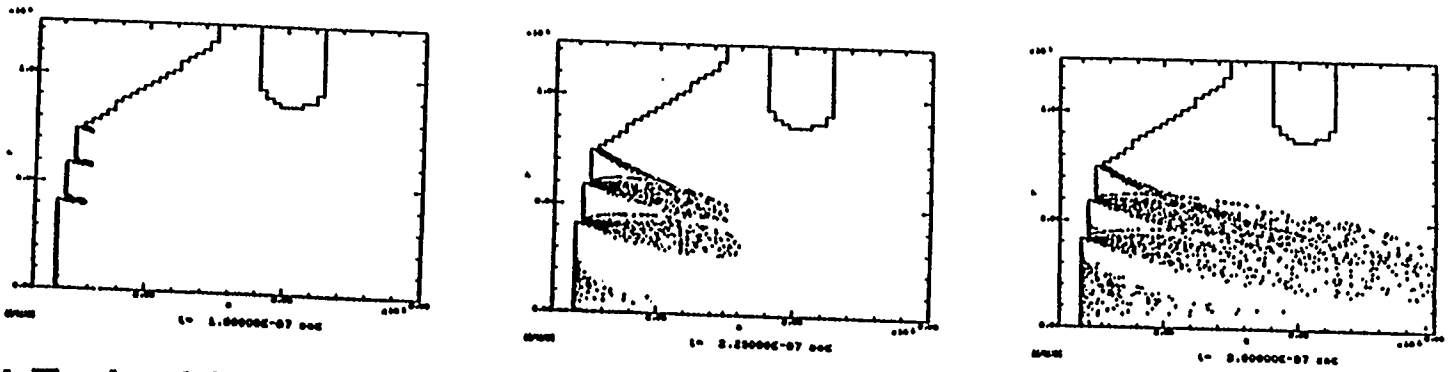

Best Embedded Curved Boundary (12/8/94)

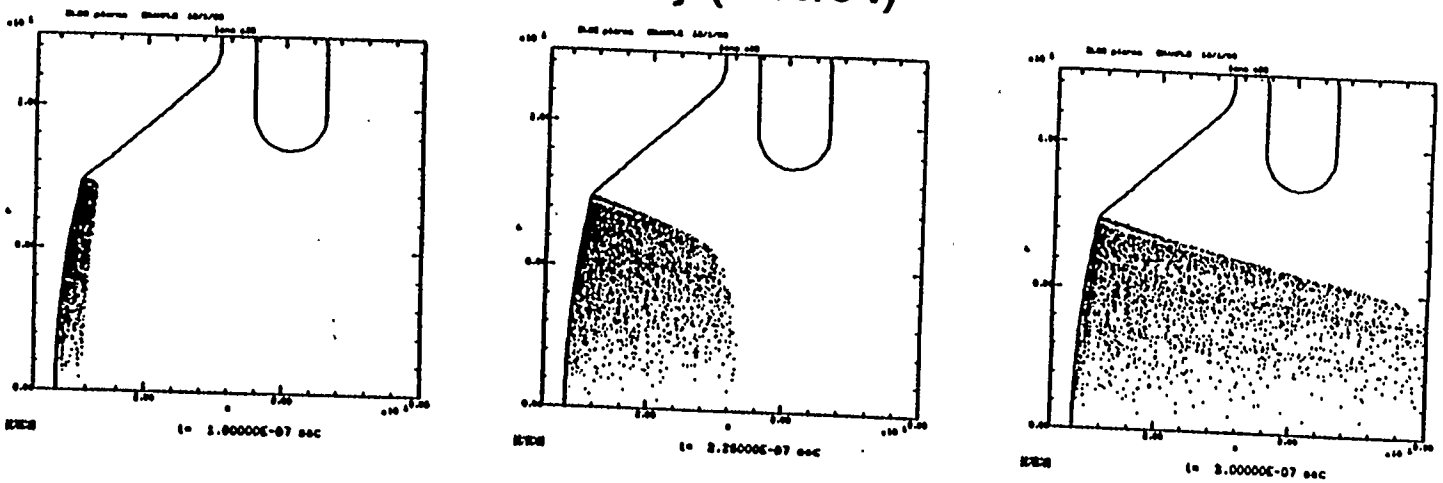

New method promises better results with far fewer grid points...as soon as the obvious problem is fixed

A difficulty may be in finding the volume of a cell so that the correct density can be determined.

Summary

A piecewise linear boundary is used to represent structures embedded within an orthogonal mesh

This Embedded Curved Boundaries (ECB) technique is almost as good as adaptive triangles...
and
allows our continued use of fast ADI methods

ECB can be viewed as a finite element boundary whose defining information is held by a "scaffold", the underlying orthogonal mesh

The underlying mesh determines the storage or "data structure"....
and
is very useful (fast!) in other areas of a typical code (such as PIC particle location and interpolation)

Recent computational progress offers a solution without explicit vector decomposition

Difficulty with the solenoidal field eqn in the traditional Darwin (radiation-free) model

$$\nabla^2 \mathbf{E}_{sol} = \frac{4\pi}{c^2}\dot{\mathbf{J}}_{sol} = \left(\mathbf{Q} + \mu\, \mathbf{E}_{sol}\right)_{sol}$$

resulted in new Streamlined Darwin Field (SDF) method

$$\nabla^2 \mathbf{E}_{sol} - \nabla^2(\nabla\psi) = \left(\mathbf{Q} + \mu\, \mathbf{E}_{sol}\right)$$

Added a new 3rd order term to compensate for the irrotational part we fail to discard.

that turns into the coupled set of PDEs

$$\boxed{\begin{aligned} \nabla^2\xi - \mu\xi &= (\mathbf{Q} + \mu\, \nabla\psi) \\ \nabla^2\psi &= -\nabla\cdot\xi \end{aligned}} \quad \text{with} \quad \mathbf{E}_{sol} = \xi + \nabla\psi$$

Initially, SDF method was prohibitive to solve--led to CEDADI technique

- 500x faster, 7x less storage (recently found another factor of 4 in speed)
- makes SDF feasible & practical.

FLAG: A Multi-dimensional Adaptive Free-Lagrange Code for Fully Unstructured Grids

Donald E. Burton
Douglas S. Miller
Todd Palmer

Lawrence Livermore National Laboratory

Workshop on
Adaptive Grid Methods for Fusion Plasmas
Pleasanton, California
December 8-9, 1994

We are developing a multidimensional (1D, 2D, 3D) free-Lagrange method

free Lagrange = { Lagrange hydro } + { unstructured polyhedra } + { reconnection, refinement, relaxation, etc. }

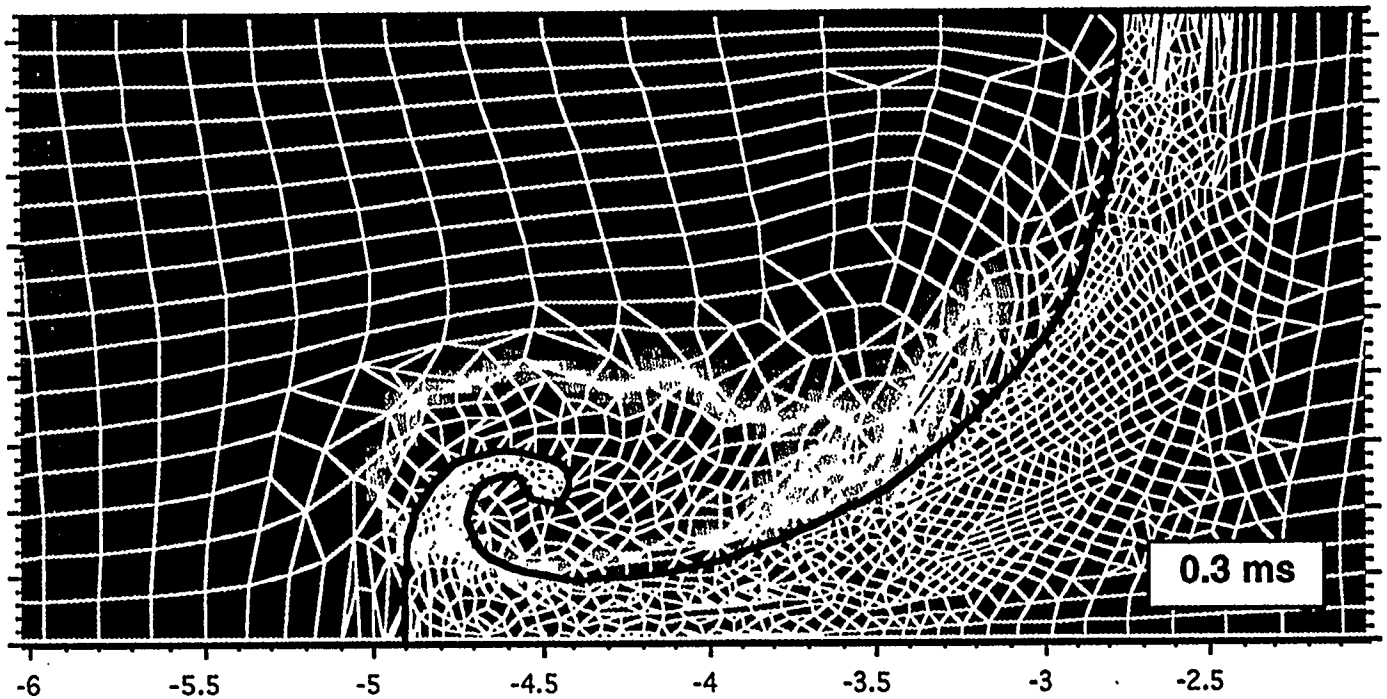

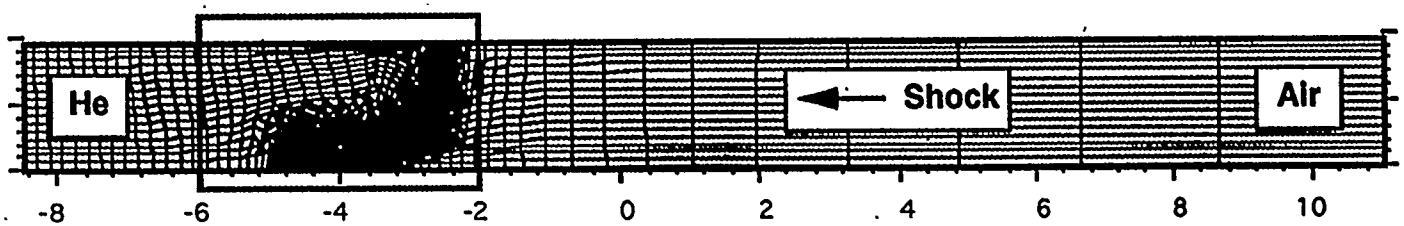

Free-Lagrange History

1959	Pasta & Ulam	Suggested concept
1965	D'yachenko	Early Russian work
1972	Glagoleva, et al	MEDUZA code
1984	Sofronov, et al	
1968	Crowley	Coins term "free-Lagrange"
1970		2D triangular grid (also called FLAG)
1985		Mixtures of triangles & quads
1985	-----	First Free Lagrange Conf. - Hilton Head
1985	Trease	3D tetrahedral grid
1990	-----	Second Free Lagrange Conf. - Jackson Hole
1991	Burton	2D adaptive free-Lagrange
1992		Multidimensional "polyhedral" formulation
FY94		Current 3-year FLAG project begins

Mesh Optimization

Adaptive free-Lagrange (AFL) is a hybrid method: 2D operators

FL - Reconnection

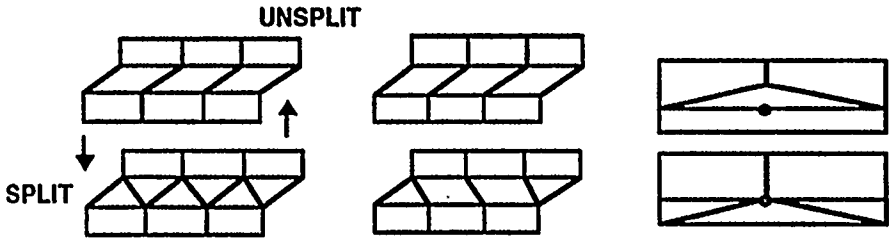

ALE - Advection

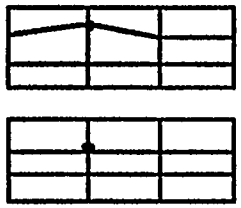

Adaptive Refinement

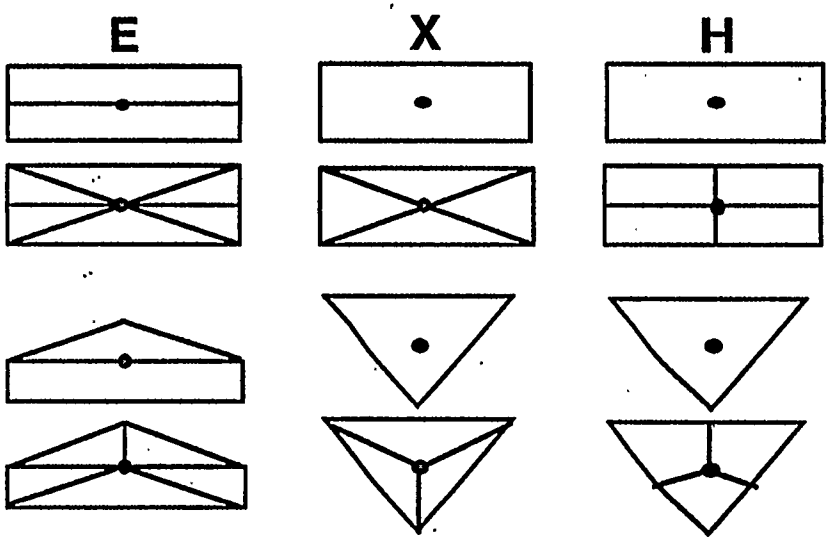

Advection Slides

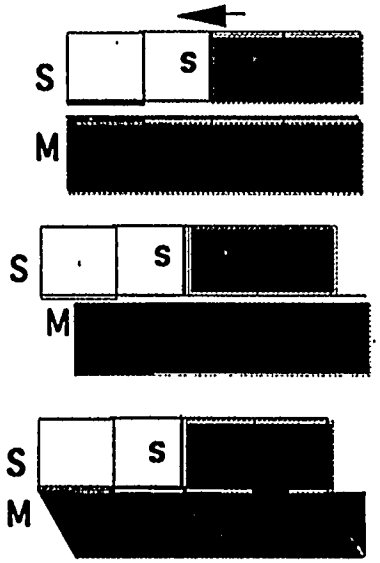

Even simple 3D free-Lagrange operations produce polyhedra outside the standard finite element set

STANDARD FINITE ELEMENT POLYHEDRA

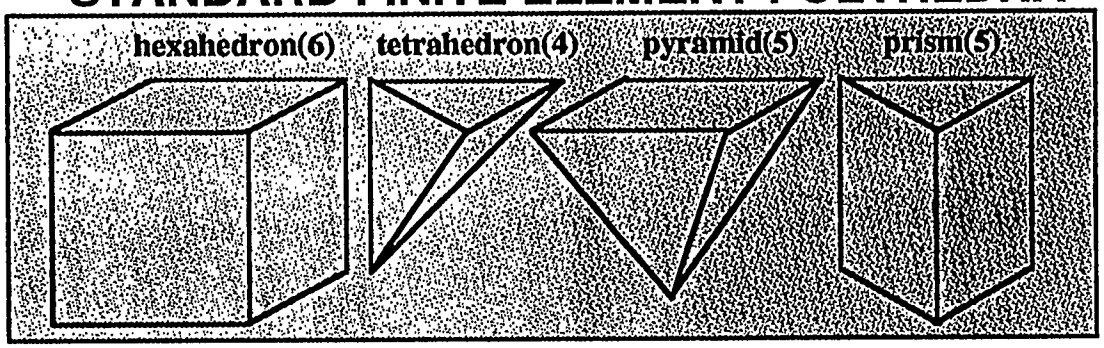

TETRAHEDRAL DECOMPOSITION

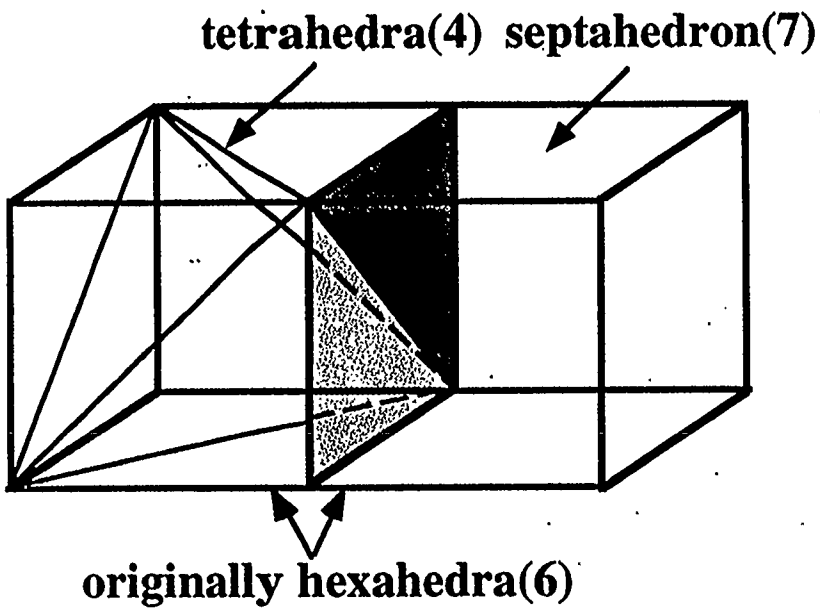

H-REFINEMENT

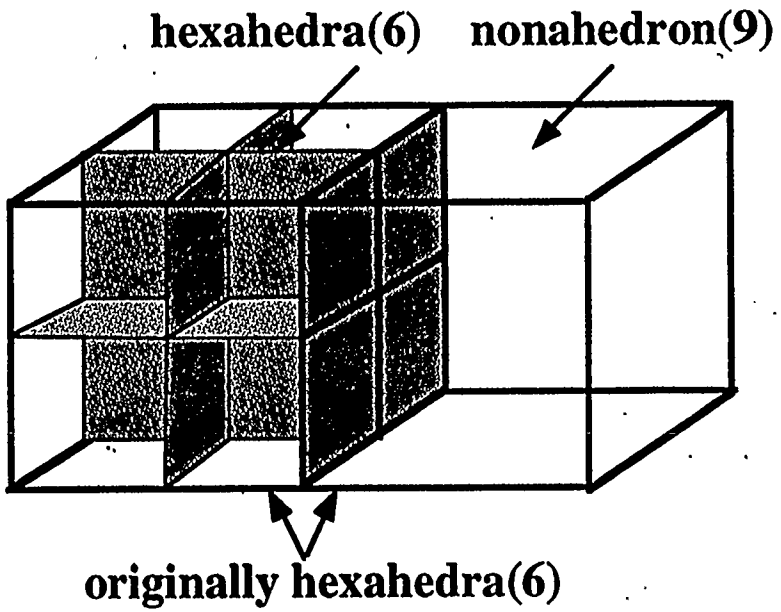

By adopting only differencing schemes appropriate for general polyhedra ...

we keep our options open with respect to mesh optimization and choice of mesh type

- Hexahedral mesh
  - Best hydro
  - Used by: (3D) DYNA3D, (2D) TENSOR, HEMP, etc
  - Options for maintaining hexahedra are limited to relaxation & regridding
  - H-refinement seems only refinement possibility

- Tetrahedral mesh (TM)
  - Relatively stiff for SGH hydro
  - Used by: (3D) X3D, (2D) 1970 FLAG, MEDUZA
  - Many reconnection & refinement options

- Standard finite-element set
  - hexahedra, tetrahedra, prisms, pyramids
  - Limited reconnection options

- Polyhedral mesh based upon a tetrahedral dual mesh (TDM)
  - SGH hydro properties relatively unexplored
  - Used by: (2D) CAVEAT-GT, HOBO, DMK
  - Many reconnection & refinement options

- H refined grids
  - Polyhedral grids are produced by H-refinement
  - Suitable for Eulerian, ALE, some Lagrange
  - Limited reconnection options

A tetrahedral based strategy illustrated in 2D

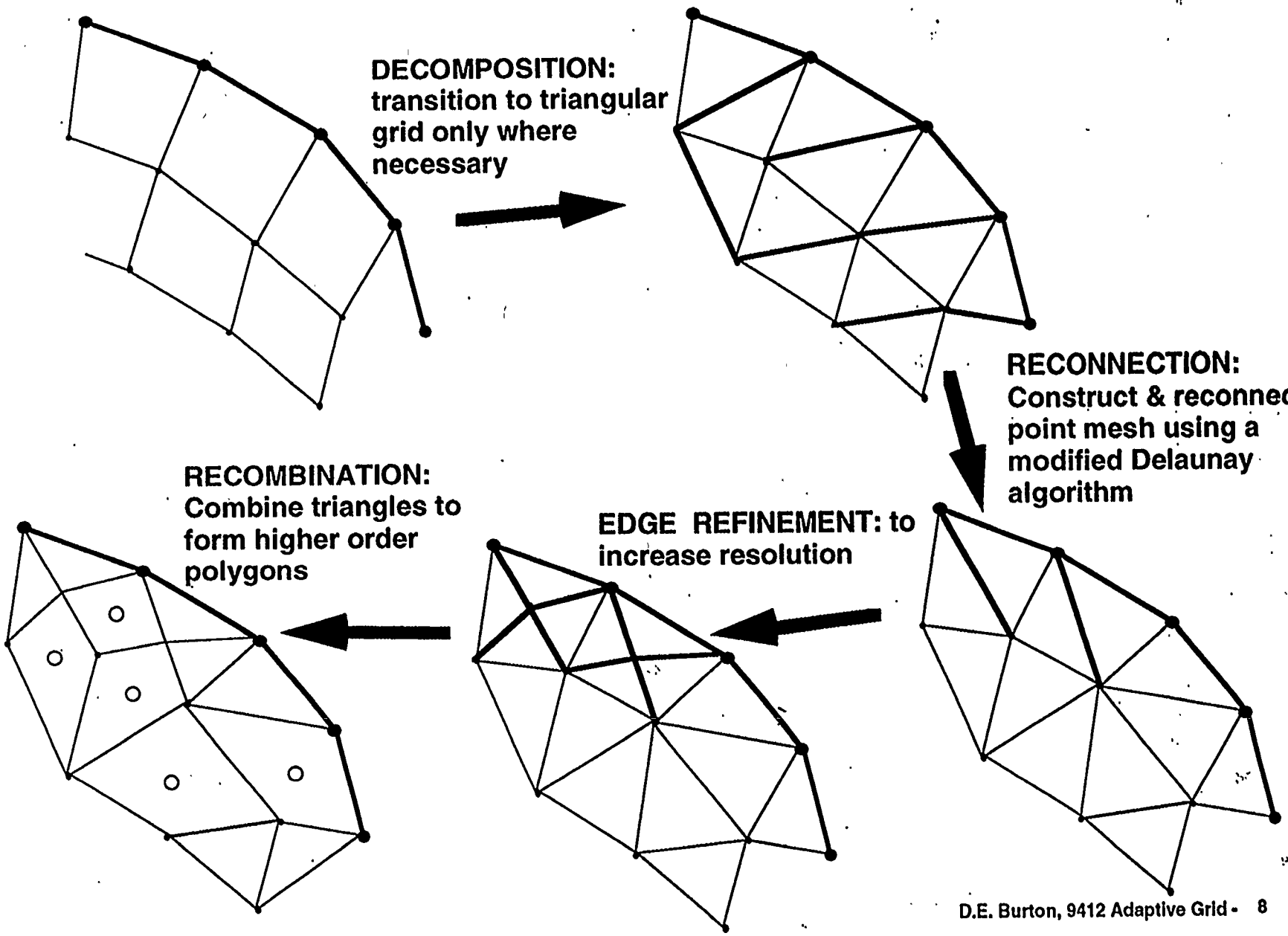

Tetrahedral based strategy applied to a 3D Coggeshall flow field

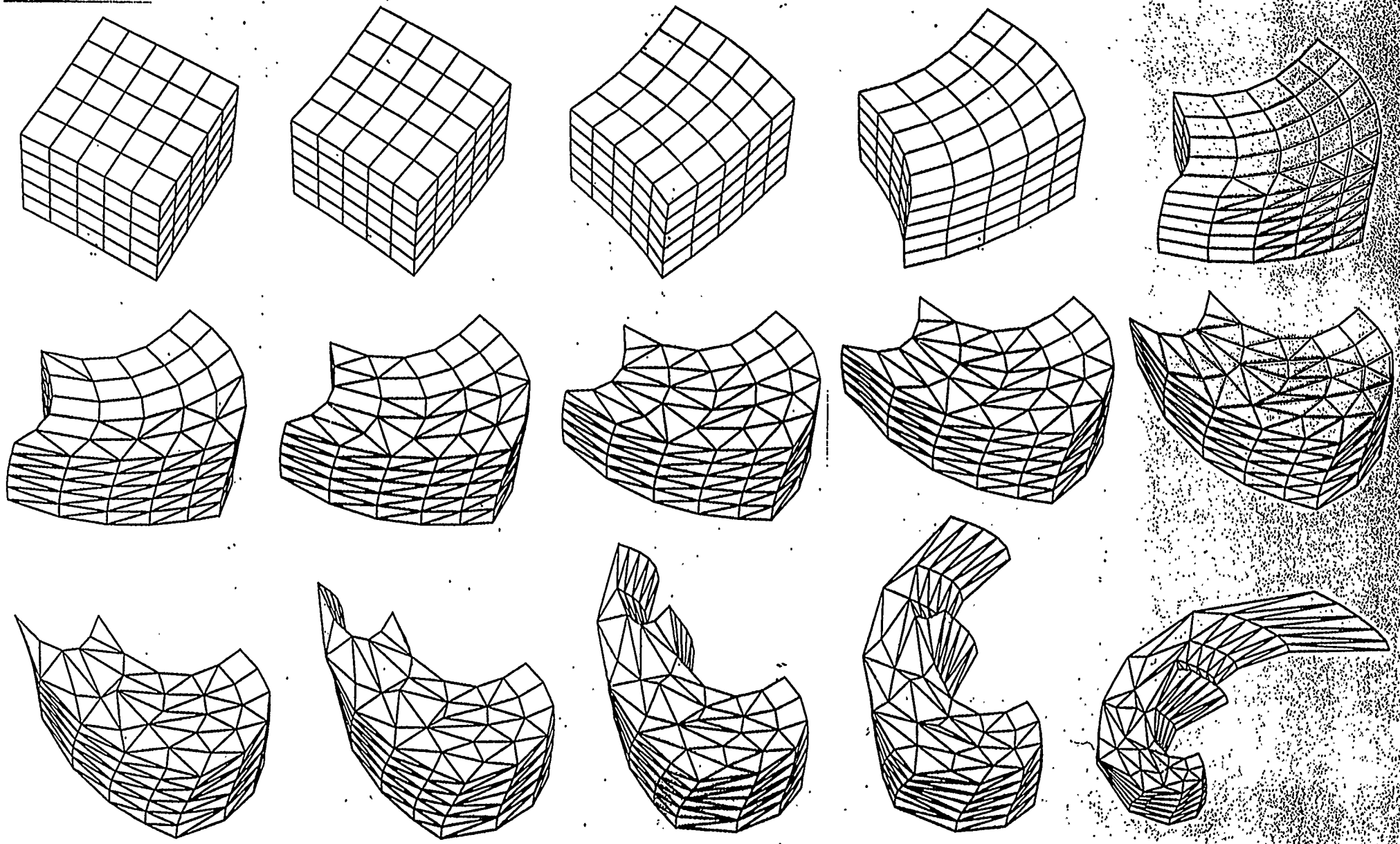

Tetrahedral based strategy applied to a 3D analytical flow field

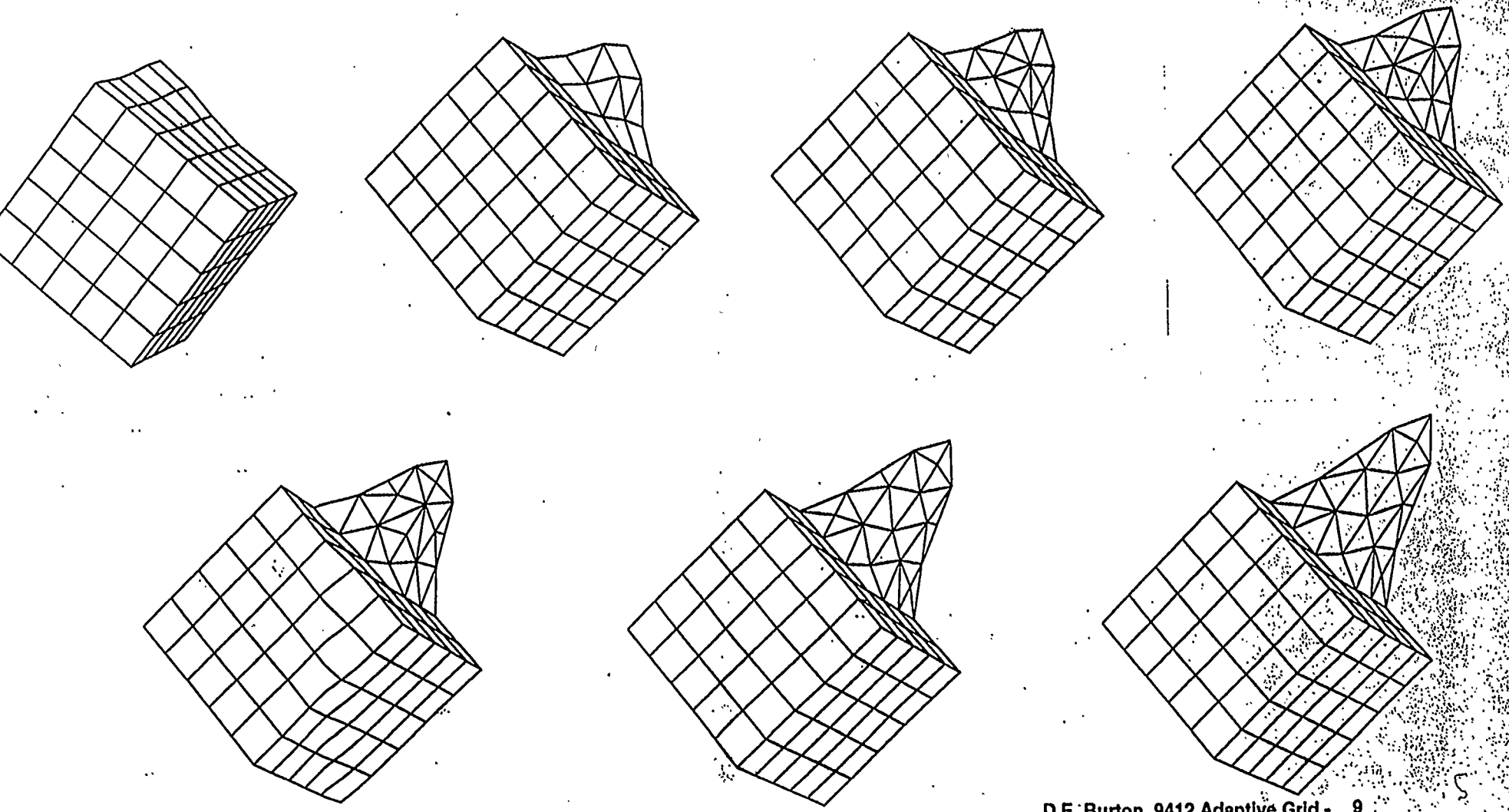

General polyhedral grid permits optimization strategies based upon a tetrahedral dual mesh

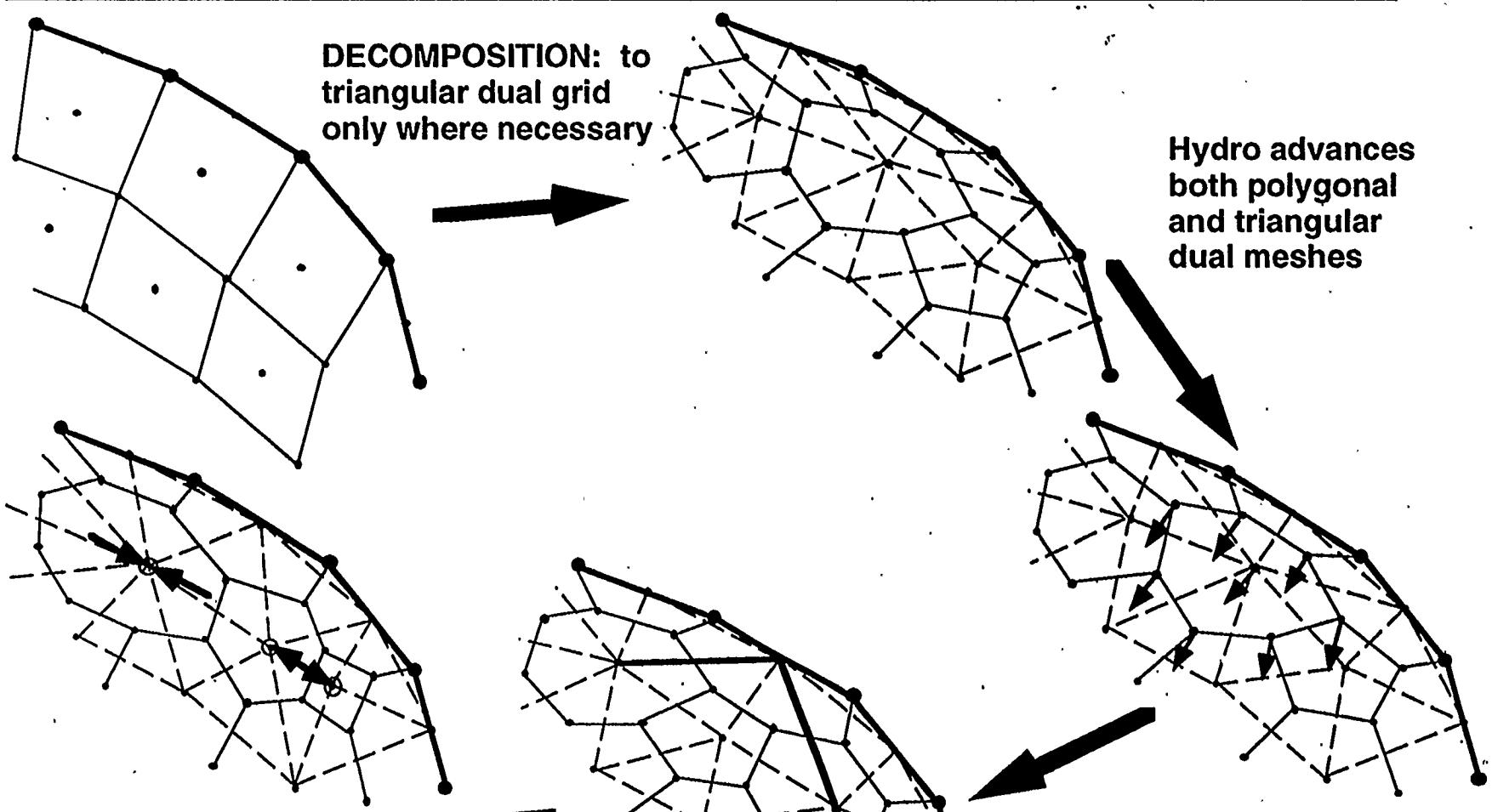

DECOMPOSITION: to triangular dual grid only where necessary

Hydro advances both polygonal and triangular dual meshes

RECONNECT dual mesh using a modified Delaunay method RECONSTRUCT polyhedral point mesh

REFINE by deleting and creating edges* in the dual mesh

*DMK: Sofronov, Rasskazova, & Shaporenko

2D illustrated for simplicity

Edge refinement only on a triangular dual mesh - DMK code (Russian)

No reconnection
is done by DMK

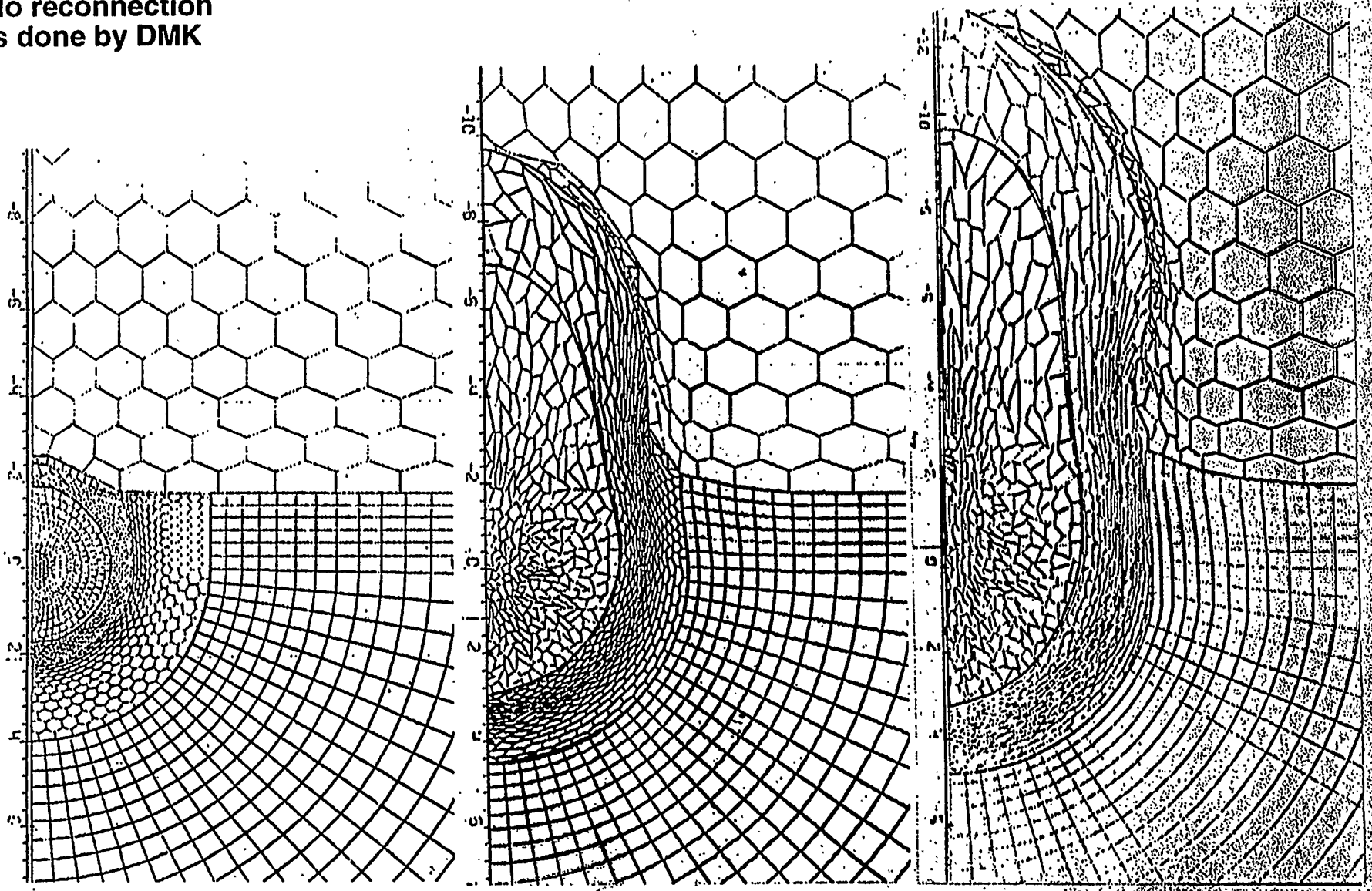

The general polyhedral grid also naturally accommodates H refinement

Method is applicable to:
- Eulerian
- ALE
- some Lagrange

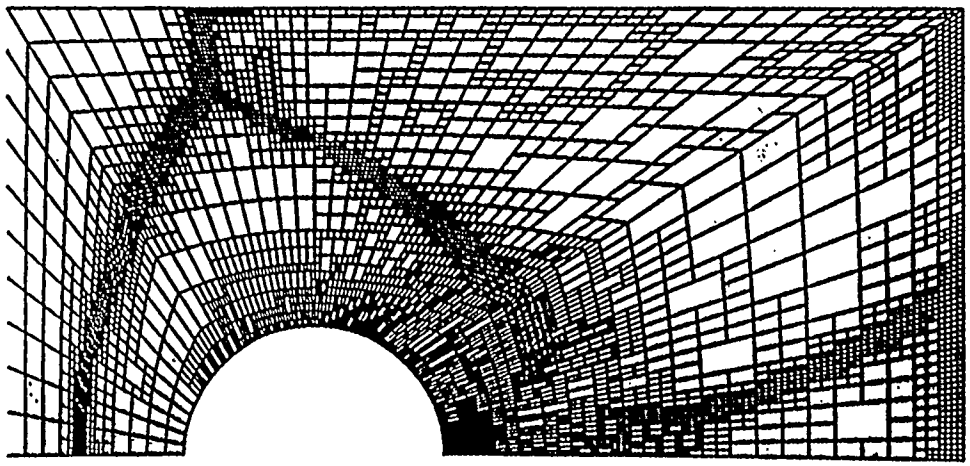

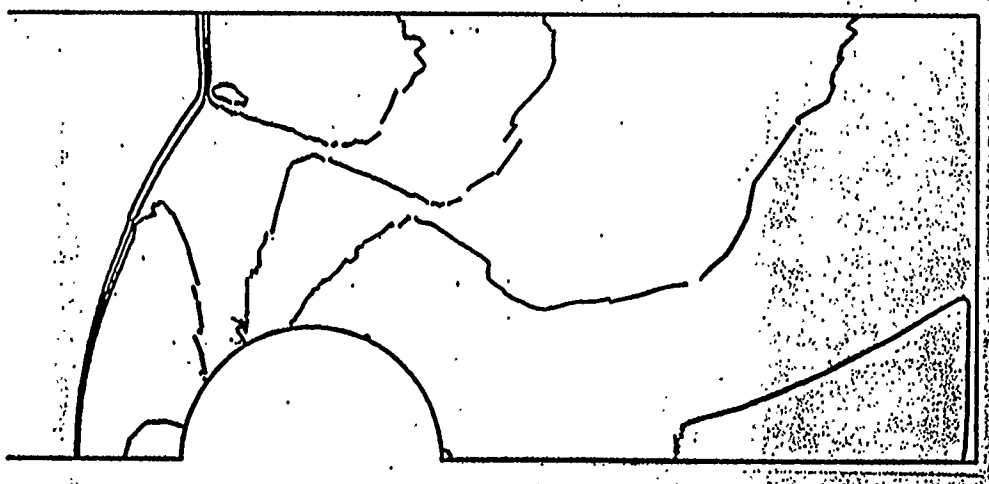

2D illustration from Crowley's LAM code

```
( -7.000e+00,  0.        ) , (  1.500e+01,  1.030e+01)
 LAM2 density at time =   1.6001e+03, nzones=  6019 bpa
 levels =   2.60e-04  1.05e-03  1.83e-03  2.62e-03  3.40e-03
```

Code Backplane

Functionality of AJAX and DELFI

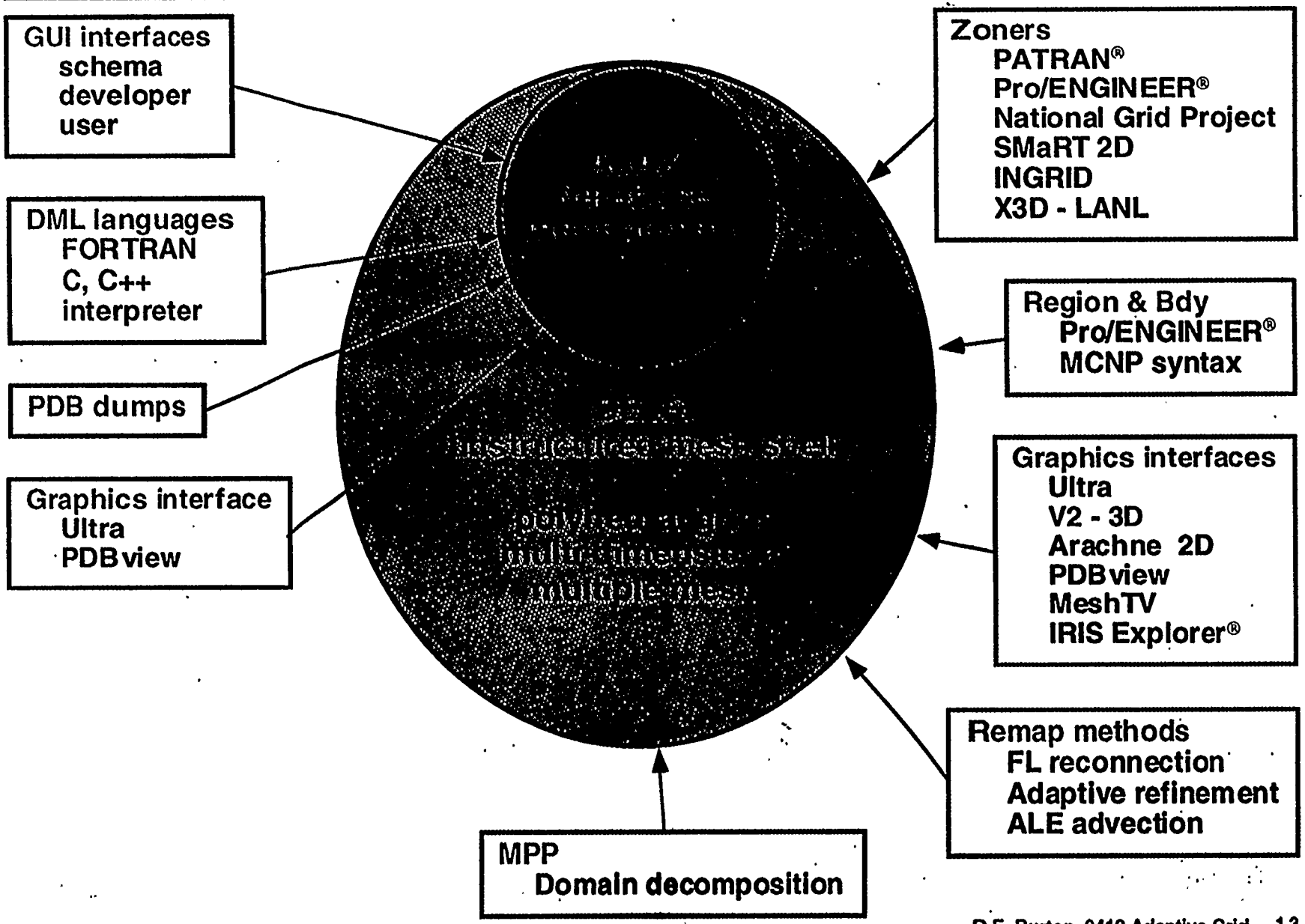

We expect AJAX & DELFI to support a family of independent physics codes

Graphics

V2

D. Lappa

Diffusion & Porous Flow

GANDI

T. Palmer
D. Burton
P. Nowak
Collaborators:
M. Adams - TAMU

Hydrodynamics

Turbulent mixing
Multiphase hydro

FLAG

D. Burton
D. Miller
A. Harrison
Collaborators:
H. Trease - LANL
M. Fritts - SAIC

Electromagnetics

???

SN transport

SNAC

P. Nowak
T. Palmer
Collaborators:
M. Dorr - CMRD
M. Adams - TAMU
E. Larsen - UMich

Parallel Monte Carlo

PMC

J. Rathkopf
Collaborators:
G. Zimmerman - P
B. Biester - B
B. Martin - UMich

The clear payoff: By factoring out common mesh machinery, we can create algorithms which can be easily coupled when necessary.

The AJAX hierarchical object-oriented database helps to isolate and modularize physics modules

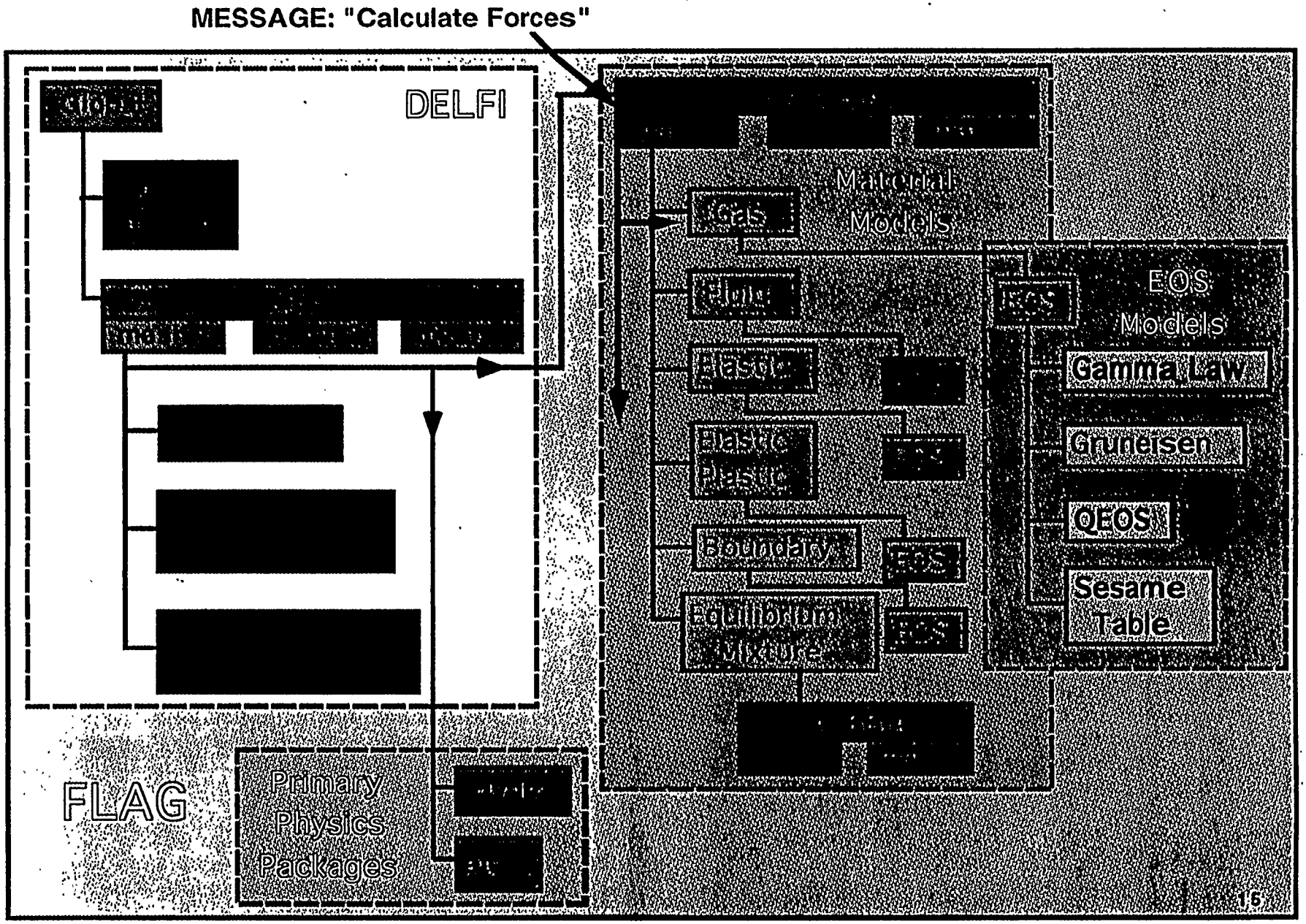

Multiple meshes of different dimensionality can be coupled to model complex processes

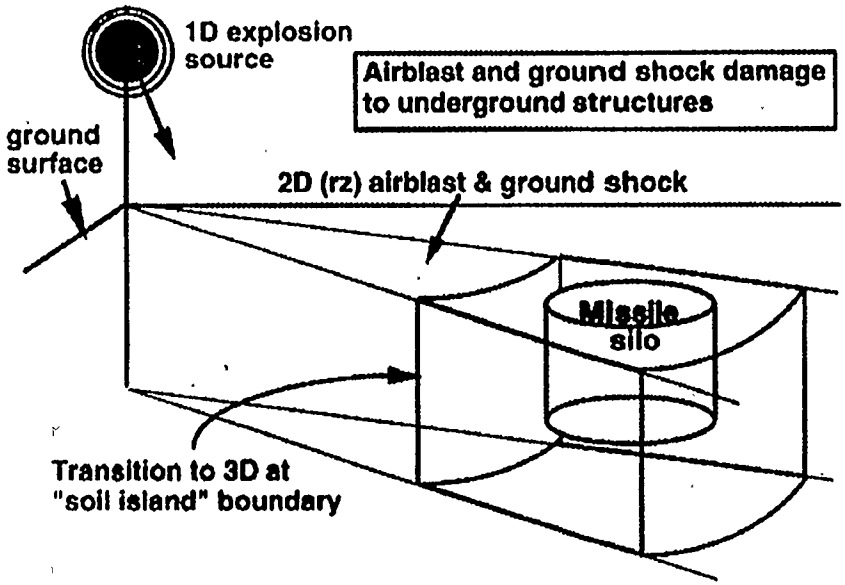

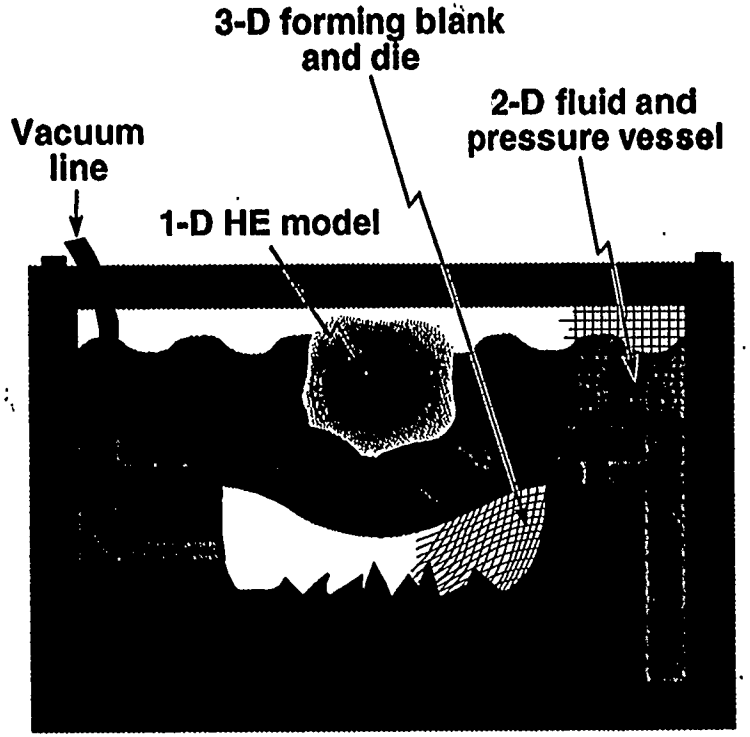

Explosive forming in a closed die

We have demonstated the multiple mesh capability of our code system

by simultaneously computing in meshes of different dimensionality

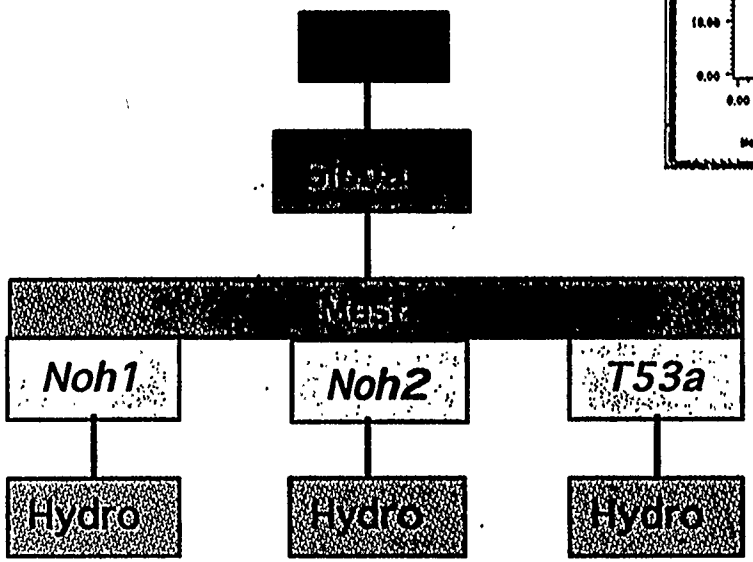

3 mesh data layout

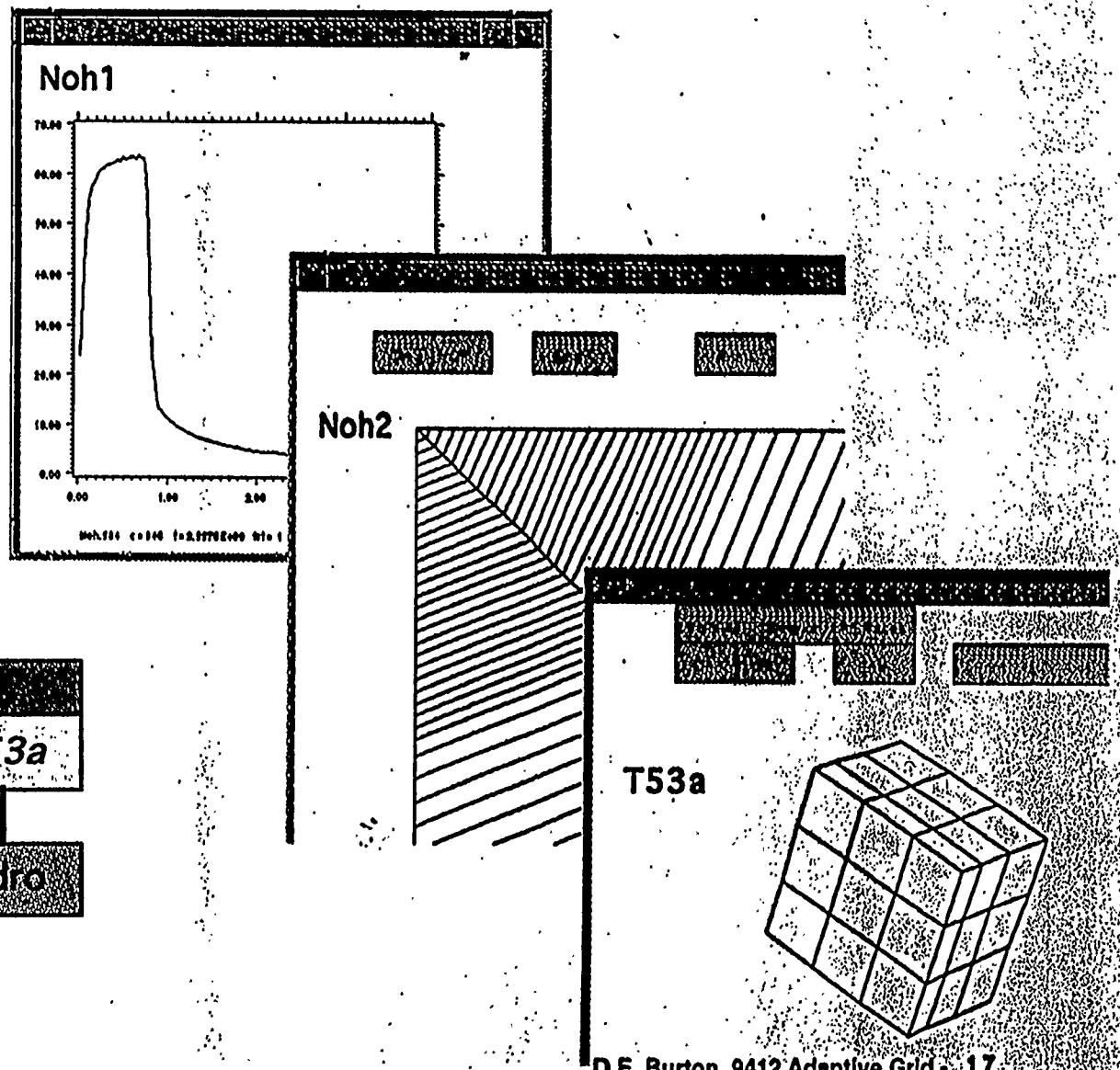

Uses for multiple instances of meshes

- Multi-dimensional combinations
  - 1D source + 2D propagation + 3D soil island
  - 2D Lagrange hydro + 3D Eulerian instability layer
- Mesh blocks
  - Slide surfaces
  - Zoning discontinuities
  - Independent timestep
  - MIMD parallelization
  - Composite meshes
- Physics dependent
  - Lagrange hydro mesh + regular transport mesh
  - Lagrange hydro mesh + smooth particle hydro (SPH) region
- Ensemble averages
  - Stochastic backscatter
  - Instability modeling
  - Parameter studies on material variations

- Managing the data is the difficult part
- Strong support from the database makes this possible

We are developing the visualization tools necessary for viewing data on unstructured FLAG grids

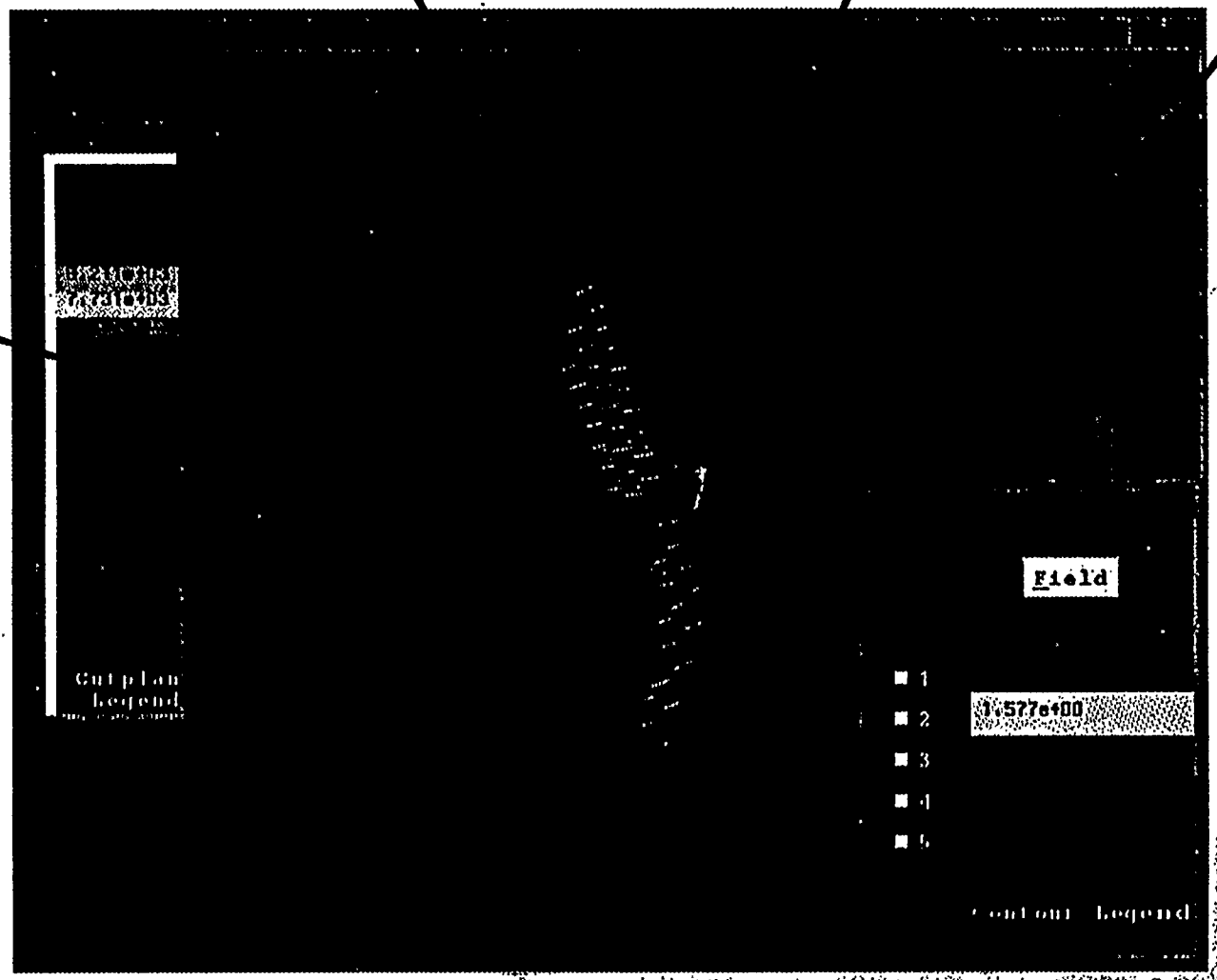

3D Richtmyer-Meshkov instability

Staggered Grid Lagrange Hydrodynamics

General polyhedra are easily described by the finite volume discretization method

The finite volume method uses surface integrals to discretize numerical operators

General polygons or polyhedra are assembled using triangular or tetrahedral templates called corners (i)

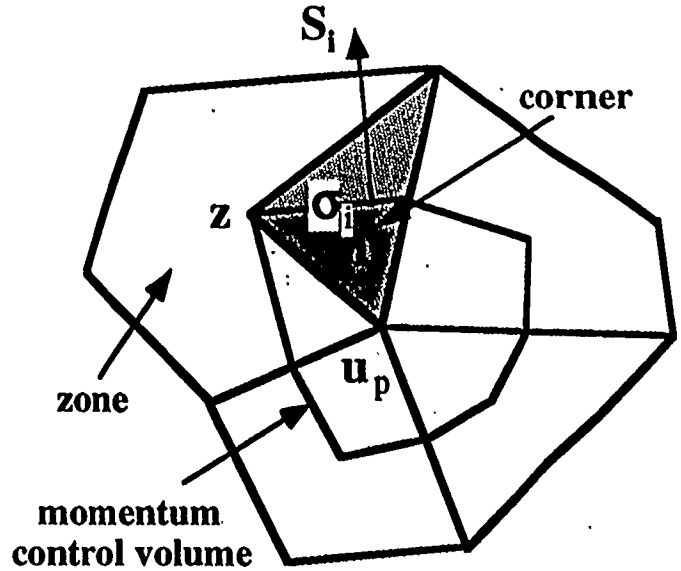

A side (s) has 2 corners (i)

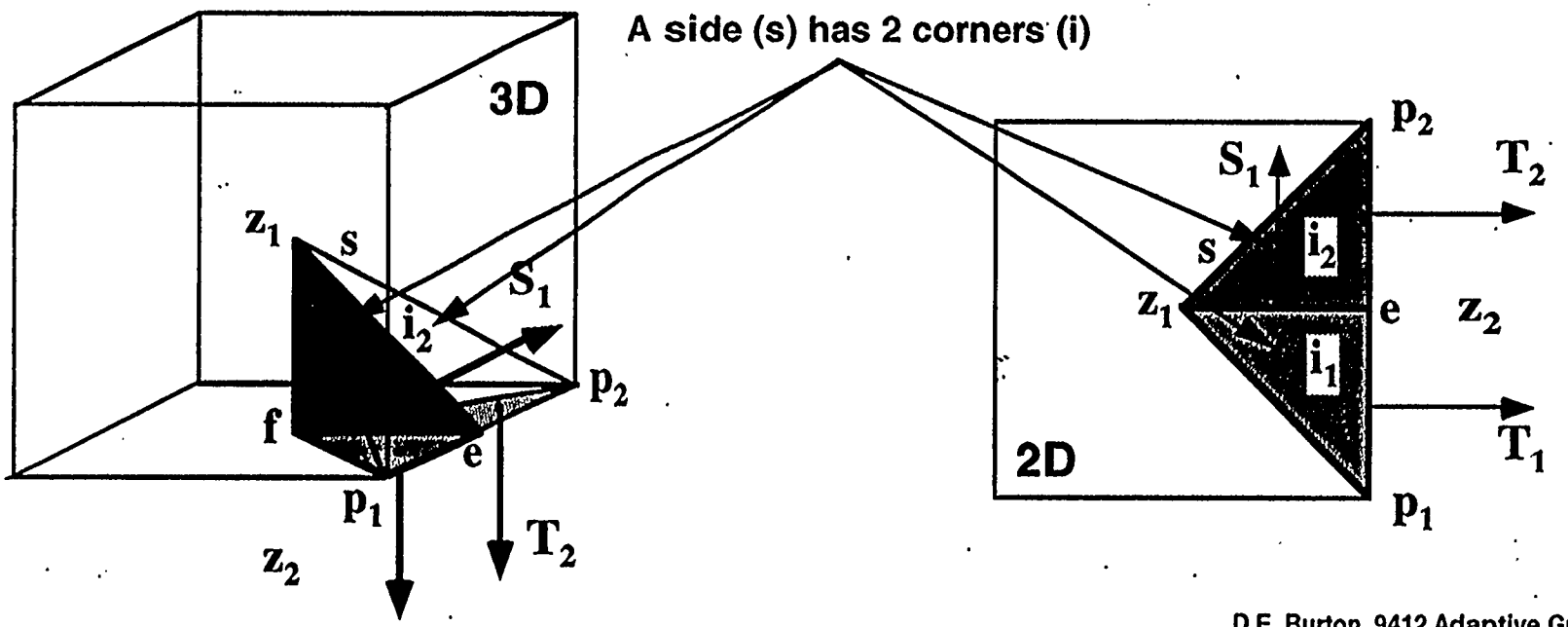

We have derived a consistent formulation of staggered-grid hydrodynamics

Once mass and momentum are specified, the discrete forms of nearly all else can be derived and should not be independently postulated

Typical Formulation

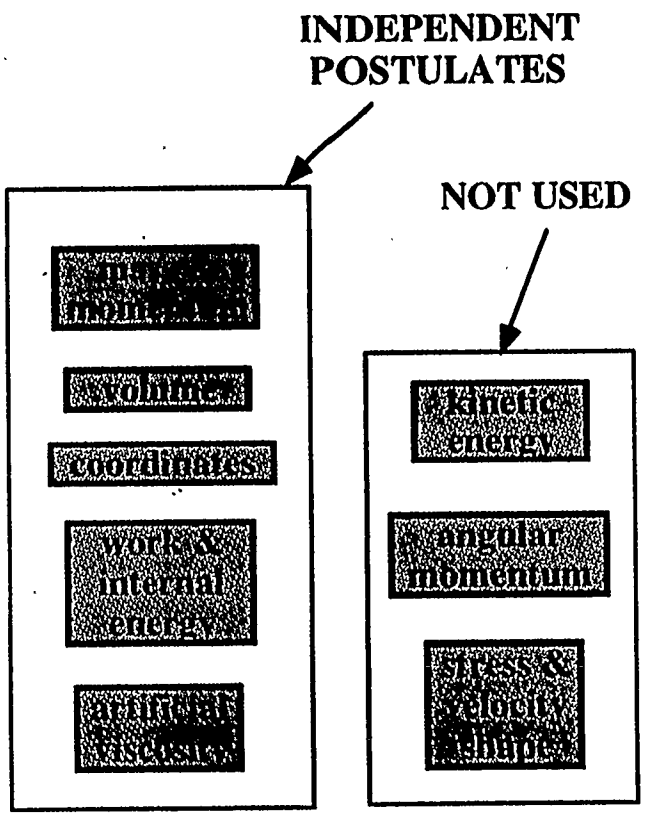

Consistent Formulation

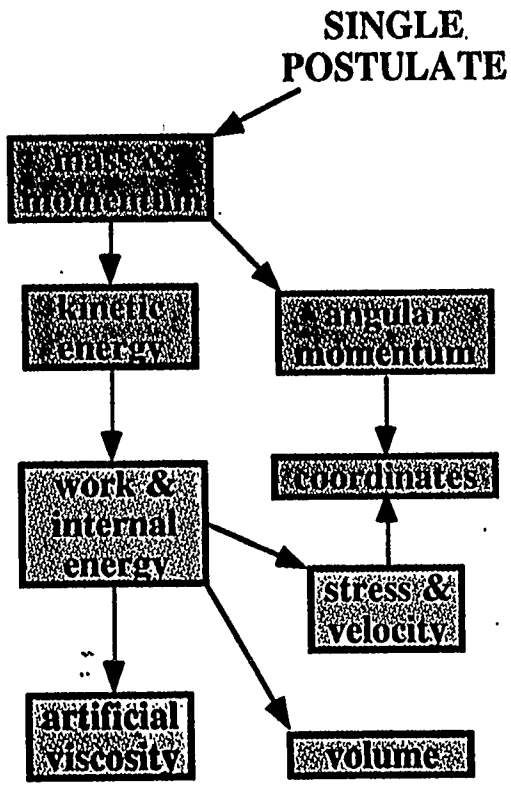

We have been able to derive a remarkable number of properties from these starting postulates

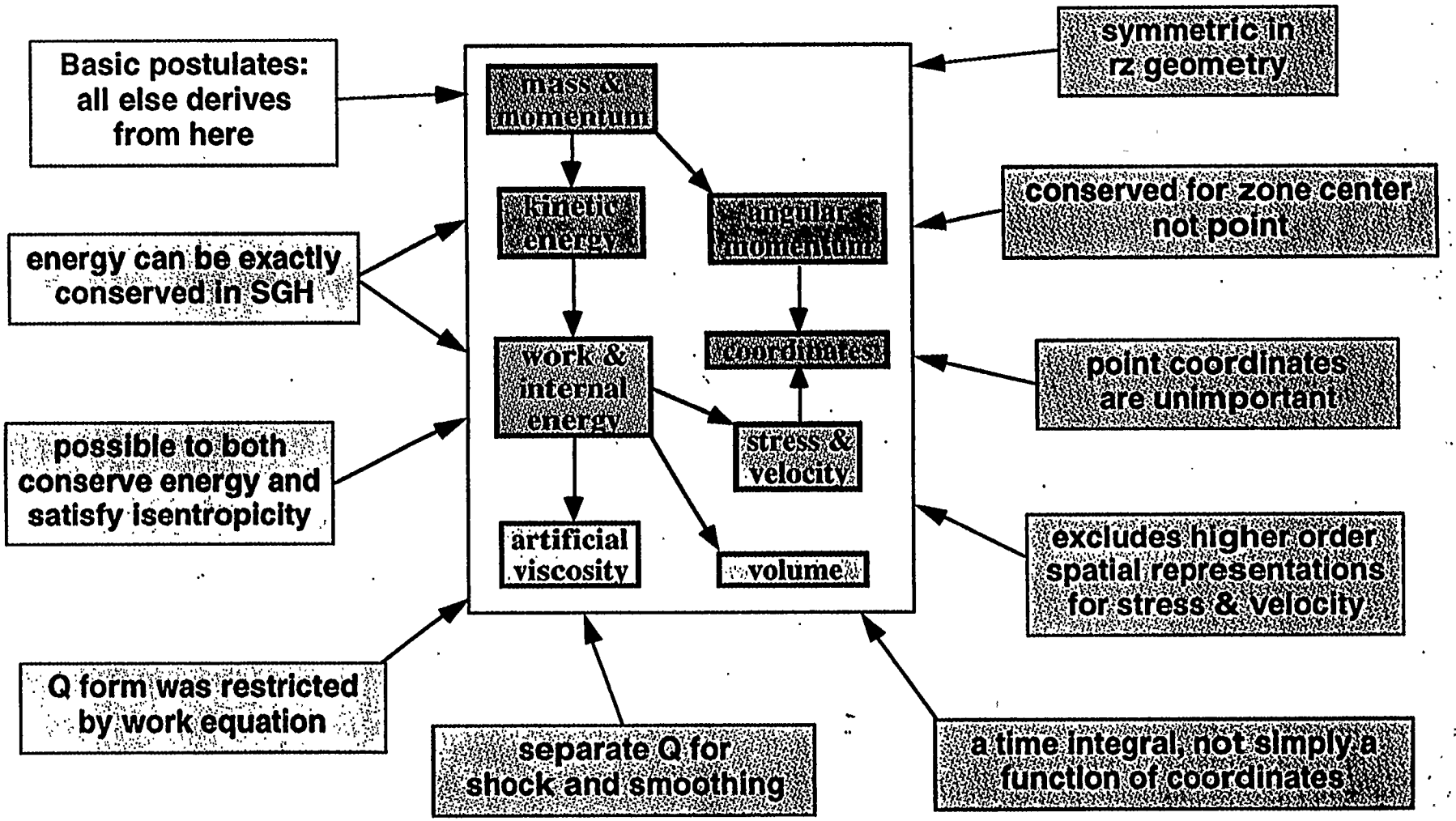

Test Problem: 2D Noh (3 K-Line)

This method

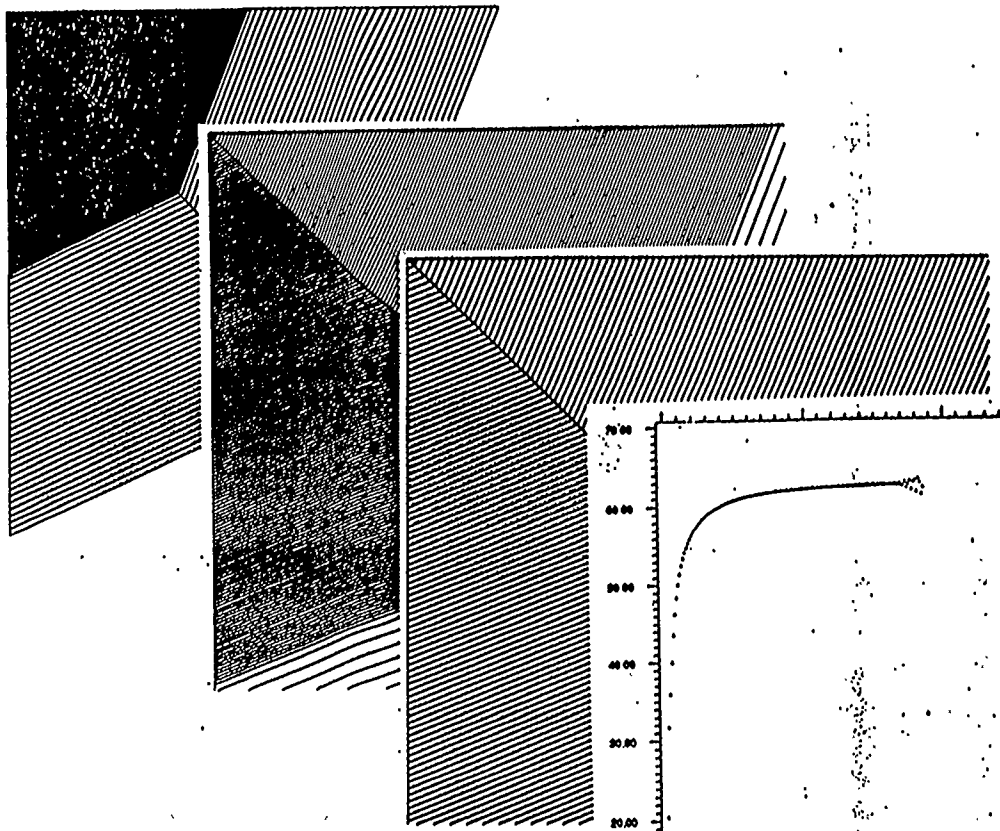

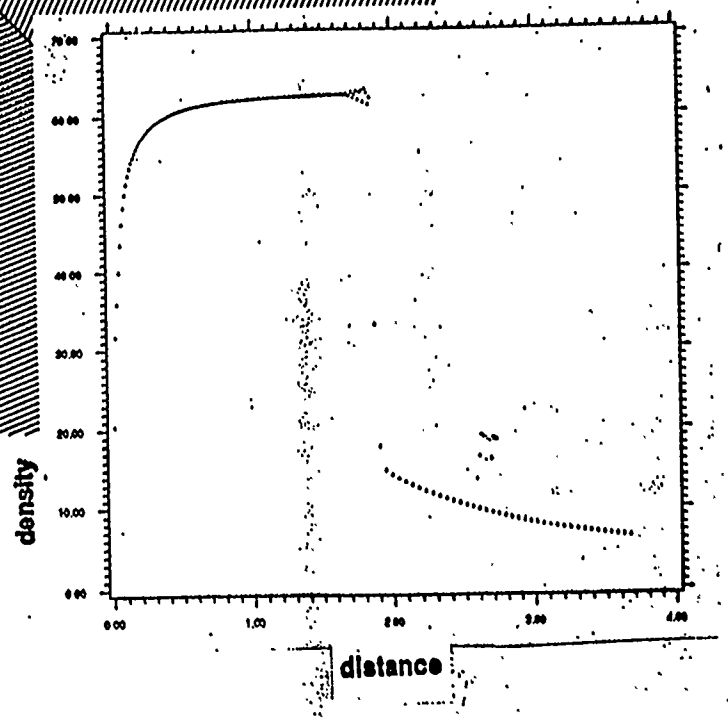

A non-symmetrical method

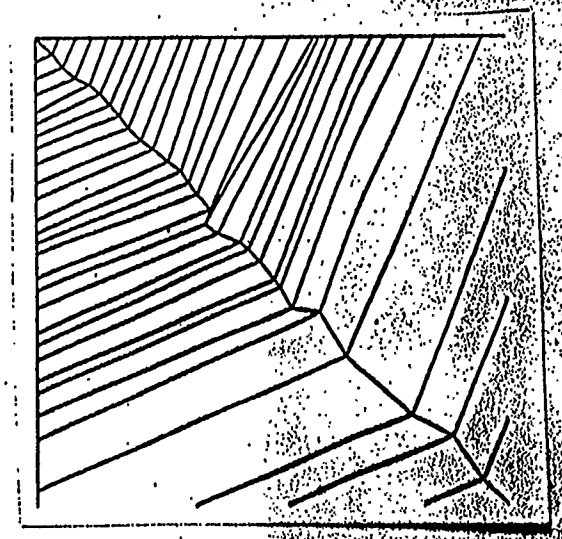

Test Problem: Schulz ellipse

This method

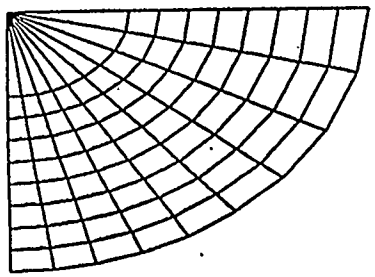

grid at 0.

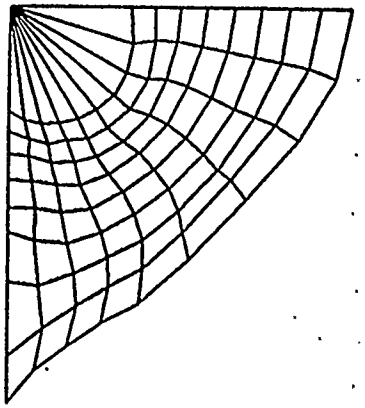

grid at 75.

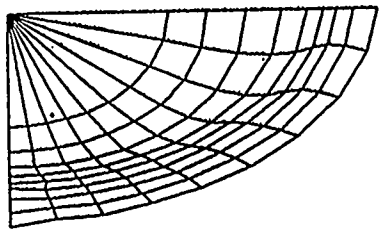

grid at 25.

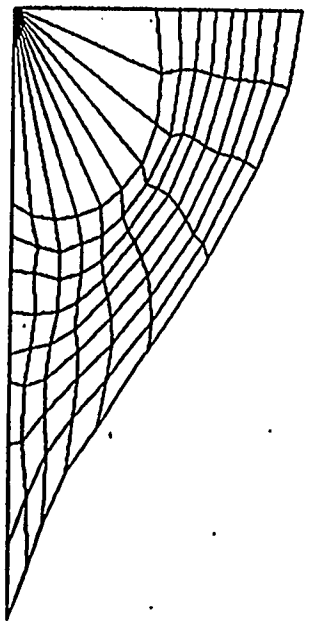

grid at 100.

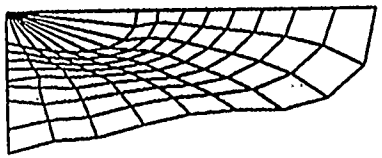

grid at 50.

Similar problem, Schulz 1964

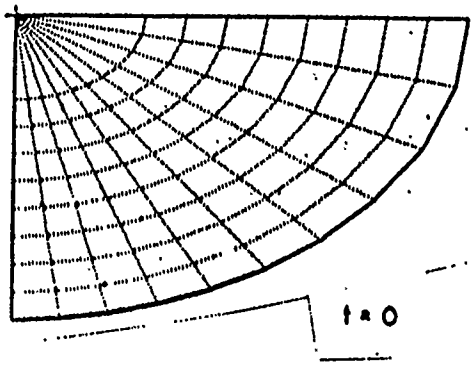

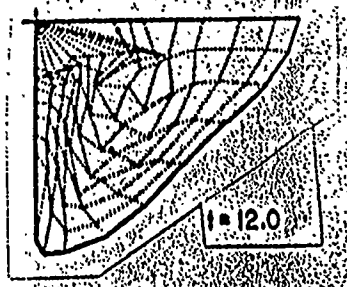

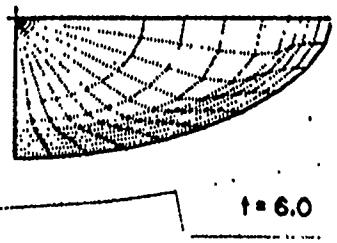

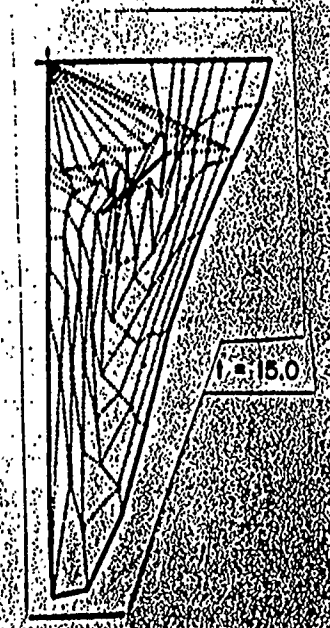

Test Problem: Saltzman piston

This method

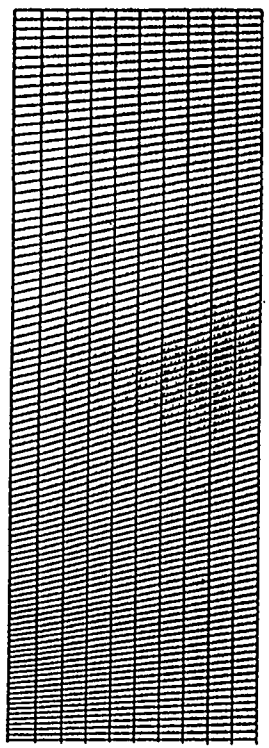

t = 0

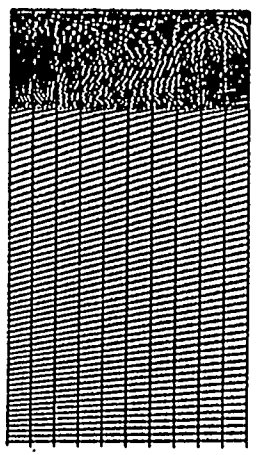

t = 0.4

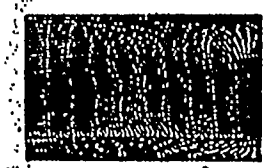

t = 0.8

Typical Lagrange method

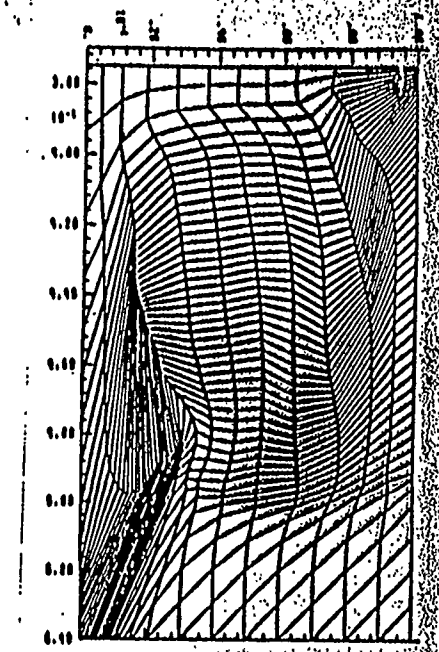

t= 0.29

Diffusion on Unstructured Grids

A collaborative effort has produced the definitive diffusion algorithm for unstructured grids

The work is motivated by needs for:

- generic multi-dimensional diffusion operator for fully unstructured grids
- prototype spatial discretization for an implicit hydrodynamics algorithm

- Works for unstructured grids of polyhedra (3D) and polygons (2D)
- Preserves linear solutions
- Is second order accurate
- Has a non-symmetric matrix (uses a biconjugate gradient solver)

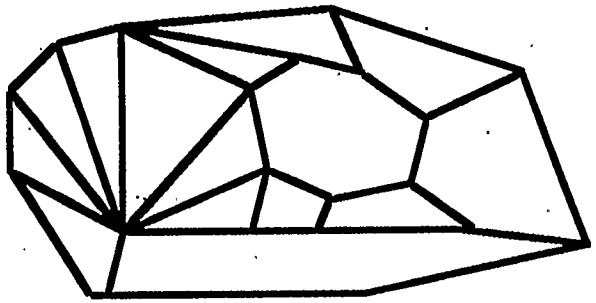

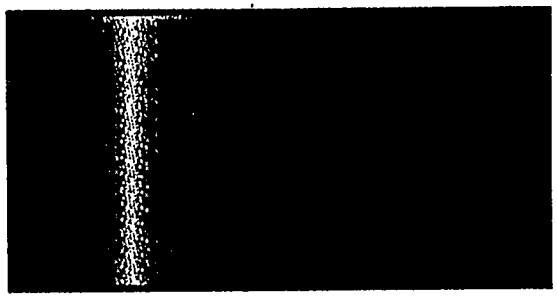

The spatial discretization of the diffusion and hydrodynamics operators is analogous

Current	$\mathbf{J} \leftrightarrow \sigma$	Stress
Flux	$\varphi \leftrightarrow \mathbf{u}$	Velocity

$$\varphi_z = \sum_c w_c(\varphi + \delta\mathbf{r} \bullet \nabla_z \varphi)$$

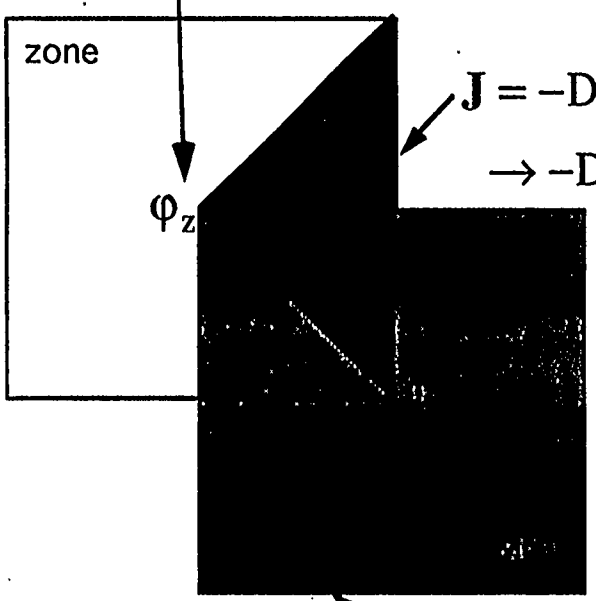

$$\mathbf{J} = -D\nabla\varphi$$

$$\rightarrow -D\sum_s \mathbf{S}\,\varphi$$

$$\sigma_a\varphi = -\nabla \bullet \mathbf{J} + q$$

$$\rightarrow -\sum_p \mathbf{S} \bullet \mathbf{J} + q$$

$$\mathbf{u}_z = \sum_c w_c \mathbf{u}$$

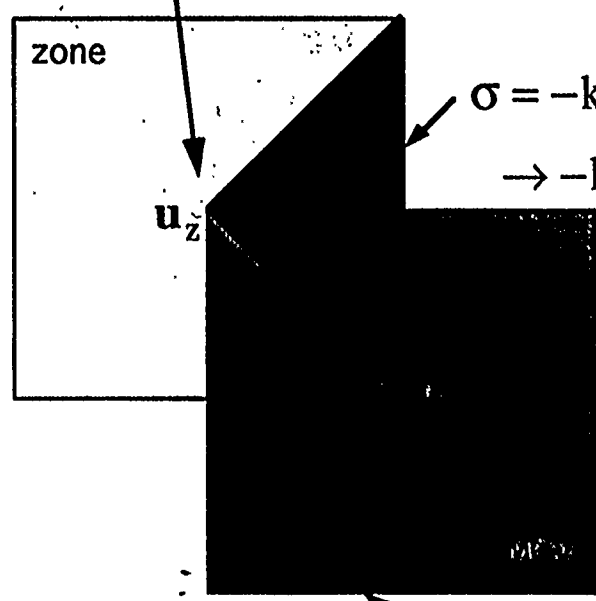

$$\sigma = -k\delta t\,\nabla\mathbf{u} + \sigma_0$$

$$\rightarrow -k\delta t\sum_s \mathbf{S}\,\mathbf{u} + \sigma_0$$

$$\rho\mathbf{u} = \nabla \bullet \sigma + \rho\mathbf{u}_0$$

$$\rightarrow \sum_p \mathbf{S} \bullet \sigma + \rho\mathbf{u}_0$$

The linear solution is obtained on a 3D version of Kershaw's Z-mesh problem

$$-D\left(\frac{\partial^2}{\partial x^2}+\frac{\partial^2}{\partial y^2}+\frac{\partial^2}{\partial z^2}\right)\phi=0$$

Exact solution for the flux is linear $\phi=\dfrac{x+2D}{1+4D}$

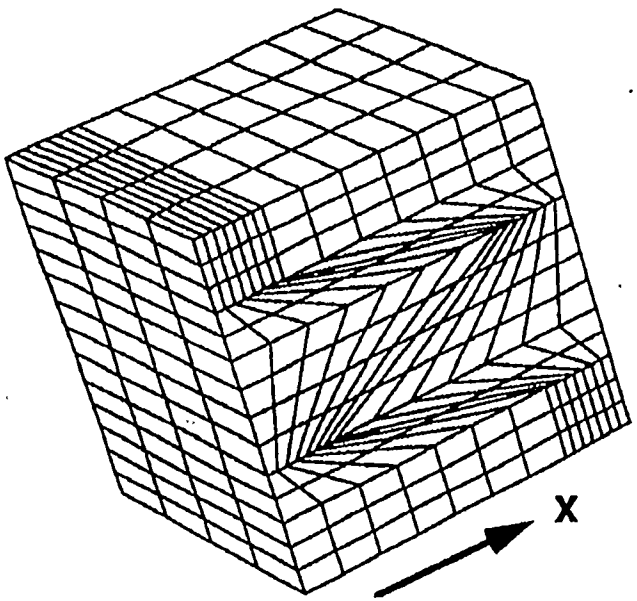

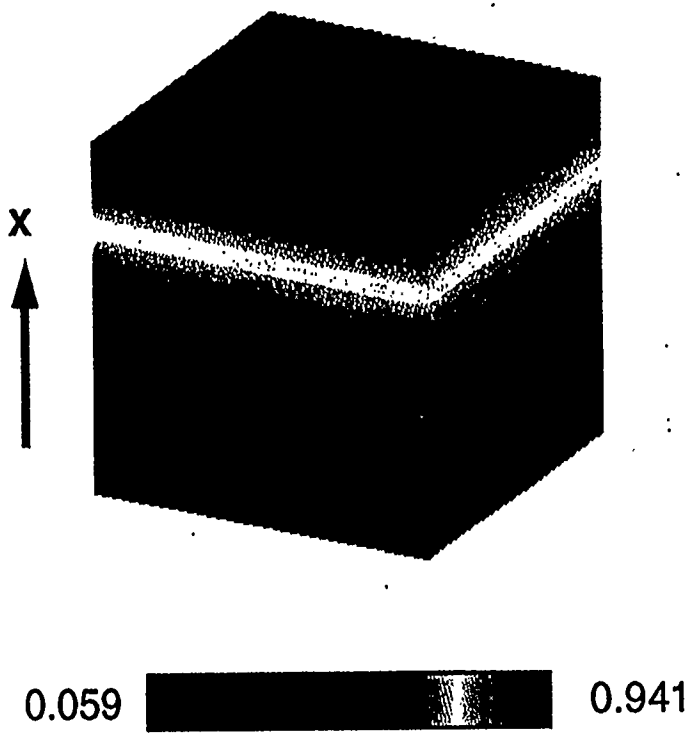

The diffusion method is second-order accurate

$$-D\left(\frac{\partial^2}{\partial x^2}+\frac{\partial^2}{\partial y^2}+\frac{\partial^2}{\partial z^2}\right)\phi = z^2$$

Exact solution is quartic

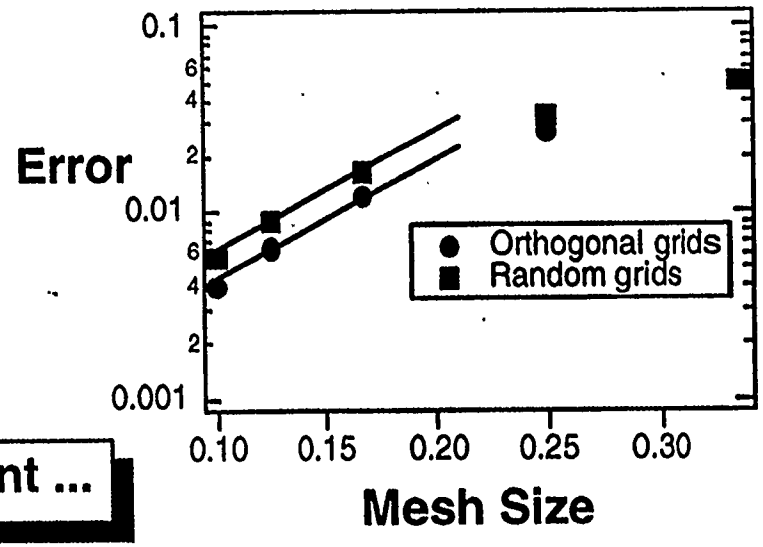

3D results are excellent ...

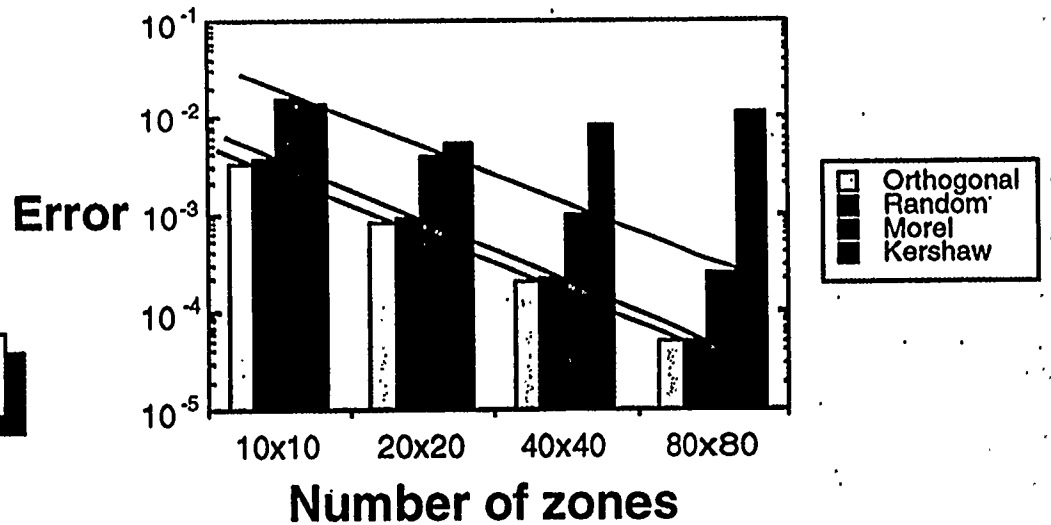

... as are the 2D

Summary

Code Backplane

- AJAX object-oriented hierarchical database
- DELFI polyhedral grid environment
- Multiple mesh concept

Mesh Optimization

- Tetrahedral strategy
  - decomposition, reconnection, refinement, recombination
- Tetrahedral dual mesh
- H-refinement
- ALE

Lagrange hydrodynamics

- Finite volume discretization
- Consistent staggered grid formulation

Diffusion on unstructured grids

- Obtains linear solutions
- Second order accuracy

3D Unstructured Mesh
Discontinuous Finite Element Hydro

Manoj K. Prasad, David S. Kershaw, and Michael J. Shaw
Lawrence Livermore National Laboratory

$$\frac{\partial \vec{\mathbf{A}}}{\partial t} + \nabla_i \vec{\mathbf{F}}_i(\vec{\mathbf{A}}) = 0$$

Motivation

- Higher order Godunov scheme using finite element (space) and fully explicit (time) discretization.

Model

1. Piecewise Linear finite element discretization in space.
2. Roe upwind surface flux & Roe averaging.
3. Explicit second-order Runge-Kutta time stepping.
4. Nonlinear VanLeer stabilization by Quadratic Programming.

Implementation

- 3D Unstructured arbitrarily moving mesh hydro code (Eulerian & Almost-Lagrangian modes) with an Interface tracker.
- Object oriented C++ design allows mesh geometry to be untangled from the physics coding.

3D LINEAR FINITE ELEMENT BASIS SET

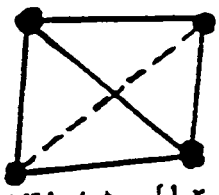

NV=4 $\phi = [1, x, y, z]$

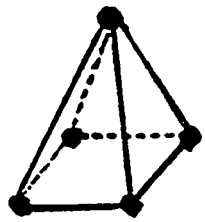

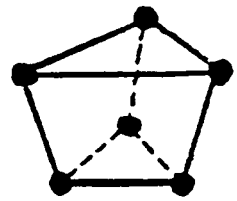

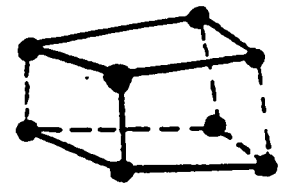

NV=8 $\phi = [1, x, y, z, xy, xz, yz, x$

LINEAR FINITE ELEMENT REPRESENTATION of $\vec{A}$

$$\vec{A}(x, y, z, t) \approx \sum_{i=1}^{NV} \vec{A}_i(t)\phi_i(x, y, z)$$

$\vec{A}_i \equiv$ *Value of* $\vec{A}$ *at NODE* i

$\phi_i \equiv$ *linear interpolation function* $= \delta_{ij}$ *at NODE* j

Galerkin eqns for $\vec{A}_i$ *in EACH element* K:

$$\int_K \phi_j \left[\frac{\partial \vec{A}}{\partial t} + \nabla_i \vec{F}_i(\vec{A})\right] d(\vec{x}) = 0 \quad , (j=1,2...NV)$$

Using the divergence theorem

$$\partial_t \int_K \phi_j \vec{A} d(\vec{x}) = -\int_{\partial K} \phi_j n_i \vec{F}_i d(\Gamma) + \int_K \vec{F}_i (\partial_i \phi_j) d(\vec{x})$$

$n_i \equiv$ *outward unit normal of element surface*

WHAT IS THE SURFACE FLUX $n_i\vec{\mathbf{F}}_i$?

For EACH point on surface LINEARIZE eqns:

$$\frac{\partial\vec{\mathbf{A}}}{\partial t} + \nabla_i\vec{\mathbf{F}}_i(\vec{\mathbf{A}}) = 0 \;\rightarrow\; \frac{\partial\vec{\mathbf{A}}}{\partial t} + \mathbf{W}_i^*\nabla_i\vec{\mathbf{A}} = 0$$

look for *wave-like solutions* $\vec{\mathbf{A}} = \vec{\mathbf{A}}(n_i x_i - \lambda^* t)$

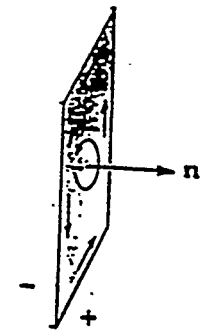

ROE AVERAGE(*) *defined through:*

$$n_i\vec{\mathbf{F}}_i(\vec{\mathbf{A}}^-) - n_i\vec{\mathbf{F}}_i(\vec{\mathbf{A}}^+) \equiv \mathbf{W}^*(\vec{\mathbf{A}}^- - \vec{\mathbf{A}}^+)$$

$$\mathbf{W}^* \equiv \frac{\partial n_i\vec{\mathbf{F}}_i^{\,*}}{\partial\vec{\mathbf{A}}^*} = R^*\Lambda^*R^{*-1}$$

Upwinding wrt sign of λ^* *gives*

ROE UPWIND SURFACE FLUX:

$$n_i\vec{\mathbf{F}}_i^{\,Roe} \equiv \frac{1}{2}[n_i\vec{\mathbf{F}}_i^{\,-} + n_i\vec{\mathbf{F}}_i^{\,+} + R^*\,sign(\Lambda^*)R^{*-1}(n_i\vec{\mathbf{F}}_i^{\,-} - n_i\vec{\mathbf{F}}_i^{\,+})]$$

Note: if *all* $\lambda^* > 0$ [< 0] *then* $n_i\vec{\mathbf{F}}_i^{\,Roe} = n_i\vec{\mathbf{F}}_i^{\,-}$ [$= n_i\vec{\mathbf{F}}_i^{\,+}$].

EXPLICIT Runge Kutta TIME STEPPING

In EACH element have system of ODE for *NODAL* $\vec{A}$:

$$\frac{\partial \vec{A}_i}{\partial t} = FaceIntegral + CellIntegral \quad , \quad (i=1,2,...NV)$$

Solve by EXPLICIT 2nd–order Runge–Kutta time discretization $\rightarrow \vec{A}^{RK}$

Use COURANT type time–step control:

$$\Delta t < Min \text{ over all elements } \left[\frac{volume \ of \ element \ K}{\int_{\partial K} |\lambda_{incoming \ waves}| (d\Gamma)} \right]$$

For smooth flows, resulting scheme has 2nd–order space–time accuracy.

NONLINEAR VanLeer STABILIZATION

For hydro, physical stability requires: $\rho > 0$, $P > 0$.
Need to ENFORCE this stability requirement

In EACH element NODAL Q_i *are FLUCTUATIONS about AVERAGE* $\bar{Q}$
VanLeer Nonlinear Stability $\rightarrow$ *LIMIT* Q_i:

$$\bar{Q}_i^{\min} \le Q_i \le \bar{Q}_i^{\max} \quad (**)$$

$\bar{Q}_i^{max/min} \equiv$ *max/min* $\bar{Q}$ *OVER ALL ELEMENTS WHICH SHARE NODE* i

In general, Q^{RK} *will VIOLATE* (**). *We then MODIFY* $Q^{RK} \rightarrow Q^M$:

QUADRATIC PROGRAMMING

$$\text{Minimize } L = \frac{1}{2}\sum_{i=1}^{NV} \alpha_i [Q_i^M - Q_i^{RK}]^2 \text{ , subject to:}$$

$$\bar{Q}_i^{\min} \le Q_i^M \le \bar{Q}_i^{\max} \quad (i=1,2...NV) \quad **$$

$$\sum_{i=1}^{NV} Q_i^M \alpha_i = \bar{Q} \quad (\alpha_i > 0) \quad ***$$

Note: In 1D with NV=2 this reduces to VanLeer's Minmod slope limiter.

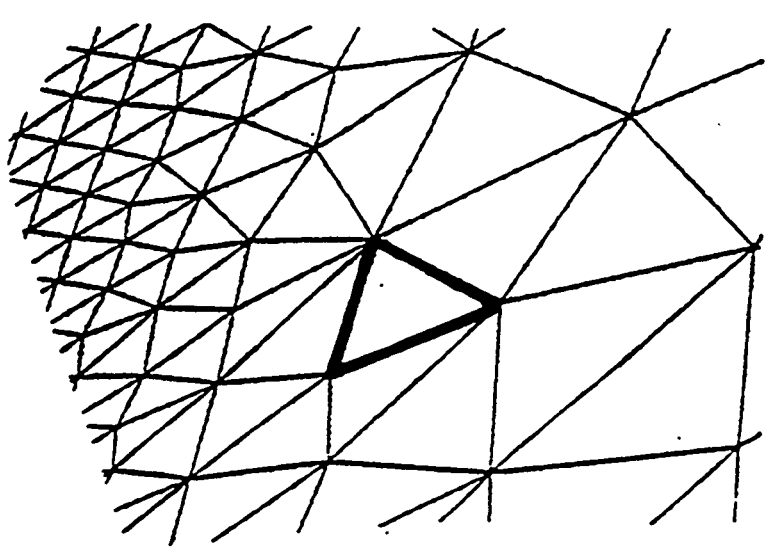

3D MOVING MESH HYDRO Eqns: $\dfrac{\partial \vec{\mathbf{A}}}{\partial t} + \dfrac{\partial \vec{\mathbf{F}}_i}{\partial x^0{}_i} = 0$

$$\vec{\mathbf{A}} = J\begin{bmatrix} \rho \\ \rho v_1 \\ \rho v_2 \\ \rho v_3 \\ \rho E \end{bmatrix} \quad , \quad \vec{\mathbf{F}}_i = \eta_{ji}\begin{bmatrix} \rho(v_j - v^g{}_j) \\ \delta_{1j}P + \rho v_1(v_j - v^g{}_j) \\ \delta_{2j}P + \rho v_2(v_j - v^g{}_j) \\ \delta_{3j}P + \rho v_3(v_j - v^g{}_j) \\ P v_j + \rho E\,(v_j - v^g{}_j) \end{bmatrix}$$

Independent Variables: t , $x^0{}_i \equiv x^g{}_i(t{=}0)$.

Piecewise Linear: ρ , v_i , P $\quad [E \equiv \frac{1}{2} v_i v_i + I(\rho, P)]$.

Continuous Linear Mesh: $x^g{}_i$, $v^g{}_i \equiv \dfrac{\partial x^g{}_i}{\partial t}$ $\quad [J_{ij} \equiv \dfrac{\partial x^g{}_j}{\partial x^0{}_i}$, $\eta_{ji} = JJ^{-1}{}_{ji}]$.

Eulerian Hydro $\rightarrow v^g{}_i{=}0 \rightarrow J{=}1 \rightarrow x^g{}_i{=}x^0{}_i$

Lagrangian Hydro $\rightarrow v^g{}_i{=}v_i \rightarrow$ *Discontinuous Mesh ??*

Almost–Lagrangian Hydro $\rightarrow v^g{}_i{=}$(*Roe*) *Average* v_i

1–**Step Solution** (*Unlike* 2–*Step*: *Lagrange* + *Remap*).

Interface Tracker:

$\mathbf{A}^\alpha = J\rho f_\alpha$, $\mathbf{F}^\alpha{}_i = \eta_{ji}\rho f_\alpha(v_j - v^g{}_j)$

$f_\alpha(t{=}0) \equiv \delta_{\alpha\beta}$ for *material species* β.

C++ OBJECT ORIENTED CODE

C++ CLASS STRUCTURE:

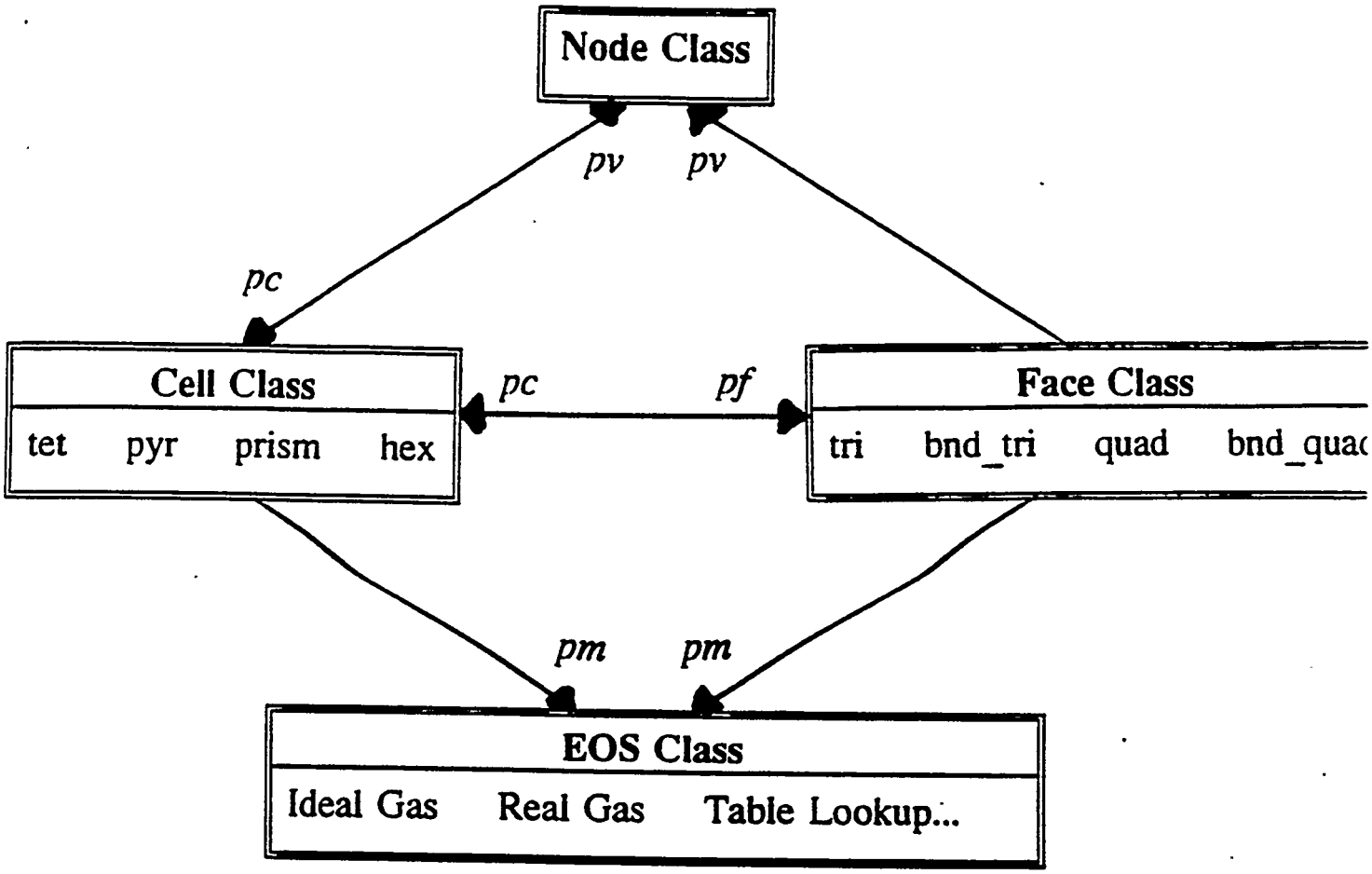

- Mesh Generator *creates* class *objects* and appropriate *pointers* across the various classes.

- Physics Modules process *objects* through class *virtual functions* using *pointers* to access data across classes.

  for(int fn=0;fn<nft;fn++) pf[fn]->Faceint();

- C++ code runs under *Basis* environment (Paul Dubois, Zane Motteler) --> user friendly graphics, interactive running, post processing, ...

WORK IN PROGRESS

- Implementing diffusive transport (electron, ion, multigroup radiation):
  1. Working uniprocessor unstructured mesh ICCG matrix solver.
  2. Dedicated C++ ICCG class sets up data structures for simple ICCG coding and modularity.

- Multiprocessing with domain decomposition:
  1. C++ classes to support ghost cell/node exchange.
  2. C++ classes to encapsulate machine dependent message passing library.
  3. Try new ideas on multiprocessing ICCG. (*Alek Shestakov*)

- Improving Basis/C++ interface. (*Zane Motteler*)

- Cylindrical (r,z,θ) and spherical (r,θ,ϕ) coordinate codes. (*Jeff Painter*)

- Incorporating the Sandia/Rhale group's C++ EOS class structure. (*Nick Gentile*)

PLANAR RIEMANN SHOCK TUBE (*Sod's Test Problem*)

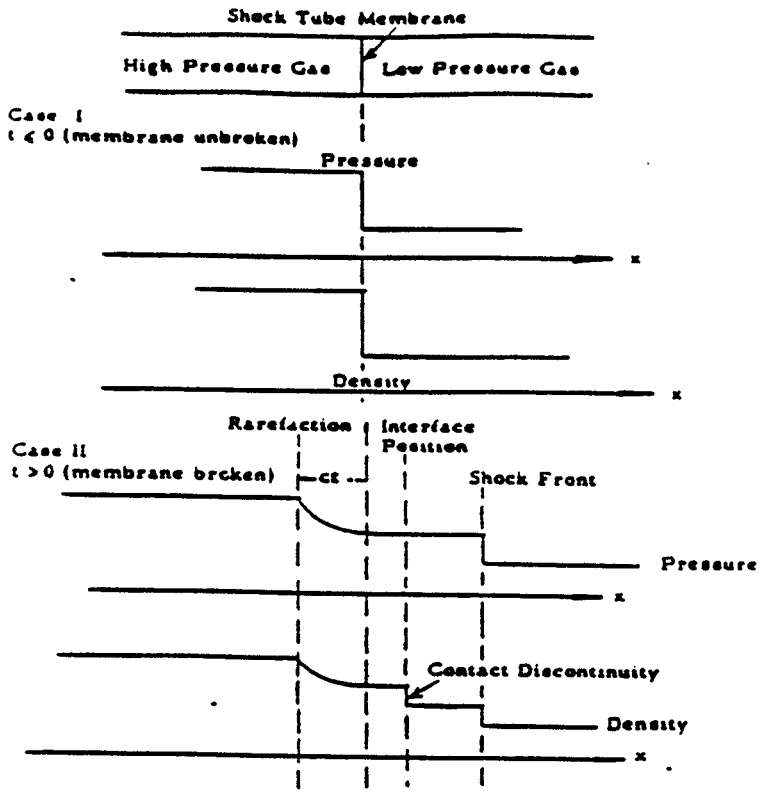

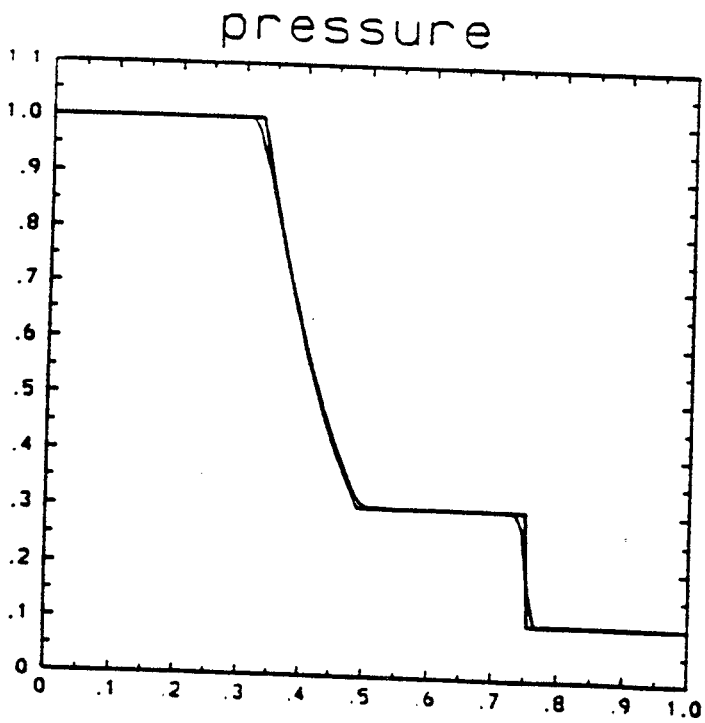

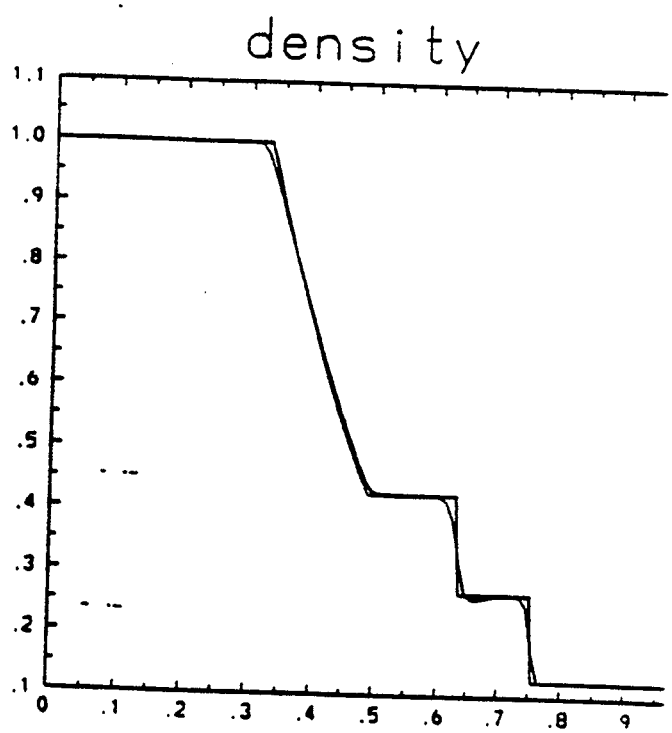

Test Problem I. : Sod's 1D Shock Tube Problem
– Comparison with LASNEX

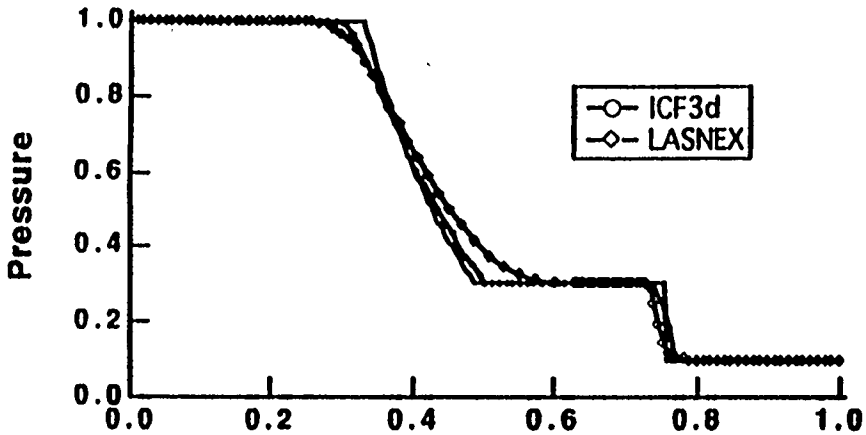

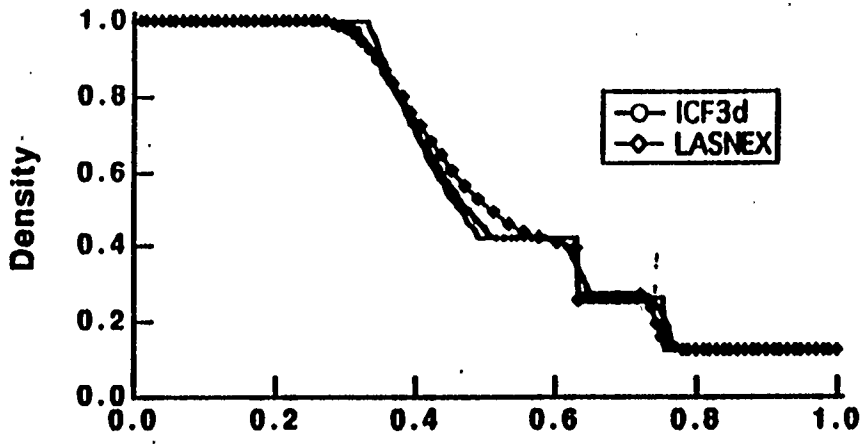

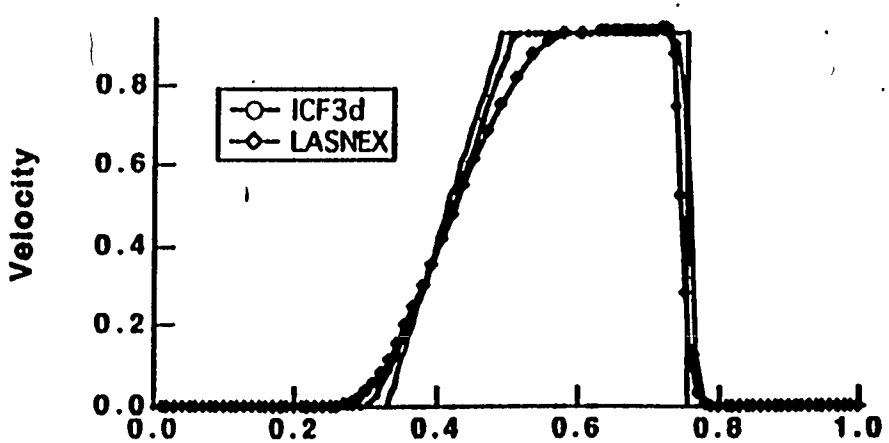

Comparison of ALE and Eulerian versions of code – Sod's shock tube

- 100 zones, $\Delta t = 0.2 \times$ Courant limit

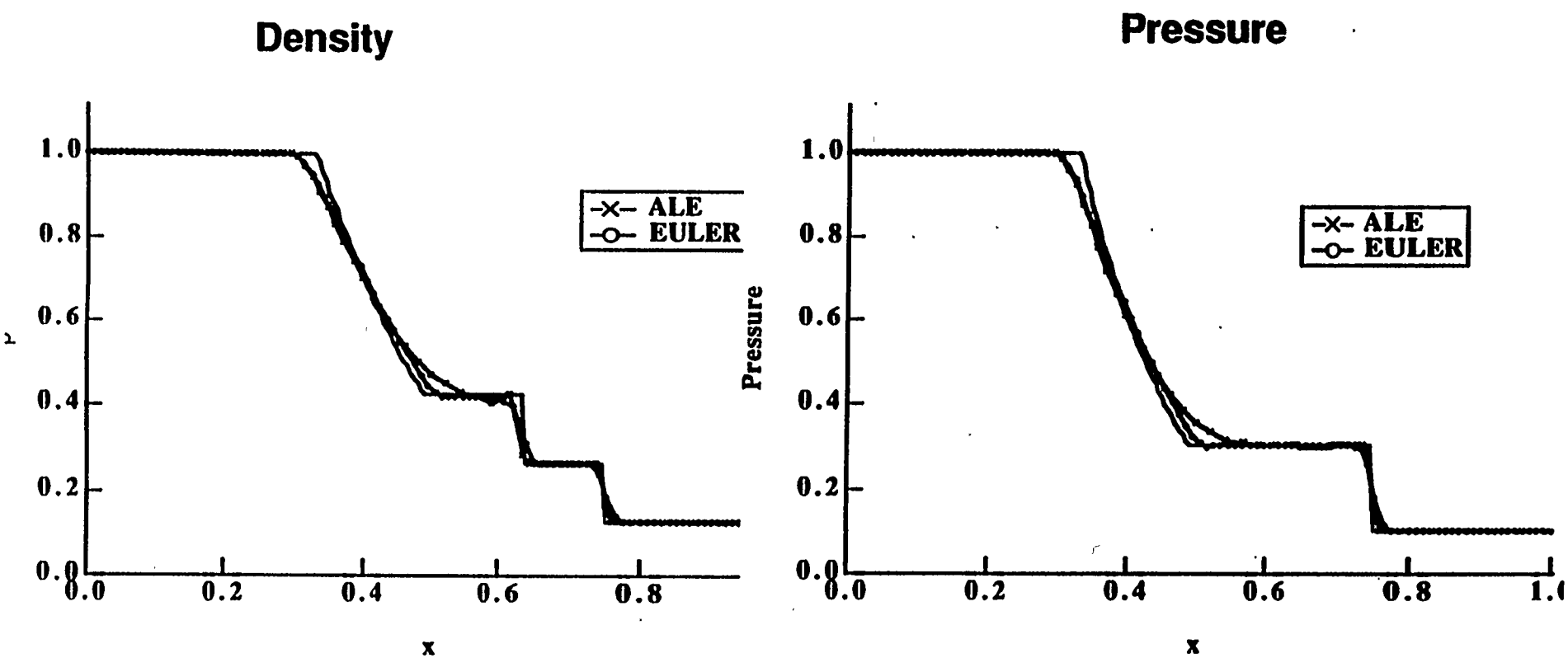

Test Problem III : Cylindrical Sod Shock Problem

- 2–D modification of Sod shock tube problem
  - High pressure fluid contained in cylindrical (at 0.5,0.5) with radius of 0.25
- Test of symmetry and 2–D capabilities of code

t = 0

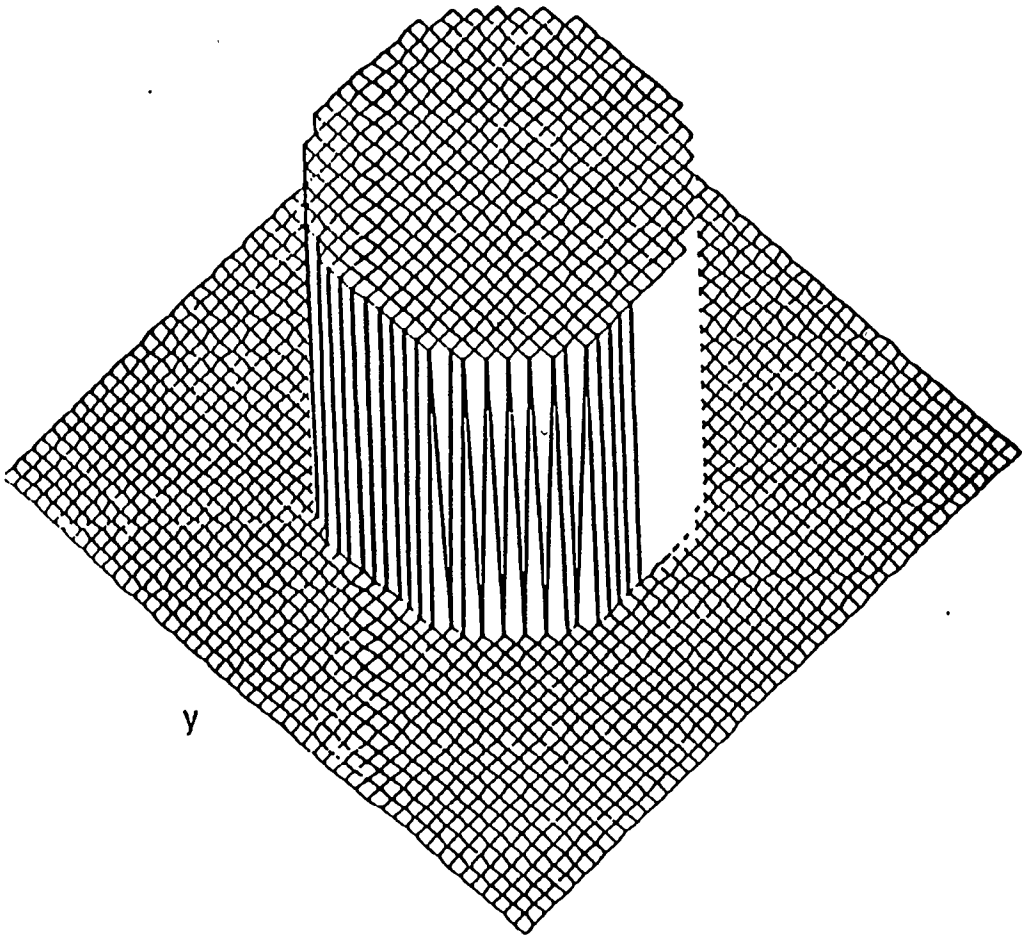

t = 0.1

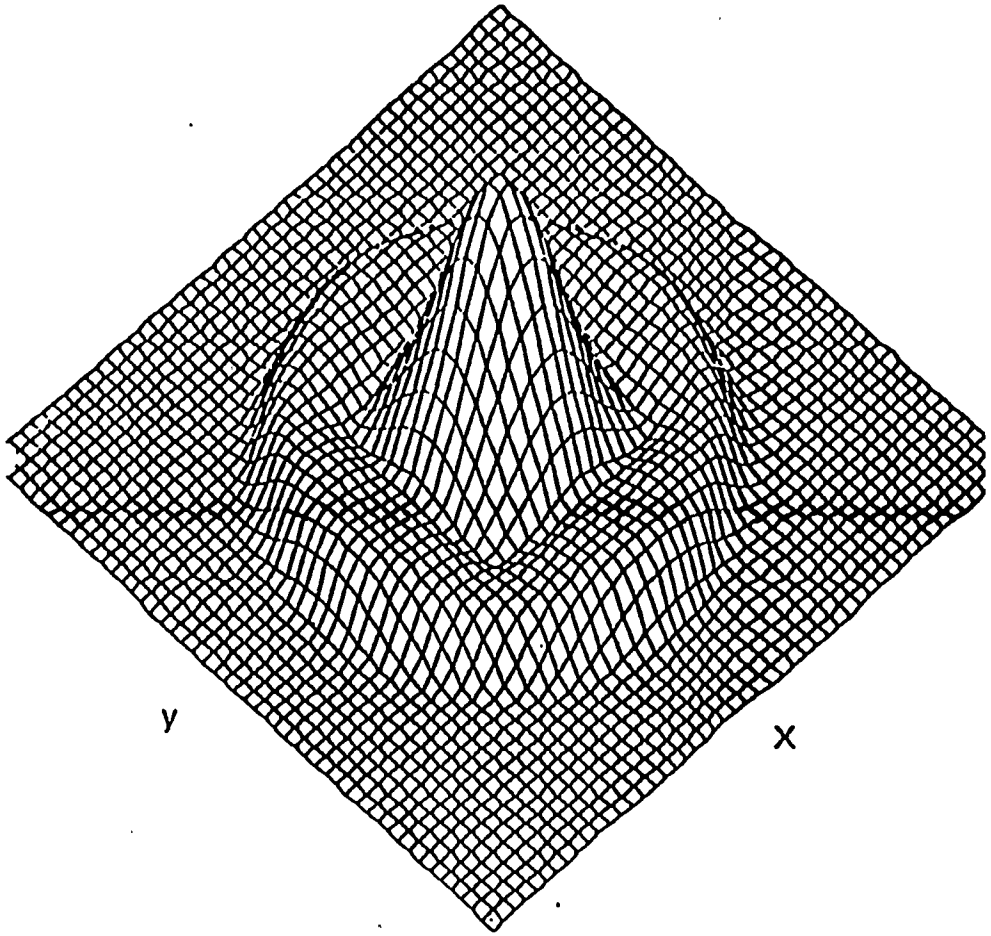

Test Problem III : Cylindrical Sod Shock Problem
– Comparison with LASNEX

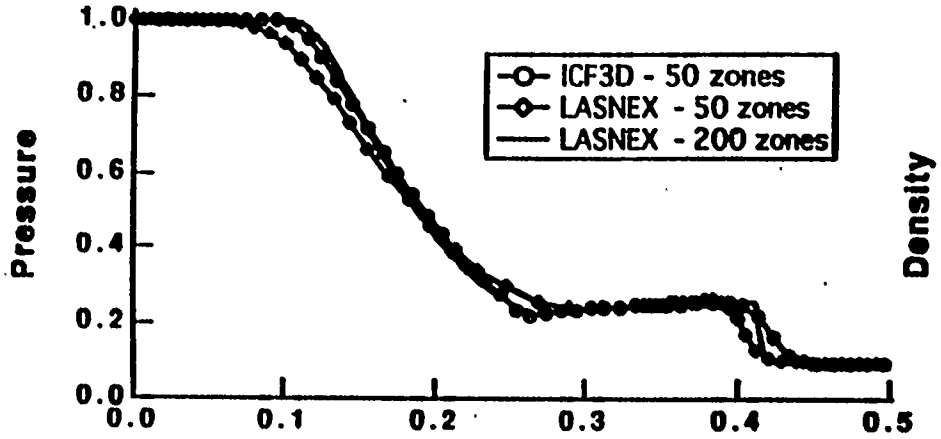

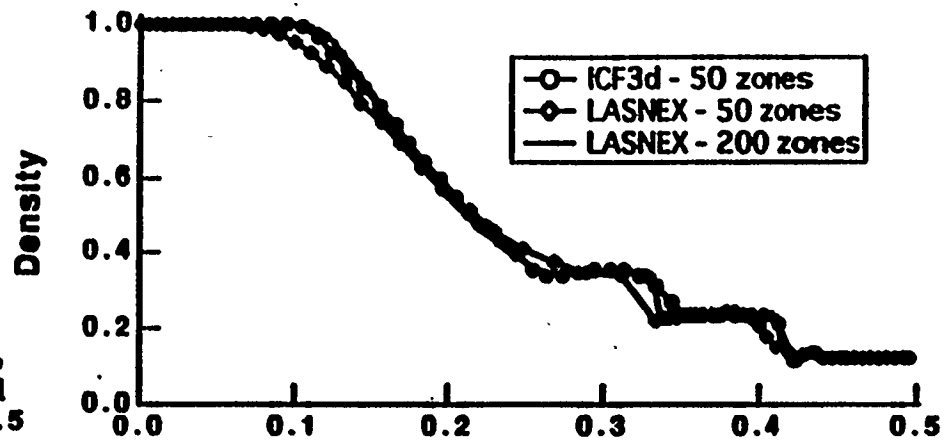

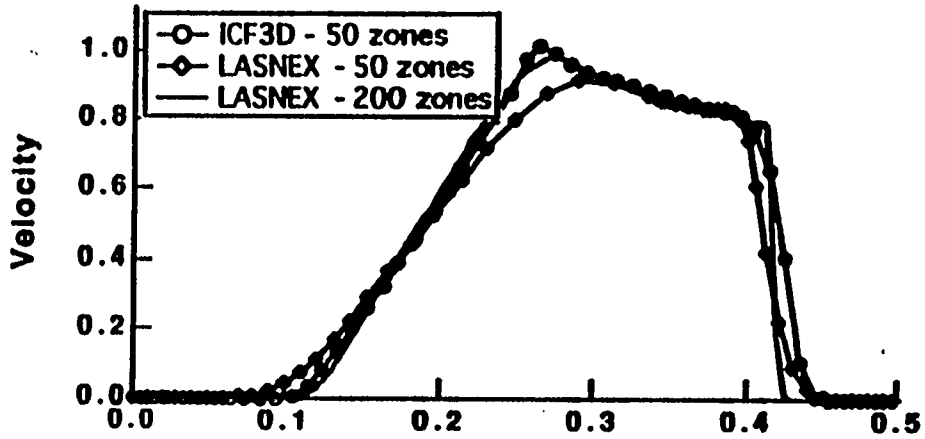

Zimmerman's slide line problem - description of initial conditions and numerical grid

Initial Conditions

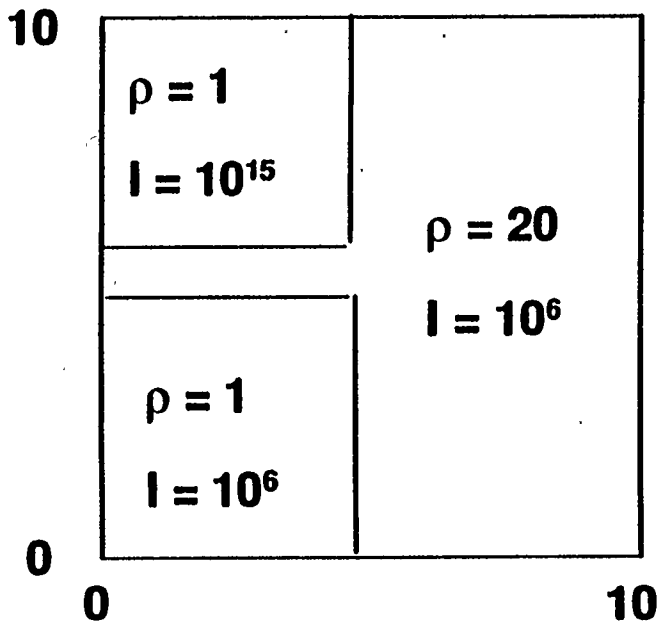

Numerical Grid

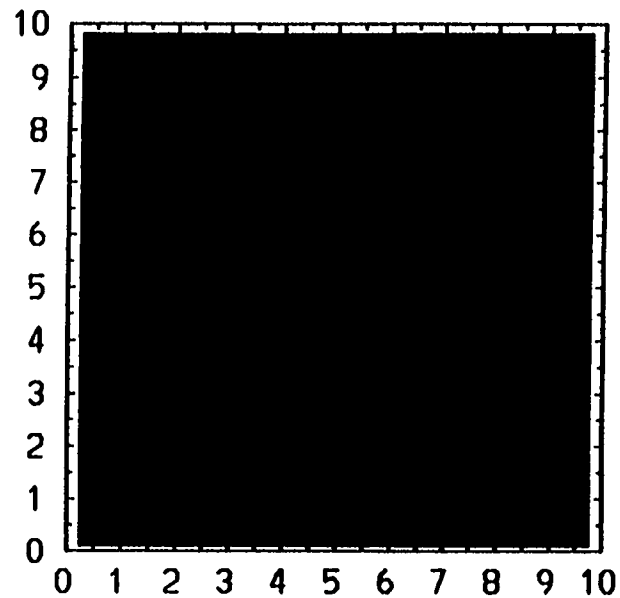

- density = g/cc; energy = erg/g

Zimmerman's slide line problem - Comparison of results (20, 60, and 100 sh)

- **Eulerian AMR results (28500 final zones)**

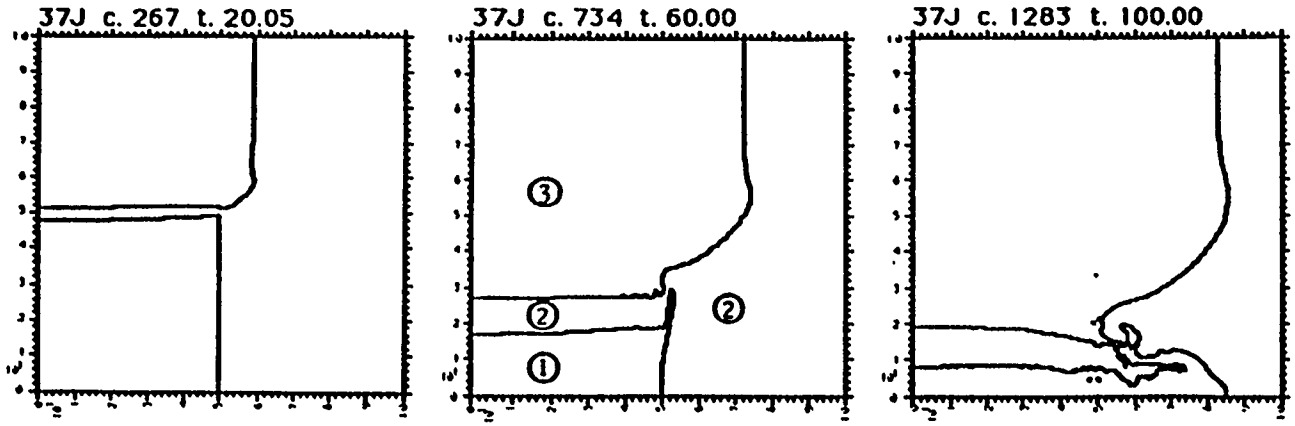

- **ICF3D, Eulerian mode (1350 zones)**

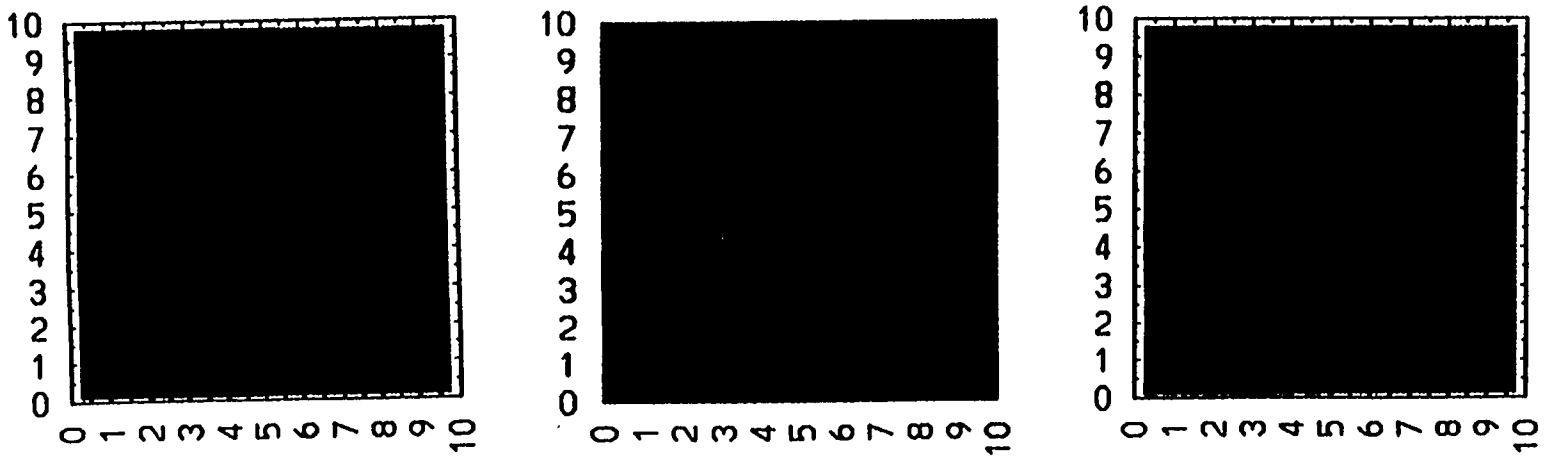

"TRIM: A FINITE-VOLUME MHD ALGORITHM FOR AN UNSTRUCTURED, ADAPTIVE MESH"

D. D. SCHNACK

I. LOTTATI

Z. MIKIĆ

P. SATYANARAYANA

SCIENCE APPLICATIONS INTERNATIONAL CORPORATION
10260 CAMPUS POINT DRIVE
SAN DIEGO, CA 92121

AND

A. TURNBULL

GENERAL ATOMICS
SAN DIEGO, CA 92121

Presented talk at the Adaptive Grid Worskhop in Pleasanton, CA
December 8-9, 1994

MOTIVATION

- SIMULATION OF PLASMA DYNAMICS IN *REALISTIC TOROIDAL GEOMETRY*
- POLOIDAL CROSS-SECTION OF MODERN TOKAMAKS CAN HAVE COMPLEX GEOMETRY
- DESIRABLE TO SIMULTANEOUSLY REPRESENT DETAILED FLUID MOTION NEAR DIVERTORS AND LIMITERS SIMULTANEOUSLY WITH LONGER SPATIAL SCALE MOTIONS IN THE PLASMA CORE
- REQUIREMENT TO SIMULATE EVOLUTION AND DYNAMICS OF VERY FINE POLOIDAL SPATIAL SCALE STRUCTURES SUCH AS *CURRENT SHEETS* AND *EDGE DENSITY GRADIENTS*
- APPLY *UNSTRUCTURED, ADAPTIVE MESH* TO TOKAMAK POLOIDAL PLANE
- USE FOURIER TRANSFORM FOR TOROIDAL REPRESENTATION
- INITIAL APPLICATION: *RESISTIVE MHD EQUATIONS*

COMPUTATIONAL MESHES

- STRUCTURED MESH:
  - A PRODUCT OF 2 (OR MORE) MESH ARRAYS (E.G., $x(i)$ AND $y(j)$) WITH INDICES i AND j ORDERED BY INCREASING COORDINATE VALUE
  - CELLS ARE GENERALLY RECTANGULAR
  - THE MESH IS STRUCTURED LOGICALLY SO THE CELLS $(i+1, j)$ AND $(i, j+1)$ ARE ADJACENT TO CELL (i, j)
  - ADDING AND DELETING POINTS AFFECTS THE INDEXING OF ALL POINTS ON THE MESH
  - BOUNDARY SHAPES OTHER THAN $x = CONSTANT$ OR $y = CONSTANT$ ARE DIFFICULT TO REPRESENT

- UNSTRUCTURED MESH:
  - A SET OF ARBITRARILY ORDERED CELLS; A CELL IS IDENTIFIED BY A SINGLE INDEX i
  - CELLS ARE GENERALLY *NOT* RECTANGULAR; USUALLY TRIANGULAR; ALLOWS ARBITRARY BOUNDARY SHAPES
  - CELL i AND CELL $i+1$ ARE NOT NECESSARILY ADJACENT
  - ADDING OR DELETING POINTS DOES *NOT* AFFECT CELL INDEXING

UNSTRUCTURED, ADAPTIVE MESH

- IDENTIFIED AND MANIPULATED BY MEANS OF PRIMARY AND SECONDARY DATA SETS

- PRIMARY DATA SET CONSISTS OF A LIST OF MESH ELEMENTS, E.G.:

  — CELLS (TRIANGLES)
  — ASSOCIATED VERTICES
  — CONNECTING EDGES

- SECONDARY DATA SETS DEFINE CONNECTIVITY BETWEEN PRIMARY MESH ELEMENTS, E.G.:

  — CROSS-INDEXING OF ELEMENTS OF PRIMARY DATA SET
  — CELLS TO THE LEFT AND RIGHT OF EACH EDGE
  — INDICES OF THREE VERTICES AND THREE EDGES OF EACH CELL

- CELLS ADDED OR DELETED BASED ON LOCAL PHYSICAL CRITERIA

- DATA SETS ARE UPDATED AS CELLS ARE ADDED OR DELETED

PRIMARY AND DUAL MESHES

- COMPUTATIONAL MESH NOT ONLY DESCRIBES GEOMETRY, BUT ALSO DEFINES DIFFERENTIAL OPERATORS

- PRIMARY AND DUAL MESHES USEFUL FOR EFFICIENT OPERATOR DEFINITION

STRUCTURED MESH:

— STAGGERED, INTERLOCKING MESHES OF RECTANGLES

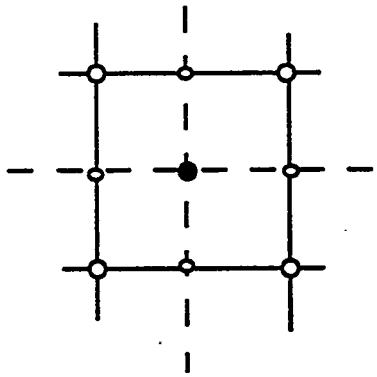

STRUCTURED, STAGGERED (DUAL) MESHES

UNSTRUCTURED MESH:

PRIMARY MESH: TRIANGLES

DUAL MESH: POLYGONS

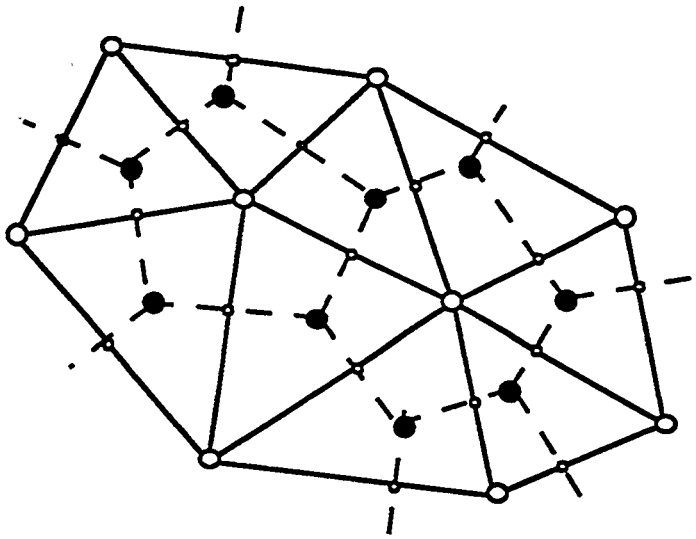

BARYCENTER, OR CENTROID, DUAL MESH

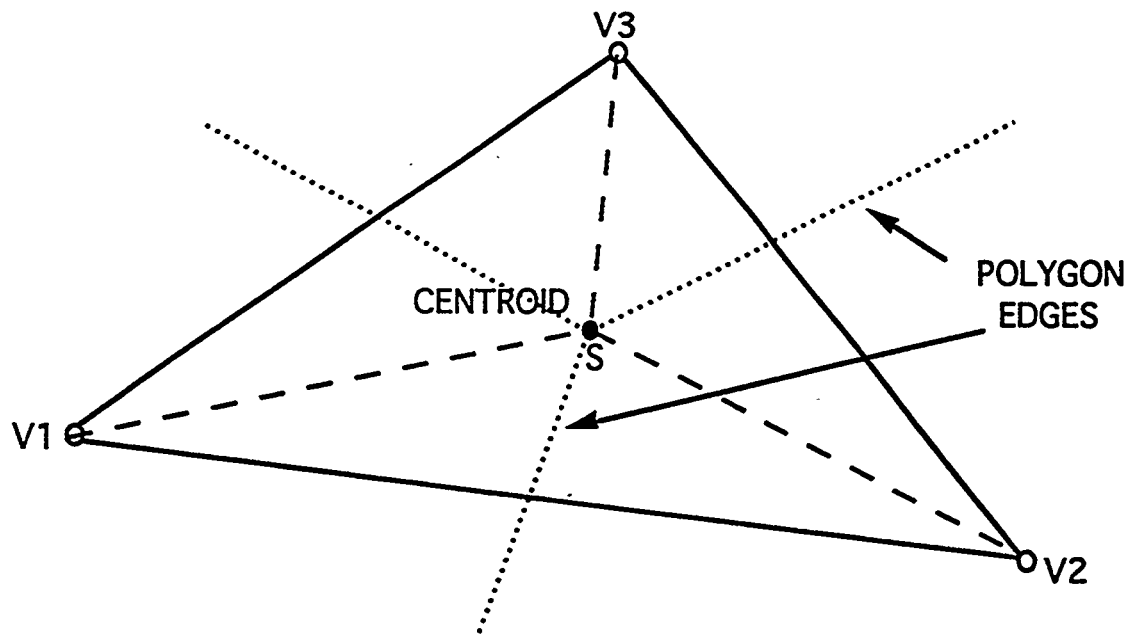

$$\mathbf{r}_s = (\mathbf{r}_{v1} + \mathbf{r}_{v2} + \mathbf{r}_{v3})/3$$

- DUAL POLYGON VERTEX ALWAYS LIES WITHIN TRIANGLE.

RESISTIVE MHD EQUATIONS

$$\mathbf{E} = -\mathbf{v}\times\mathbf{B} + \eta\mathbf{J}$$

$$\frac{\partial \mathbf{A}}{\partial t} = -\mathbf{E}$$

$$\mathbf{B} = \nabla\times\mathbf{A}$$

$$\mathbf{J} = \nabla\times\mathbf{B}$$

$$\frac{\partial \rho\mathbf{v}}{\partial t} = -\nabla\cdot\left[\rho\mathbf{v}\mathbf{v} - \mathbf{B}\mathbf{B} + \frac{1}{2}\left(p + B^2\right)\mathbf{I}\right]$$

$$\frac{\partial \rho}{\partial t} = -\nabla\cdot(\rho\mathbf{v})$$

$$\frac{\partial u}{\partial t} = -\nabla\cdot\left[\left(\rho v^2 + \frac{\gamma}{\gamma-1}p\right)\mathbf{v} + 2\mathbf{E}\times\mathbf{B}\right]$$

$$u = \rho v^2 + B^2 + \frac{p}{\gamma-1}$$

CONTROL VOLUME FOR FINITE VOLUME APPROXIMATION

TRIANGLES

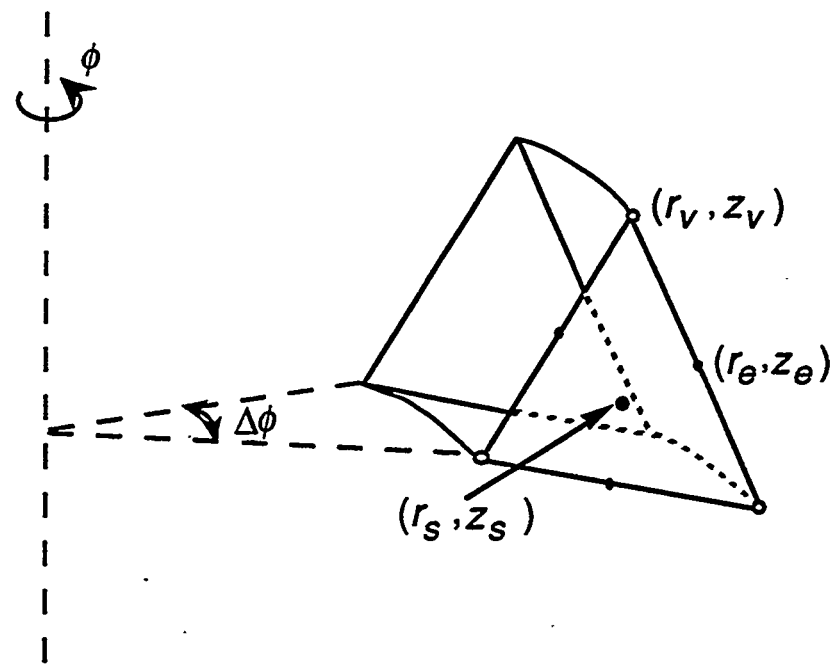

THREE-DIMENSIONAL TRIANGULAR CONTROL VOLUME

- ASSUME ALL FUNCTIONS ARE OF THE FORM:

$$f(r,\phi,z,t) = \sum_n f_n(r,z,t)e^{in\phi}$$

- DEFINE DIFFERENTIAL OPERATORS BY INTEGRAL RELATIONS APPLIED OVER THE CONTROL VOLUME:

GRADIENT OF A SCALAR

$$\int \nabla f dV = \oint f \mathbf{n} dS$$

DIVERGENCE OF A VECTOR

$$\int \nabla \cdot \mathbf{A} dV = \oint \mathbf{n} \cdot \mathbf{A} dS$$

DIVERGENCE OF A TENSOR

$$\int \nabla \cdot \mathbf{T} dV = \oint \mathbf{n} \cdot \mathbf{T} dS$$

CURL OF A VECTOR

$$\int \nabla \times \mathbf{A} dS = \oint \mathbf{A} \cdot \mathbf{t} d\ell$$

PLACEMENT OF VARIABLES

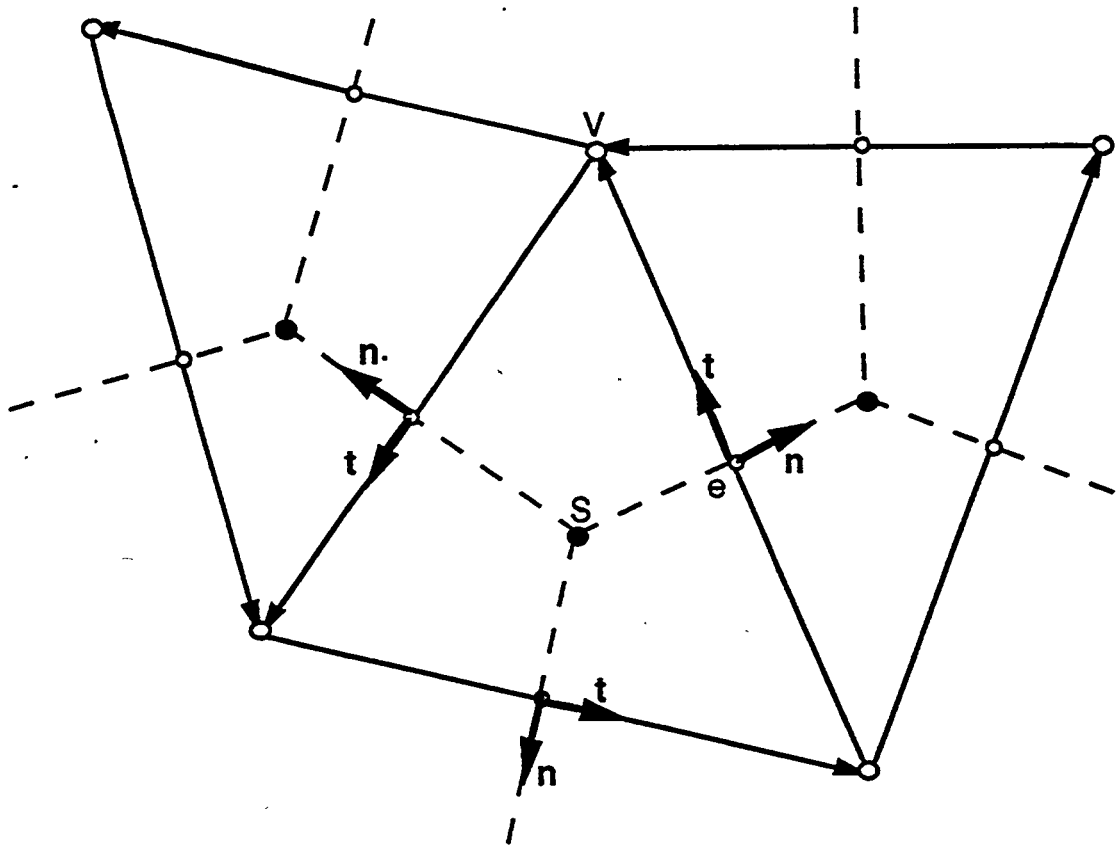

- EDGES ∘ $A_r, A_z, B_r, B_z, E_r, E_z, J_r, J_z \; (v_r, v_\phi, v_z)$
- CENTERS • $u,\ p,\ \rho,\ B_\phi,\ \rho v_r,\ \rho v_\phi,\ \rho v_z,\ A_\phi,\ J_\phi$

TRIANGLE GEOMETRY

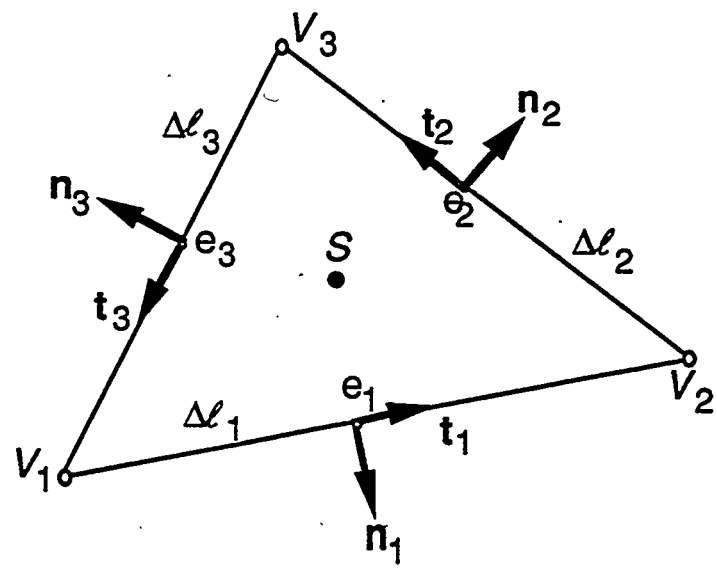

POLOIDAL PROJECTION OF TRIANGULAR CONTROL VOLUME

- UNIT VECTORS:

$$\mathbf{e}_\phi = \mathbf{t}_e \times \mathbf{n}_e$$

- GEOMETRIC VECTORS:

$$\boldsymbol{\ell}_1 + \boldsymbol{\ell}_2 + \boldsymbol{\ell}_3 = 0 \qquad \boldsymbol{\ell}_e = \Delta r_e \mathbf{e}_r + \Delta z_e \mathbf{e}_z = \Delta \ell_e \mathbf{t}_e$$

$$\mathbf{n}_e = \frac{\Delta z_e \mathbf{e}_r - \Delta r_e \mathbf{e}_z}{\Delta \ell_e} \qquad V_{ne} = \mathbf{V}\cdot\mathbf{n}_e \quad V_{te} = \mathbf{V}\cdot\mathbf{t}_e$$

$$\Delta as = \frac{1}{2}\left|\boldsymbol{\ell}_1 \times \boldsymbol{\ell}_2\right| = \frac{1}{2}\left|\boldsymbol{\ell}_2 \times \boldsymbol{\ell}_3\right| = \frac{1}{2}\left|\boldsymbol{\ell}_3 \times \boldsymbol{\ell}_1\right|$$

DIFFERENTIAL OPERATORS

- GRADIENT OF A SCALAR:

$$(\nabla\psi)_S = \frac{1}{r_S \Delta a_S} \sum_{e=1}^{3} \mathbf{n}_e \Delta\ell_e r_e \psi_e - \frac{\psi_S}{r_S}\mathbf{e}_r + \frac{in}{r_S}\psi_S \mathbf{e}_\phi$$

- DIVERGENCE OF A VECTOR:

$$(\nabla\cdot\mathbf{V})_S = \frac{1}{r_S \Delta a_S} \sum_{e=1}^{3} r_e \Delta\ell_e V_{ne} + \frac{in}{r_S} V_{\phi S}$$

- CURL OF A VECTOR, $\mathbf{U} = \nabla \times \mathbf{V}$:

$$U_{ne} = -\frac{1}{r_e \Delta\ell_e}\left(r_{v+}V_{\phi v+} - r_{v-}V_{\phi v-}\right) + \frac{in}{r_e}\mathbf{V}_e \cdot \mathbf{t}_e$$

$$U_{\phi S} = -\frac{1}{\Delta a_S}\sum_{e=1}^{3} \mathbf{V}_e \cdot \boldsymbol{\ell}_e$$

— IT IS EASY TO VERIFY THAT $(\nabla \cdot \mathbf{U})_S = 0$.

- DIVERGENCE OF A TENSOR:

$$(\nabla\cdot\mathbf{T})_S = \frac{1}{r_S \Delta a_S}\sum_{e=1}^{3} r_e \Delta\ell_e \Big[\mathbf{e}_r(\mathbf{n}_e\cdot\mathbf{T}_e)_r + \mathbf{e}_\phi(\mathbf{n}_e\cdot\mathbf{T}_e)_\phi$$

$$+ \mathbf{e}_z(\mathbf{n}_e\cdot\mathbf{T}_e)_z\Big] + \frac{in}{r_S}\left[\mathbf{e}_r T_{\phi r_S} + \mathbf{e}_\phi T_{\phi\phi_S} + \mathbf{e}_z T_{\phi z_S}\right]$$

$$+ \frac{1}{r_S}\left[\mathbf{e}_\phi T_{\phi r_S} - \mathbf{e}_r T_{\phi\phi_S}\right]$$

FLUX AT TRIANGLE EDGES

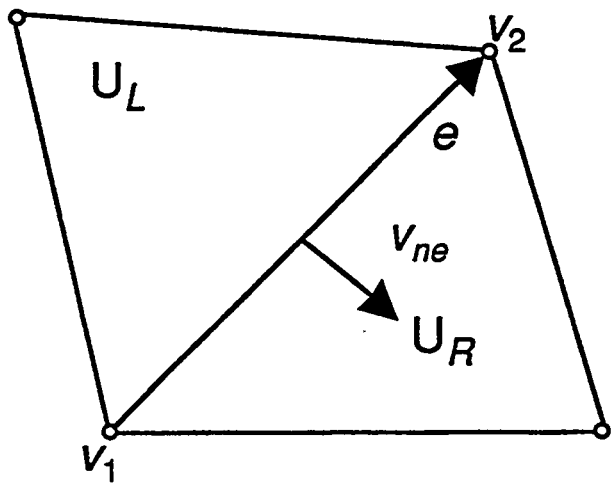

$$\mathbf{F} = U\mathbf{v}$$

$$\hat{n}_e \cdot \mathbf{F}_e = \tilde{U}_e \; v_{ne}$$

$\tilde{U}_e$ — AN APPROXIMATION TO U AT THE EDGE e.

<u>FIRST ORDER</u>:

$$\tilde{U}_e = \begin{cases} U_L & v_{ne} > 0 \\ U_R & v_{ne} < 0 \end{cases}$$

DIFFUSIVE! $D = \dfrac{v_{ne}\delta}{2}$

<u>HIGHER ORDER</u>: SOME APPROXIMATION TO THE RIEMANN PROBLEM

TIME ADVANCEMENT

- EXPLICIT LEAP-FROG WITH PREDICTOR-CORRECTOR FOR ADVECTION

$$\mathbf{U}^{*} = \mathbf{U}^{n} + \Delta t \cdot \mathbf{F}_{\exp}$$

- SEMI-IMPLICIT ADVANCE IF CFL > 1

$$\left(1-\alpha_{\mathrm{SI}}\Delta t\nabla^{2}\right)\ \mathbf{U}^{**} = \mathbf{U}^{*} - \alpha_{\mathrm{SI}}\Delta t\nabla^{2}\ \mathbf{U}^{n}$$

$$\alpha_{\mathrm{SI}} = \frac{1}{4}\left(\left(\frac{\Delta t}{\Delta t_{\mathrm{CFL}}}\right)^{2} - 1\right)$$

- IMPLICIT VISCOSITY

$$\left(1-\nu\Delta t\,\nabla^{2}\right)\ \mathbf{U}^{n+1} = \mathbf{U}^{**}$$

- STABLE FOR ARBITRARY Δt

SCALAR LAPLACIAN

$$u_e = \frac{1}{2}\left(u_{S_L} + u_{S_R}\right)$$

$$(\nabla u)_S = \frac{1}{r_S \Delta a_S} \sum_{e=1}^{3} \mathbf{n}_e \Delta \ell_e r_e u_e - \frac{u_S}{r_S}\ \mathbf{e}_r$$

$$+ \frac{in}{r_S}\ u_S\ \mathbf{e}_\phi$$

$$(\nabla u)_e = \frac{1}{2}\left[(\nabla u)_{S_L} + (\nabla u)_{S_R}\right]$$

$$\nabla^2 u_S = \frac{1}{r_S \Delta a_S} \sum_{e=1}^{3} r_e \Delta \ell_e \mathbf{n}_e \cdot (\nabla u)_e - \frac{n^2}{r_S^2}\ u_S$$

- SELF-ADJOINT FORMULATION
- MATRIX INVERSION BY CONJUGATE GRADIENT METHOD WITH DIAGONAL PRECONDITIONING

MESH ADAPTION

- TAG TRIANGLE FOR REFINEMENT BY
  - — ESTIMATING CHANGE IN TRIANGLE QUANTITIES BY SUMMING EDGE FLUXES, OR
  - — ESTIMATING GRADIENT OF QUANTITIES
- ADD VERTEX INSIDE TRIANGLE AND MAKE 3 NEW TRIANGLES:

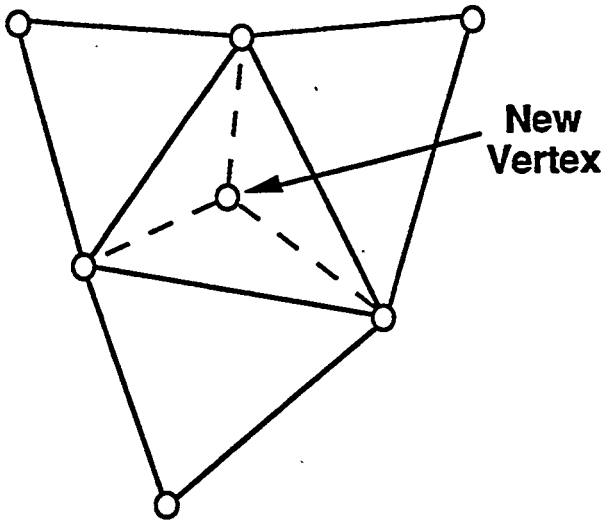

- SWAP EDGES, IF REQUIRED

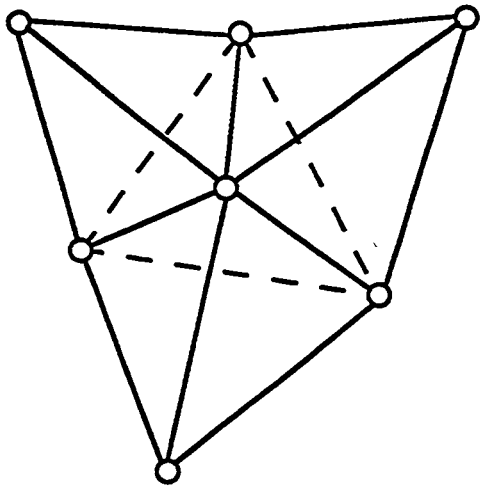

"SOD" HYDRODYNAMIC SHOCK PROBLEM

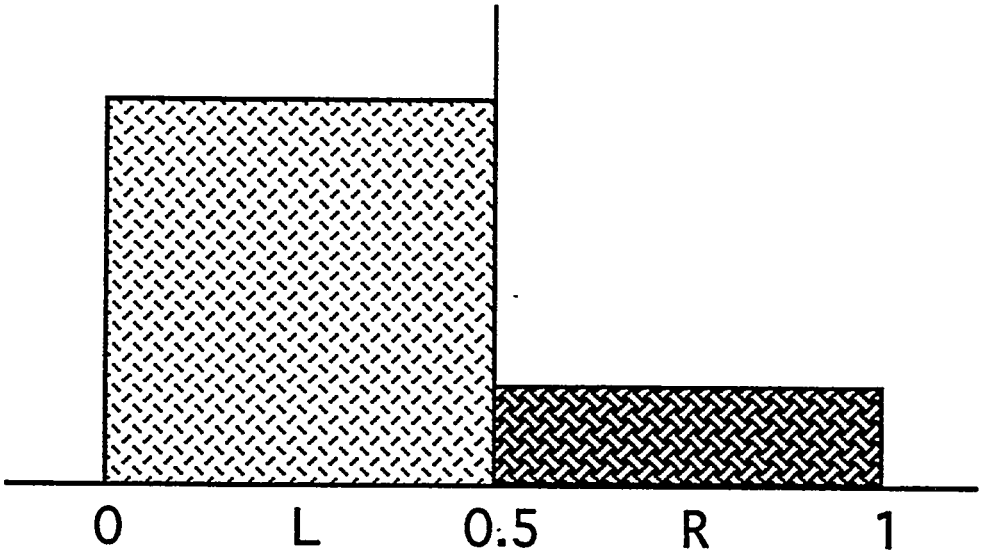

$p_L = 1$ $\qquad$ $p_R = 0.1$

$\rho_L = 1$ $\qquad$ $\rho_R = 0.125$

$u_L = 0$ $\qquad$ $u_R = 0$

$$\gamma = 1.4$$

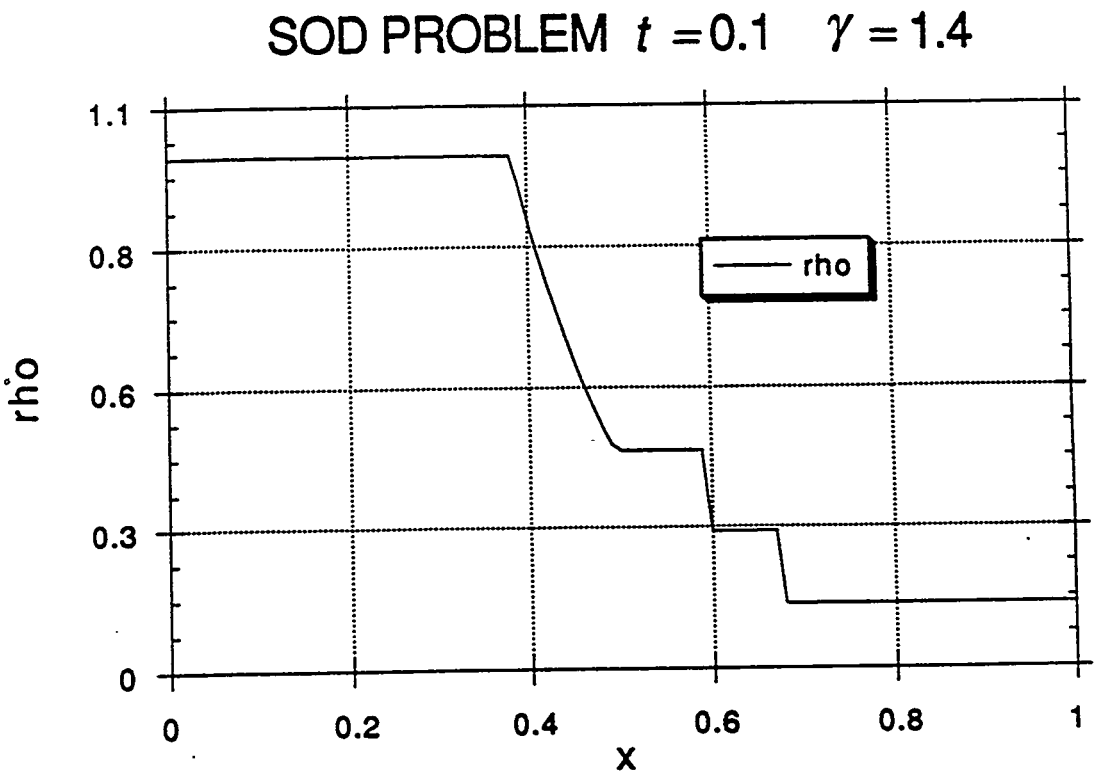
SOD PROBLEM $t = 0.1$ $\gamma = 1.4$
rho
1.1
0.8
0.6
0.3
0
0
0.2
0.4
0.6
0.8
1
X
rho

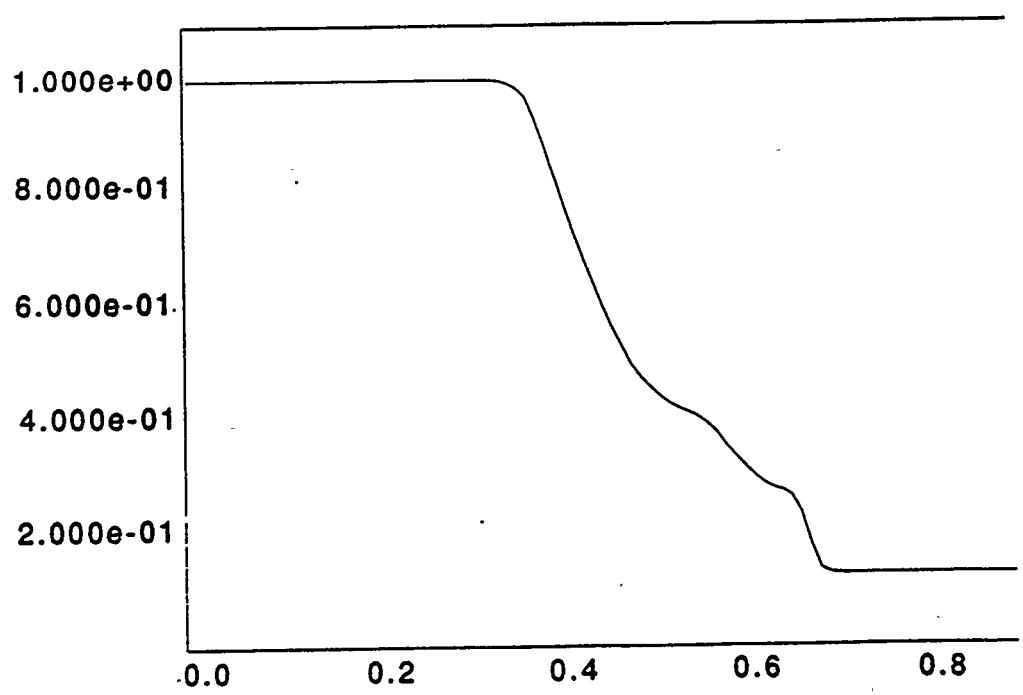
1.000e+00
8.000e-01
6.000e-01
4.000e-01
2.000e-01
0.0
0.2
0.4
0.6
0.8

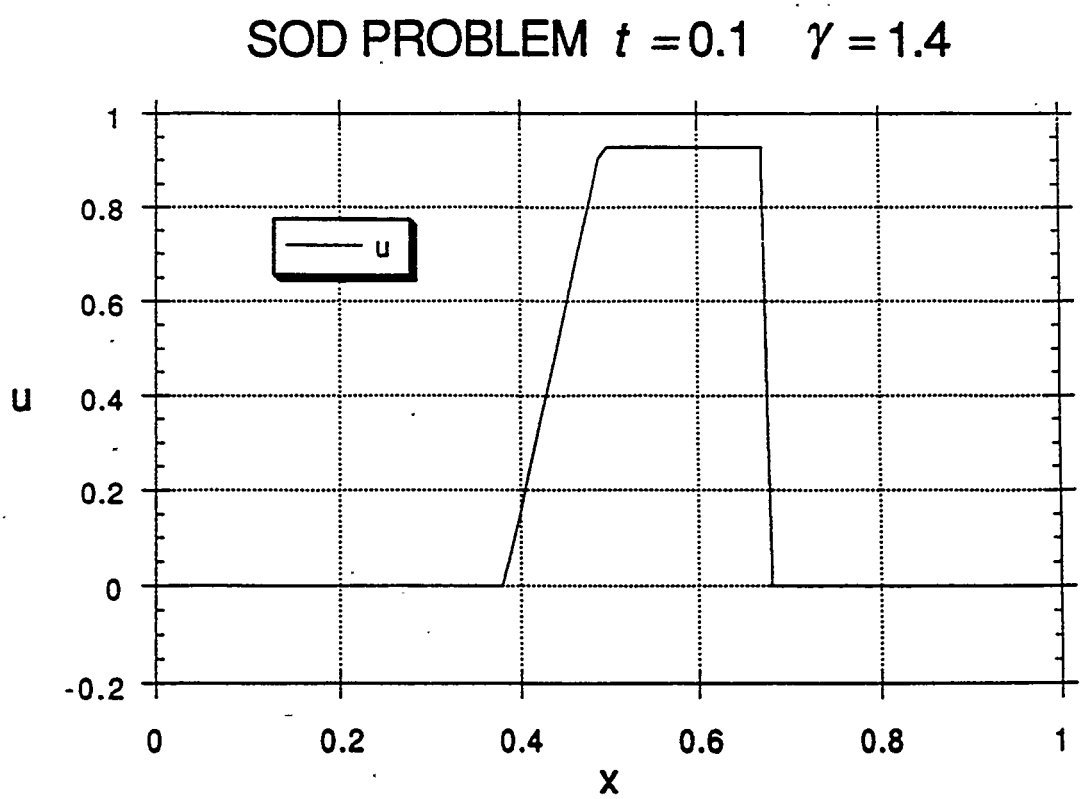
SOD PROBLEM $t = 0.1$ $\gamma = 1.4$
u
1
0.8
0.6
0.4
0.2
0
-0.2
0
0.2
0.4
0.6
0.8
1
x

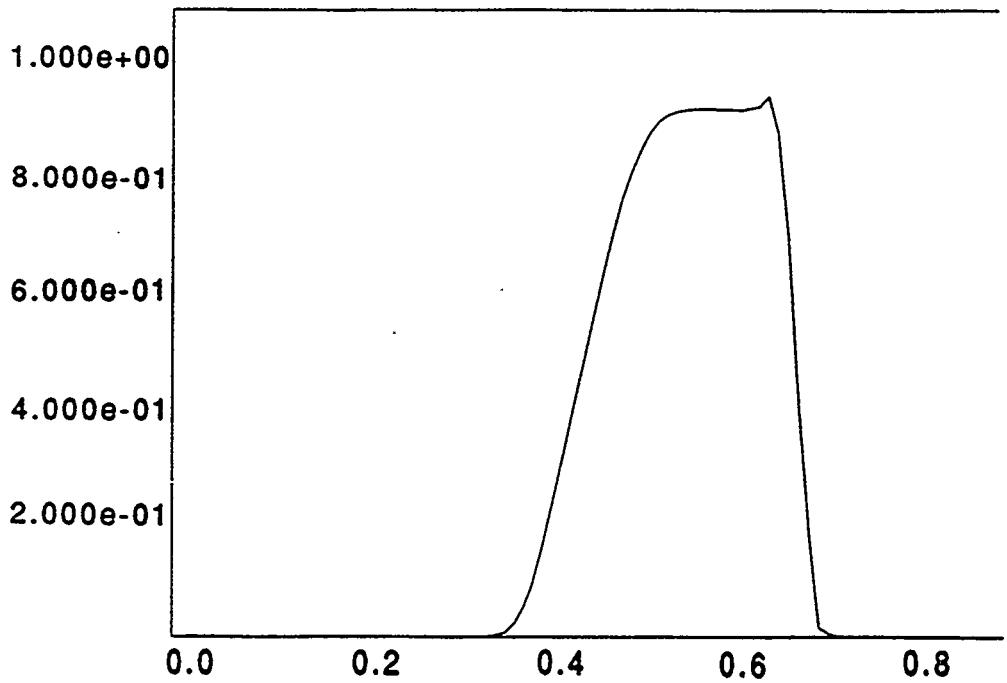
1.000e+00
8.000e-01
6.000e-01
4.000e-01
2.000e-01
0.0
0.2
0.4
0.6
0.8

SOD PROBLEM $t = 0.1 \quad \gamma = 1.4$

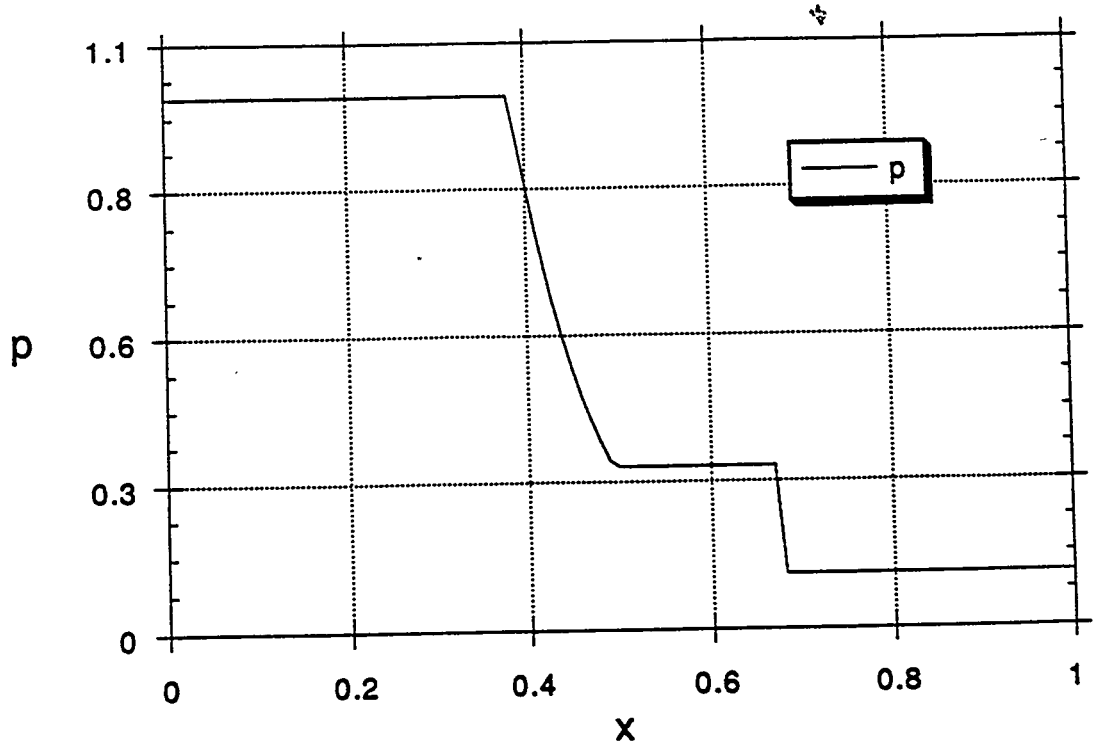

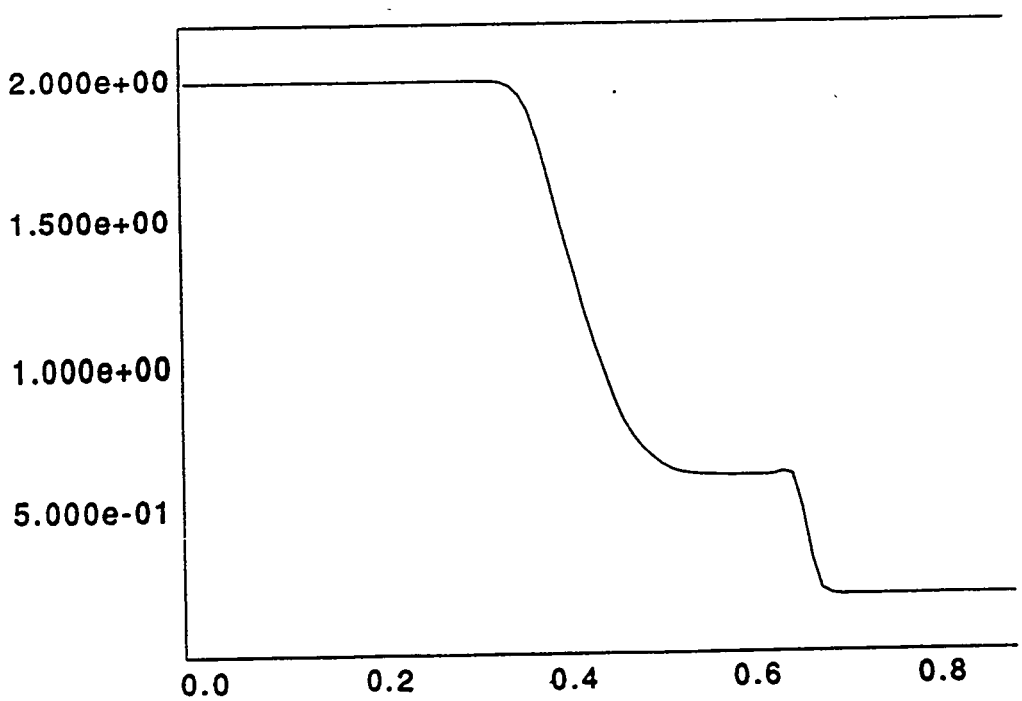

BRIO-WU MHD SHOCK PROBLEM

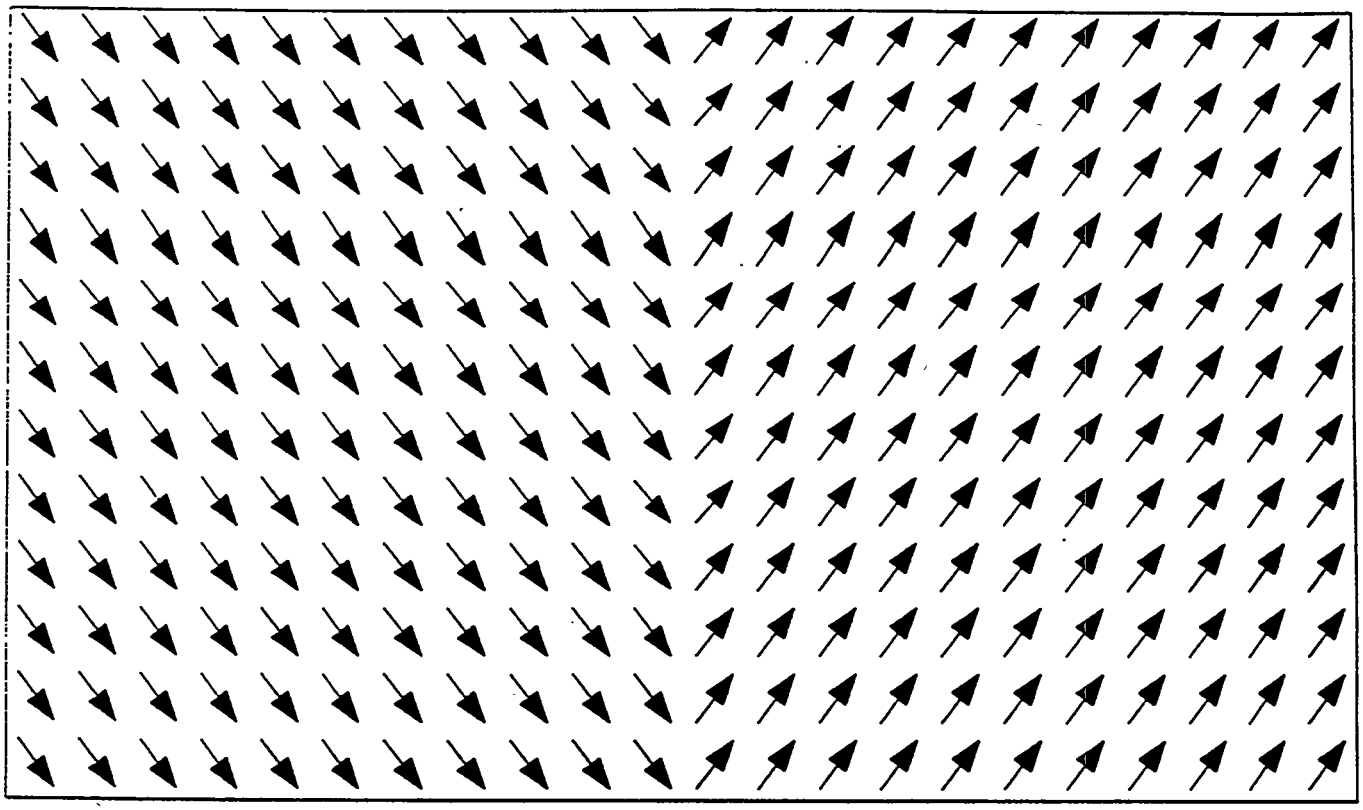

$$p_L = 1 \qquad p_R = 0.1$$
$$\rho_L = 1 \qquad \rho_R = 0.125$$
$$u_L = 0 \qquad u_R = 0$$
$$B_{r_L} = 1 \qquad B_{r_R} = -1$$

$$B_z = 0.75$$
$$\gamma = 1.4$$

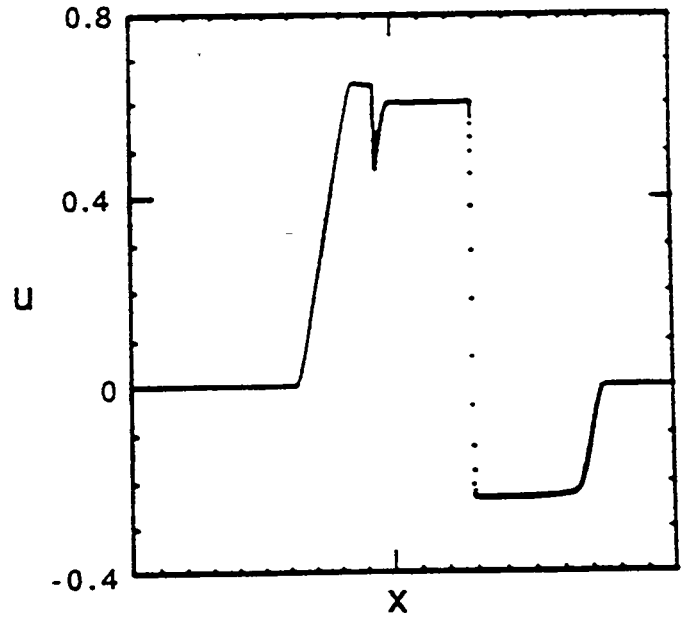
0.8
0.4
u
0
-0.4
x

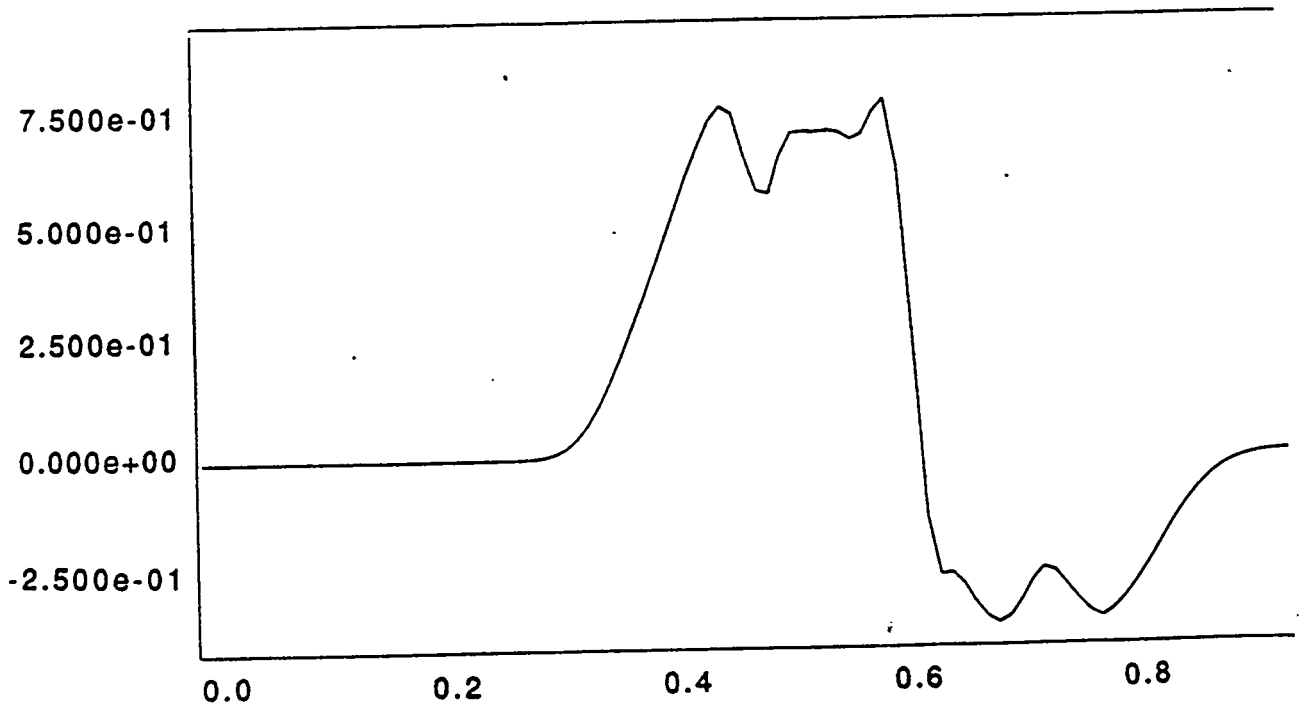
7.500e-01
5.000e-01
2.500e-01
0.000e+00
-2.500e-01
0.0
0.2
0.4
0.6
0.8

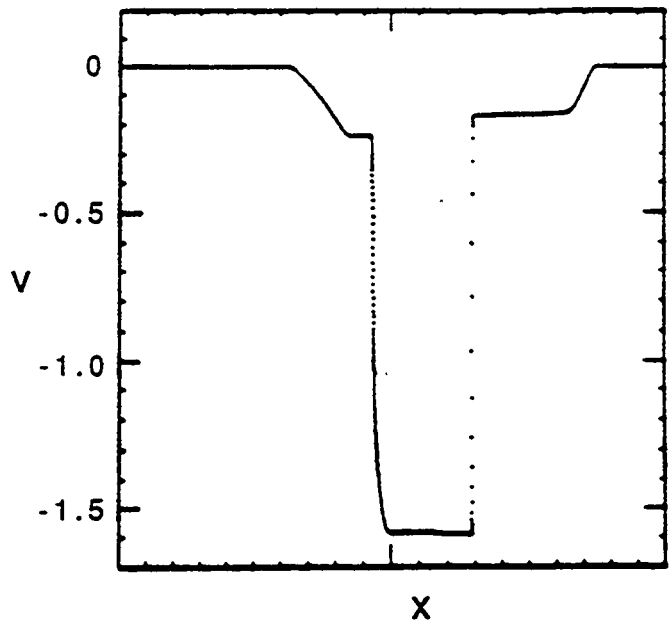
0
-0.5
V
-1.0
-1.5
X

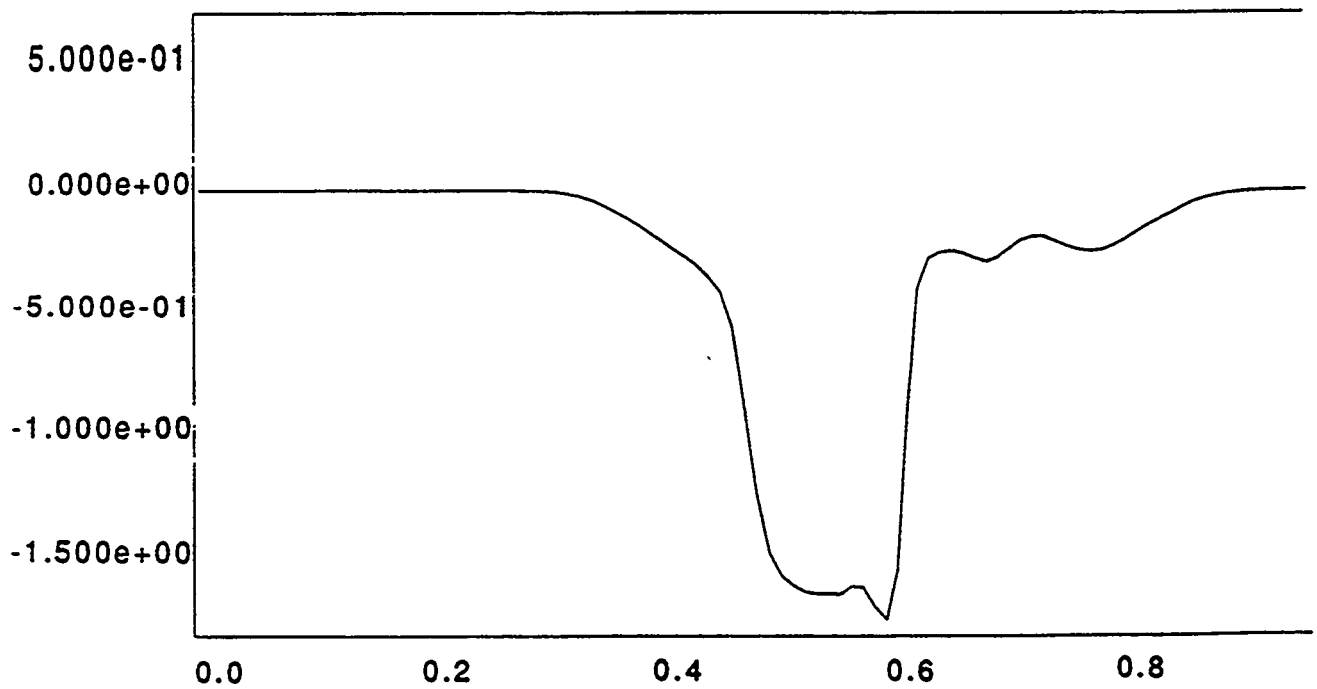
5.000e-01
0.000e+00
-5.000e-01
-1.000e+00
-1.500e+00
0.0
0.2
0.4
0.6
0.8

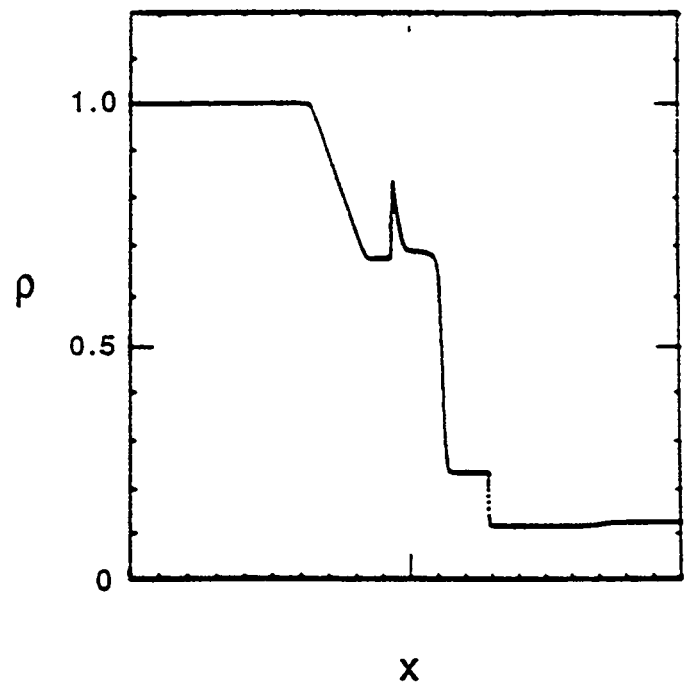
1.0
ρ
0.5
0
x

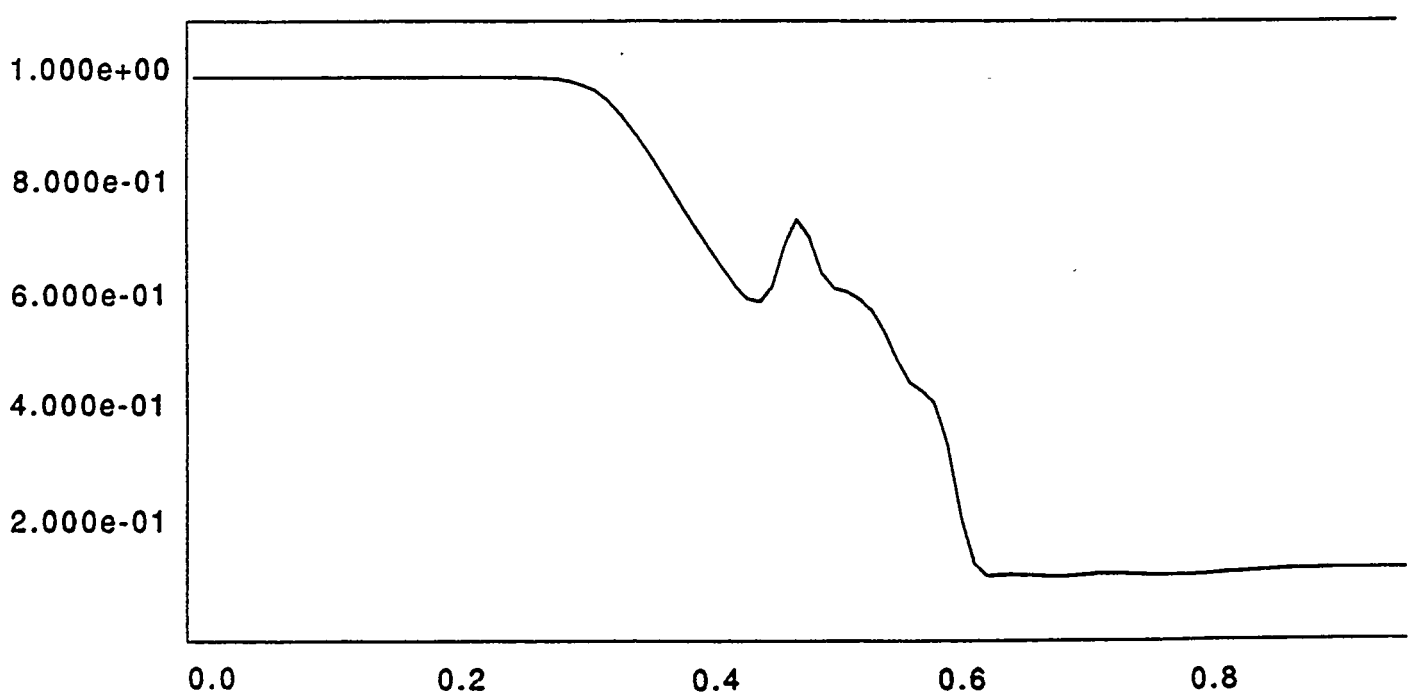
1.000e+00
8.000e-01
6.000e-01
4.000e-01
2.000e-01
0.0
0.2
0.4
0.6
0.8

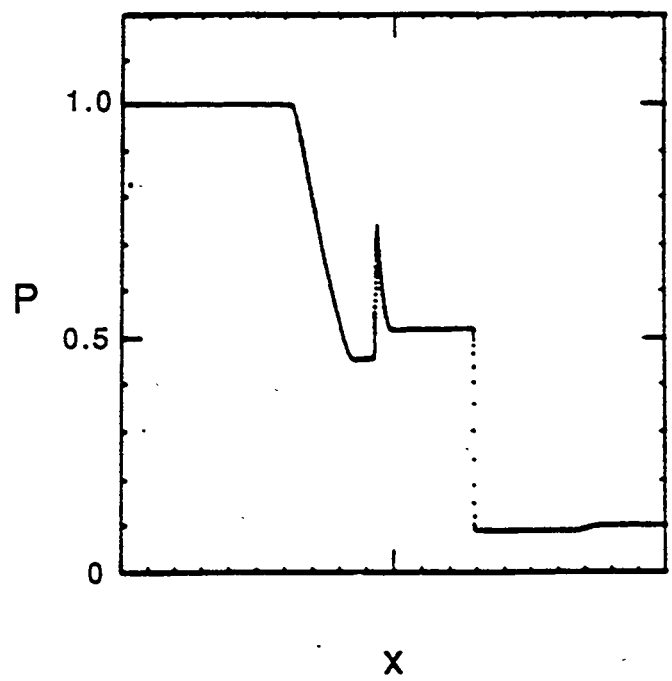
1.0
P
0.5
0
x

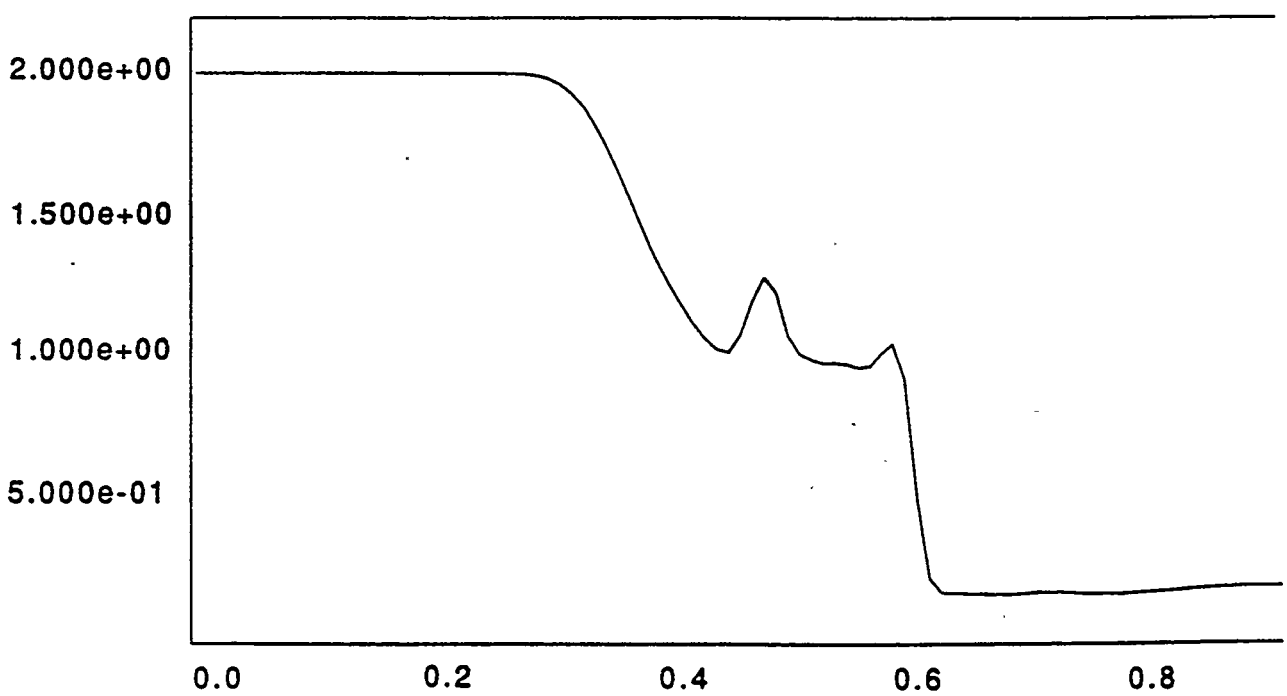
2.000e+00
1.500e+00
1.000e+00
5.000e-01
0.0
0.2
0.4
0.6
0.8

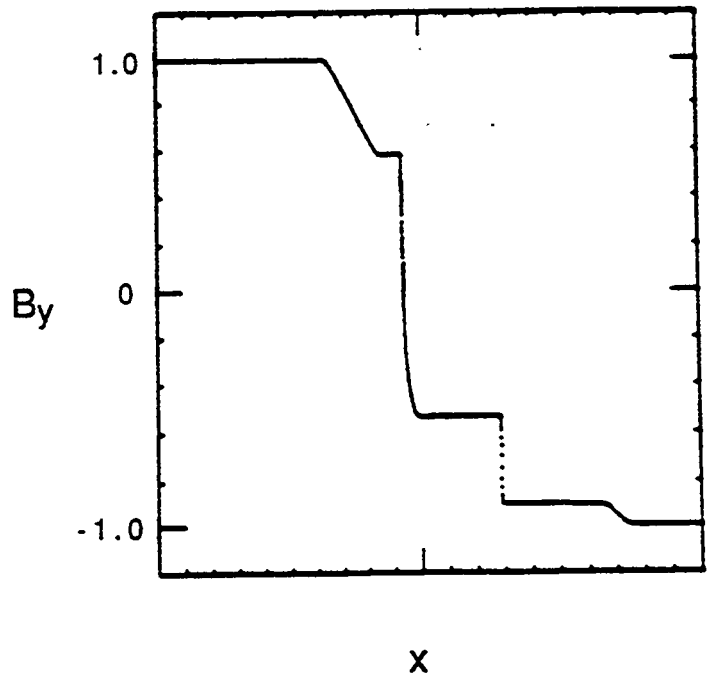
1.0
0
-1.0
By
x

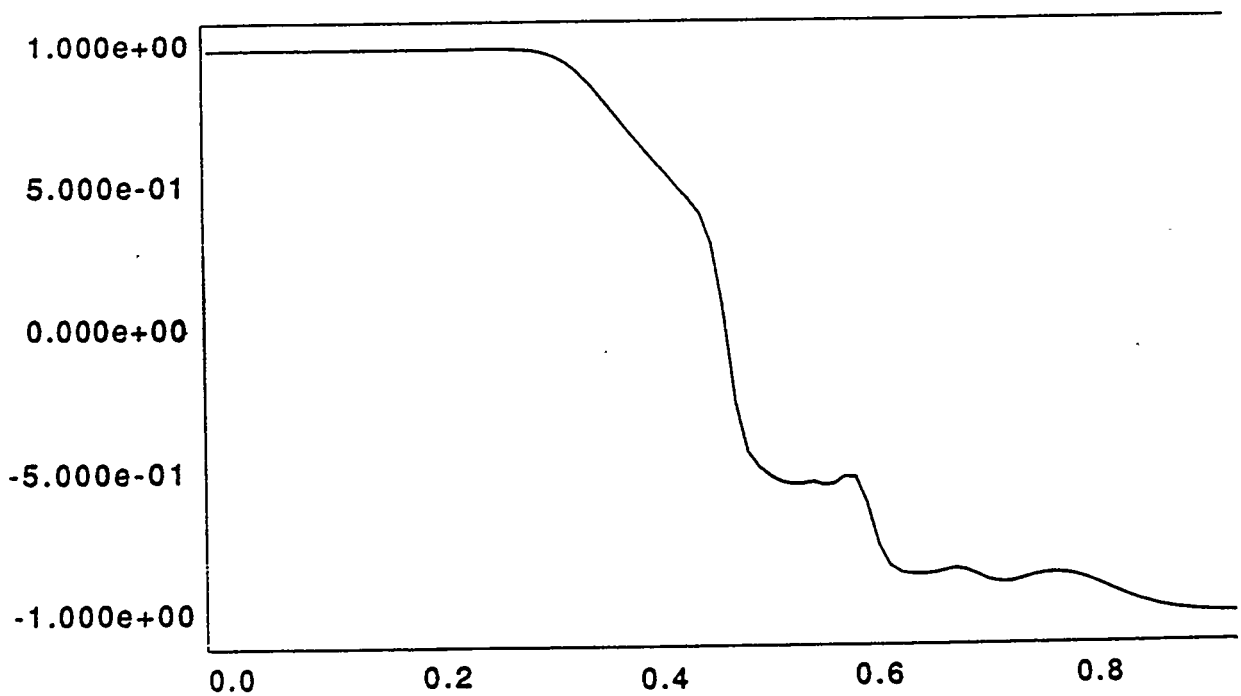
1.000e+00
5.000e-01
0.000e+00
-5.000e-01
-1.000e+00
0.0
0.2
0.4
0.6
0.8

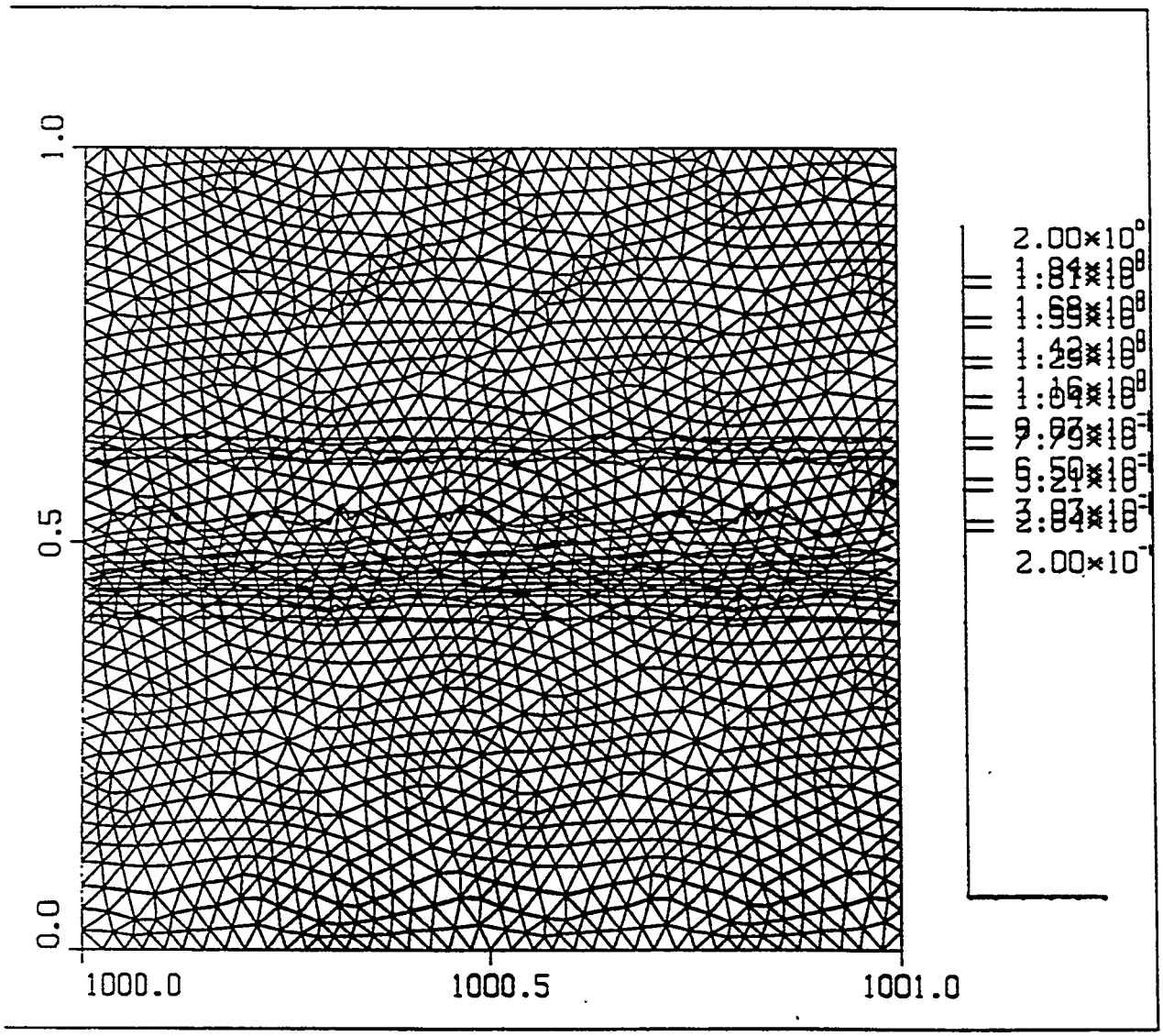
1.0
0.5
0.0
1000.0
1000.5
1001.0
2.00×10⁰
1.84×10⁻¹
1.68×10⁻¹
1.42×10⁻¹
1.16×10⁻¹
9.87×10⁻²
7.79×10⁻²
6.50×10⁻²
5.21×10⁻²
3.87×10⁻²
2.00×10⁻²

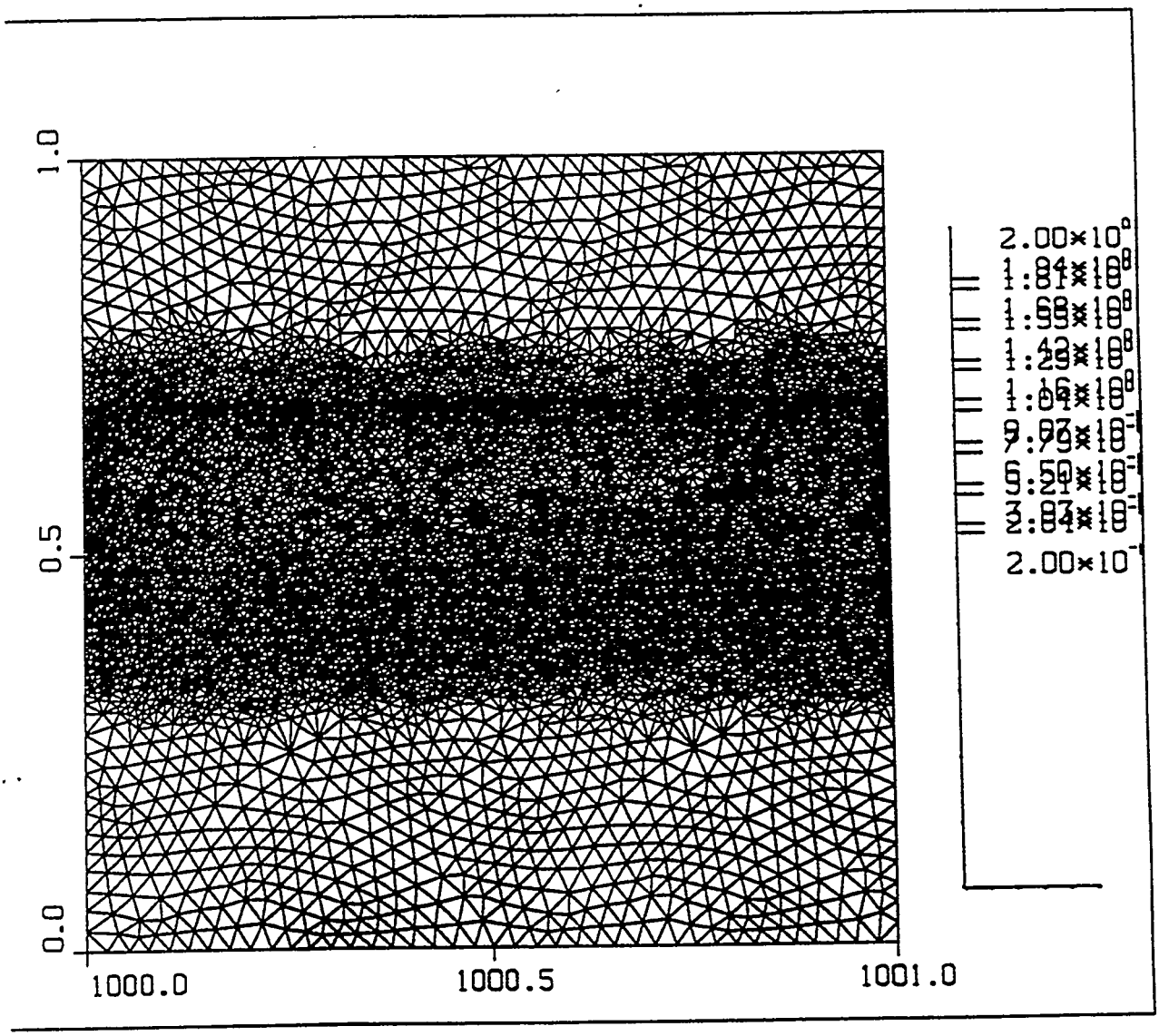
1.0
0.5
0.0
1000.0
1000.5
1001.0
2.00×10^0
1.84×10^0
1.68×10^0
1.53×10^0
1.37×10^0
1.21×10^0
1.06×10^0
9.07×10^-1
7.79×10^-1
6.50×10^-1
5.21×10^-1
3.93×10^-1
2.64×10^-1
2.00×10^-1

SOD PROBLEM t = 0.1

NO ADAPTION

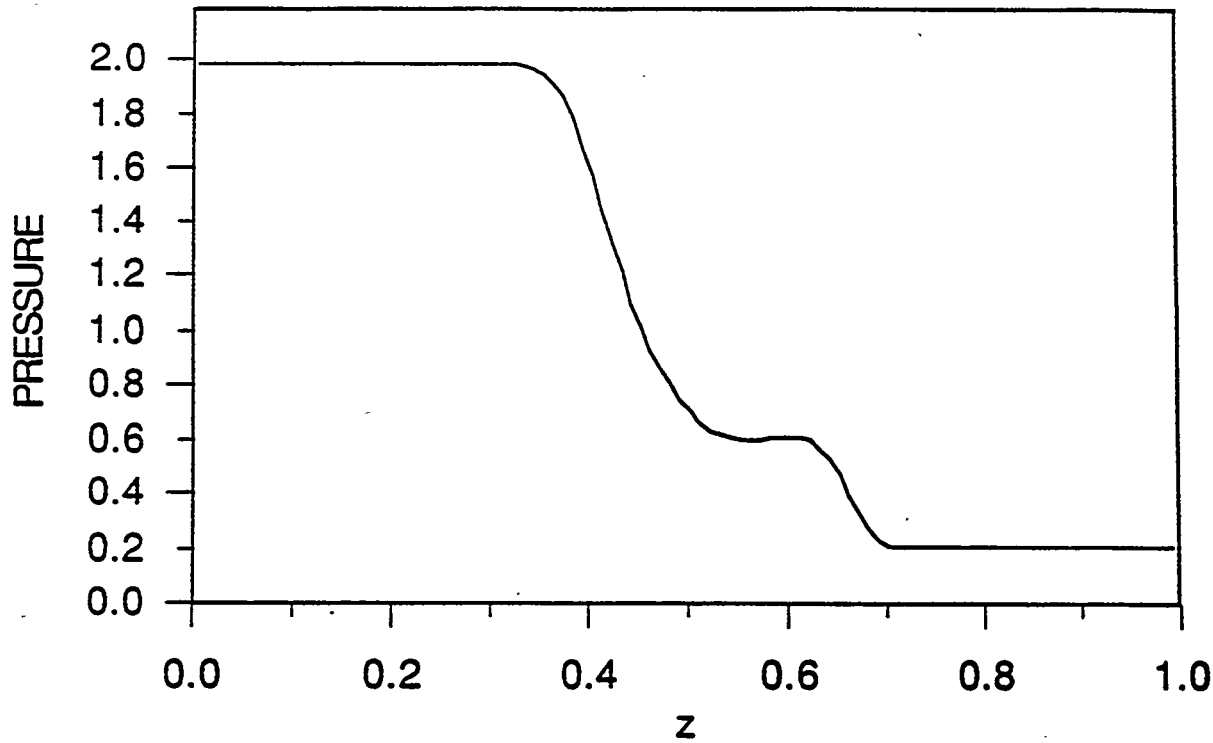

ADAPTIVE MESH

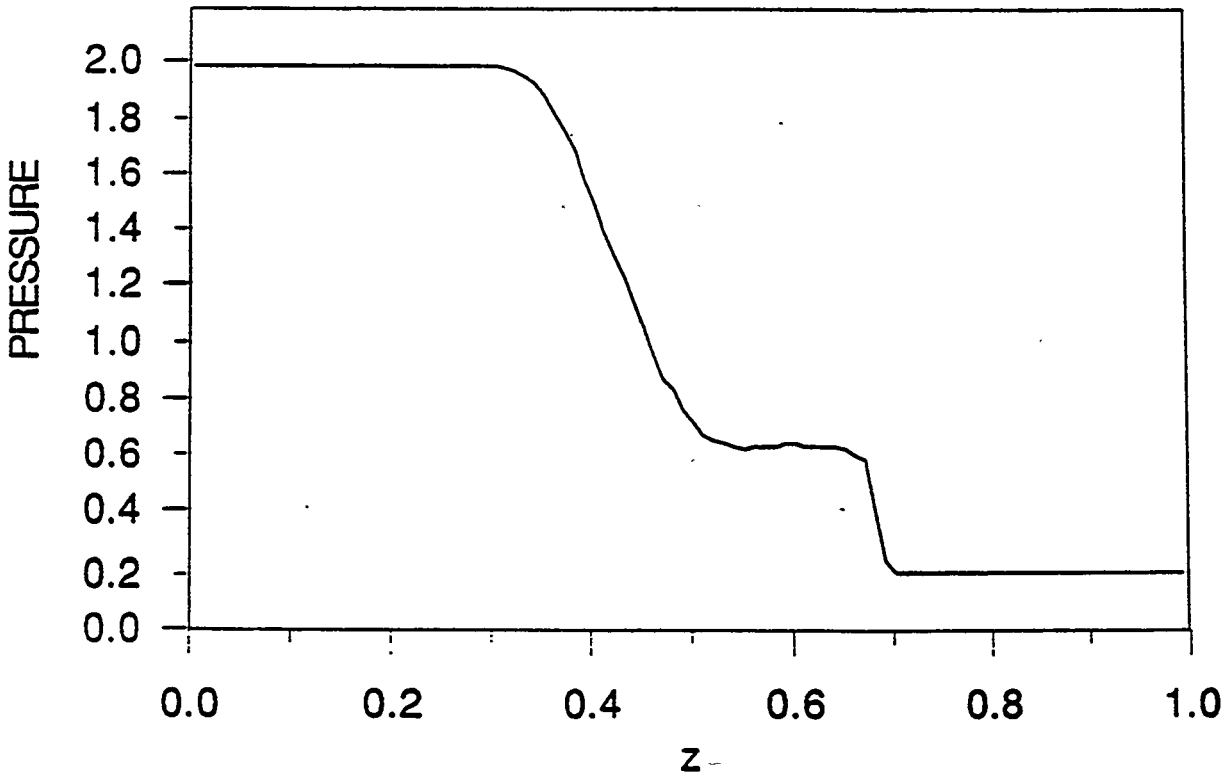

SOD PROBLEM t = 0.1

NO ADAPTION

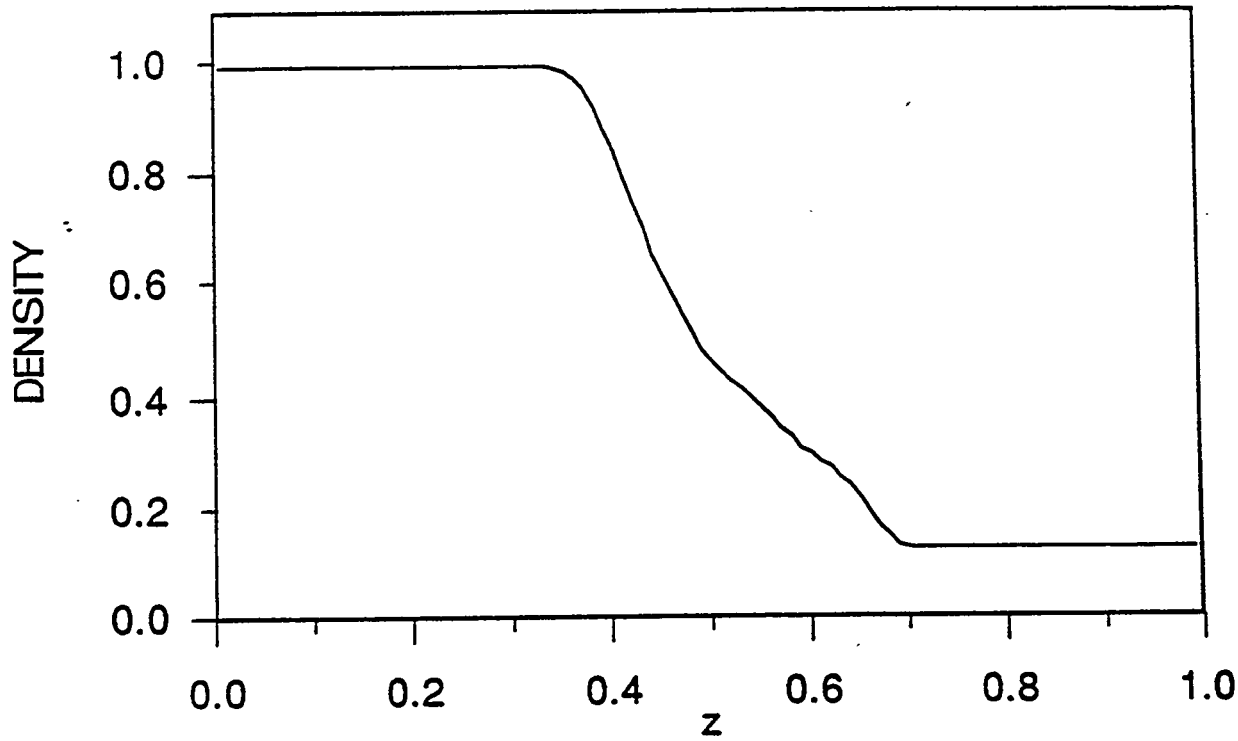

ADAPTIVE MESH

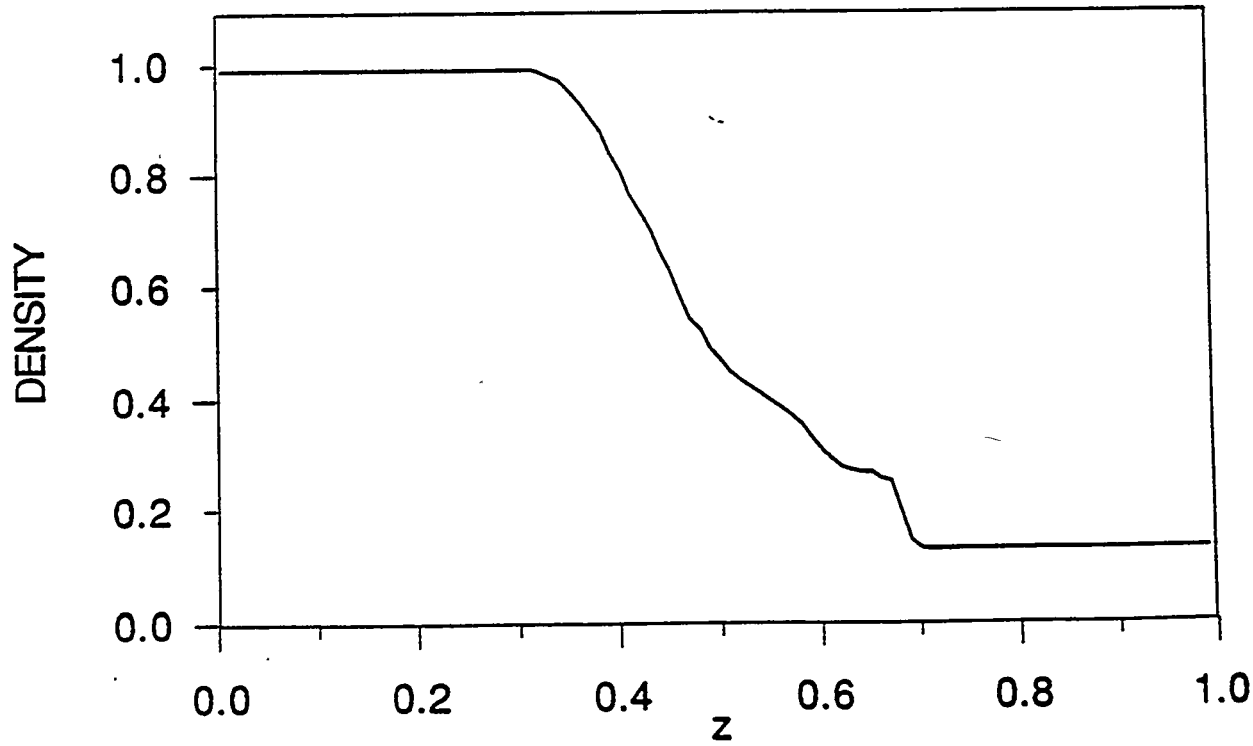

SOD PROBLEM t = 0.1

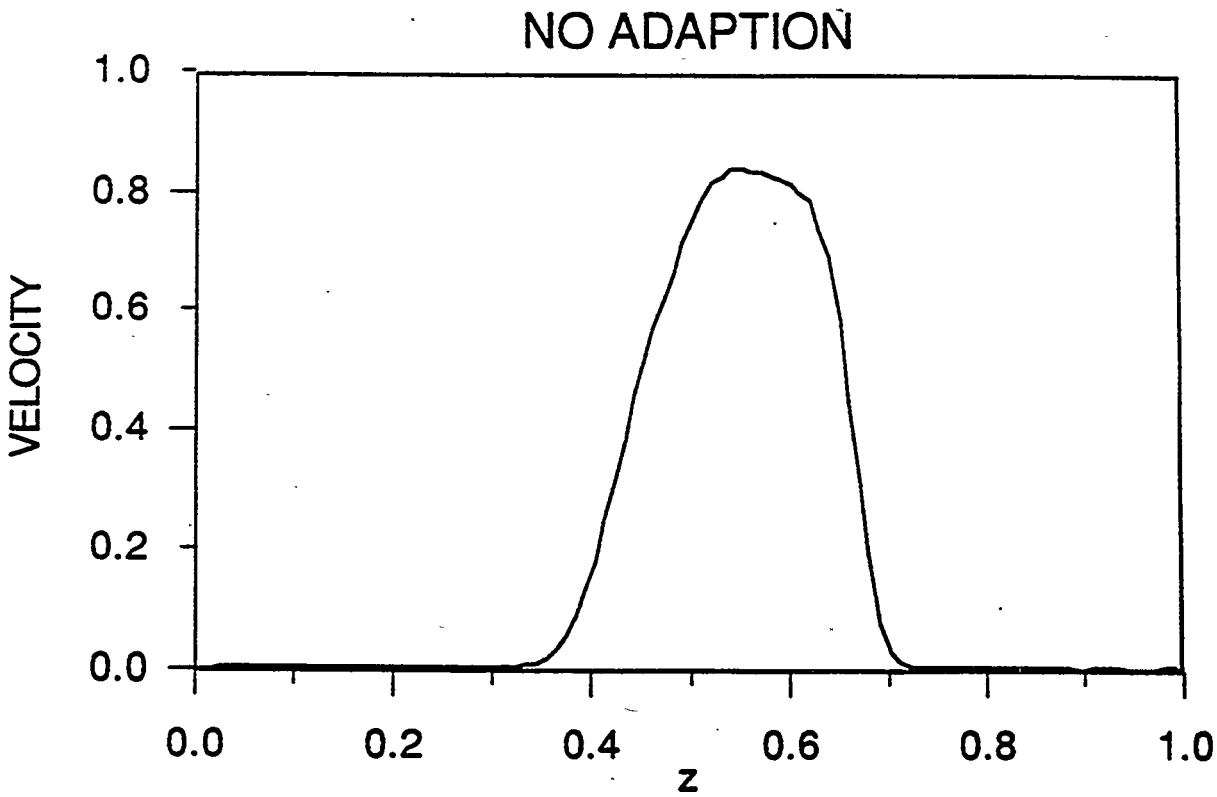

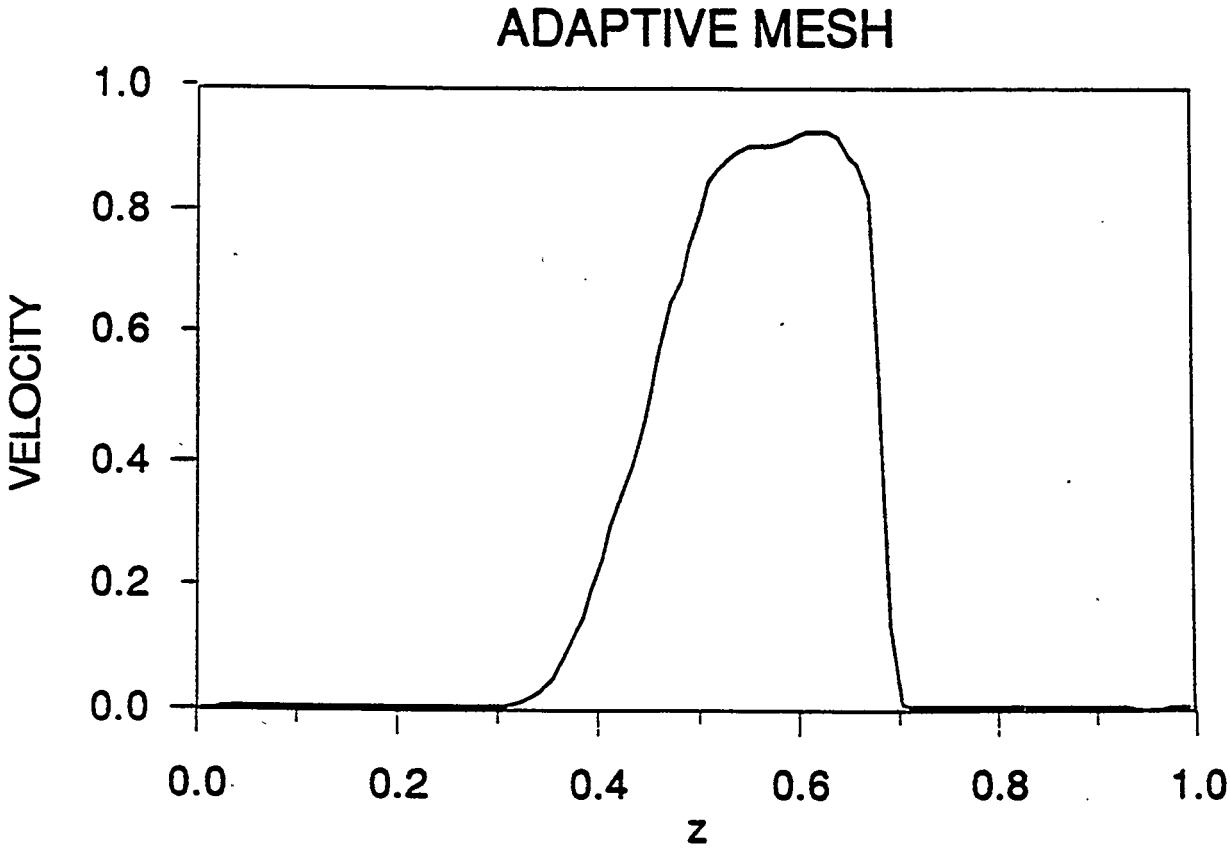

UNSTABLE ITER EQUILIBRIUM

- NONCIRCULAR, LOW ASPECT RATIO TOKAMAK EQUILIBRIUM
- MADE UNSTABLE BY LOWERING q-PROFILE; $q(0) \approx 0.4$
- INTERNAL MODES:
  - Unstable $n = 2, 4$
  - Marginally stable $n = 3$
  - Stable $n = 1$
- OBTAIN $n = 2$ LINEAR EIGENFUNCTION AND GROWTH RATE
- NONLINEAR SATURATION

PLASMA GUN

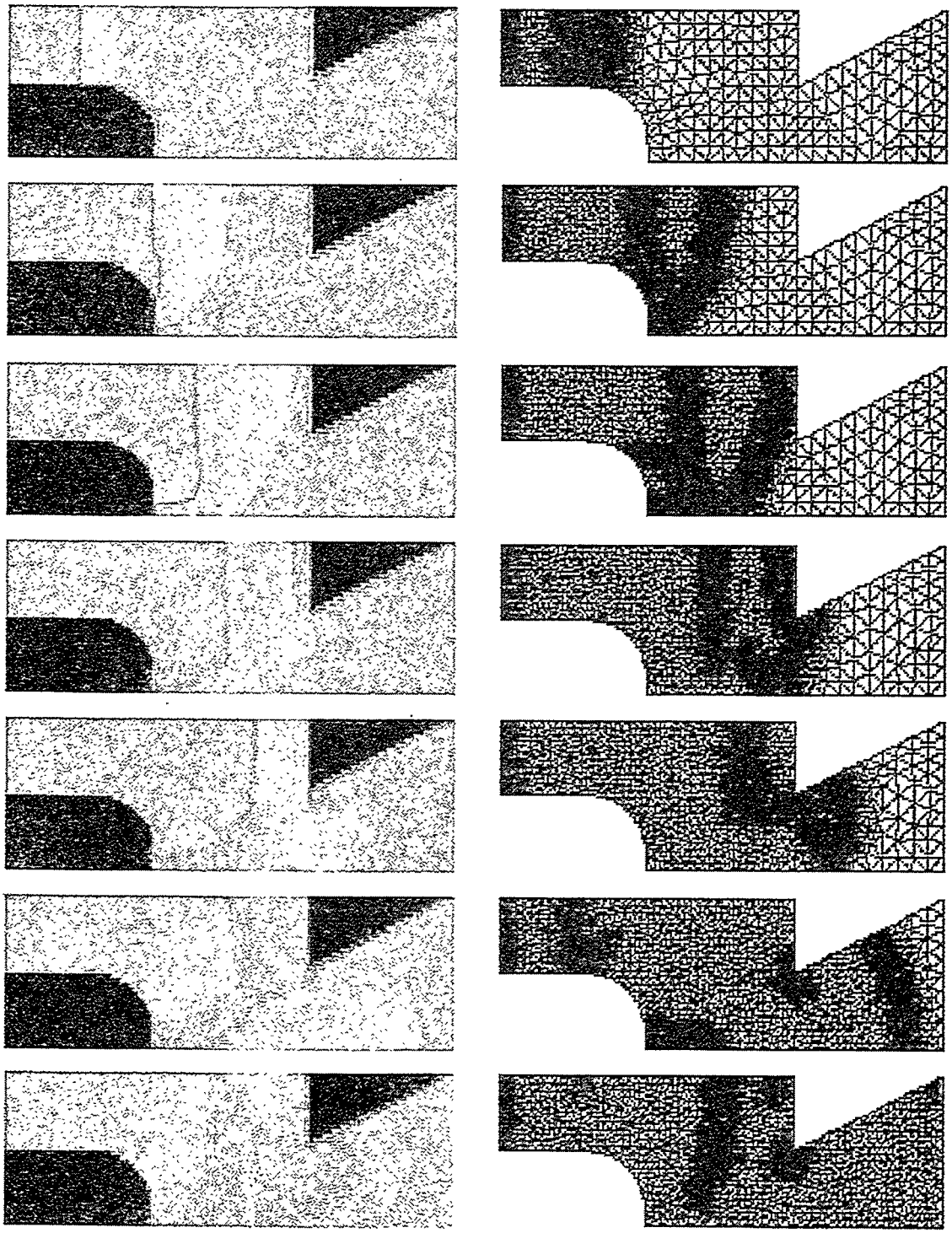

UNSTABLE ITER EQUILIBRIUM SAFETY FACTOR versus POLOIDAL FLUX

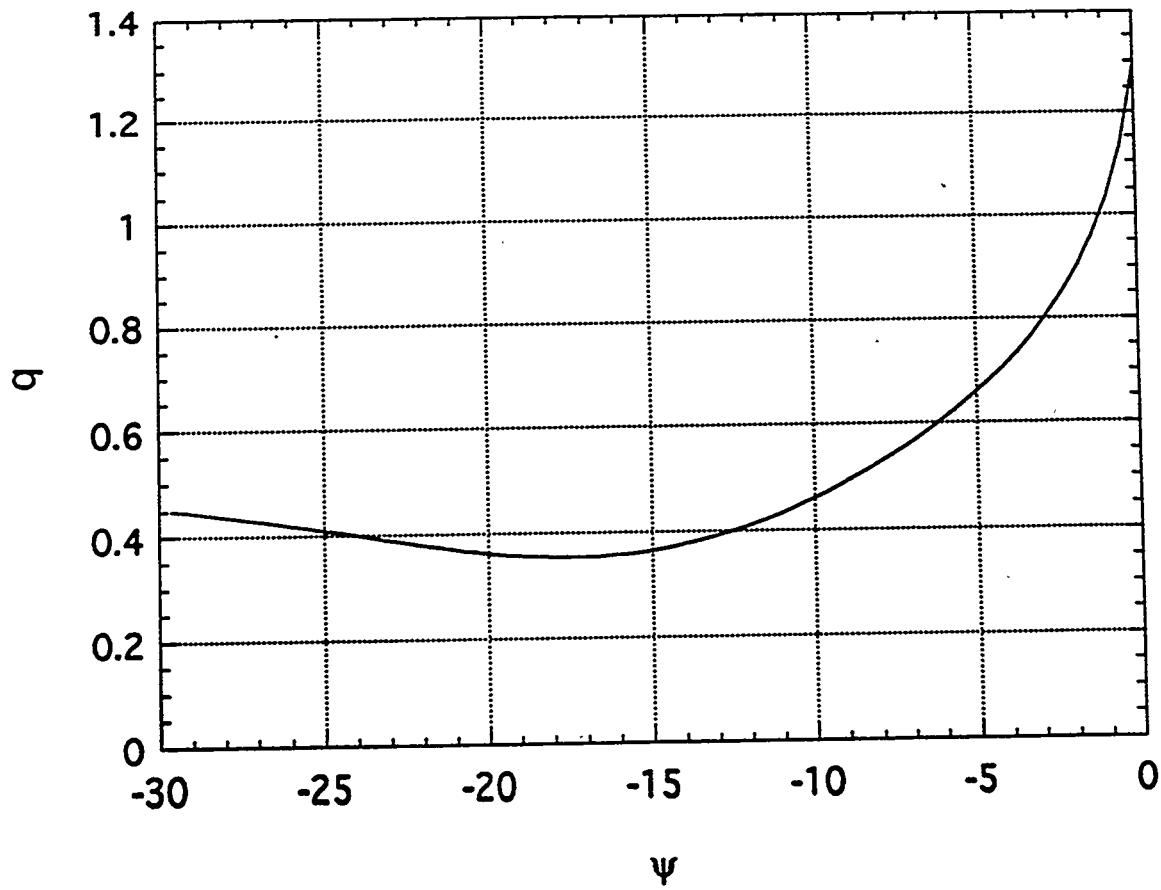

UNSTABLE ITER EQUILIBRIUM PRESSURE versus POLOIDAL FLUX

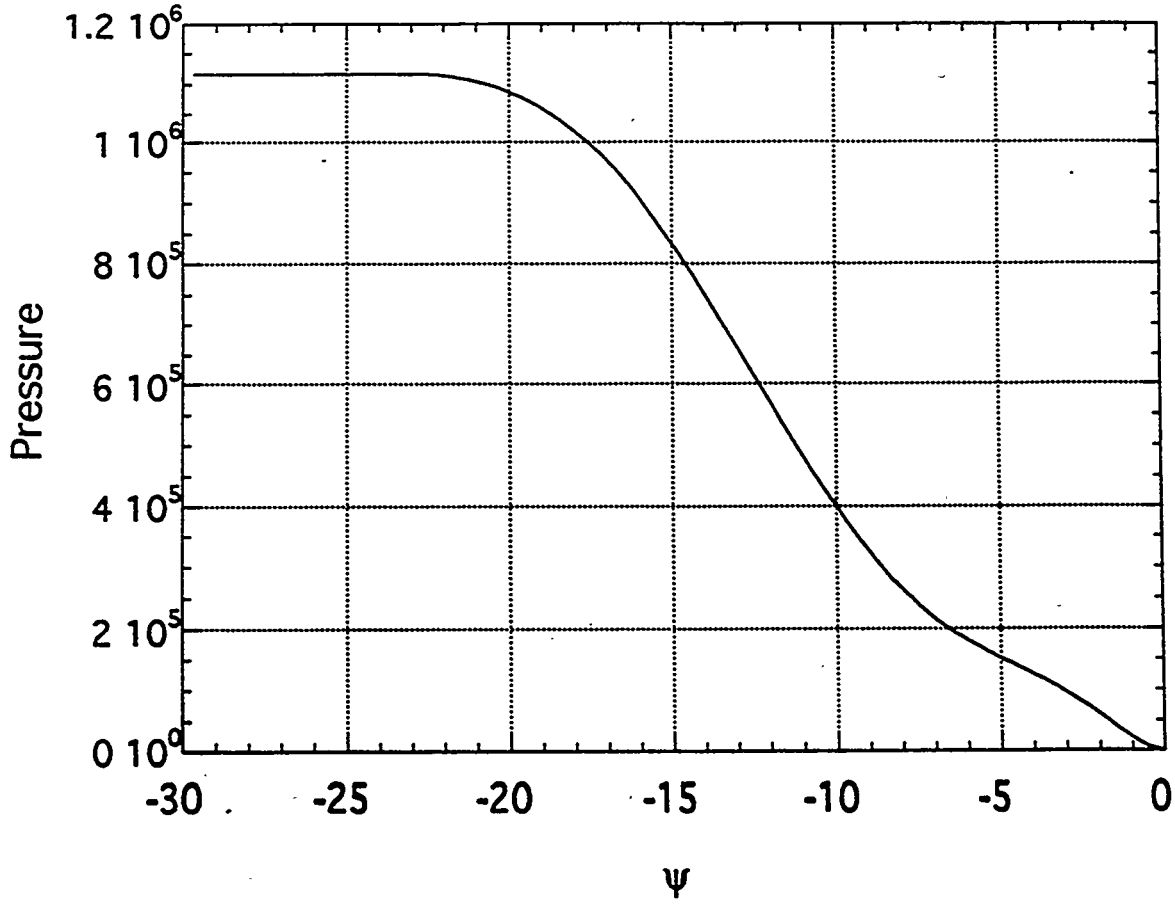

UNSTABLE ITER EQUILIBRIUM
$F = rB_\phi$
versus
POLOIDAL FLUX

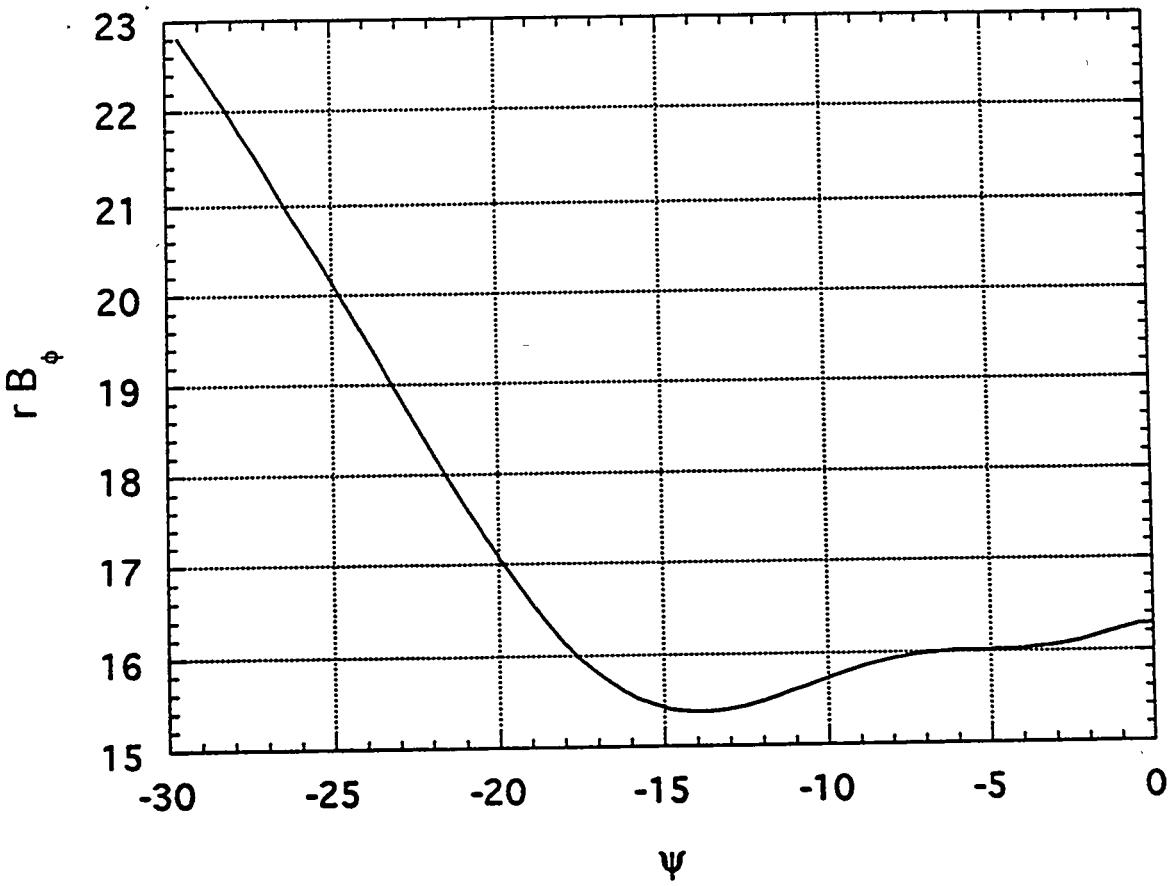

ITER POLOIDAL CROSS-SECTION

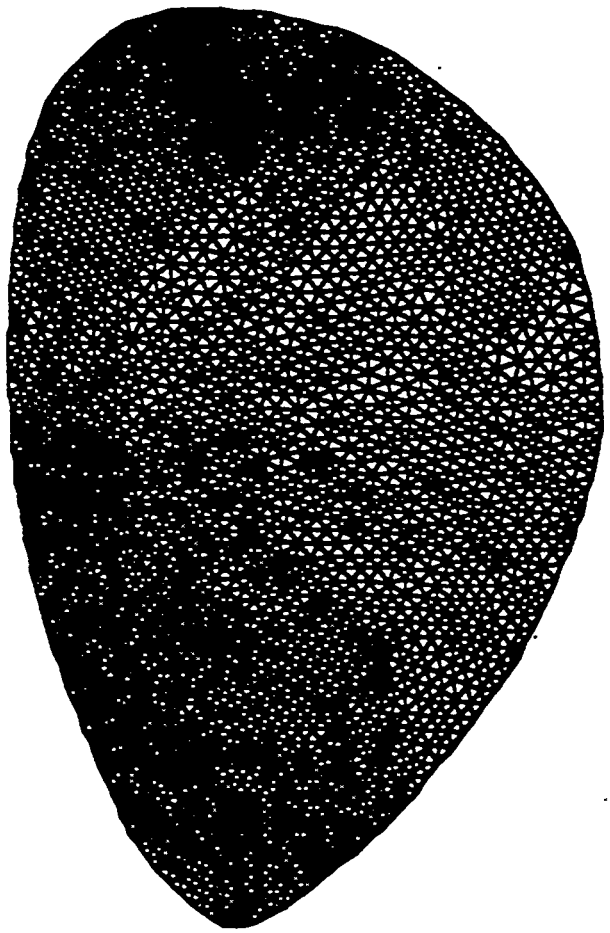

TRIANGULATION INSIDE
LAST CLOSED FLUX SURFACE

ITER EQUILIBRIUM

FLUX

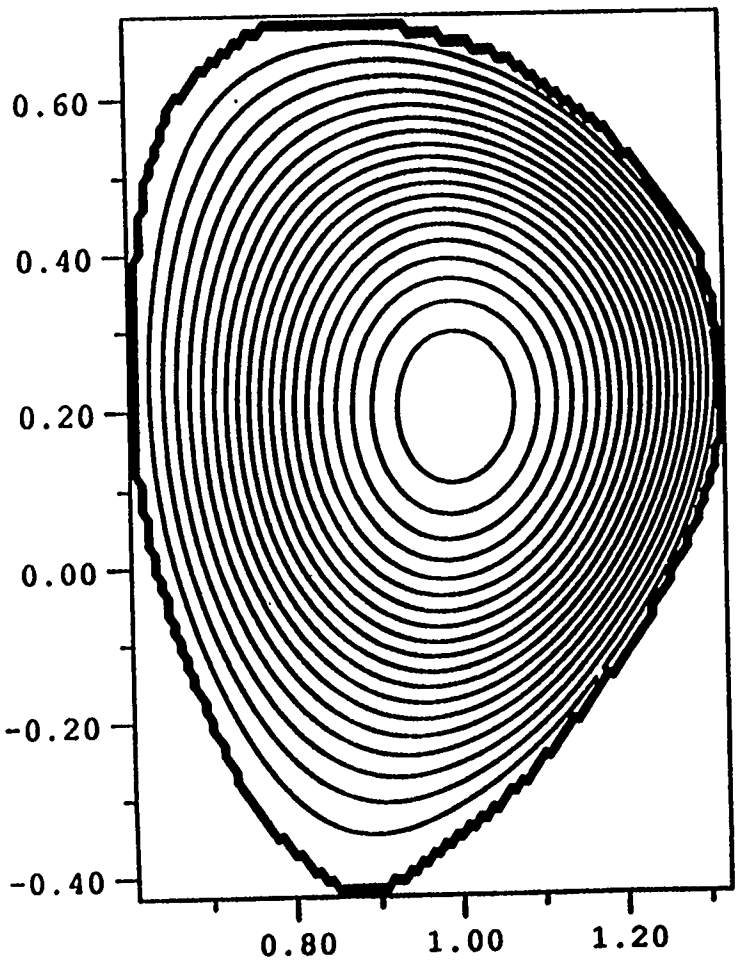

PRESSURE

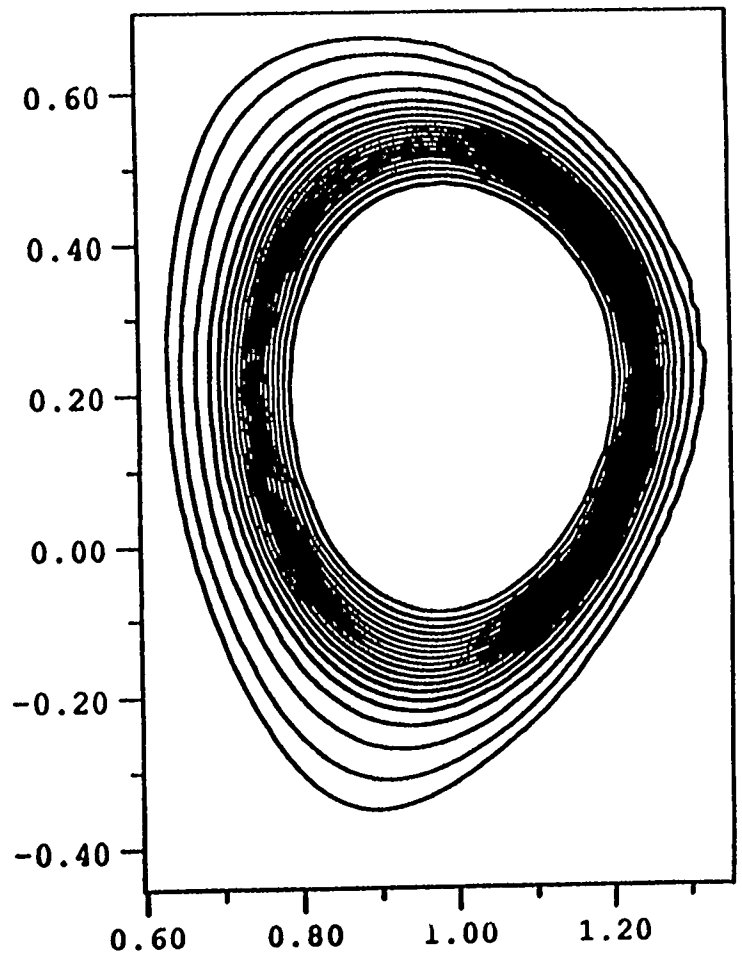

2-SCHNACK.11

ITER STABILITY MODEL
KINETIC ENERGY
versus
TIME

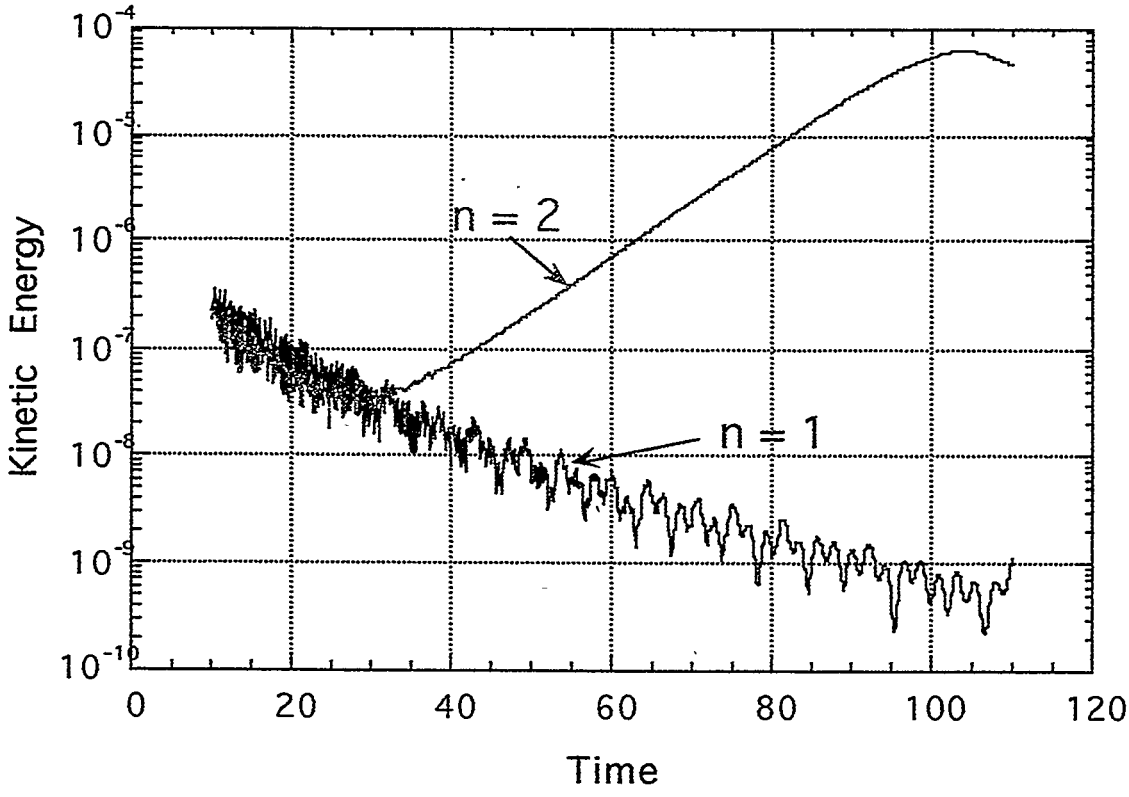

n = 2 EIGENMODE

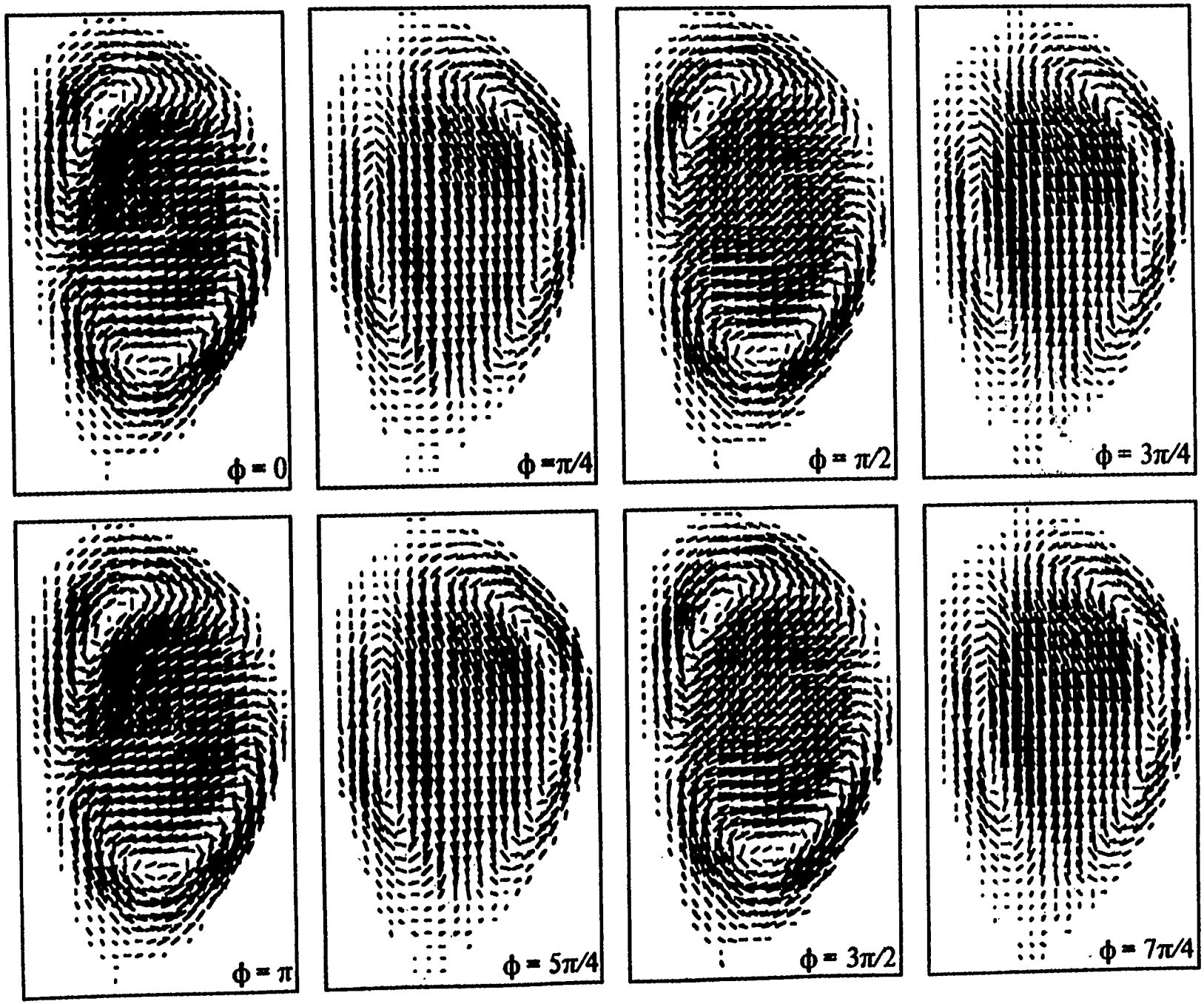

n = 2 EIGENMODE
TOROIDAL VELOCITY

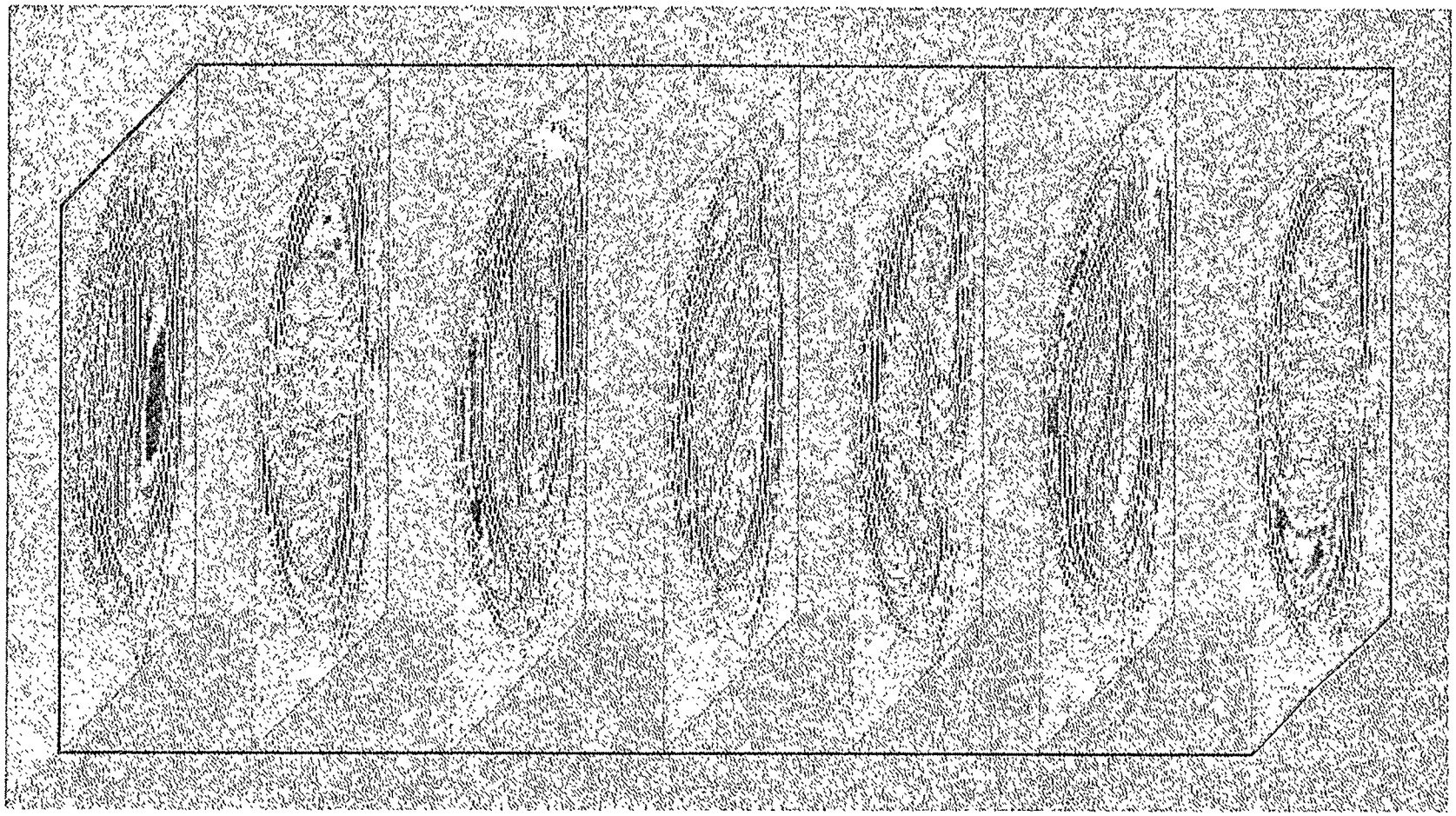

CPU TIME (sec) per e-FOLDING TIME VERSUS COURANT NUMBER

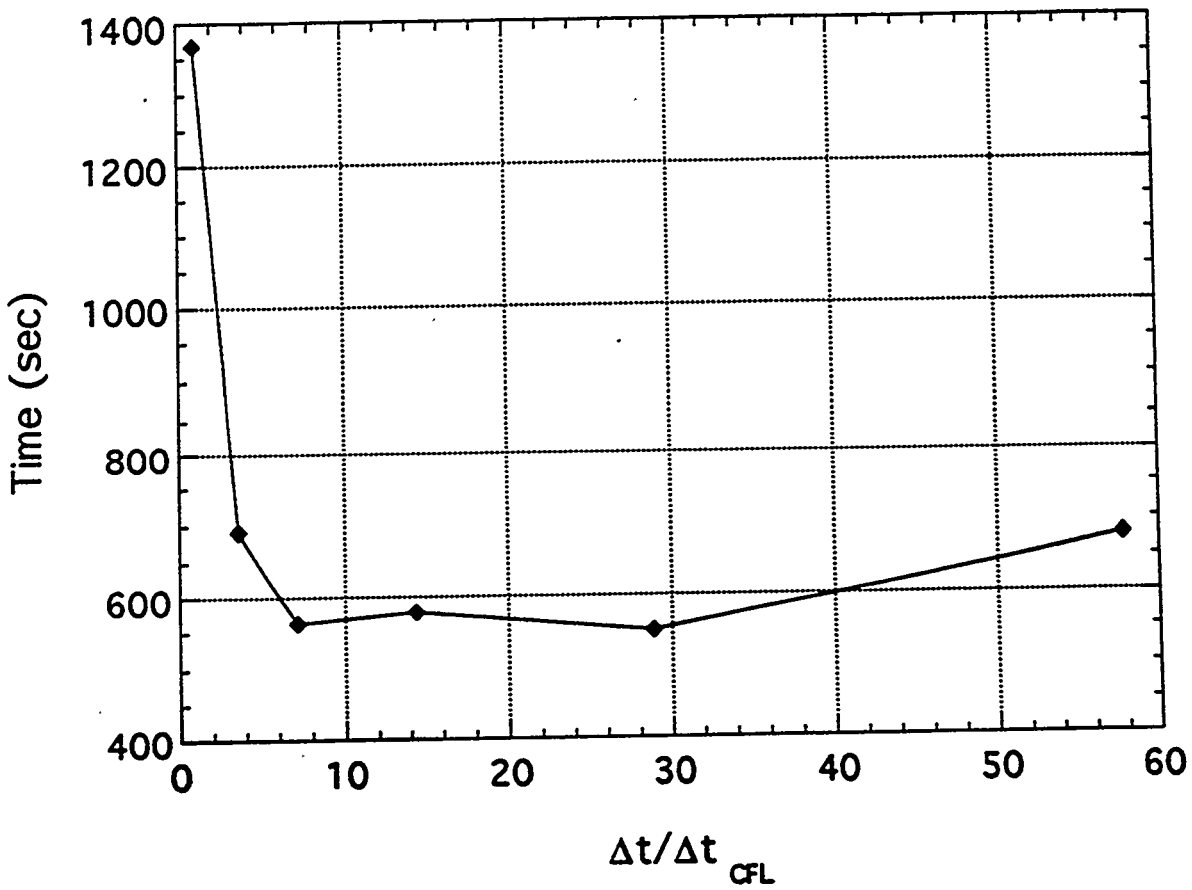

CPU TIME PER TIMESTEP (sec) versus COURANT NUMBER

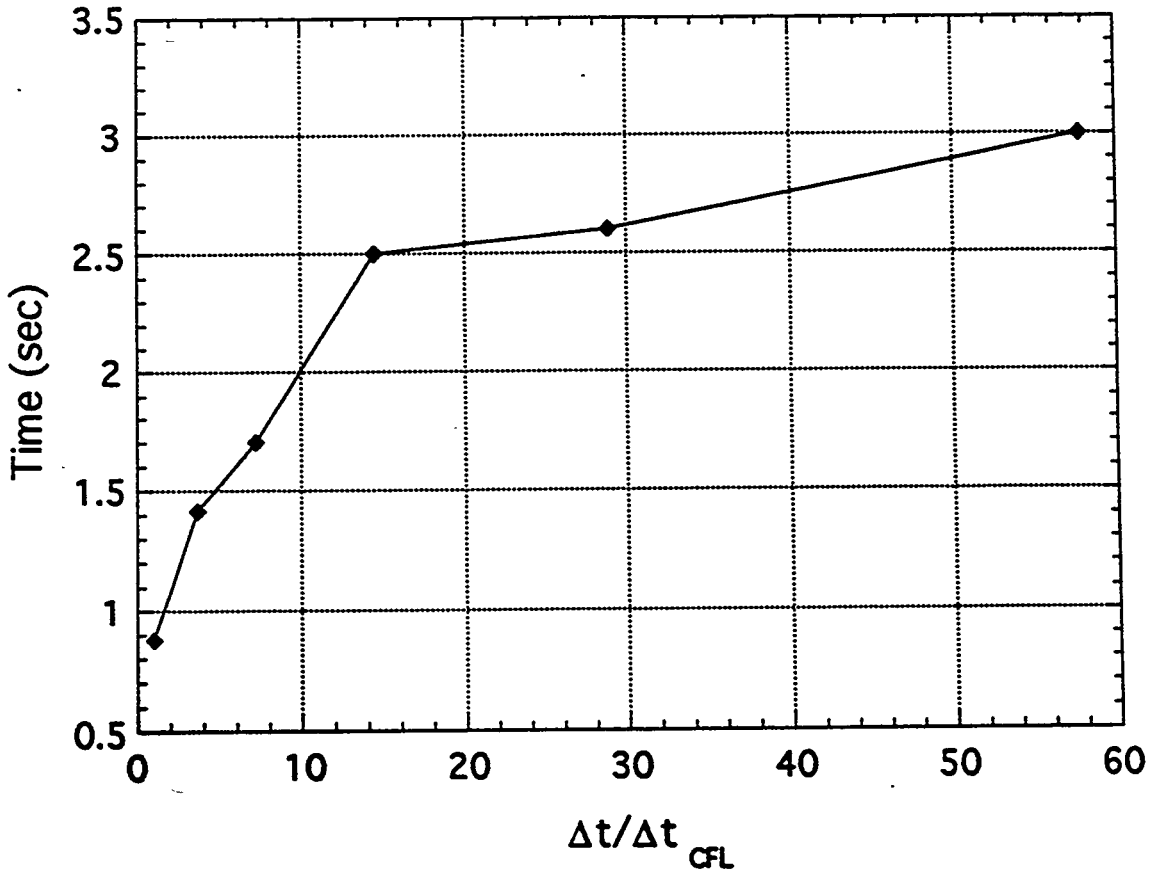

NUMBER OF CG ITERATIONS PER SOLVE VERSUS COURANT NUMBER

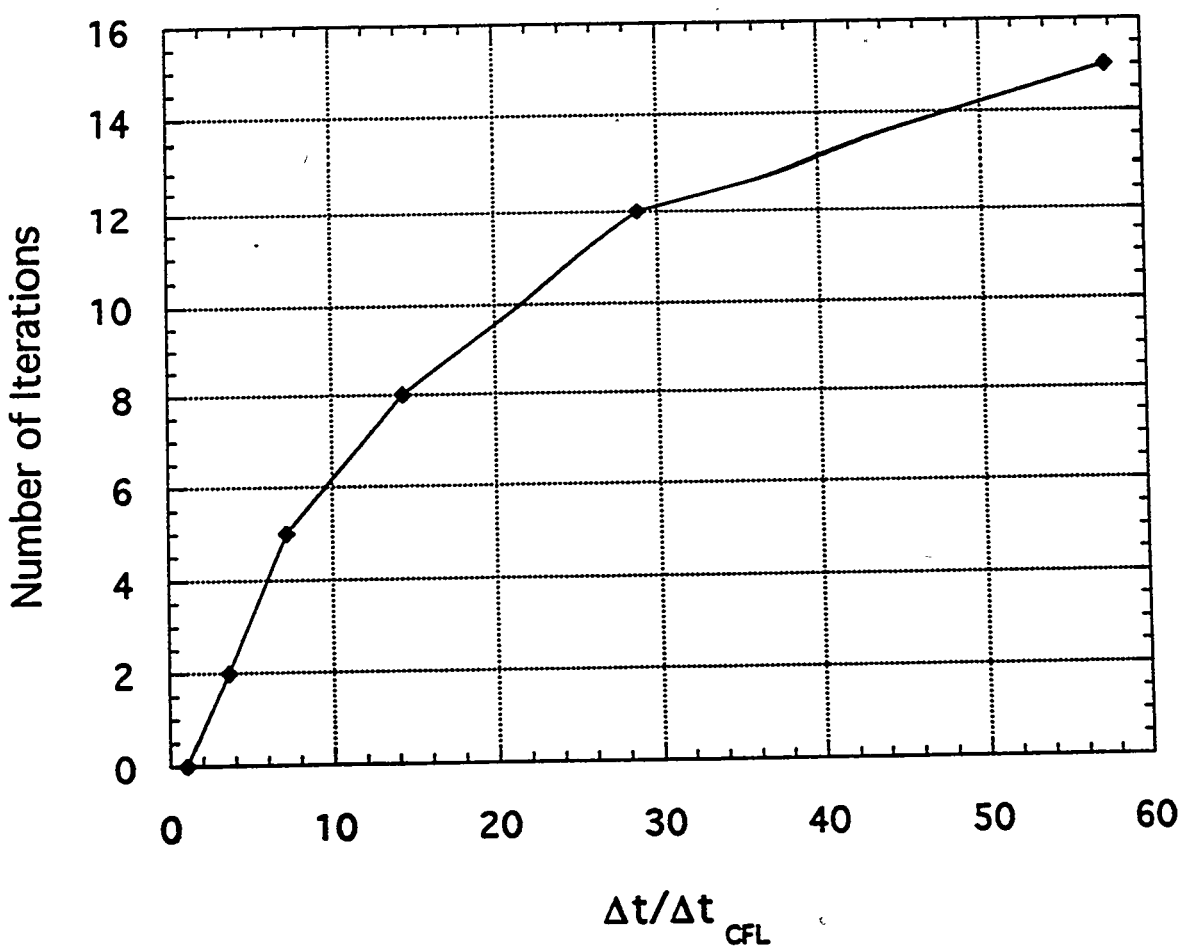

UNSTABLE ITER EQUILIBRIUM GROWTH RATE $\gamma\tau_{A\phi}$ versus COURANT NUMBER n = 2 MODE

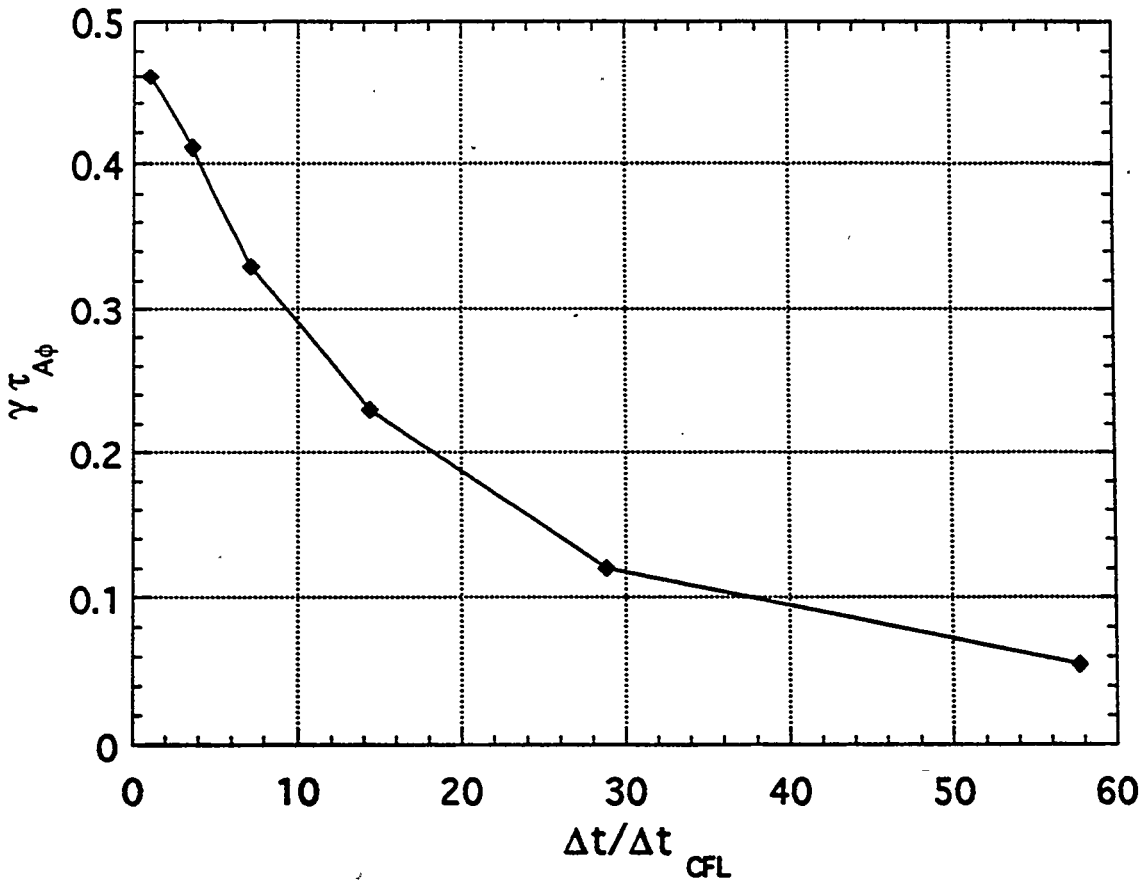

SOD PROBLEM

WITHOUT ADAPTION

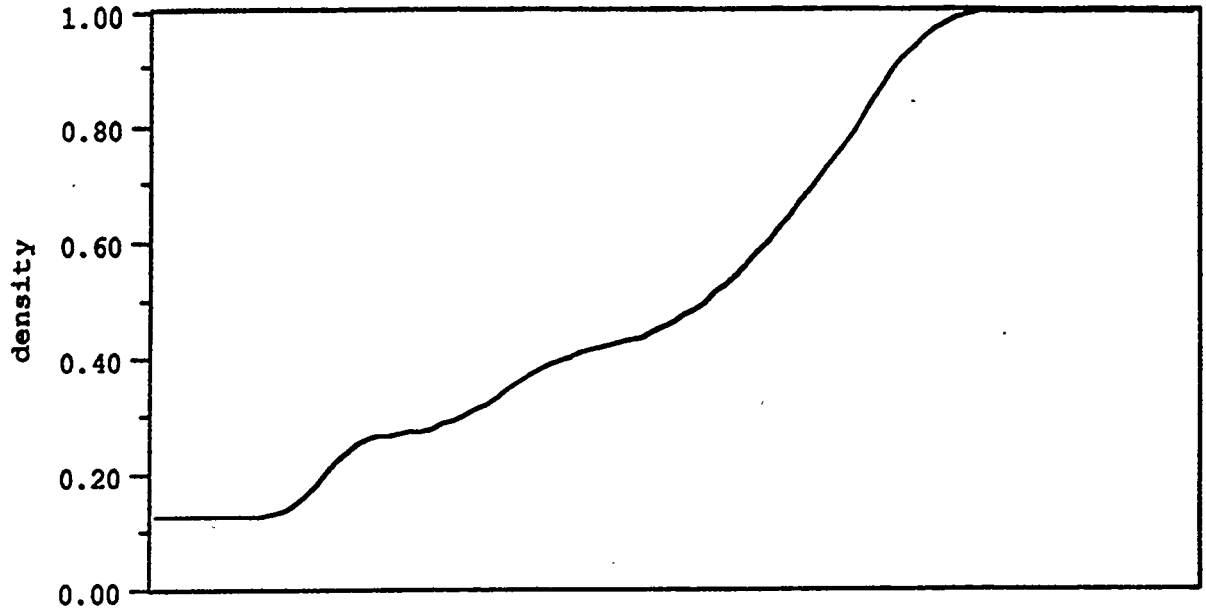

WITH ADAPTION

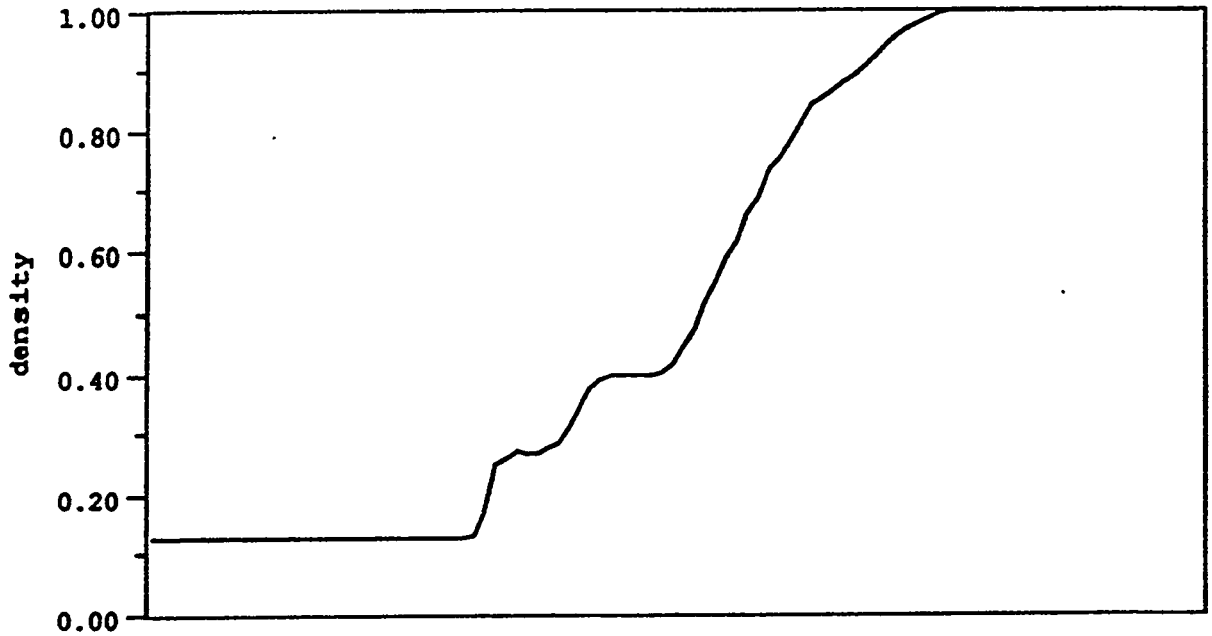

RESEARCH ISSUES

- RESULTS SENSITIVE TO TRIANGLE SHAPE
  - Equilateral triangles best
  - How to arrange vertices to optimize mesh?
- INTERPOLATION
  - Simplest schemes have low order accuracy
  - Results sensitive to interpolation errors
  - Wrong choice can destroy self-adjointness
- ADAPTION
  - Mechanics of refinement/coarsening well defined and operational
  - Criteria for refinement/coarsening for hydrodyrodynamics well defined and operational
  - Criteria for refinement/coarsening for MHD not well understood.

STATUS

- COMPUTED GROWTH AND SATURATION OF INTERNAL MODES IN NON-CIRCULAR, TOROIDAL GEOMETRY
- MESH ADAPTION WORKS FOR 2-D SHOCK TEST PROBLEMS

FUTURE DIRECTIONS

- APPLY MESH ADAPTION TO 3-D TOROIDAL PROBLEMS
- VACUUM REGION/EXTERNAL MODES
- RESISTIVE WALLS
- EDGE MODELS

High-Performance Computing at NERSC: Present and Future

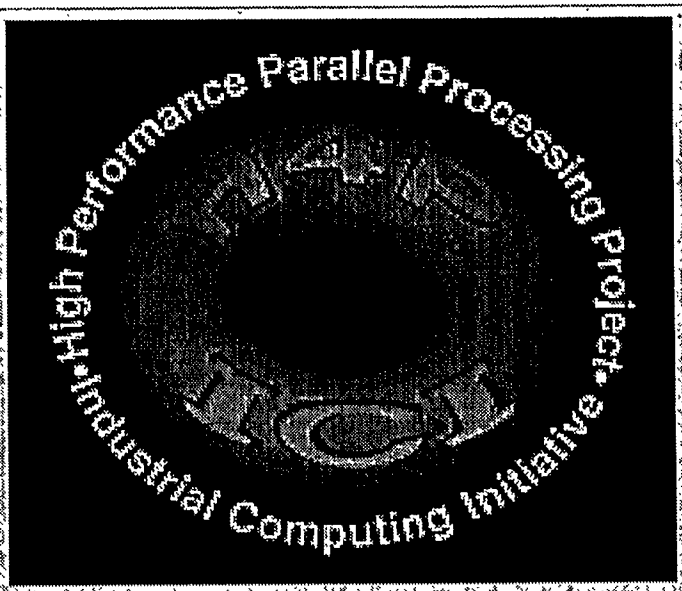

Alice E. Koniges
H4P-ICI Project Leader

Outline

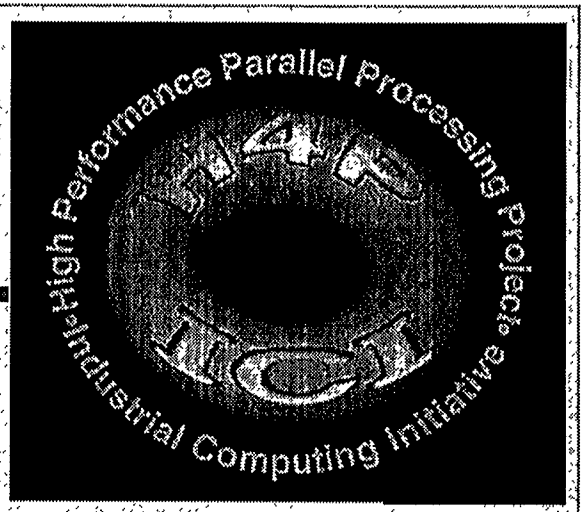

- **High-Performance Computing at NERSC**
  - Intro to MPP
  - Hardware and Software
  - Performance Issues on MPP's
  - The ICI projects
- **Trends and Limitations in Computer Architectures**
- **Benchmark Performance**
- **Future**
  - Heterogeneous Computing
  - Role of MPP's

What is MPP?

Parallel Processor

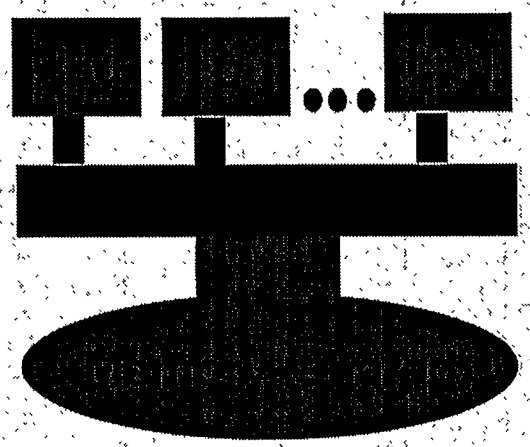

2-32 processors today
Memory shared
High powered Processors (C90)

Not Scalable

MPP Massively Parallel Processor

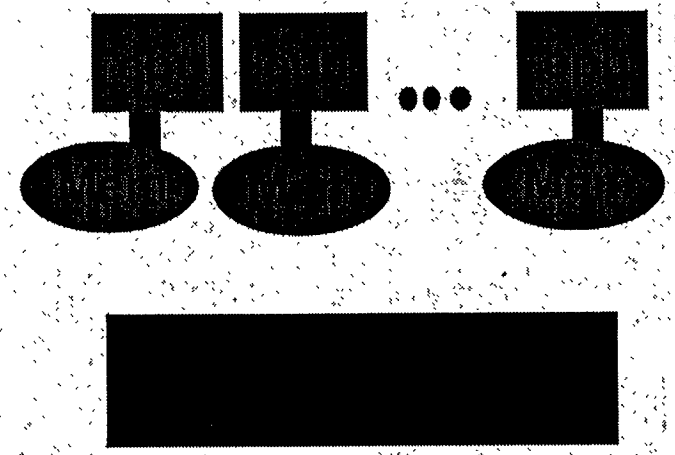

64 - up today
Memory physically distributed
High Powered Micros (Alpha)

Scalable

MPP Today

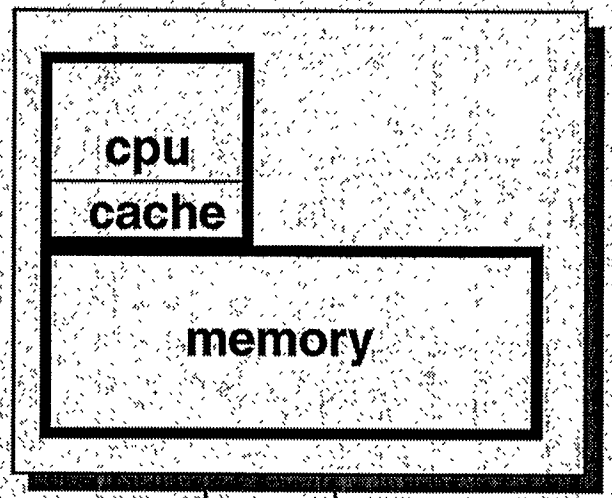

Processor

RS6000 - IBM
Dec Alpha - Cray
Sparc - TMC, Meiko

Memory

16 MBytes - 256 MBytes
Ram per processor

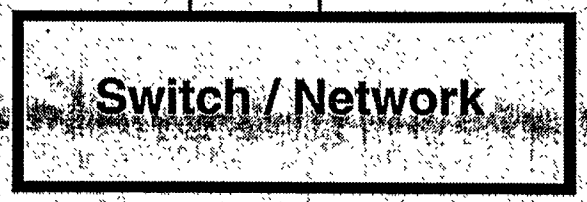

Network

omega — IBM SP2, Meiko
3D Torus — Cray T3D

IBM SP-2

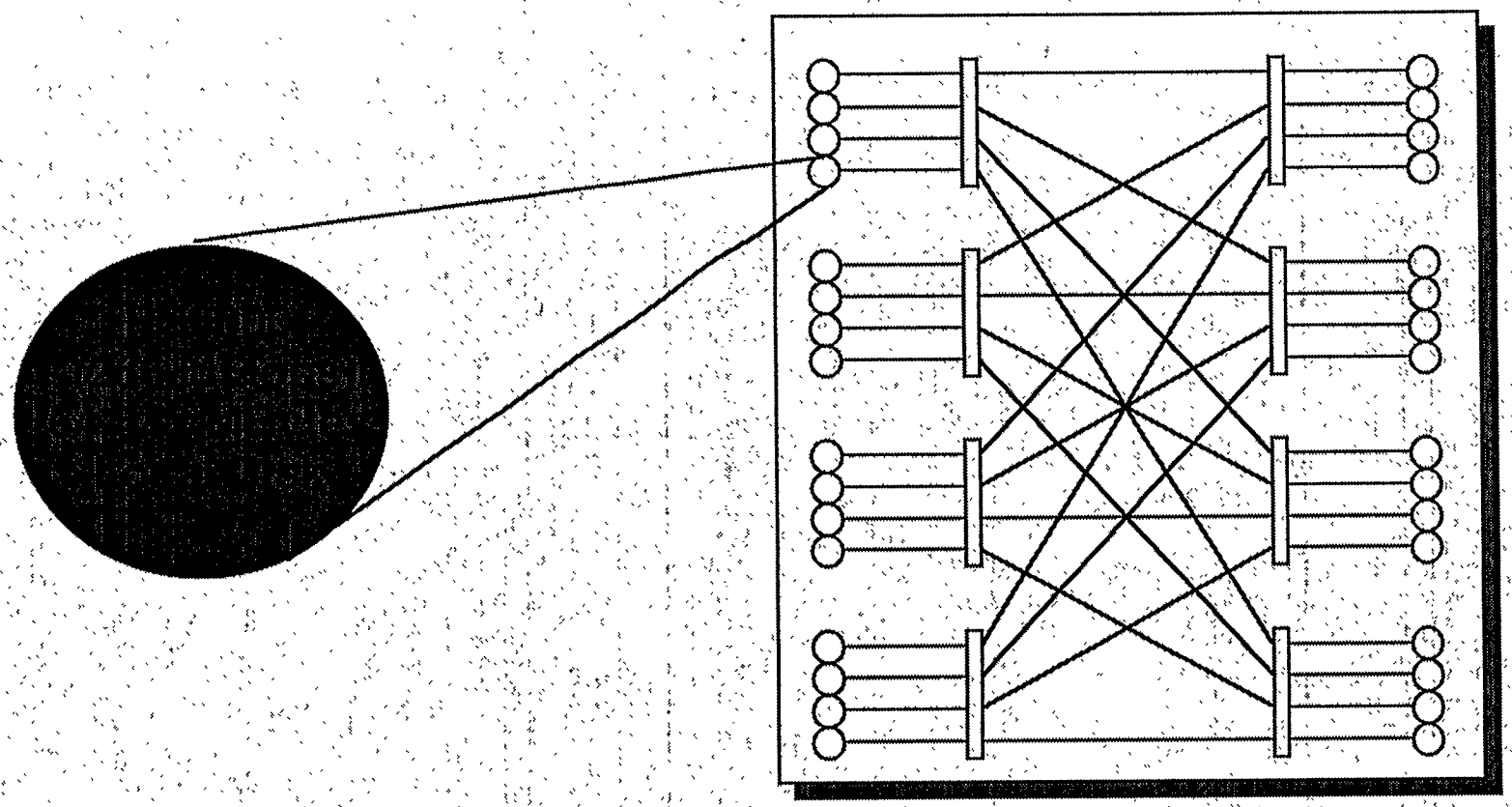

http://ibm/tc/cornell.edu/ibm/pps/sp2/index.html

Cray T3D

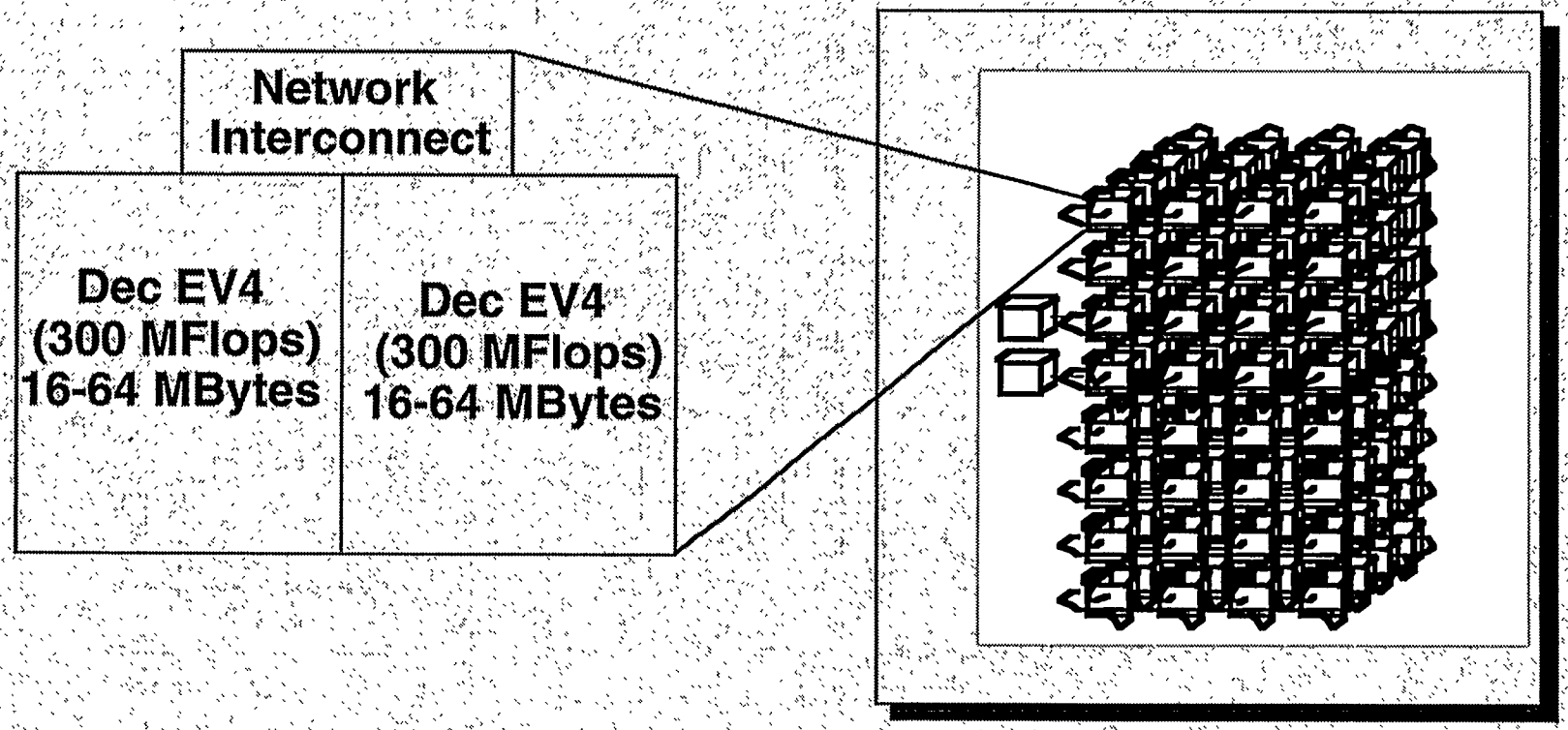

http://www.cray.com/PUBLIC/product-info/mpp/CRAY_T3D.html

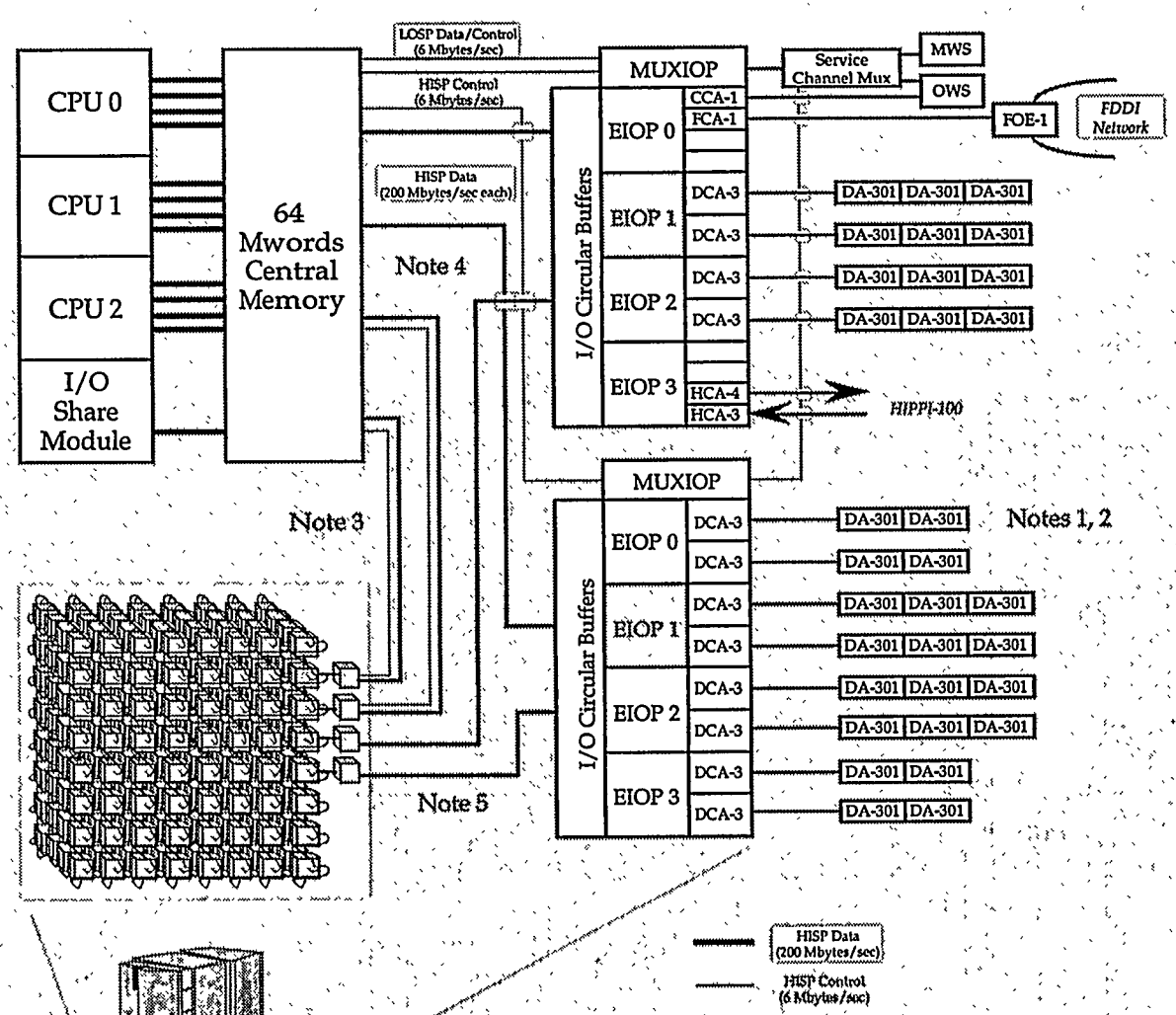

CRAY T3D SC256-8/364

Note 1: 180 Gbytes Disk Capacity
2: 432 Mbytes/sec Disk Bandwidth
3: 400 Mbytes/sec bi-directional to/from T3D and Cray host
4: 400 Mbytes/sec bi-directional to/from Cray host and IOCs
5: 400 Mbytes/sec bi-directional to/from T3D and IOCs (I/O Phase 2 only)

Software: Programming Models

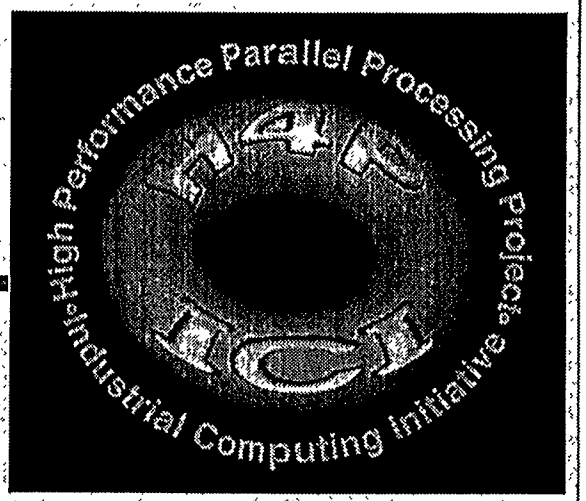

In fact the advent of parallel programming may do something to revive the pioneering spirit in programming, which seems to be degenerating into a rather dull and routine occupation.

- S. Gill, "Parallel Programming", Computer Journal, Vol. 1, 1958.

Shared memory

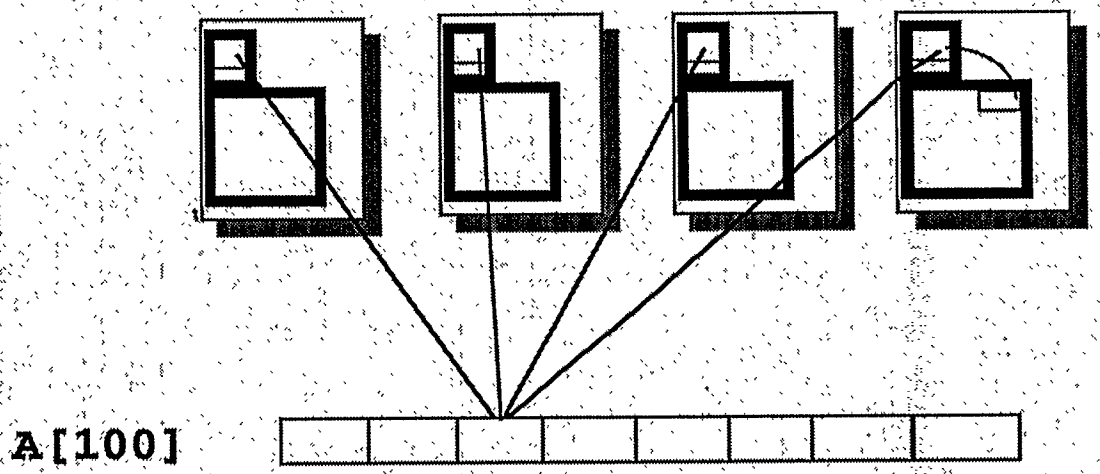

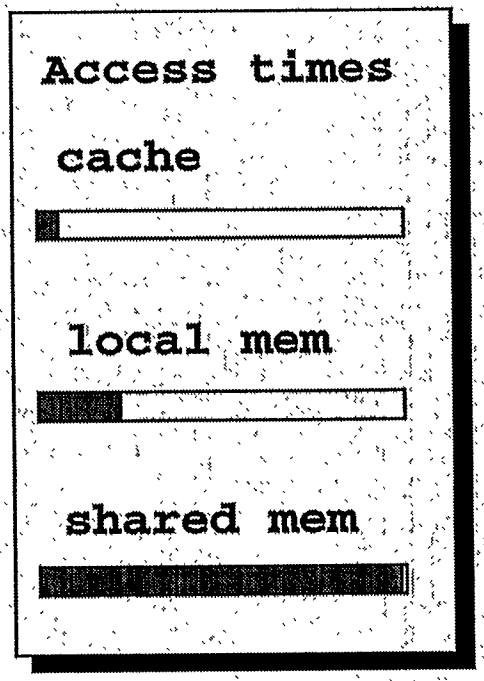

All processors access the same variable A

Message Passing

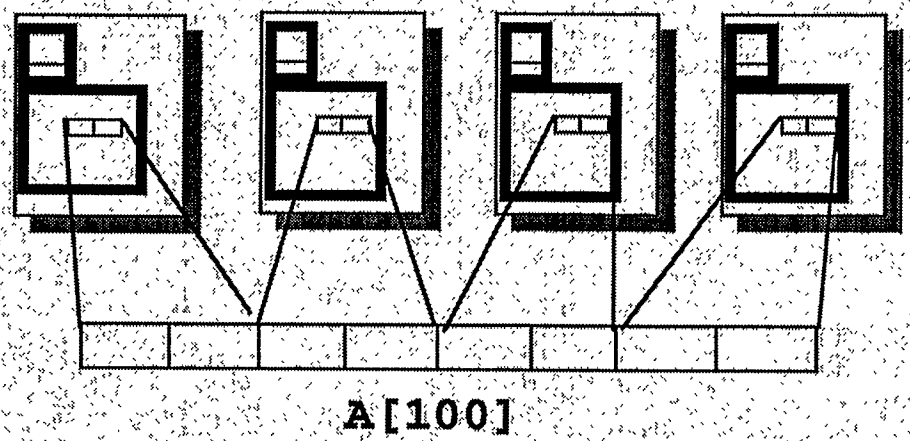

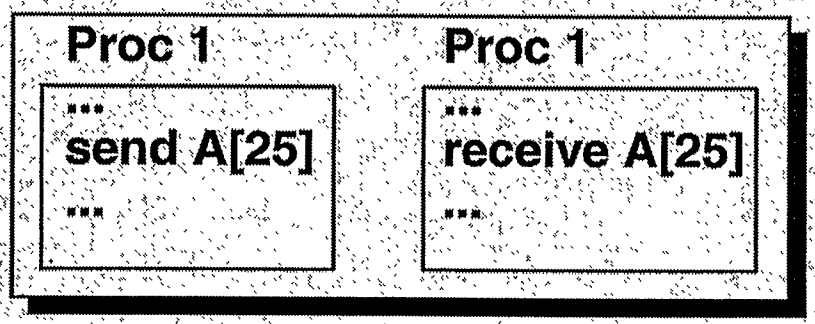

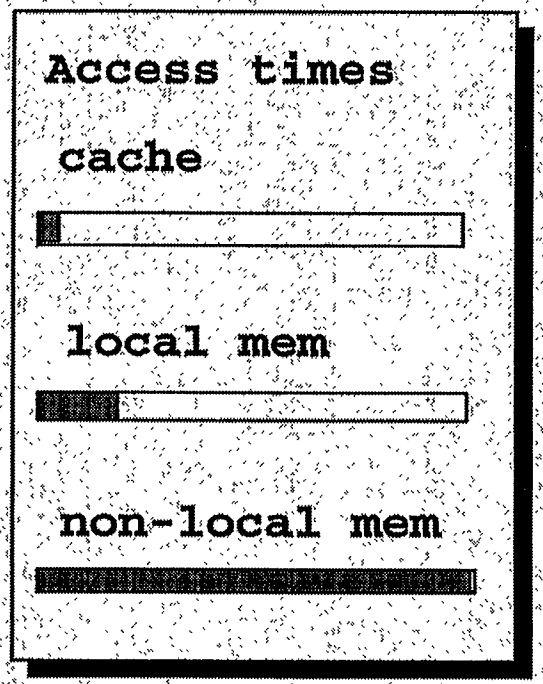

Each Processing Element (PE) owns part of the data.
Other PE's must generate messages to access memory.

Data Parallel

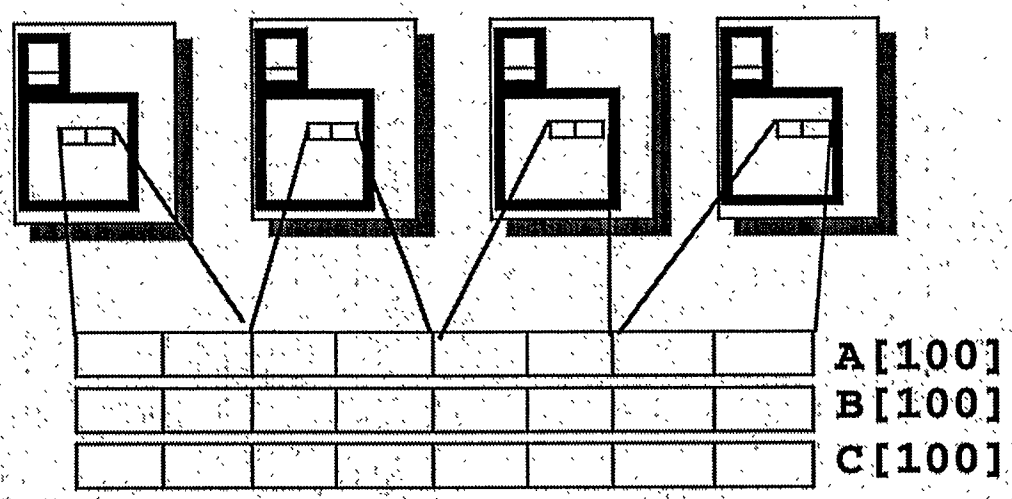

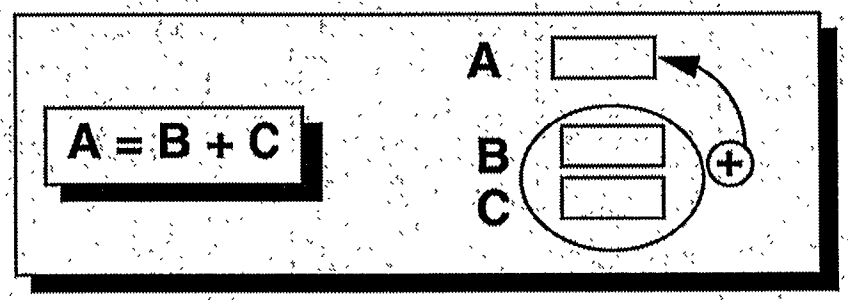

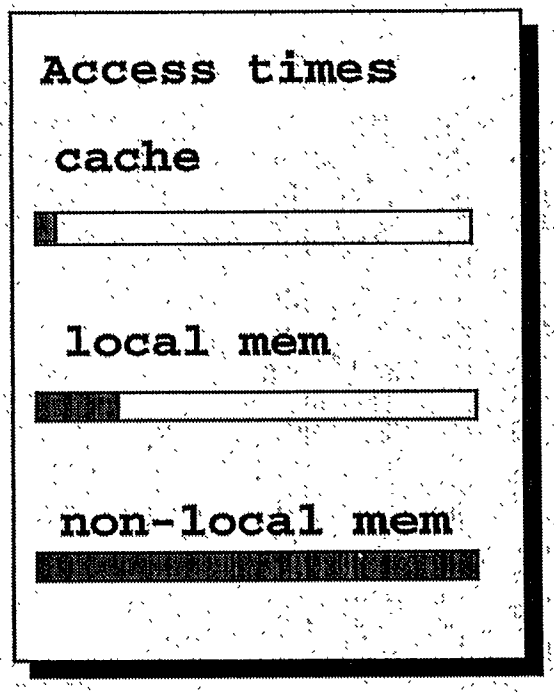

Each Processing Element (PE) owns part of the data. The language has implicit communications and attempts to use local memory whenever possible.

Performance of a Plasma PIC Code

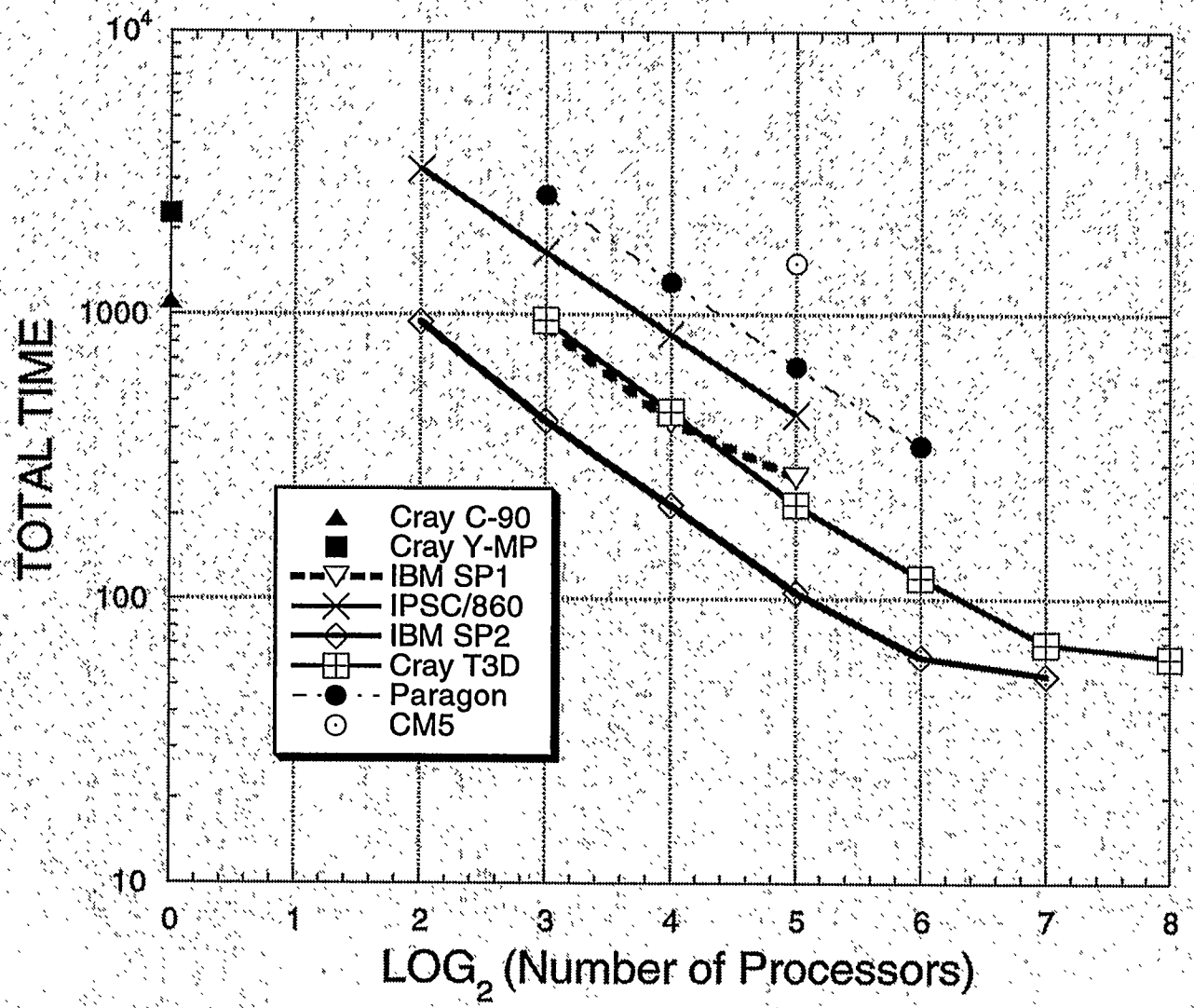

V. Decyk

Scalability

Sample:

ATMOSPHERIC GENERAL CIRCULATION MODEL

2° x 2.5° x 9 Levels

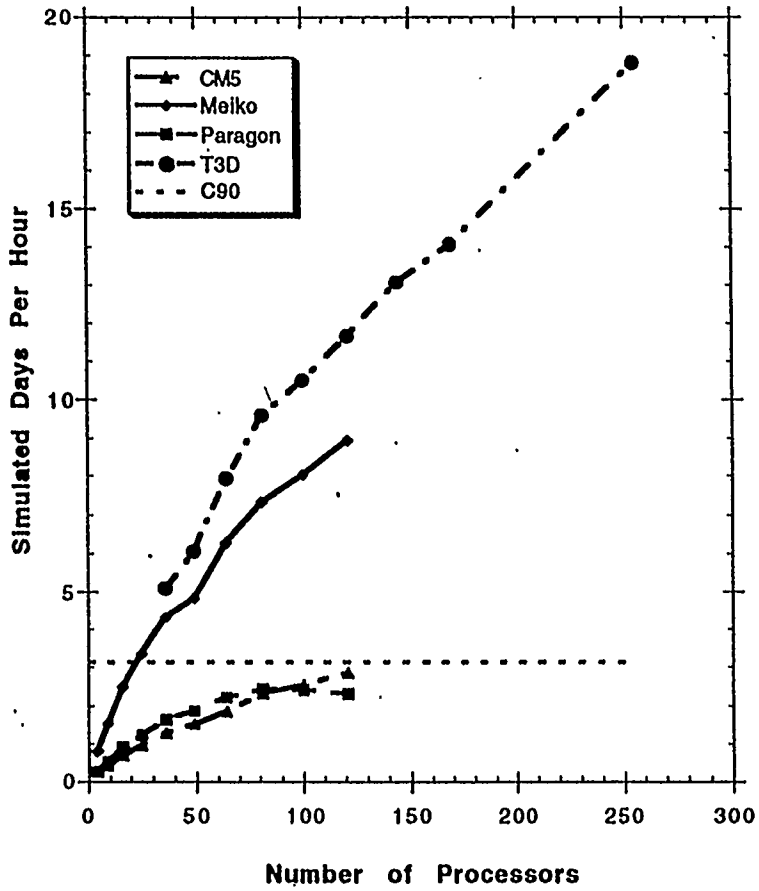

Performance

Sample:

77 Gflops

With Optimized

Well-Logging

Code

1024 Processors

Performance of PCGPP on Cray T3D

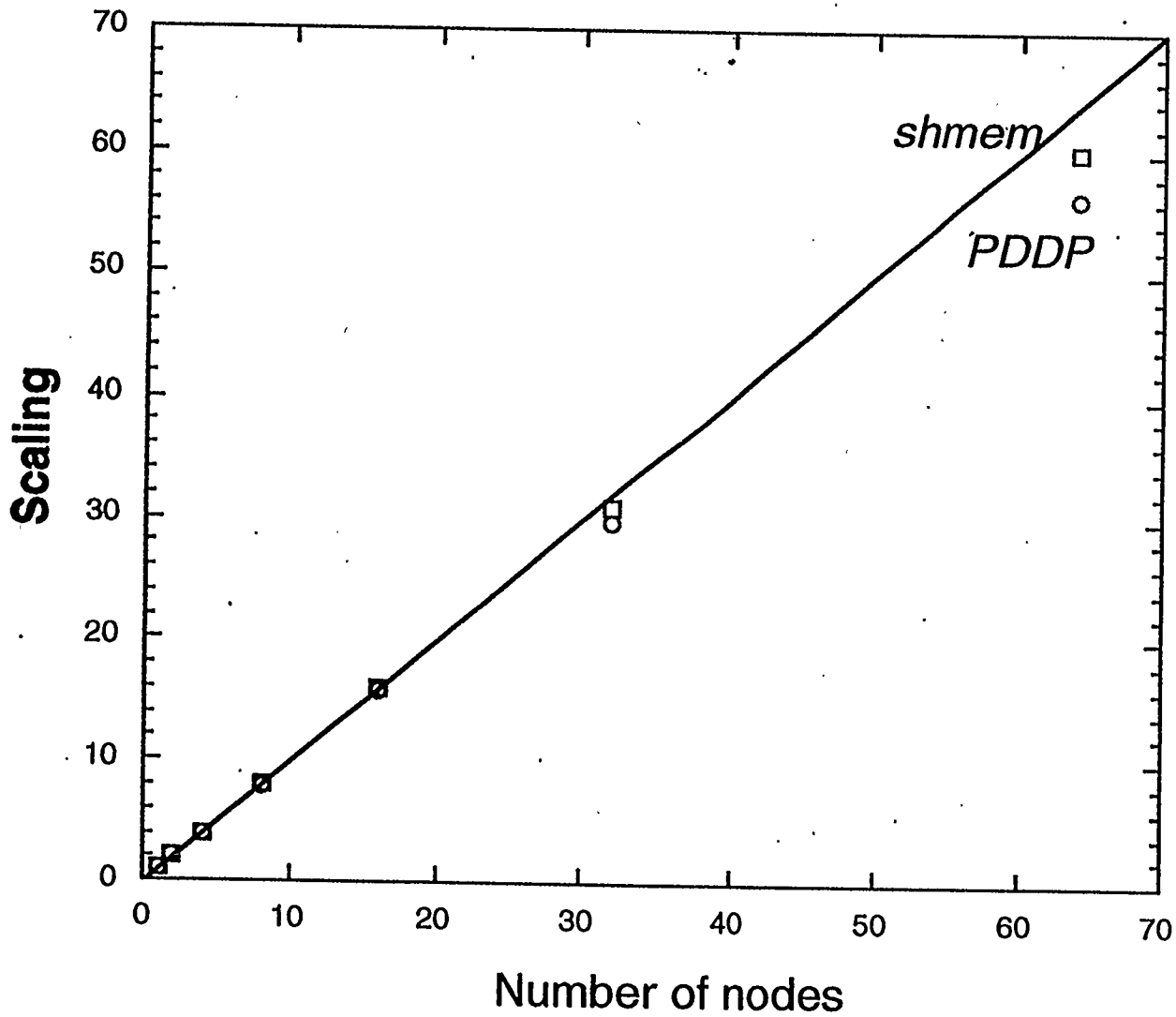

Problem size: 46 Mbypes of memory and 96 Mbytes of data.

The H4P-ICI and related ACISE funding provides MPP facilities for 13 CRADA's, UC Collaborations, and LLNL Projects

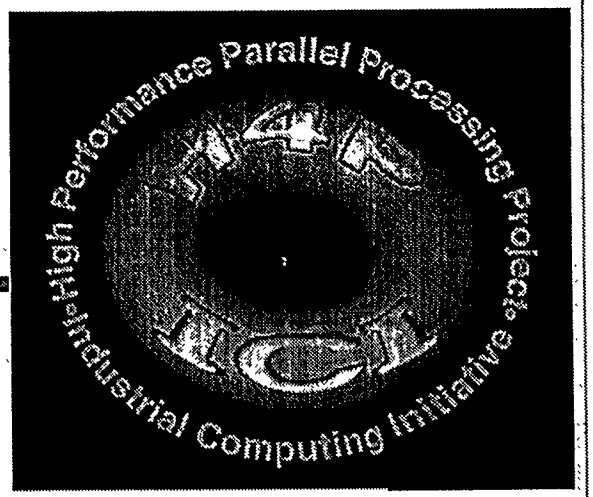

CRI T3D - 128 Proc. Upgrade
256 Processors Total

HIPPI

Meiko CS-2 - 16 Proc. Upgrade
64 Processors Total

http://www.nersc.gov/doc/Parallel_Processing/h4p/h4p.html

http://www.nersc.gov/doc/ACISE/index.html

Easy Way: NERSC home page www.nersc.gov
go to Parallel Processing...

H4P - ICI

High Performance Parallel Processing Project
- a collaborative research project aimed at putting real applications on MPPs.

Cray T3D - 128 Processors

Industry Partners

- Alcoa
- Amoco
- Arete Associates
- AT&T
- Berea
- Biosym Tech Inc.
- Olin Rocket Research
- Xerox

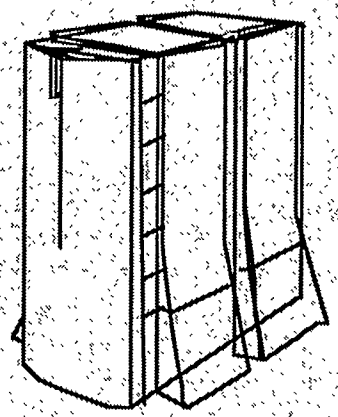

- Boeing
- Exxon
- General Motors
- Halliburton
- Hughes
- IT Corp.
- Schlumberger

NERSC Procurement

Two Machines:

FCM

Fully Configured Machine
Production-quality

PEP

Pilot Early Production
A smaller, less capable machine

Less powerful Processing Elements
Less Useful software